

ABSTRACT

OLSEN, KRISTEN M. Fine Scale Modeling of Agricultural Air Quality over the Southeastern United States: Application and Evaluation of Two Air Quality Models. (Under the direction of Dr. Yang Zhang).

Three-dimensional air quality models are vital tools for air quality research. The models are under continuous development as the knowledge and understanding of atmospheric processes improve. Once a model has been evaluated retrospectively against available observations, sensitivity studies can be conducted to determine possible causes for discrepancies between the model and observations and to assess potential impact of future emission changes. This research will evaluate the performance of two air quality models, the Community Multiscale Air Quality (CMAQ) model and the Comprehensive Air Quality Model with extensions (CAMx), at a fine scale over the southeastern United States in January and July 2002. The air quality in the southeast is of particular interest because of the high NH_3 emissions from agriculture which play a key role in the nutrient and nitrogen cycle, act to neutralize acids in the air, and participate in the formation of $\text{PM}_{2.5}$.

The baseline simulations are completed at a horizontal grid spacing of 4-km using both CMAQ and CAMx. The evaluation of meteorological variables, chemical concentrations, wet and dry deposition, column mass, and visibility is completed using available observations from surface measurements and satellite data. The evaluation protocol involves analysis through domain-wide statistics, spatial distribution, and temporal variations. Additionally, two sensitivity studies are conducted. In order to assess the model sensitivity to horizontal grid spacing, a sensitivity study evaluates the performance of CMAQ at 12-, 4-, and 1.33-km horizontal grid spacings. The second sensitivity study evaluates the sensitivity of CMAQ to emission reductions of SO_2 , NO_x , and agricultural-livestock NH_3 .

In the baseline simulation, O_3 and $\text{PM}_{2.5}$ are overpredicted by both models in January and underpredicted by both models in July, with CAMx predicting higher values than CMAQ in both months. The overprediction by the models in January is likely influenced by simulated weaker vertical mixing than what occurred in the true atmosphere. In July, underestimated emissions of precursor species or overpredicted wet deposition may be contributing to the underpredicted O_3 and $\text{PM}_{2.5}$. The spatial distribution of the adjusted gas

ratio indicates that the regions of high NH_3 emissions in the eastern NC and northeastern GA are NH_3 -rich and reductions of NH_3 alone would do little to reduce $\text{PM}_{2.5}$ pollution, which will be further evaluated in the second sensitivity study. When compared to satellite data, CMAQ shows good agreement for CO and NO_2 in both months, with larger biases for O_3 and AOD. These discrepancies may be due to uncertainties in the boundary conditions of the model and the calculation of AOD from the model predictions, as well as assumptions made in the satellite retrieval algorithms.

CMAQ shows some improvement for O_3 and $\text{PM}_{2.5}$ using finer grid spacings in January, but no improvement in July. One cause for this seasonal variation is the increased mass removed through wet deposition at finer scales in both months. This reduces the overprediction of PM species in January, but exacerbates the underprediction in July. Additional factors impacting the sensitivity to horizontal grid resolution are the sensitivity of the meteorology model and emissions. Through the emission sensitivity study, it was found that NH_3 emission reductions have a larger impact than SO_2 or NO_x emission reductions on $\text{PM}_{2.5}$ in January, while SO_2 emission reductions result in the largest decrease in $\text{PM}_{2.5}$ in July. Combining NH_3 emission reductions with the projected SO_2 and NO_x emission reductions act to reduce $\text{PM}_{2.5}$ more than SO_2 and NO_x emission reductions alone in both January and July.

Fine Scale Modeling of Agricultural Air Quality over the Southeastern United States:
Application and Evaluation of Two Air Quality Models

by
Kristen M. Olsen

A thesis submitted to the Graduate Faculty of
North Carolina State University
in partial fulfillment of the
requirements for the degree of
Master of Science

Marine, Earth, and Atmospheric Sciences

Raleigh, North Carolina

2009

APPROVED BY:

Dr. Yang Zhang
Committee Chair

Dr. Nicholas Meskhidze

Dr. Wayne Robarge

Dr. John T. Walker

BIOGRAPHY

Kristen Olsen was born and raised in Wilmington, DE where her interest in meteorology began as a childhood fear of thunderstorms. Upon graduating from high school in 2001, she entered Millersville University of Pennsylvania to pursue a Bachelor's degree in meteorology. During her undergraduate studies, she was an active member of the university's chapter of the American Meteorological Society and participated in meteorological forecasting activities including the Campus Weather Service and the National Forecasting Contest (now "WxChallenge"). She also volunteered time at the campus radio station to provide the weekend forecast during the 5 o'clock news segment on Fridays. During her final undergraduate semester, she completed an internship with the meteorologists at the local NBC station, WGAL-TV8. Through coursework and forecasting experience, her interests shifted from operational forecasting to forecast modeling. She graduated from Millersville University in May 2005 with a Bachelor of Science degree in meteorology and a minor in mathematics. Kristen worked for Access Group, Inc, a graduate student loan company, for two years before continuing on to obtain her Master's degree. She was accepted to North Carolina State University's Marine, Earth, and Atmospheric Science Graduate Program in July 2007 and began working with Dr. Yang Zhang's Air Quality Forecasting Laboratory in August 2007.

ACKNOWLEDGMENTS

I would first like to thank my committee members, Drs. Yang Zhang, Nicholas Meskhidze, Wayne Robarge, and John Walker. I additionally want to thank Dr. Zhang for providing me with the opportunity to conduct this research and present the findings at conferences throughout my graduate studies. I also want to thank my undergraduate professors (Drs. Richard Clark, Sepi Yalda, and Alex DeCaria) in the meteorology department at Millersville University of Pennsylvania for providing the knowledge base required to further my education, as well as the encouragement to continue to a higher degree.

I would like to acknowledge and thank the USDA Cooperative State Research, Education, and Extension Service Air Quality Program for funding this project through the National Research Initiative Competitive Grant no. 2008-35112-18758. Thanks are also due to numerous people who have contributed to this research in one way or another: Pat Brewer, Mike Abraczinskas, George Bridgers, Bebhinn Do, Chris Misenis, Hoke Kimball, and Wayne Cornelius, North Carolina Department of Environmental and Natural Resources; Don Olerud, Baron Advanced Meteorological Systems; Dennis McNally and Cyndi Loomis, Alpine Geophysics, Inc; Ryan Boyles, North Carolina State Climate Office; Alice Gilliland, Steve Howard, and Shao-Cai Yu, U.S. Environmental Protection Agency; and Shiang-Yuh Wu, Clark County Department of Air Quality and Environmental Management.

I also want to thank the past and current members of the Air Quality Forecasting Lab at NC State for their endless guidance and camaraderie. I've enjoyed sharing stories with you and learning of foreign culture while taking breaks from research. To my family; my mom, dad, and sister, thank you for everything; for the endless love, support, and motivation, not only during these two years, but through out my life. And to Ryan, you always knew just what to say to lift my spirits when I needed it the most and I couldn't have done this without your love and encouragement.

TABLE OF CONTENTS

LIST OF TABLES	vi
LIST OF FIGURES	viii
ACRONYMS	xiv
1. INTRODUCTION	1
1.1 Background and Motivations	1
1.1.1 Sources, Emissions, and Roles of NH ₃	1
1.1.2 Impacts of PM _{2.5}	4
1.2 Objectives	5
2. LITERATURE REVIEW	6
2.1 Comparison of Model Treatments	6
2.2 Sensitivity to Horizontal Grid Spacing	11
2.3 Sensitivity to Emissions	14
3. DESCRIPTION OF MODEL CONFIGURATIONS, EPISODE, DATABASE, AND METHODOLOGY	20
3.1 Modeling System	20
3.1.1 MM5	20
3.1.2 SMOKE	23
3.1.3 CMAQ and CAMx	24
3.2 Description of Episode Selected for Model Simulations	24
3.3 Observational Data	27
3.3.1 Meteorological Observations	28
3.3.2 Chemical and Optical Observations	28
3.3.3 Quality of Observational Data	32
3.4 Evaluation Protocol	34
3.4.1 Statistical Evaluation	34
3.4.2 Spatial Evaluation	35
3.4.3 Temporal Evaluation	35

3.4.4 Column Mass of Chemical Species	36
4. BASELINE SIMULATIONS: INTERCOMPARISON OF CMAQ AND CAM _x	37
4.1 Meteorology.....	37
4.2 Chemical Concentrations of Gaseous and PM Species	50
4.3 Dry and Wet Deposition Fluxes.....	73
4.4 Column Mass of Chemical Species	89
4.5 Visibility	97
4.6 Summary.....	102
5. SENSITIVITY TO HORIZONTAL GRID SPACING AND EMISSION REDUCTIONS	106
5.1 Sensitivity to Horizontal Grid Spacing.....	106
5.1.1 Meteorology.....	106
5.1.2 Emissions	116
5.1.3 Chemical Concentrations of Gaseous and PM Species	124
5.1.4 Dry and Wet Deposition Amounts.....	132
5.1.5 Visibility	138
5.2 Sensitivity to Emission Reduction.....	143
5.2.1 Agricultural Livestock Ammonia (AL-NH ₃) Reduction	146
5.2.2 NO _x Reduction.....	149
5.2.3 SO ₂ Reduction.....	149
5.2.4 Combination of NH ₃ , NO _x , and SO ₂ Emission Reductions.....	149
5.2.5 Summary.....	155
6. CONCLUSIONS AND RECOMMENDATIONS	159
7. REFERENCES	164

LIST OF TABLES

Table 2.1.	A list of the chemical mechanisms and physical schemes available in the CMAQ and CAMx versions used in this research.....	7
Table 2.2.	Recent studies on model sensitivity to horizontal grid spacing.....	12
Table 2.3.	Characterization of NH ₃ -rich and NH ₃ -poor regions based on GR and AdjGR (Ansari and Pandis (1998); Pinder et al. (2008); modified from Takahama et al. (2004) and Dennis et al. (2008)).....	17
Table 2.4.	Recent research on the sensitivity of AQMs to emission reductions.....	18
Table 3.1.	MM5 model configurations used in this research.....	22
Table 3.2.	CMAQ and CAMx model configurations used in this research.....	25
Table 3.3.	The observational networks and satellites used in model evaluation, as well as the variables evaluated, the sampling frequency, and the number of sites within the 4-km and 1.33-km modeling domains	29
Table 4.1.	Performance statistics for meteorological variables for January 2002	38
Table 4.2.	Performance statistics for meteorological variables for July 2002.....	40
Table 4.3.	Performance statistics for gaseous and PM species in January 2002	55
Table 4.4.	Performance statistics for gaseous and PM species in July 2002	59
Table 4.5.	Performance statistics for dry and wet deposition in January 2002.....	74
Table 4.6.	Performance statistics for dry and wet deposition in July 2002	77
Table 4.7.	Performance statistics for satellite derived variables in January	90
Table 4.8.	Performance statistics for satellite derived variables in July	91
Table 4.9.	Values of $f(RH)$ used to calculate β_{ext} for CAMx at the IMPROVE sites within the 4-km domain (U.S. EPA, 2003).....	99
Table 4.10.	Statistics for visibility parameters in January 2002	100

Table 4.11.	Statistics for visibility parameters in July 2002	101
Table 5.1.	Mean biases and NMBs of meteorological variables for January at 12-, 4-, and 1.33-km horizontal grid spacing	107
Table 5.2.	Mean biases and NMBs of meteorological variables for July at 12-, 4-, and 1.33-km horizontal grid spacing	109
Table 5.3.	Statistics for gaseous and PM species in January at 12-, 4-, and 1.33-km horizontal grid spacing	125
Table 5.4.	Statistics for gaseous and PM species in July at 12-, 4-, and 1.33-km horizontal grid spacing	126
Table 5.5.	Statistics for wet and dry deposition in January at 12-, 4-, and 1.33-km horizontal grid spacings	133
Table 5.6.	Statistics for wet and dry deposition in July at 12-, 4-, and 1.33-km horizontal grid spacings	134
Table 5.7.	Percent change in annual NO _x emissions from each source type in each state contained in the 4-km domain, based on projected annual emissions reported by MACTEC, Inc. (2008)	144
Table 5.8.	Percent change in annual NO _x emissions from each source type in each state contained in the 4-km domain, based on projected annual emissions reported by MACTEC, Inc. (2008)	145
Table 5.9.	Absolute (abs., in $\mu\text{g m}^{-3}$) and percent (perc., %) change in domain-wide average PM _{2.5} , NH ₄ ⁺ , SO ₄ ²⁻ , and NO ₃ ⁻ as a result of emission reductions	157

LIST OF FIGURES

Figure 1.1.	Percentage of ammonia-nitrogen emissions from different sources in the U.S. in 1994 (adapted from Battye et al., 1994)	2
Figure 3.1.	The three modeling domains used in this research	21
Figure 4.1.	The spatial distribution of monthly-mean temperatures at 2-m in (a) January and (b) July as simulated by MM5 (background color) overlaid with observations (diamonds) from CASTNET, STN, and NC SCO	43
Figure 4.2.	The spatial distribution of monthly-mean relative humidities at 2-m in (a) January and (b) July as simulated by MM5 (background color) overlaid with observations (diamonds) from CASTNET, STN, and NC SCO	44
Figure 4.3.	Temporal variation of temperatures in January at Beaufort, NC (coastal), Kinston, NC (central), Great Smoky Mountains (mountain), TN, and Raleigh, NC (urban).....	46
Figure 4.4.	Temporal variation of temperatures at 2-m in July at Beaufort, NC (coastal), Kinston, NC (central), Great Smoky Mountains (mountain), TN, and Raleigh, NC (urban).....	47
Figure 4.5.	Temporal variation of relative humidity at 2-m in January at Beaufort, NC (coastal), Kinston, NC (central), Great Smoky Mountains (mountain), TN, and Raleigh, NC (urban).....	48
Figure 4.6.	Temporal variation of relative humidity at 2-m in July at Beaufort, NC (coastal), Kinston, NC (central), Great Smoky Mountains (mountain), TN, and Raleigh, NC (urban).....	49
Figure 4.7.	Temporal variation of wind speeds at 10-m in January at Beaufort, NC (coastal), Kinston, NC (central), Great Smoky Mountains (mountain), TN, and Raleigh, NC (urban).....	51
Figure 4.8.	Temporal variation of wind speeds at 10-m in July at Beaufort, NC (coastal), Kinston, NC (central), Great Smoky Mountains (mountain), TN, and Raleigh, NC (urban).....	52

Figure 4.9.	Temporal variation of wind direction at 10-m in January at Beaufort, NC (coastal), Kinston, NC (central), Great Smoky Mountains (mountain), TN, and Raleigh, NC (urban).....	53
Figure 4.10.	Temporal variation of wind direction at 10-m in July at Beaufort, NC (coastal), Kinston, NC (central), Great Smoky Mountains (mountain), TN, and Raleigh, NC (urban).....	54
Figure 4.11.	Spatial distribution of the monthly-mean PM _{2.5} concentrations as simulated by CMAQ (top) and CAMx (bottom) in January (left) and July (right) overlaid with observations (diamonds) from IMPROVE and STN	65
Figure 4.12.	Hourly O ₃ mixing ratios as simulated by CMAQ and CAMx, compared to observations at Beaufort, NC and Great Smoky Mountains, TN	66
Figure 4.13.	Hourly O ₃ as simulated by CMAQ and CAMx, compared to observed hourly O ₃ mixing ratios, at Beaufort, NC, Kinston, NC, Great Smoky Mountains, TN, and Raleigh, NC	67
Figure 4.14.	Observed PM _{2.5} concentrations compared to modeled PM _{2.5} concentrations in January (left) and July (right) at Raleigh (top) and Kinston (bottom).....	69
Figure 4.15.	Monthly-mean spatial distribution of the ratio NH ₄ ⁺ /NH _x (in percentage) as simulated by (a) CMAQ in January, (b) CMAQ in July, (c) CAMx in January, and (d) CAMx in July	70
Figure 4.16.	Monthly-mean spatial distribution of AdjGR as simulated by (a) CMAQ in January, (b) CMAQ in July, (c) CAMx in January, and (d) CAMx in July	71
Figure 4.17.	SO ₂ dry deposition velocity in January (top) and July (bottom) as simulated by MLM, CMAQ, and CAMx at Beaufort, NC (left) and Great Smoky Mountains, TN (right).....	82
Figure 4.18.	SO ₂ dry deposition flux in January (top) and July (bottom) as simulated by MLM, CMAQ, and CAMx at Beaufort, NC (left) and Great Smoky Mountains, TN (right).....	83

Figure 4.19.	HNO ₃ dry deposition velocity in January (top) and July (bottom) as simulated by MLM, CMAQ, and CAMx at Beaufort, NC (left) and Great Smoky Mountains, TN (right).....	84
Figure 4.20.	HNO ₃ dry deposition flux in January (top) and July (bottom) as simulated by MLM, CMAQ, and CAMx at Beaufort, NC (left) and Great Smoky Mountains, TN (right).....	85
Figure 4.21.	NH ₄ ⁺ dry deposition velocity in January (top) and July (bottom) as simulated by MLM, CMAQ, and CAMx at Beaufort, NC (left) and Great Smoky Mountains, TN (right).....	86
Figure 4.22.	SO ₄ ²⁻ dry deposition flux in January (top) and July (bottom) as simulated by MLM, CMAQ, and CAMx at Beaufort, NC (left) and Great Smoky Mountains, TN (right).....	87
Figure 4.23.	NO ₃ ⁻ dry deposition velocity in January (top) and July (bottom) as simulated by MLM, CMAQ, and CAMx at Beaufort, NC (left) and Great Smoky Mountains, TN (right).....	88
Figure 4.24.	Monthly-mean column CO as derived from MOPITT (top) and from the CMAQ simulation (bottom) for January (left) and July (right)	93
Figure 4.25.	Monthly-mean column NO ₂ as derived from GOME (top) and from the CMAQ simulation (bottom) for January (left) and July (right)	94
Figure 4.26.	Monthly-mean column O ₃ as derived from TOMS (top) and from the CMAQ simulation (bottom) for January (left) and July (right)	95
Figure 4.27.	Monthly-mean aerosol optical depth (AOD) as derived from MODIS (top) and from the CMAQ simulation (bottom) for January (left) and July (right).....	96
Figure 4.28.	The monthly-mean (a) extinction coefficient, (b) haziness index, and (c) visual range in January, based on the CMAQ simulation, overlaid with observations from IMPROVE (diamonds)	103
Figure 4.29.	The monthly-mean (a) extinction coefficient, (b) haziness index, and (c) visual range in July, based on the CMAQ simulation, overlaid with observations from IMRPOVE (diamonds)	104

Figure 5.1.	Spatial distribution of monthly-mean temperature in January at a grid spacing of (a) 12-km, (b) 4-km, and (c) 1.33-km, all overlaid with observations from CASTNET, STN, and NC SCO.....	110
Figure 5.2.	Spatial distribution of monthly-mean temperature in July at a grid spacing of (a) 12-km, (b) 4-km, and (c) 1.33-km, all overlaid with observations from CASTNET, STN, and NC SCO.....	111
Figure 5.3.	Spatial distribution of monthly-mean relative humidity in January at a grid spacing of (a) 12-km, (b) 4-km, and (c) 1.33-km, all overlaid with observations from CASTNET and NC SCO	112
Figure 5.4.	Spatial distribution of monthly-mean relative humidity in July at a grid spacing of (a) 12-km, (b) 4-km, and (c) 1.33-km, all overlaid with observations from CASTNET and NC SCO	113
Figure 5.5.	Time series for meteorological variables at Candor, NC in January at 12-, 4-, 1.33-km horizontal grid spacing.....	114
Figure 5.6.	Time series for meteorological variables at Candor, NC in July at 12-, 4-, 1.33-km horizontal grid spacing.....	115
Figure 5.7.	Spatial distributions of the percentage difference of monthly-mean NH ₃ emissions at 1.33-km compared to 4-km (left) and 12-km (right) in January (top) and July (bottom).....	117
Figure 5.8.	Spatial distributions of the percentage difference of monthly-mean SO ₂ emissions at 1.33-km compared to 4-km (left) and 12-km (right) in January (top) and July (bottom).....	118
Figure 5.9.	Spatial distributions of the percentage difference of monthly-mean NO ₂ emissions at 1.33-km compared to 4-km (left) and 12-km (right) in January (top) and July (bottom).....	119
Figure 5.10.	Spatial distributions of the percentage difference of monthly-mean NO emissions at 1.33-km compared to 4-km (left) and 12-km (right) in January (top) and July (bottom).....	120
Figure 5.11.	Spatial distributions of the percentage difference of monthly-mean PM _{2.5} emissions at 1.33-km compared to 4-km (left) and 12-km (right) in January (top) and July (bottom).....	121

Figure 5.12.	Spatial distributions of the percentage difference of monthly-mean SO_4^{2-} emissions at 1.33-km compared to 4-km (left) and 12-km (right) in January (top) and July (bottom).....	122
Figure 5.13.	Spatial distributions of the percentage difference of monthly-mean NO_3^- emissions at 1.33-km compared to 4-km (left) and 12-km (right) in January (top) and July (bottom).....	123
Figure 5.14.	Spatial distribution of monthly-mean $\text{PM}_{2.5}$ as simulated in January by CMAQ at (a) 12-km, (b) 4-km, and (c) 1.33-km overlaid with observations (diamonds) from STN and CASTNET	127
Figure 5.15.	Spatial distribution of monthly-mean $\text{PM}_{2.5}$ as simulated in January by CMAQ at (a) 12-km, (b) 4-km, and (c) 1.33-km overlaid with observations (diamonds) from STN and CASTNET	129
Figure 5.16.	Time series for O_3 at the CASTNET site in Candor, NC as simulated at 12-, 4-, and 1.33-km horizontal grid spacings	130
Figure 5.17.	Time series for $\text{PM}_{2.5}$ at Raleigh, NC (hourly) and Kinston, NC (24-hour average) as simulated at 12-, 4-, and 1.33-km horizontal grid spacings	131
Figure 5.18.	Time series of NH_4^+ dry deposition flux at Candor, NC in January and July as simulated by CMAQ at 12-, 4-, and 1.33-km and compared to the MLM	135
Figure 5.19.	Time series of SO_4^{2-} dry deposition flux at Candor, NC in January and July as simulated by CMAQ at 12-, 4-, and 1.33-km and compared to the MLM	136
Figure 5.20.	Time series of NO_3^- dry deposition flux at Candor, NC in January and July as simulated by CMAQ at 12-, 4-, and 1.33-km and compared to the MLM	137
Figure 5.21.	Time series of SO_2 dry deposition flux at Candor, NC in January and July as simulated by CMAQ at 12-, 4-, and 1.33-km and compared to the MLM	139
Figure 5.22.	Time series of HNO_3 dry deposition flux at Candor, NC in January and July as simulated by CMAQ at 12-, 4-, and 1.33-km and compared to the MLM	140

Figure 5.23.	Spatial distribution of the haziness index in January as simulated by CMAQ at horizontal grid spacings of (a) 12-km, (b) 4-km, and (c) 1.33-km	141
Figure 5.24.	Spatial distribution of the haziness index in July as simulated by CMAQ at horizontal grid spacings of (a) 12-km, (b) 4-km, and (c) 1.33-km	142
Figure 5.25.	The absolute (left) and percentage (right) difference in $PM_{2.5}$, NH_4^+ , SO_4^{2-} , and NO_3^- in January when AL- NH_3 emissions are reduced by 50%	147
Figure 5.26.	The absolute (left) and percentage (right) difference in $PM_{2.5}$, NH_4^+ , SO_4^{2-} , and NO_3^- in July when AL- NH_3 emissions are reduced by 50%	148
Figure 5.27.	The absolute (left) and percentage (right) difference in $PM_{2.5}$, NH_4^+ , SO_4^{2-} , and NO_3^- in January when NO_x is reduced by 50%	150
Figure 5.28.	The absolute (left) and percentage (right) difference in $PM_{2.5}$, NH_4^+ , SO_4^{2-} , and NO_3^- in July when NO_x emissions are reduced by 50%	151
Figure 5.29.	The absolute (left) and percentage (right) difference in $PM_{2.5}$, NH_4^+ , SO_4^{2-} , and NO_3^- in January when SO_2 emissions are reduced by 50%	152
Figure 5.30.	The absolute (left) and percentage (right) difference in $PM_{2.5}$, NH_4^+ , SO_4^{2-} , and NO_3^- in July when SO_2 emissions are reduced by 50%	153
Figure 5.31.	The absolute (left) and percentage (right) difference in $PM_{2.5}$, NH_4^+ , SO_4^{2-} , and NO_3^- in January when AL- NH_3 , NO_x , and SO_2 emissions are reduced by 50%	154
Figure 5.32.	The absolute (left) and percentage (right) difference in $PM_{2.5}$, NH_4^+ , SO_4^{2-} , and NO_3^- in July when AL- NH_3 , NO_x , and SO_2 emissions are reduced by 50%	156

ACRONYMS

3-D	Three-Dimensional
ACM	Asymmetric Convective Mixing
AdjGR	Adjusted Gas Ratio
AERONET	Aerosol Robotic Network
AIRS-AQS	Aerometric Information Retrieval System – Air Quality Subsystem
AL-NH ₃	Agricultural Livestock NH ₃
AOD	Aerosol Optical Depth
AQM	Air Quality Model
ASOS	Automated Surface Observing System
AWOS	Automated Weather Observing System
BC	Black Carbon
BCON	Boundary Condition
CAMx	Comprehensive Air Quality Model with Extensions
CASTNET	Clean Air Status and Trends Network
CB05	2005 version Carbon Bond Mechanism
CB-IV	Carbon Bond IV
CCN	Cloud Condensation Nuclei
CF	Coarse-Fine (Bisectional) Scheme
CMAQ	Community Multiscale Air Quality modeling system
CMU	Carnegie Mellon University
CO	Carbon Monoxide
CoCoRaHS	Community Collaborative Rain, Hail, and Snow Network
CONUS	Continental U.S.
DSN	Degree of Sulfate Neutralization
ECONet	Environment and Climate Observing Network
EGU	Electric Generating Unit
ENVISAT	Environmental Satellite

ERS-2	2 nd European Remote Sensing satellite
FB	Fractional Bias
FDDA	Four Dimensional Data Assimilation
FGE	Fractional Gross Error
GOME	Global Ozone Monitoring Experiment
GR	Gas Ratio
H ₂ O	Water
H ₂ O ₂	Hydrogen Peroxide
H ₂ SO ₄	Sulfuric Acid
HNO ₃	Nitric Acid
ICON	Initial Conditions
IMPROVE	Interagency Monitoring of Protected Visual Environments
IMS95	1995 Integrated Monitoring Study
LPV-2	Long Path Visibility – 2
LSM	Land Surface Model
MADRID	Model of Aerosol Dynamics, Reaction, Ionization, and Dissolution
MAGE	Mean Absolute Gross Error
MAQSIP	Multiscale Air Quality Simulation Platform
MB	Mean Bias
MCIP	Meteorology-Chemistry Interface Processor
MM5	PSU/NCAR 5 th generation Mesoscale Model
MNB	Mean Normalized Bias
MNGE	Mean Normalized Gross Error
MNGFE	Mean Normalized Gross Fractional Error
MODIS	Moderate Resolution Imaging Spectroradiometer
MOPITT	Measurements of Pollution in the Troposphere
NAAQS	National Ambient Air Quality Standard
NADP	National Atmospheric Deposition Program
NC	North Carolina

NCAR	National Center for Atmospheric Research
NCDENR	NC Department of Environmental and Natural Resources
NDSC	Network for the Detection of Stratospheric Change
NEI	National Emission Inventory
NET	National Emissions Trends
NGN-2	Next Generation Nephelometer – 2
NH ₃	Ammonia
NH ₄ ⁺	Ammonium Ion
(NH ₄) ₂ SO ₄	Ammonium Sulfate
NH ₄ HSO ₄	Ammonium Bisulfate
NH ₄ NO ₃	Ammonium Nitrate
NH _x	Reduced Nitrogen (NH ₃ + NH ₄ ⁺)
NMB	Normalized Mean Bias
NMBF	Normalized Mean Bias Factor
NME	Normalized Mean Error
NMEF	Normalized Mean Error Factor
NMFB	Normalized Mean Fractional Bias
NMFGE	Normalized Mean Fractional Gross Error
NO	Nitric Oxide
NO ₂	Nitrogen Dioxide
NO ₃ ⁻	Nitrate Ion
NO _x	Nitrogen Oxides
NR	Non-road
NWS	National Weather Service
O ₃	Ozone
OC	Organic Carbon
OM	Organic Matter
PM	Particulate Matter
PPM	Piecewise Parabolic Method

Precip	Precipitation
PSU	Penn State University
RADM	Regional Acid Deposition Model
REMSAD	Regional Modeling System for Aerosols and Deposition
RH2	Relative Humidity at 2-m
RMSE	Root Mean Square Error
RRTM	Rapid Radiative Transfer Model
SAPRC99	1999 version State Air Pollution Research Center module
SCAN	Soil Climate Analysis Network
SEARCH	Southeastern Aerosol Research and Characterization
SIP	State Implementation Plan
SMOKE	Sparse Matrix Operator Kernel Emissions
SO ₂	Sulfur Dioxide
SO ₄ ²⁻	Sulfate Ion
SOA	Secondary Organic Aerosol
SOAP	Secondary Organic Aerosol Partitioning
SORGAM	Secondary Organic Aerosol Model
STN	Speciation Trends Network
T2	Temperature at 2-m
TC	Total Carbon
TOMS	Total Ozone Mapping Spectrometer
TOR	Thermal Optical Reflectance
TOT	Thermal Optical Transmittance
U.S.	United States
U.S. EPA	U.S. Environmental Protection Agency
VISTAS	Visibility Improvement State and Tribal Association of the Southeast
VOC	Volatile Organic Compound
VR	Visual Range
WDR10	Wind Direction at 10-m

WSP10

Wind Speed at 10-m

1. INTRODUCTION

1.1 Background and Motivations

Three-dimensional air quality models (3-D AQMs) are powerful tools in air quality research. As the knowledge and understanding of atmospheric processes improve, they are applied to the models to improve the representation of the true atmosphere. For example, current 3-D AQMs have adapted a “one-atmosphere” approach to simulate ozone, aerosols, and deposition simultaneously in an attempt to accurately represent interactions among the pollutants. As improvements are integrated into the models, the results must be verified against observations before the model can be applied to additional research and forecasting. The detailed, one-atmosphere science then allows for sensitivity studies to assess the impacts of future emission changes. The research presented in this thesis work will focus on fine scale air quality modeling over a portion of the southeastern United States (U.S.) using the Pennsylvania State University (PSU)/National Center for Atmospheric Research (NCAR) 5th generation Mesoscale Model (MM5) (Grell et al., 1994) and two commonly-used 3-D AQMs, the Models-3 Community Multiscale Air Quality (CMAQ) model (Byun and Ching, 1999; Binkowski and Roselle, 2003; Byun and Schere, 2006) and ENVIRON’s Comprehensive Air Quality Model with extensions (CAMx) (ENVIRON, 2006). The air quality in the southeastern U.S. is of particular interest because of high ammonia (NH₃) emissions from agricultural sources and their impacts on the regional air quality and environment.

1.1.1 Sources, Emissions, and Roles of NH₃

Ammonia (NH₃) plays a key role in many aspects of the ecosystem, including the nutrient and nitrogen cycle, neutralizing acids in the air, and participating in the formation of particulate matter having an aerodynamic diameter of 2.5 μm or less (PM_{2.5}). The percentage contribution of NH₃-nitrogen from different emission sources is displayed in Figure 1.1 with the major sources being livestock (cattle, swine, and poultry). The wet and dry deposition of NH₃ to the soil is a source of nitrogen to the nitrogen cycle, which provides nutrients to

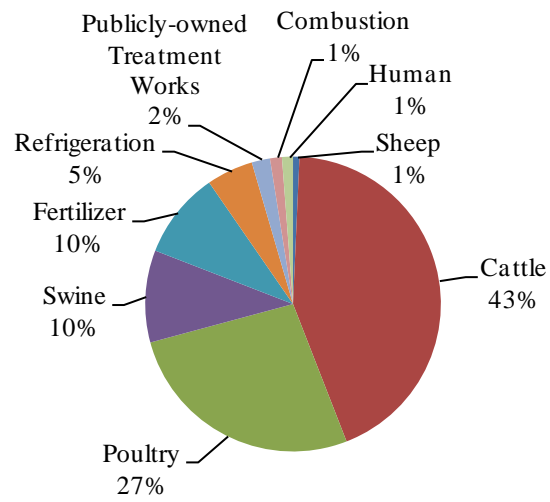


Figure 1.1. Percentage of ammonia-nitrogen emissions from different sources in the U.S. in 1994 (adapted from Battye et al., 1994).

plants; however, too much nitrogen runoff into coastal waterways and estuaries can lead to eutrophication, increasing harmful algal blooms (Kinzig and Socolow, 1994; Paerl, 1997). Additionally, NH_3 is the most abundant gaseous base in the atmosphere and acts to neutralize acids in the air, such as nitric acid (HNO_3) and sulfuric acid (H_2SO_4) (Li and Aneja, 1992; Lefer et al., 1999). This neutralization can result in the formation of salts, such as ammonium sulfate ($(\text{NH}_4)_2\text{SO}_4$), ammonium bisulfate (NH_4HSO_4), or ammonium nitrate (NH_4NO_3), which are major components of $\text{PM}_{2.5}$. The ammonium ion (NH_4^+) contained in the salts has a longer lifetime (up to 15 days) (Aneja et al., 2001) than NH_3 (up to 10 days) (Seinfeld and Pandis, 2006), thus capable of transporting and depositing the nitrogen to regions further from the source. NH_3 emissions can also cause odors, impacting the lifestyles of people in the area. For these reasons, an accurate understanding of the emissions, fate, and transport of agricultural livestock NH_3 (AL- NH_3) emissions is important in improving the air quality of the surrounding areas. Thus, sensitivity simulations will be completed in this research to evaluate the impacts of NH_3 emission reductions in conjunction with the federally-required reductions of sulfur dioxide (SO_2) and nitrogen oxides (NO_x).

Some research has indicated that NH_3 may play an important role in the formation of new particles through nucleation (Coffman and Hegg, 1995; Napari et al., 2002; Yu, 2006). Research has indicated that binary nucleation theory, in which new particles form from gas phase H_2SO_4 and water (H_2O), may underestimate the nucleation rate under some conditions (Weber et al., 1999). The ternary nucleation theory adds another species (e.g., NH_3) to the binary nucleation theory in an attempt to increase the predicted nucleation rates to more accurately represent observed rates (Coffman and Hegg, 1995; Napari et al., 2002; Yu, 2006). Smith et al. (2005) collected data on nucleation events in Atlanta, GA during the month of August, 2002. They found that the new particles, ranging from 8-13 nanometers (nm) in diameter, were composed of ammonium and sulfate. None of the other compounds that could be identified by the instrument, including nitrate and numerous organic compounds, could be found in the new particles (Smith et al., 2005). This confirms that NH_3 is a major component of new particle formation in some regions.

1.1.2 Impacts of PM_{2.5}

As just mentioned, NH₃ participates in the formation of PM_{2.5}, which is monitored by the U.S. Environmental Protection Agency (U.S. EPA) because of its negative impacts on human health, visibility, and climate. Exposure to PM_{2.5} can result in respiratory problems because fine particles are more likely to penetrate deeper into the lungs compared to larger particles that are trapped and removed by the upper respiratory system (Hinds, 1999). Visibility degradation occurs when particles that are nearly the same size as the wavelength of light, scatter and absorb the light. With visible light having wavelengths ranging from 0.4 to 0.7 μm, most visibility degradation occurs because of fine particles in the atmosphere (Malm, 1999). The scattering and absorption of light not only impacts visibility but directly affects the Earth's climate by modifying the solar radiation that reaches and warms the surface. PM_{2.5} can also have several indirect effects on climate. For example, PM_{2.5} can act as cloud condensation nuclei (CCN). More PM_{2.5} in the atmosphere with the same amount of available water for condensation can result in more, but smaller, cloud drops. This makes the cloud more reflective, thus further reducing radiation to the surface. The smaller drops are also less likely to collide to form raindrops, extending the lifetime of the cloud and reducing precipitation. The U.S. EPA has developed the National Ambient Air Quality Standards (NAAQS) for PM_{2.5} and some precursor gases (i.e., SO₂ and NO_x) to help protect people and the environment from these detrimental effects, however, there have been no federal rules implemented to control NH₃ emissions. Some states have implemented laws to control agricultural emissions. For example, the state of NC has banned the construction of new hog waste open-air lagoons since 1997 (<http://www.uswaternews.com/archives/arepolicy/7lawmothe4.html>) and in 2007 passed the Swine Farm Environmental Performance Standards Act continuing the ban on new hog waste lagoons, but also includes provisions to improve existing lagoons and initiate a methane capture program (http://www.edf.org/documents/6979_NC_Swine_Performance_Act.pdf).

1.2 Objectives

The objectives of this research are to:

- (1) evaluate the performances of MM5/CMAQ and MM5/CAMx using available observations and their seasonal variations (January and July 2002) at a 4-km horizontal grid spacing;
- (2) complete diagnostic analyses and sensitivity simulations to identify likely causes for discrepancies between observations and model predictions and between predictions from both models;
- (3) examine the sensitivity of CMAQ predictions to horizontal grid resolution (i.e., 12-, 4-, and 1.33-km);
- (4) assess the impacts of AL-NH₃ emissions on air quality and their potential regulatory controls (e.g., reducing agricultural NH₃ emissions by 50%) individually and in combination with reductions in the emissions SO₂ and NO_x.

2. LITERATURE REVIEW

The U.S. EPA requires the use of 3-D AQMs for demonstrating the attainment of the NAAQS, however, the model to be used is not specified (U.S. EPA, 2007). Thus, it is important to understand the differences between the models and the implications on the model's performance prior to selecting a model. Additionally, the performance of the model is affected by the choice of horizontal grid spacing. This thesis will analyze the performance of two commonly-used 3-D AQMs, CMAQ and CAMx, over the southeastern U.S at a horizontal grid spacing of 4-km. A comparison of the model treatments is detailed in Section 2.1, followed by a literature review of previous research conducted at various horizontal grid spacings in Section 2.2. The final section of this chapter (2.3) presents recent research on the sensitivity of AQMs to emission reductions, paying particular attention to the interactions of SO₂, NO_x and NH₃ because of the high NH₃ emissions in the southeast.

2.1 Comparison of Model Treatments

The two air quality models used in this research are CMAQ (Byun and Ching, 1999; Byun and Schere, 2006) version 4.51 with a revised secondary organic aerosol (SOA) module by ENVIRON (Morris et al., 2007) (referred to as CMAQ for simplicity hereafter) and CAMx version 4.42 (ENVIRON, 2006). Both models are 3-D Eulerian, one-atmosphere air quality models. They combine gas and particle emissions, chemistry, transport, and deposition in an effort to accurately represent processes occurring in the troposphere. The models are capable of using nested grids to simulate air quality over a range of spatial scales (hemispheric to urban). Both CMAQ and CAMx are modular in nature, allowing the user to select different chemical mechanisms or physics schemes; however, the available options differ for each model, as shown in Table 2.1. Some of the available modules are the same in both models, for example, the Carbon Bond IV (CB-IV) gas phase mechanism, the ISORROPIA inorganic aerosol thermodynamic module, and the modified version of the cloud chemistry in the Regional Acid Deposition Model (RADM), however there are several differences between the models.

Table 2.1. A list of the chemical mechanisms and physical schemes available in the CMAQ and CAMx versions used in this research.

	CMAQ v4.51	CAMx v4.42
Horizontal Advection	PPM, Yamartino-Blackman Cubic	Bott, PPM
Horizontal Diffusion	Explicit	Explicit
Vertical Advection	PPM, Yamartino-Blackman Cubic	Implicit
Vertical Diffusion	Semi-implicit K-theory, ACM	Implicit
Gas phase Chemistry	CB-IV, SAPRC99, CB05 (beta)	CB-IV, SAPRC99
Aqueous Phase Chemistry	RADM	RADM
PM Size Representation	Modal (i.e., nuclei, accumulation, coarse)	Sectional (i.e., 2 or more bins)
Inorganic Aerosol Thermodynamics	ISORROPIA v1.5	ISORROPIA v1.6
Secondary Organic Aerosol	SORGAM	SOAP
Dry Deposition	The Wesely (1989) resistance theory, M3DRY	The Wesely (1989) resistance theory
Wet Deposition	Accumulation and coarse mode particles completely absorbed in cloud water; Nuclei mode slowly scavenged; Henry's law equilibrium for gases	All PM assumed in cloud water; Henry's law equilibrium for gases

CB-IV: Carbon Bond IV

SAPRC99: State Air Pollution Research Center module, 1999 version

CB05: Carbon Bond, 2005 version

RADM: Regional Acid Deposition Model

ACM: Asymmetric Convective Mixing

ISORROPIA: Thermodynamic equilibrium model

SORGAM: Secondary Organic Aerosol Model

SOAP: Secondary Organic Aerosol Partitioning

PPM: Piecewise Parabolic Method

One of the major differences between CMAQ and CAMx is the treatment of vertical mixing. The Yamartino-Blackman Cubic advection option in CMAQ utilizes the Piecewise Parabolic Method (PPM) for horizontal advection, and then uses the density from the driving meteorology model to calculate the vertical velocity at each grid cell that satisfies the continuity equation (http://www.cmascenter.org/help/model_docs/cmaq/4.5.1/ADVECTION_DIFFUSION.txt). CAMx calculates vertical diffusion and advection implicitly (ENVIRON, 2006). Studies have found that the different treatments of vertical mixing between CMAQ and CAMx result in a weaker vertical mixing by CAMx than CMAQ (Liang et al., 2004; Zhang et al., 2004). Weaker vertical mixing can result in higher concentrations of directly emitted (primary) and non-reactive species (i.e., carbon monoxide (CO), black carbon (BC)). If primary species are not mixed vertically, the secondary species that form from them may also have higher concentrations in the lower troposphere compared to a simulation with stronger vertical mixing.

A second difference between the two models is how they represent PM size distributions. CMAQ represents PM size using a modal approach (i.e., three log-normally-distributed modes: nuclei, accumulation, and coarse) (Binkowski, 1999), whereas CAMx uses a sectional approach (e.g., 2 or more bins as specified by the user) (ENVIRON, 2006). To actually capture the size distribution using bins, a larger number of bins must be used (Binkowski, 1999). The smallest number of bins that can be used in CAMx is two, which represents the fine and coarse mode particles (i.e., the CF scheme). Using this scheme, there is no separation of the fine mode into nuclei and accumulation sections as for the case in CMAQ. Additional bins can be simulated in CAMx using the Carnegie Mellon University (CMU) scheme, with the size ranges defined by the user. Increasing the number of bins increases the number of variables to be simulated, which in turn increases the time required to complete the simulation (i.e., higher CPU cost). The CMU scheme simulates the emission and evolution of particle sizes among all bins, while the CF scheme and CMAQ separate primary emissions into the coarse and fine modes/sections and all secondary aerosols are simulated in the fine mode (Binkowski, 1999; ENVIRON, 2006).

The treatment of SOA is yet another difference between the two air quality models used in this study. Both models use the CB-IV gas phase mechanism and simulate SOA formation from the volatile organic compounds (VOCs) included in CB-IV (i.e., paraffins, olefins, ethene, toluene and other monoalkyl aromatics, xylene and other polyalkyl aromatics, formaldehyde, higher aldehyde, isoprene, methanol, ethanol). CAMx also simulates SOA formation from condensable gases that form from the VOCs (i.e., paraffins, toluene, xylene, cresol, and terpenes) (ENVIRON, 2006). The SOA module used in CMAQ for this study was enhanced by ENVIRON to include sesquiterpenes, additional SOA formation from isoprene, and polymerization of SOA species. These enhancements are detailed in Morris et al. (2006, 2007). In comparing the SOA enhancements to the default SOA module in CMAQ, Morris et al. (2006) found improved performance for organic carbon (OC) and total carbon (TC) mass when using the enhancements. This improvement was more noticeable at rural locations and in the summer because the enhancements affect biogenic SOA, which is limited in urban locations and winter months. Morris et al. (2006) also found that the SOA enhancements improved model performance in most regions of the U.S., with the exception of the western U.S. The observed degradation in performance in the arid west is attributed to an overestimation of the derived biogenic emission rates. However, for the research presented here, studying the southeastern U.S., the enhanced SOA module is applicable and utilized.

The treatment of dry deposition also differs between the models used in this research. In CAMx, dry deposition of gases is based on Wesely's (1989) resistance model (ENVIRON, 2006). This approach calculates the deposition velocity of gases using the aerodynamic, boundary layer, and surface resistances. The aerodynamic resistance is common to all gases, while the boundary layer resistance is dependent on the gas diffusivity. The surface resistance is a function of the stomatal and mesophyll resistance of plants in the upper canopy, resistance in the lower canopy, and resistance based on ground surface characteristics. CMAQ, on the other hand, has two options for dry deposition of gases available in the Meteorology-Chemistry Interface Processor (MCIP) (Byun et al., 1999). One is based on the Regional Acid Deposition Model and also uses the resistance theory of Wesely (1989). The

second option (which is the one used in this research) is the Models-3 dry (M3DRY) deposition model, which is coupled with the land-surface model (LSM) in MM5. By coupling the dry deposition model with the LSM in MM5, the stomatal resistance may be improved over a non-coupled model because of the inclusion and nudging of soil moisture (Byun and Ching, 1999). In both models, the dry deposition of particles is based on the resistance approach of Slinn and Slinn (1980), which calculates the deposition velocity using the aerodynamic and canopy resistances and the gravitational settling velocity (Binkowski and Shankar, 1995; ENVIRON, 2006).

Another major difference between the two models, which is affected by the model's representation of PM size distribution, is the removal of pollutants through wet deposition. Wet deposition is one of the major processes resulting in the transport and deposition of pollutants to the surface. In CMAQ, all accumulation and coarse mode particles within a modeled cloud are considered completely absorbed by the cloud and rain water, while particles in the nuclei mode are slowly scavenged by the cloud water. At a grid spacing of 8-km or more, CMAQ treats sub-grid sized clouds in addition to completely resolved clouds that encompass the entire grid cell. At a horizontal grid spacing of less than 8-km, the sub-grid cloud scheme is not used and only resolved clouds are treated by the model (Byun and Schere, 2006). In CAMx, aqueous chemistry is only treated in resolved clouds and all PM mass within a cloudy grid cell, regardless of particle size, is assumed to be in the cloud water (ENVIRON, 2006). These two factors may produce conflicting results. One may expect CAMx to simulate more total PM mass in cloud water than CMAQ because all particles within the cloud are contained within the cloud water. However, depending on the grid spacing, CAMx may treat aqueous-phase reactions in fewer clouds than CMAQ and thus actually simulate less total PM mass in the cloud water. The horizontal grid spacing used in the simulation will thus influence the clouds that CAMx is able to resolve, and the resultant wet deposition of PM. For gases within a cloud, both models use Henry's Law to determine the equilibrium concentrations between the cloud drops and surrounding air. Below the simulated clouds, scavenging coefficients are calculated separately for gases and particles (Roselle and Binkowski, 1999; ENVIRON, 2006).

2.2 Sensitivity to Horizontal Grid Spacing

The U.S. EPA requires state agencies to use 3-D AQMs to demonstrate that the emission reductions proposed in the State Implementation Plans (SIPs) will bring the region into attainment of the NAAQS and improve visibility in Federal Class I areas (i.e., national parks and wilderness areas) (U.S. EPA, 2007). Previous U.S. EPA reports have recommended using grid spacing of 2-5 km for urban scale ozone (O₃) modeling (U.S. EPA, 1991) and similar scales for modeling PM. Air quality modeling at finer grid scales is feasible because of advanced computational technology and improved understanding and representation of terrain, meteorology, emissions, and other atmospheric processes. However, the current ability to complete fine scale modeling does not mean that the fine scale modeling is always accurate. Some research has shown that coarser grid spacing provides similar, if not better, results than finer grid spacing due to various reasons (Mathur et al., 2005; Arunachalam et al., 2006; Cohan et al., 2006; Zhang et al., 2006a, b; Queen and Zhang, 2008), so it is up to the modeler to determine if the finer grid spacing is necessary for their selected episode and domain (U.S. EPA, 2007). Table 2.2 summarizes some of the recent research on model sensitivity to horizontal grid spacing in the eastern U.S.

The sensitivity of the AQM to the horizontal grid spacing depends on the accuracy and detail of the required input fields (i.e., meteorology, emissions, terrain, etc.). Mass et al. (2002) summarized research evaluating the sensitivity of meteorological models to horizontal grid spacing. From their review, they found that finer grid spacing does show improvement from coarse grid spacing for some events (i.e., strong forced convection, diurnal circulations, and heavy precipitation events); however it may not be a substantial improvement. Although the finer grid spacing does allow for more detailed terrain and model processes, it can also cause small errors to grow into substantial forecast errors (Mass et al., 2002). In the case of air quality modeling, the performance and sensitivity of the meteorology model can have a large impact on the performance of the AQM. For example, precipitation acts as a pollutant removal process through wet deposition. Queen and Zhang (2008) found that precipitation, particularly convective precipitation in the summer, is sensitive to the horizontal grid

Table 2.2. Recent studies on model sensitivity to horizontal grid spacing.

Models	Grid Spacing	Episode	Region	Variables		Reference
				Met.	Chem.	
MM5/ MAQSIP	36/12/4	Jun. 1996	Eastern U.S./ SE U.S./ Central NC	-----	O ₃	Mathur et al., 2005
MM5/ MAQSIP	36/12/4	Summer 1995, 1996, 1997	Eastern U.S./ SE US/ Central NC	-----	O ₃	Arunachalam et al., 2006
MM5/ CMAQ	36/12/4	Aug. 2000	Eastern U.S./ SE U.S./ Northern GA	-----	O ₃	Cohan et al., 2006
MM5/ CMAQ	32/8	Jun.-Jul. 1999	CONUS/ SE U.S.	Temp, RH, WSP, WDR	O ₃ , NO, NO ₂ , HNO ₃ , PM _{2.5} , BC, OC, NO ₃ ⁻ , NH ₄ ⁺ , SO ₄ ²⁻	Zhang et al., 2006a,b
MM5/ CMAQ	36/12/4	Aug./Dec. 2002	CONUS/ Eastern U.S./ NC	Temp, RH, WSP, WDR, Precip	O ₃ , PM _{2.5} , BC, OC, NO ₃ ⁻ , NH ₄ ⁺ , SO ₄ ²⁻ , Wet Deposition of NO ₃ ⁻ , NH ₄ ⁺ , and SO ₄ ²⁻	Wu et al., 2008a
MM5/ CMAQ	36/12/4	Aug./Dec. 2002	CONUS/ Eastern U.S./ NC	Precip	Wet Deposition of NO ₃ ⁻ , NH ₄ ⁺ , and SO ₄ ²⁻	Queen and Zhang, 2008

Met.: Meteorological

Chem.: Chemical

MAQSIP: Multiscale Air Quality Simulation Platform

CONUS: Continental U.S.

Temp: Temperature

RH: Relative Humidity

WSP: Wind Speed

WDR: Wind Direction

O₃: Ozone

NO: Nitric Oxide

NO₂: Nitrogen Dioxide

HNO₃: Nitric Acid

PM_{2.5}: Particulate matter with an aerodynamic diameter less than or equal to 2.5µm

BC: Black Carbon

OC: Organic Carbon

NO₃⁻: Nitrate Ion

NH₄⁺: Ammonium Ion

SO₄²⁻: Sulfate Ion

spacing. The finer grid spacing of 4-km more accurately predicted precipitation in the summer month (August 2002) than the 12- or 36-km simulation because the finer scale could capture the mesoscale convection better than the coarser scale. The resultant wet deposition of chemical species also improved at the finer spacing in the summer (Queen and Zhang, 2008). In the winter month (December 2002), however, the 12-km simulation performed the best for precipitation, but the worst for wet deposition of PM_{2.5} species, indicating that wet deposition is more sensitive to other factors (i.e., emissions) in the winter than in the summer, and validating the importance of episode selection on determining the best grid spacing to use. Zhang et al. (2006a, b) evaluated additional meteorological and chemical variables over the southeastern U.S. in June and July 1999 using MM5 and CMAQ at 32- and 8-km horizontal grid spacing. They found that, despite similar meteorological performance (Zhang et al., 2006a), the simulations at a coarser spacing performed better than those at a finer spacing for PM_{2.5} and maximum O₃. Wu et al. (2008a) also reported that the meteorological variables were less sensitive to the horizontal grid spacing than the chemical variables, and that some variables (i.e., NH₄⁺ and nitrate (NO₃⁻)) show more sensitivity to grid spacing in the winter than in the summer. It is therefore important to evaluate the sensitivity of meteorological variables to horizontal grid spacing, in addition to the chemical variables, to determine how much of the sensitivity of the chemical variables is due to meteorology or to other factors.

Emissions are another variable that may influence the sensitivity of an air quality model to horizontal grid spacing. With coarser grid spacing, the emissions are quickly diffused into a larger grid cell rather than being concentrated within a smaller grid cell. This can result in overpredictions in some regions, but underpredictions in others. For example, Mathur et al. (2005) reported a wider O₃ plume in central NC using 36- and 12-km horizontal grid spacing than with a 4-km horizontal grid spacing, which resulted in an overprediction of O₃ mixing ratios at most observational sites in the area. Cohan et al. (2006) also reported premature diffusion of emissions in the coarser grid spacing and found that VOC-sensitive regions show more dependence on grid scale than NO_x-sensitive regions. Although there tends to be little difference between 12- and 4-km results (Cohan et al., 2006; Arunachalam

et al., 2006), the finer spacing is important for studying localized variability in pollutant concentrations (Mathur et al., 2005; Cohan et al., 2006), which is impacted by the diffusion of emissions into the grid cell.

2.3 Sensitivity to Emissions

Once a representative grid spacing is selected for the episode and region of interest, simulations can be completed to evaluate the sensitivity of the model to estimated changes in emissions of pollutants and precursor species. This is important in the development of SIPs, demonstrating whether the proposed emission reductions will bring the region into attainment of the NAAQS. While meteorological conditions are also expected to change in the future, some research has shown that the emission control strategies have a larger impact on future pollutant concentrations than the meteorological changes (Tagaris et al., 2007; Liao et al., 2007; Nolte et al., 2008). Reducing SO₂ and NO_x has continuously been the focus of emission control strategies in an effort to mitigate the acid deposition problem and reduce PM_{2.5} and O₃ pollution. The formation mechanisms of both PM_{2.5} and O₃ vary across the country because of different emission sources and atmospheric conditions, so the emission control strategies must be tailored to the specific region. Additionally, pollutant formation is often non-linear, meaning reducing the precursor species does not result in an equal reduction in the secondary pollutant. In fact, reducing a precursor species may cause no change, or even increase, the secondary pollutant. For example, O₃ formation, which involves NO_x and VOCs, is NO_x-limited in the southeastern U.S. because of the large biogenic VOC emissions and less NO_x emissions (Chameides and Cowling, 1995; Cowling and Furiness, 2001; Liao et al., 2007; Zhang et al., 2009b). Thus, controlling NO_x in the southeast can reduce O₃. However, in other regions, O₃ formation is limited by VOCs and a decrease in NO_x can actually increase O₃. It is therefore important to understand the pollutant formation mechanisms and limiting factors in a particular region before implementing pollutant control strategies.

When evaluating PM_{2.5} and its sensitivity to emission reductions, it is important to consider the components (i.e., sulfate (SO₄²⁻), NO₃⁻, NH₄⁺, BC, and OC), not just the total

PM_{2.5} mass. This detailed analysis is beneficial in determining and understanding the sensitivity of the individual species to emission reductions. Baker (2004) reported a decrease in PM NO₃⁻ when NO_x and NH₃ were reduced by 30% and a decrease in PM SO₄²⁻ when SO₂ was decreased by 30%, as would be expected. However, changes in PM_{2.5} are more sensitivity to NO_x emission reductions in the winter and SO₂ reductions in the summer (Baker, 2004; Liao et al., 2007). Transport of the pollutants is also an important process to consider and Baker (2004) reported that decreases in NO_x and NH₃ had more of a localized impact, whereas decreases in SO₂ impacted PM_{2.5} predictions over a larger region. This understanding of seasonal and regional variations of sensitivity to reduced pollutants is important in developing emission control strategies.

Regions of significant NH₃, SO₂, and NO_x emissions have a complex sensitivity to emission reductions (Ansari and Pandis, 1998; Tsimpidi et al., 2007; Pinder et al., 2007, 2008). All SO₂ will be oxidized to the aerosol phase (SO₄²⁻) because of its low vapor pressure. NH₃, if available, is converted to the aerosol phase (NH₄⁺) and acts to neutralize SO₄²⁻. If HNO₃ is included in the system, then the available concentrations of NH₃, SO₄²⁻, and NO₃⁻, as well as atmospheric conditions, play an important role in PM formation. Regions with sufficient NH₃ to completely neutralize SO₄²⁻ to (NH₄)₂SO₄ are considered NH₃-rich. Some of these regions may even have sufficient NH₃ to neutralize any HNO₃ in the system. NH₃-poor regions do not contain sufficient NH₃ to completely neutralize SO₄²⁻ and thus also lack excess NH₃ for neutralizing HNO₃. To identify NH₃-rich and NH₃-poor regions, Ansari and Pandis (1998) proposed a gas ratio (GR):

$$GR = \frac{TA - 2 \times (TS)}{TN} \quad (2.1)$$

where TA is the total ammonia (NH₃ + NH₄⁺) concentration, TS is the sulfate concentration, and TN is the total nitrate (NO₃⁻ + HNO₃) concentration. When GR is greater than 0, the region is considered NH₃-rich, while a region with GR less than 0 is considered NH₃-poor. The GR, however, assumes that SO₄²⁻ is fully neutralized by NH₄⁺ to form (NH₄)₂SO₄ which may not always be the case (i.e., winter temperatures) (Pinder et al., 2008; Wu et al., 2008b). Therefore, Pinder et al. (2008) proposed an alternative, or adjusted, GR (AdjGR) defined as

$$AdjGR = \frac{TA - DSN \times (TS)}{TN} = \frac{NH_3 + NO_3^-}{TN} \quad (2.2)$$

They developed this ratio by replacing the 2 in the GR with the degree of sulfate neutralization (DSN), defined as

$$DSN = \frac{NH_4^+ - NO_3^-}{SO_4^{2-}} \quad (2.3)$$

When there is sufficient NH_4^+ to fully neutralize SO_4^{2-} , $DSN = 2$, Equation 2.2 is thus the same as Equation 2.1. The values of GR and AdjGR associated with NH_3 -rich and NH_3 -poor regions are summarized in Table 2.3. In NH_3 -rich regions, where there is excess NH_3 after neutralizing SO_4^{2-} and NO_3^- (GR and $AdjGR > 1$), reducing NH_3 emissions will result in little to no change in PM (Pinder et al., 2008). Reducing SO_2 and/or NO_x emissions in NH_3 -rich regions can lead to reduced PM, but frees up more reduced nitrogen ($NH_x = NH_3 + NH_4^+$). This additional NH_x can then be deposited to the surface (Pinder et al., 2008), impacting vegetation and waterways. In NH_3 -poor regions, only reducing SO_2 will reduce PM SO_4^{2-} , but has the potential to increase PM NO_3^- by releasing up to two NH_4^+ for reaction with available HNO_3 (Ansari and Pandis, 1998; Takahama et al, 2004). Reducing NH_3 in NH_3 -poor or transition regions can decrease NO_3^- and thus decrease PM (Pinder et al., 2008) while also decreasing the amount of NH_x deposited to the surface. These complex interactions of NH_4^+ , SO_4^{2-} , and NO_3^- again verify the importance of regional selection when developing emission control strategies.

Table 2.4 summarizes some recent research on the sensitivity of AQMs to emission reductions, particularly SO_2 , NO_x , and NH_3 . Research indicates that the most effective control strategy for $PM_{2.5}$ in the eastern U.S. is reducing NH_3 in January and SO_2 in July (Tsimpidi et al., 2007; Pinder et al., 2007, 2008). Reducing SO_2 in January releases NH_4^+ for reaction with available NO_3^- , thus increasing NO_3^- , cancelling out the reduction of SO_4^{2-} , resulting in little change in $PM_{2.5}$ in January (Tsimpidi et al., 2007; Pinder et al., 2007). Reducing SO_2 in July also frees up NH_4^+ , however there is less NO_3^- available in the summer in the southeast, so there is a larger reduction in $PM_{2.5}$ (Tsimpidi et al., 2007; Pinder et al., 2007). Reducing NH_3 has little impact on SO_4^{2-} , but acts to reduce NH_4^+ and NO_3^- . Because

Table 2.3. Characterization of NH₃-rich and NH₃-poor regions based on GR and AdjGR (Ansari and Pandis (1998); Pinder et al. (2008); modified from Takahama et al. (2004) and Dennis et al. (2008)).

GR	AdjGR	Description
< 0	<< 1	NH ₃ -poor: Insufficient NH ₃ to neutralize sulfate to (NH ₄) ₂ SO ₄
0 ≤ GR < 1	~1	Transition: Sufficient NH ₃ to neutralize sulfate, but not nitrate
≥ 1	>> 1	NH ₃ -rich: Sufficient NH ₃ to neutralize sulfate and nitrate

Table 2.4. Recent research on the sensitivity of AQMs to emission reductions.

Model(s)	Episode	Region	Emission Adjustments	Emission Inventory	Reference
Box Model	January 4-6, 1996	San Joaquin Valley, CA	NO _x by -50%, VOC by -50%	Based on 1995 Integrated Monitoring Study (IMS95)	Pun and Seigneur, 2001
CMAQ	July 1-10, 1999	Southeastern U.S.	NH ₃ and Primary OM by a factor of 1.5	NET 96	Zhang et al., 2006c
PMCAMx	July 2001, January 2002	Eastern U.S.	SO ₂ by -25%, -50%, NH ₃ by -25%, -50%	LADCO BaseE, derived from NEI 1999 v2.0	Tsimpidi et al., 2007
PMCAMx	July 12-25, 2001, January 9-22, 2002	Central and Eastern U.S.	125 scenarios combining 0%, 10%, 20%, 30%, and 50% of baseline emissions of SO ₂ , NO _x , and NH ₃	LADCO BaseE, derived from NEI 1999 v2.0	Pinder et al., 2007
CMAQ	August and December 2002	NC	0% of baseline NH ₃ , changes in total NH ₃ and diurnal variations of NH ₃ emissions	Developed by VISTAS, based on NEI 1999 v2.0	Wu et al., 2008b
CMAQ, CMAQ-MADRID, REMSAD	June 29 – July 10, 1999	CONUS and Southwest U.S.	50% reduction in SO ₂ , NO _x , and VOCs	NET 96	Pun et al., 2008
CMAQ	January, April, July, October, 2001	CONUS	NH ₃ by -10%	NEI 1999 v3.0 with adjusted NH ₃ emissions from Gilliland et al., 2006	Pinder et al., 2008
CMAQ-MADRID	December 25, 2000 – January 7, 2001	Central CA (San Joaquin Valley)	Reduced primary PM, NO _x , NH ₃ , VOC by 50%	California Air Resources Board	Pun et al., 2009

OM: Organic Matter

NET: National Emissions Trends

PMCAMx: the first version of CAMx to simulate PM

LADCO: Lake Michigan Air Directors Consortium

NEI: National Emission Inventory

MADRID: Model of Aerosol Dynamics, Reaction, Ionization, and Dissolution

REMSAD: Regional Modeling System for Aerosols and Deposition

CONUS: Continental U.S.

NO_3^- is a larger component of $\text{PM}_{2.5}$ in January compared to July in the southeastern U.S., reduction of NH_3 in January is more effective at reducing NO_3^- in January (Tsimpidi et al., 2007; Pinder et al., 2007). Wu et al. (2008b) conducted a simulation using CMAQ in which all AL- NH_3 emissions in NC in August 2002 were removed. Reducing the AL- NH_3 emissions resulted in significant reductions in NH_4^+ and NO_3^- , particularly in the regions with the highest baseline NH_3 emissions. As with the 50% reductions in NH_3 , completely eliminating NH_3 has little impact on SO_4^{2-} concentrations (Wu et al., 2008b). Zhang et al. (2006c) conducted a sensitivity simulation with increased NH_3 by a factor of 1.5 in July 1999 which resulted in an increase in NO_3^- concentrations. This brought the model simulation closer to observed NO_3^- values, indicating that the NH_3 emission inventory used may have underestimated NH_3 emissions (Zhang et al., 2006c). In California, NO_3^- concentrations have been found to be most sensitive to NO_x emission reductions, with some regions slightly sensitive to VOC emission reductions due to the decrease in oxidizing agents (i.e., OH and O_3) (Stockwell et al., 2000; Pun and Seigneur, 2001; Kleeman et al., 2005; Pun et al., 2009). However, reducing VOCs in the eastern U.S. displays complex sensitivities by reducing OM, but increasing SO_4^{2-} and NO_3^- (Pun et al., 2008). Thus, reducing VOCs in the eastern U.S. is less effective in reducing $\text{PM}_{2.5}$ than reducing SO_2 and NH_3 .

3. DESCRIPTION OF MODEL CONFIGURATIONS, EPISODE, DATABASE, AND METHODOLOGY

Two modeling systems, MM5/CMAQ and MM5/CAMx, are used in this research to simulate air quality over the southeastern U.S. in January and July 2002. The two inner domains of Figure 3.1, labeled D03 and D04 at horizontal grid spacing of 4-km over the southeastern U.S. and 1.33-km over the central and eastern NC, respectively, are the domains simulated in this research. D01 (not shown) and D02 at a horizontal grid spacing of 36-km over the continental U.S. and 12-km over the eastern U.S., respectively, were simulated by the Visibility Improvement State and Tribal Association of the Southeast (VISTAS). In order to evaluate the model sensitivity to horizontal grid spacing, the model configurations and physics used in this research for MM5 and CMAQ are consistent with the Phase II of the modeling study completed by VISTAS at 36- and 12-km horizontal grid spacing (see <http://www.vistas-sesarm.org/documents/FinalDocs.asp>). When available, similar physical schemes and chemical mechanisms are used in both CMAQ and CAMx to reduce the potential sources of discrepancies and allow for a fair model inter-comparison. In addition to the inter-comparison, both models are evaluated against available observations using statistics, spatial distributions, temporal analysis, and column mass. More details are provided in the following sections.

3.1 Modeling System

3.1.1 MM5

MM5 (Grell et al., 1995) version 3.7 with Four Dimensional Data Assimilation (FDDA) was used to derive the meteorological fields provided to the Sparse Matrix Operator Kernel Emissions (SMOKE) modeling system, CMAQ and CAMx. The configurations used in both the 4- and 1.33-km MM5 simulations are listed in Table 3.1 and are consistent with the MM5 simulations completed by Olerud and Sims (2004) for VISTAS. Cumulus parameterization and shallow convection scheme were turned off because all clouds are assumed to be resolved at the finer grid scales (Roselle and Binkowski, 1999). FDDA with

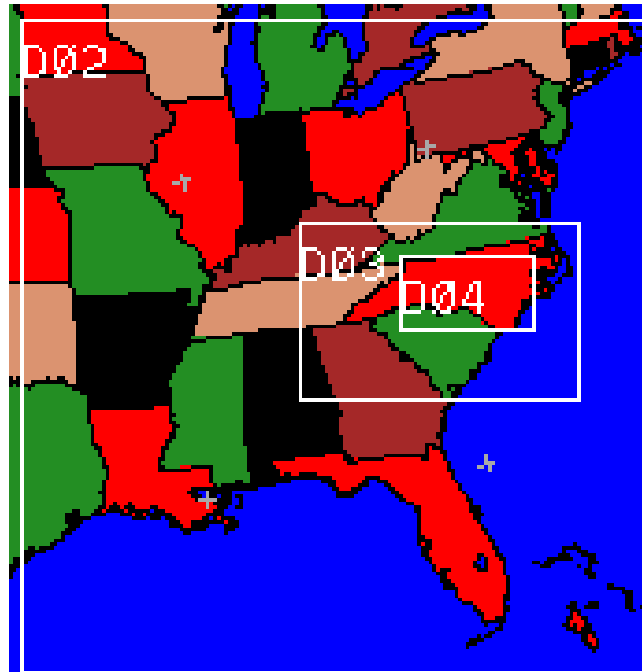


Figure 3.1. The three modeling domains used in this research: 12-km horizontal grid spacing over the eastern U.S. (D02, completed by VISTAS), 4-km horizontal grid spacing over the southeastern U.S. (D03), and 1.33-km horizontal grid spacing over the central and eastern NC (D04) (modified from Morris et al., 2007).

Table 3.1. MM5 model configurations used in this research.

	MM5 v3.7
Horizontal Spacing	4- and 1.33-km
Vertical Spacing	34 layers from 0 to approximately 15 km, with first model layer height of 36 m
Land Surface Model	Pleim-Xu
Planetary Boundary Layer Model	Pleim-Xu (ACM)
Cloud Microphysics	Reisner 1 (Mixed Phase)
Cumulus Scheme	None
Shallow Convection	None
Longwave Radiation	Rapid Radiative Transfer Model (RRTM)
Shortwave Radiation	Cloud-Radiation
Analysis Nudging	
Temperature	Aloft (nudging coefficient: 1×10^{-4})
Moisture	Aloft (nudging coefficient: 1×10^{-5})
Wind (u and v)	Surface and Aloft (nudging coefficient: 1×10^{-4})
Observational Nudging	None

analysis nudging is conducted aloft for temperature, moisture, and winds and at the surface for winds using reanalysis data from NCAR (ds464.0 and ds353.4, <http://dss.ucar.edu/datasets/ds464.0/>, <http://dss.ucar.edu/datasets/ds353.4/>) (Olerud and Sims, 2004). The initial and boundary conditions (ICONS and BCONs) are derived from the VISTAS 12-km MM5 simulation that was completed in 6 day segments with 12 hours of overlap of each segment for spin up (Olerud and Sims, 2003). The meteorological fields are prepared for CMAQ using MCIP (Byun et al., 1999) version 3.1 and for CAMx using the MM5CAMx preprocessor available from ENVIRON (<http://www.camx.com/download/support.php>).

3.1.2 SMOKE

The emission inventory used in this research was developed by VISTAS (MACTEC, 2008) and prepared for CMAQ using SMOKE (<http://www.smoke-model.org/index.cfm>) version 2.1. The inventory was based on the 1999 National Emission Inventory (NEI) version 2 with supplemental data for the VISTAS states gathered and developed by E. H. Pechan and Associates, Inc., MACTEC Engineering and Consulting, Inc., and Alpine Geophysics, Inc. (MACTEC, 2008). SMOKE converts area, mobile, fire, point, and biogenic source emissions from the emission inventory into hourly, gridded, speciated files, formatted for use in CMAQ. Biogenic emissions are modeled within SMOKE using the Biogenic Emission Inventory System, version 3 (BEIS3) and mobile sources are modeled using MOBILE6. SMOKE output files must be converted into a separate format for use in CAMx using the preprocessor tool CMAQ2CAMx available from ENVIRON (<http://www.camx.com/download/support.php>). The list of emitted species remains the same; however CAMx uses separate files for surface and elevated emissions. The elevated emissions are determined within CAMx using stack parameters (e.g., height, diameter, exit velocity, and temperature) and ambient meteorology conditions (ENVIRON, 2006). So while SMOKE generates a 3-D file for use by CMAQ containing surface and elevated emissions, CAMx uses two 2-D files; one containing surface emissions and one containing

emission rates and stack parameters. As mentioned in Chapter 2, the primary PM emissions in CMAQ and CAMx using the CF scheme are modeled as both coarse and fine particles.

3.1.3 CMAQ and CAMx

The configurations selected for this research from Table 2.1 are displayed in Table 3.2. CMAQ is configured identical to VISTAS Phase II modeling (see <http://www.vistas-sesarm.org/documents/FinalDocs.asp>). Similar options were selected for CAMx when available, for example, CB-IV and ISORROPIA. The RADM aqueous chemistry is used in CMAQ along with a sub-grid treatment for convective clouds (<http://www.epa.gov/asmdnerl/CMAQ/release45.html>) based on ACM. As discussed in Section 2.1, the sub-grid treatment is not used when the horizontal grid spacing is 4-km or less so the aqueous chemistry used in both models is similar at the fine grid spacing used in this research. VISTAS completed the simulations at 36- and 12-km horizontal grid spacing as nested simulations and used a 15-day spin up (Morris et al., 2007). The ICONs and BCONs for the 36-km simulation were based on the 2002 simulation of GEOS-CHEM, a global circulation/chemistry model, and the 36-km simulation provided BCONs for the 12-km simulation through one-way nesting. The ICONs and BCONs for the simulation completed with a horizontal grid spacing of 4-km were then derived from the VISTAS 12-km simulation without spin up. The ICONs and BCONs for the simulation using 1.33-km horizontal grid spacing were derived from the completed simulation at 4-km. More details regarding the differences between the models have been provided in Section 2.1.

3.2 Description of the Episode Selected for Model Simulations

As mentioned previously, the simulations for this thesis are completed for January and July, 2002 using MM5/CMAQ and MM5/CAMx. In Morris et al. (2007), an explanation is provided for the selection of 2002 by VISTAS for their base year simulations. 2002 was selected in order to meet EPA guidelines under the Regional Haze Rule, which include modeling a representative year that captures the best 20% and worst 20% visibility days at Class I monitoring sites between the years 2000-2004 (U.S. EPA, 2007). At the time that

Table 3.2. CMAQ and CAMx model configurations used in this research.

	CMAQ v4.51	CAMx v4.42
Horizontal Advection	Yamartino-Blackman Cubic	PPM
Horizontal Diffusion	Explicit	Explicit
Vertical Advection	Yamartino-Blackman Cubic	Implicit
Vertical Diffusion	Semi-implicit K-theory	Implicit
Gas-Phase Chemistry	CB-IV	CB-IV
Aqueous-Phase Chemistry	RADM	RADM
PM Size Representation	Modal (i.e., nuclei, accumulation, coarse)	Sectional (2 bins)
Inorganic Aerosol Thermodynamics	ISORROPIA v1.5	ISORROPIA v1.6
Secondary Organic Aerosol	SORGAM	SOAP
Dry Deposition	M3DRY	The Wesely (1989) resistance theory
Wet Deposition	Accumulation and coarse mode particles completely absorbed in cloud water; Nuclei mode slowly scavenged; Henry's law equilibrium for gases	All PM assumed in cloud water; Henry's law equilibrium for gases

VISTAS was initiating their research and simulations, observational data in the Class I areas from the Interagency Monitoring of Protected Visual Environments (IMPROVE) were more complete for 2002 than the data from 2000 and 2001, and 2003-2004 IMPROVE data were not yet available. In terms of meteorology, 2002 appeared to be more representative of a typical year, while 2003, for example, was colder and wetter than 2002. While VISTAS completed simulations for the complete year of 2002 at a coarse horizontal grid spacing, January and July were selected to represent a winter and summer month, respectively, for the fine scale simulations completed in this thesis.

Selecting a winter and summer month allows for the assessment of the impact of seasonal variability of meteorology and emissions on air quality modeling. January temperatures in 2002, both nationally and in the southeastern region, were warmer than historical averages (see <http://lwf.ncdc.noaa.gov/oa/climate/research/2002/jan/national.html>). Nationally, January 2002 was the 7th warmest January during the period of 1895-2002 with a + 2.5°C (+ 4.5°F) departure from the average. In the Southeast, temperature departures were less than + 4°C (+ 7.2°F) from the 1961-1990 average temperatures. Precipitation in January 2002 was near historic averages, both nationally and in the southeastern states. However, there was an extreme snow storm that swept through Georgia and the Carolinas in the beginning of the month (January 2nd and 3rd) that resulted in up to 14 inches of snow in central NC.

Nationally, July 2002 was also warmer than the national average, ranking the 5th warmest from 1895 to 2002 with a departure of + 1.2°C (+ 2.2°F) from the average (see <http://www.ncdc.noaa.gov/oa/climate/research/2002/jul/national.html>). The mean temperature in the majority of the southeast was near normal, with some regions in the Carolinas reporting temperature departures up to + 1.7°C (+ 3°F) from the 1971 to 2000 averages. While precipitation nationally was near average, ranking the 53rd driest July out of the last 108 years, the precipitation in the southeast was below normal (e.g., South Carolina recorded the 12th driest July in the last 108 years).

Emissions of pollutants in the southeastern U.S. are typically higher in July than in January which have resulted in regions of O₃ and PM_{2.5} non-attainment in the summer

months. Additionally, in the first week of July 2002, there were several wildfires burning in Quebec, Canada (see <http://www.ncdc.noaa.gov/oa/climate/extremes/2002/july/extremes0702.html>) and smoke from the fires was advected southward into the U.S. and out over the Atlantic Ocean. While the smoke mainly impacted the northeastern states (i.e., New York, New Jersey, and Pennsylvania), some of the smoke also impacted PM concentrations over the eastern NC.

3.3 Observational Data

In order to evaluate the meteorology and air quality model performance, the simulations are compared to available observations. Numerous observational networks have been established in order to monitor pollutant concentrations, which can then be used to verify attainment of the NAAQSs and develop SIPs. Some networks have been developed on a national level (e.g., the Clean Air Status and Trends Network (CASTNET), the Speciation Trends Network (STN), and IMPROVE), while others have been established and maintained by state, local, and private agencies (e.g., the Southeastern Aerosol Research and Characterization (SEARCH) Study). In addition to chemical data, some of the networks also collect ambient meteorological data. The networks and special studies used for model evaluation in this thesis include CASTNET (<http://www.epa.gov/castnet>), STN, IMPROVE (<http://vista.cira.colostate.edu/improve>), SEARCH (<http://www.atmospheric-research.com/studies/SEARCH/index.html>), the Aerometric Information Retrieval System – Air Quality Subsystem (AIRS-AQS) (<http://www.epa.gov/ttn/airs/airsaqs>), and the National Atmospheric Deposition Program (NADP) (<http://nadp.sws.uiuc.edu>). Additional surface observations have been provided by the North Carolina Department of Environmental and Natural Resources (NCDENR) and the North Carolina State Climate Office (NC SCO). All these networks and special studies provide pointwise observational data for near the surface. Satellite data are used to evaluate model performance through the depth of the troposphere, which is important for examination of simulated vertical mixing and long-range transport of pollutants and integrated column abundances and properties. Satellite data also allow for more complete spatial representation of pollution that is not captured by the limited,

pointwise surface observations. Data from the following satellite instruments are used in this thesis: the Moderate Resolution Imaging Spectroradiometer (MODIS) (<http://modis.gsfc.nasa.gov>), the Measurements of Pollution in the Troposphere (MOPITT) (<http://terra.nasa.gov/About/MOPITT/index.php>), the Global Ozone Monitoring Experiment (GOME) (<http://earth.esa.int/ers/gome/>), and the Total Ozone Mapping Spectrometer (TOMS) (<http://jwocky.gsfc.nasa.gov>). Table 3.3 summarizes information on the networks and satellites, with additional details provided in the following sections.

3.3.1 Meteorological Observations

2-m temperature (T2), 2-m relative humidity (RH2), 10-m wind speed (WSP10), and 10-m wind direction (WDR10) are recorded at the CASTNET, SEARCH, NCDENR, and NC SCO monitoring sites. T2 is also recorded at the STN sites. MCIP produces T2, WSP10, and WDR10, which are used in the model evaluation against observations. RH2 is not directly produced by MCIP, so it is calculated for the first layer using variables from MCIP (i.e., water vapor mixing ratio, temp, and pressure) and the Clausius-Clapeyron Equation as follows:

$$RH = \frac{QV * 100\%}{\left(\frac{18.0153}{28.9628}\right) * \left\{ 611 * \exp\left(19.8644 - \frac{5423}{TA}\right) \right\} \left/ \left[PRES - 611 * \exp\left(19.8644 - \frac{5423}{TA}\right) \right] \right\}} \quad (3.1)$$

where QV, TA and PRES are the water vapor mixing ratio, temperature, and pressure, respectively, from MCIP. Weekly total precipitation is measured at the NADP sites (<http://nadp.sws.uiuc.edu/nadpoverview.asp>).

3.3.2 Chemical and Optical Observations

The monitoring networks collect data on both gas and PM species. O₃, being a criteria pollutant regulated by the EPA, is monitored by numerous networks, including AIRS-AQS, CASTNET, SEARCH, and NCDENR. The O₃ analyzers used on-site allow for continuous O₃ measurements, which are typically reported as hourly averages (<http://www.atmospheric-research.com/studies/search/SEARCHFactSheet.pdf>,

Table 3.3. The observational networks and satellites used in model evaluation, as well as the variables evaluated, the sampling frequency, and the number of sites within the 4-km and 1.33-km modeling domains.

Network	Variables			Sampling Frequency	Number of Sites	
	Met.	Gas	PM		4-km	1.33-km
AIRS-AQS	-----	O ₃	-----	Hourly	14	4
IMPROVE (mostly remote sites)	-----	-----	PM _{2.5} , SO ₄ ²⁻ , NO ₃ ⁻ , NH ₄ ⁺ , EC, OC, β _{ext} , HI	24-hour average (1-in-3 day)	6	0
CASTNET (mostly rural sites)	T2, RH2, WSP10, WDR10	O ₃ , SO ₂ , HNO ₃	SO ₄ ²⁻ , NO ₃ ⁻ , NH ₄ ⁺	7-day average (hourly O ₃ and met.)	9	1
STN (urban sites)	T2	-----	PM _{2.5} , SO ₄ ²⁻ , NO ₃ ⁻ , NH ₄ ⁺ , BC, OC	24-hour average (daily, 1-in-3, or 1-in-6 day)	18	9
NADP	Precip	-----	Wet Deposition of SO ₄ ²⁻ , NO ₃ ⁻ , NH ₄ ⁺	Weekly totals	19	5
SEARCH	T2, RH2, WSP10, WDR10	O ₃ , CO, SO ₂ , NO _x , HNO ₃	PM _{2.5} , SO ₄ ²⁻ , NO ₃ ⁻ , NH ₄ ⁺ , BC, OM	24-hour average and continuous	2	0
NCDENR ¹	T2, RH2, WSP10, WDR10	O ₃ , CO, SO ₂ , NO ₂	PM _{2.5}	Hourly, 24-hour average (1-in-3 day)	73	60
NC SCO	T2, RH2, WSP10, WDR10	-----	-----	Hourly	117	45
MODIS	-----	-----	AOD	Global coverage every 1-2 days	Domain wide	Domain wide
MOPITT	-----	CO	-----	3-day global coverage	Domain wide	Domain wide
GOME	-----	NO ₂	-----	3-day global coverage	Domain wide	Domain wide
TOMS	-----	O ₃	-----	Daily global coverage	Domain wide	Domain wide

¹ There are a total of 73 NCDENR sites in the 4-km domain, some with collocated observations (46 sites with hourly O₃ observations, 37 sites with 24-hour average PM observations, 8 sites with hourly PM observations, and 8 sites with hourly meteorology observations).

http://www.epa.gov/castnet/docs/CASTNET_factsheet_2007.pdf). O₃ data for the depth of the troposphere for 2002 are obtained from the TOMS instrument onboard the Aura satellite. The satellite data consist of global daily measurements, with the satellite passing over the same location around the same time every day. Some O₃ and PM precursor gases (i.e., SO₂, nitrogen dioxide (NO₂), HNO₃) are also monitored at some sites (i.e., IMPROVE, CASTNET, SEARCH, NCDENR) in order to provide more complete information on the partitioning and formation mechanisms of secondary pollutants. The tropospheric column NO₂ is derived from GOME observations, onboard the European Remote Sensing (ERS-2) satellite. Another gas that is monitored through SEARCH and NCDENR, as well as MOPITT, is CO, a moderately long-lived O₃ precursor. Monitoring CO is beneficial to air quality model evaluation because its long lifetime leaves it susceptible to transport. The horizontal transport has been found to be negligible in comparison to vertical transport (Jang et al., 1995), so observed CO mixing ratios compared to modeled values can provide some insight into the ability of the model to capture vertical transport of pollutants.

PM_{2.5} is monitored at IMPROVE, STN, SEARCH, and NCDENR. Speciation of ambient PM is monitored at the CASTNET sites, while wet deposition of PM species is monitored at the NADP sites. The volatility of some PM_{2.5} components has made the collection method of PM_{2.5} very important. Using filters to collect PM_{2.5} can be costly for both the materials and manual work required, thus filter samples are typically taken for 24-hour periods once every three or six days. Some sites (e.g., SEARCH, NCDENR) have adopted the use of continuous measurement methods, such as TEOM, however, for demonstration of the NAAQS attainment, the EPA requires data be obtained using the filter-based Federal Reference Method (FRM) or Federal Equivalent Method (FEM). NCDENR, SEARCH, and STN all use the FRM or FEM to collect PM_{2.5} and its components, in compliance with EPA regulations. IMPROVE was established in 1985 to monitor visibility and regional haze, not PM_{2.5} attainment, and continues to use the IMPROVE Modular Aerosol Sampler, which consists of four sampling modules. Each module uses a Teflon, Nylon, or quartz filter which is sent to a lab to identify PM_{2.5} mass, components, or optical absorption. Some sites also use an Optec Long Path Visibility - 2 (LPV-2) Transmissometer

and an Optec Next Generation Nephelometer – 2 (NGN-2) Integrating Nephelometer to measure light extinction and scattering, respectively. The visibility variables available through IMPROVE include the extinction coefficient (β_{ext}) and haziness index (HI), reported as deciviews (dcv). The haziness index was designed so that changes in haziness correspond to uniform increments of perceived changes in visibility (U.S. EPA, 2003; Pitchford and Malm, 1994) and is calculated based on β_{ext} as follows:

$$\text{HI (dcv)} = 10 \times \ln (\beta_{\text{ext}} / 0.01 \text{ km}^{-1}) \quad (3.2).$$

The Aerosol Optical Depth (AOD) is a dimensionless measurement of the attenuation of radiation by particles in the atmosphere integrated over the path (Seinfeld and Pandis, 2005). The observed AOD values for the vertical column of the atmosphere above the surface can be derived from the MODIS instruments onboard the Terra and Aqua satellites. While AOD does not provide direct measurements of PM_{2.5} mass at the surface, it can, in some cases, correlate well with PM concentrations (Engel-Cox et al., 2004a, b).

CASTNET and NADP were established to monitor dry and wet deposition of pollutants, respectively, as opposed to ambient concentration measurements for demonstration of NAAQS attainment. CASTNET uses a three-stage filter pack to collect gases and particles on a weekly basis. Meteorological measurements from CASTNET, combined with a description of the local vegetation (i.e., leaf area index, plant reactivity to light and temperature, type and height of vegetation, and minimum stomatal resistance), are used in the Multilayer Model (MLM) to determine dry deposition velocities (Meyers et al., 1998; Finkelstein et al., 2000). The dry deposition flux is determined by multiplying the modeled dry deposition velocity by the concentration of the chemical specie in the air. Wet deposition flux is determined through the collection and analysis of precipitation at the NADP sites. Precipitation is collected in a bucket that automatically closes when the precipitation stops in order to prevent contamination from dry deposition (<http://nadp.sws.uiuc.edu/lib/brochures/insideRain.pdf>).

3.3.3 Quality of Observational Data

There are uncertainties and errors associated with observational data and the agency in charge of the monitoring station has the responsibility of validating the data and estimating the uncertainties. Most of the long-standing observational networks, such as CASTNET, NADP, and IMPROVE, use highly detailed procedures to determine the data quality using indicators, including precision, accuracy, completeness, representativeness, and comparability (MACTEC, 2007; Aubertin et al., 1991; IMPROVE, 2002). Precision and accuracy are evaluated using co-located sites, either within the same network or from another network. Completeness is a determination of the number of valid observations made compared to the expected total observations. The representativeness is associated with selecting the location of the monitor, which is also based on very detailed procedures. The comparability of the data is the confidence that the dataset can be compared with another, including co-located data, and site-by-site, year-by-year, and network-to-network comparison. CASTNET and IMPROVE have published their precision and accuracy criteria, which are generally within ± 5 -10% depending on the variable. Temperature, wind speed, and wind direction, as measured at the CASTNET sites, are to fall within ± 0.5 -1°C, ± 5 m/s, and $\pm 5^\circ$, respectively. Both networks also publish quarterly and yearly quality assurance reports. The maximum allowable bias (precision) at NADP varies depending on the measured amount compared to the detection limit of the individual species ($\pm 100\%$ at the detection limit, $\pm 20\%$ at 10 times the detection limit, and $\pm 10\%$ at 100 times the detection limit). STN also uses comparability and completeness, and the completeness is determined separately for specified values, precisions, accuracies, and validities (Chow and Watson, 1998). The validity of STN data is determined at three levels. The first level is completed in the field or laboratory and eliminates or flags invalid data based on computer or equipment data logs. The second level evaluates the consistency of the data based on known relationships (e.g., $PM_{2.5}$ concentrations are always less than PM_{10} concentrations, and charge balances). The third and final level of validation of suspicious values begins with an assumption of measurement error, which is further researched. If no error can be traced, the value is assumed valid due to an environmental cause (Chow and Watson, 1998). AIRS-

AQS and NC SCO are databases that collect data from numerous other sources. AIRS-AQS includes data collected by the EPA, state, local, and tribal air pollution control agencies and is validated by the submitting agency (http://www.epa.gov/ttn/airs/airsaqs/basic_info.htm). NC SCO data is collected from the National Weather Service (NWS) Automated Surface Observing System (ASOS), the Automated Weather Observing System (AWOS), buoys, NWS cooperative observers (volunteers), the Environment and Climate Observing Network (ECONet), the Soil Climate Analysis Network (SCAN), and the Community Collaborative Rain, Hail, and Snow Network (CoCoRaHS) (volunteers) (<http://www.nc-climate.ncsu.edu/cronos/about.php>). The volunteers are trained in making and reporting the measurements to help eliminate some error and guarantee consistency.

The validation of satellite data can be more difficult than validation surface observations. There are some ground-based measurements used in the validation process of MODIS, MOPITT, GOME, and TOMS data, including the Aerosol Robotic Network (AERONET) and the Network for the Detection of Stratospheric Change (NDSC) (Chu et al., 2003; Lambert, 2002). Additionally, observations from aircrafts have also been used (<http://www.acd.ucar.edu/mopitt/validation/val-retr.shtml>). In order to complete the validations using surface observations or aircraft measurements, the data has to be matched up in time and space with the satellite overpass. Depending on the availability of data, this may range from within 30 minutes of the overpass for MODIS validation with AERONET sites (Chu et al., 2003), to a 3 hour window for MOPITT Level-1 validation using aircraft measurements (<http://www.acd.ucar.edu/mopitt/validation/val-rads-status.shtml>). Validation of satellite data have given the following results: MODIS derived AOD values (τ) fall within the range of retrieval error of $\Delta\tau = \pm 0.05 \pm 0.20\tau$ (Chu et al., 2003); MOPITT Level-2 data (mixing ratios) have been within $6.2 \pm 11.4\%$ (<http://www.acd.ucar.edu/mopitt/validation/val-retr.shtml>); differences in column NO_2 data is typically less than 1.5×10^{15} molecules cm^{-2} (Lambert, 2002); and TOMS data has a mean difference of $0.5 \pm 0.7\%$ from surface observations of tropospheric O_3 (McPeters et al., 1996).

3.4 Evaluation Protocol

The model performance and comparison are completed using statistics, spatial distributions, and temporal analyses. A fourth form of comparison is completed using column mass of the pollutant derived from satellite observations. These four forms of evaluation allow for multiscale and multi-layer comparison, from domain-wide down to site specific variations and from total column to the surface.

3.4.1 Statistical Evaluation

To compare the model performance with observations, the simulated values are extracted from the grid cell that contains the point measurement site and statistics are calculated. The statistics calculated in this study include: normalized mean bias (NMB), normalized mean error (NME), correlation coefficient (corr), mean bias (MB), mean absolute gross error (MAGE), root mean square error (RMSE), mean normalized bias (MNB), mean normalized gross error (MNGE), fractional bias (FB), fractional gross error (FGE), normalized mean fractional bias (NMFB), normalized mean fractional gross error (NMFGE), mean normalized fractional bias (MNFB), mean normalized gross fractional error (MNGFE), normalized mean bias factor (NMBF), and normalized mean error factor (NMEF). The analysis of performance statistics focuses on the mean (average) values, MB, NMB, and NME. The NMB and NME are defined as follows (Yu et al., 2006):

$$NMB = \frac{\sum_{i=1}^N (M_i - O_i)}{\sum_{i=1}^N O_i} \quad (3.3)$$

$$NME = \frac{\sum_{i=1}^N |M_i - O_i|}{\sum_{i=1}^N O_i} \quad (3.4)$$

where M_i and O_i are the modeled and observed values, respectively, at a specific time and location, i , with N pairs of data. NMB and NME can be presented as a percentage by

multiplying the above equations by 100%. NMB can be a positive or negative value, indicating an over or underprediction, respectively; however the underprediction is bounded by -1 (-100%), while there is no bound on the overprediction. Using NME only considers the magnitude of the difference between modeled and observed values and does not provide any information as to whether the model over or underpredicts the variable. While, individually, NMB and NME have advantages and disadvantages, combined, they can provide useful information in determining the models ability to represent observed values. The statistics presented in this thesis are separated by networks because of their varying characteristics in terms of sampling frequency and resolution and monitoring approach and type of area (e.g., urban vs. rural) following Eder and Yu (2006) and Queen et al. (2008). It is also important to note that the statistics are evaluated based on a single point measurement while the simulated value is a grid volume average in the area of the monitoring station.

3.4.2 Spatial Evaluation

The use of spatial plots allows for evaluation of the spatial distribution of variables across the whole domain, including insight into the fine scale variability and spatial gradients of the plotted variable. Spatial plots presented in this thesis include monthly-mean simulated values overlaid with monthly-mean observed values, as well as absolute and percent difference plots when completing the sensitivity analysis. All spatial plots are created using the Package for Analysis and Visualization of Environmental data (PAVE) (http://www.ie.unc.edu/cempd/EDSS/pave_doc/index.shtml).

3.4.3 Temporal Evaluation

The third type of evaluation used in this thesis is temporal analysis. This is completed by plotting the observed and modeled values against time. When hourly observations are available, the temporal evaluation allows for interpretation of how well the model captures diurnal variations. When hourly observations are not available, the temporal analysis can still be completed, however only the longer trends based on available observations can be evaluated (e.g., modeled daily 24-hour averages compared to 1-in-3 day

24-hour average observed values). The time series analysis also allows for the identification of particular trends at different geographical locations (i.e., urban vs. mountain sites).

3.4.4 Column Mass of Chemical Species

The satellite data and evaluation of the column mass of chemical species is presented as spatial distribution plots. The total mass within the column is considered and presented as a single value per grid cell. The AOD is evaluated by extracting the simulation hours closest to overpass time of the satellite (10 AM and 11 AM local time, daily) and averaged for the month. The satellite data has some limitations, including cloud cover preventing the satellite sensor from retrieving data and limitations on the algorithms used to derive the variable of interest (Engel-Cox et al., 2004a). For example, the AOD algorithm eliminates very low and very high AOD values to remove the influence of clouds, shadows, or other contamination (Engel-Cox et al., 2004a). Additionally, the AOD algorithm depends on geolocated reflectances, and cloud mask and meteorology data (Remer et al., 2005). There are also separate algorithms for calculating the AOD over land versus the AOD over water, so information identifying land pixels and water pixels is also required (Remer et al., 2005). When retrieving the aerosol data along coastal regions that include land and water pixels, the quality of the retrieval is reduced (Remer et al., 2005). The data required to derive the AOD increases the associated uncertainties, particularly over land (Chu et al., 2002).

4. BASELINE SIMULATIONS: INTERCOMPARISON OF CMAQ AND CAMx

The MM5/CMAQ and MM5/CAMx simulations completed at a horizontal grid spacing of 4-km for January and July are herein referred to as the baseline simulations. In this chapter, the CMAQ and CAMx baseline simulations will be evaluated using the observations and modeling protocol discussed in Chapter 3. The objectives of this model evaluation are to assess the performance and seasonal variations of the meteorology and air quality models at a fine horizontal grid resolution and identify likely causes for discrepancies between observations and model predictions and between predictions from both models.

4.1 Meteorology

Prior to completing the model evaluation for chemical species, the performance of MM5 is evaluated using available observations, as described in Chapter 3. Tables 4.1 and 4.2 provide the statistics for January and July 2002, respectively, for hourly T2, RH2, WSP10, WDR10, the u and v component of wind, and weekly total precipitation. The values are rounded to the nearest tenth. Because of possible errors when reporting calm wind speed (Olerud et al., 2005), a cutoff value, or threshold, is used in calculating the wind speed statistics. When the observed wind speed value is less than 1.5 knots (0.771 m s^{-1}) (halfway between 0.0 and the lowest observable wind speed of 3 knots (Olerud et al., 2005)), the data pair is not included in the calculations. The NMBs of T2 and RH2 are generally between $\pm 10\%$, with the exceptions of January T2 at the CASTNET, SEARCH, and NC SCO sites, and January RH2 at the SEARCH sites. WSP10 is overpredicted in both months with a better performance in January. The mean bias in WDR10 ranges from -11.3° at the NC SCO sites in July to $+12.1^\circ$ at the CASTNET sites in January. Some difficulty arises in interpreting the statistics of WDR10, which is a vector reported in degrees. This is because 0° is equal to 360° in the wind rose plot, however, the mathematical difference between 0° and 360° is large. One way to gain a better understanding of the models performance of both wind speed and direction is to evaluate the u and v components individually. Both components are overpredicted at all three networks in both months with the exception of the

Table 4.1. Performance statistics for meteorological variables for January 2002.

Variable	T2 (°C)				RH2 (%)		Precip (mm)
	CAST	STN	SEARCH	SCO	CAST	SEARCH	NADP
Number	5157	60	1360	623	6857	1455	72
MeanObs	7.87	6.33	10.02	8.46	70.69	69.59	29.30
MeanMod	7.00	6.90	7.00	7.13	75.12	80.25	26.09
NMB	-0.11	0.09	-0.30	-0.16	0.06	0.15	-0.11
NME	0.25	0.26	0.33	0.26	0.17	0.20	0.40
corr	0.89	0.89	0.85	0.89	0.68	0.70	0.79
MB	-0.87	0.57	-3.02	-1.34	4.44	10.66	-3.22
MAGE	1.93	1.61	3.31	2.19	12.26	14.02	11.73
RMSE	2.59	2.04	4.24	2.89	16.66	18.36	17.71
MNB	NaN	Inf	-0.09	Inf	Inf	0.22	0.49
MNGE	Inf	Inf	0.21	Inf	Inf	0.26	0.93
FB	12.70	-0.27	-1.01	-0.18	0.07	0.16	-0.07
FGE	-12.43	0.66	1.07	0.41	0.19	0.21	0.52
NMFB	-0.12	0.09	-0.36	-0.17	0.06	0.14	-0.12
NMFGFE	0.26	0.24	0.39	0.28	0.17	0.19	0.42
MNFB	NaN	0.35	0.32	-1.58	Inf	0.21	0.20
MNGFE	Inf	0.47	2.15	2.53	Inf	0.27	1.22
NMBF	-0.12	0.09	-0.43	-0.19	0.06	0.15	-0.12
NMEF	0.28	0.26	0.47	0.31	0.17	0.20	0.45

Inf (Infinity) and NaN (Not a Number) are a result of a small denominator compared to the numerator and mean observation (Seigneur et al., 2000) in the following equations (from Zhang et al., 2006a):

$$MNB = \frac{1}{N} \sum_{i=1}^N \frac{M_i}{O_i} - 1$$

$$MNGE = \frac{1}{N} \sum_{i=1}^N \frac{|M_i - O_i|}{O_i}$$

$$MNFB = \frac{1}{N} \sum_{i=1}^N F_i \text{ where } F_i = \frac{M_i}{O_i} - 1 \text{ for } M_i \geq O_i, \text{ or } F_i = 1 - \frac{O_i}{M_i} \text{ for } M_i < O_i$$

$$MNGFE = \frac{1}{N} \sum_{i=1}^N |F_i| \text{ where } F_i = \frac{M_i}{O_i} - 1 \text{ for } M_i \geq O_i, \text{ or } F_i = 1 - \frac{O_i}{M_i} \text{ for } M_i < O_i$$

Table 4.1. Continued.

Variable	WSP10 (m s ⁻¹)			WDR10 (°)			U-component (m s ⁻¹)			V-component (m s ⁻¹)		
	CAST	SEARCH	SCO	CAST	SEARCH	SCO	CAST	SEARCH	SCO	CAST	SEARCH	SCO
Number	6089	1295	700	7098	1455	744	6089	1302	701	6089	1302	701
MeanObs	2.98	2.95	2.66	200.45	210.27	212.15	0.91	0.39	1.18	0.05	-0.29	0.26
MeanMod	3.81	3.25	3.43	212.57	210.56	215.22	1.48	0.44	1.34	0.37	0.31	0.15
NMB	0.28	0.10	0.29	0.06	0.00	0.01	0.63	0.13	0.14	6.23	-2.07	-0.43
NME	0.43	0.36	0.36	0.31	0.26	0.07	1.39	3.39	0.60	29.00	-5.88	3.09
corr	0.59	0.60	0.72	0.45	0.57	0.90	0.66	0.71	0.91	0.77	0.53	0.93
MB	0.83	0.29	0.77	12.12	0.29	3.07	0.57	0.05	0.16	0.32	0.60	-0.11
MAGE	1.27	1.05	0.95	62.32	54.75	15.51	1.26	1.32	0.71	1.50	1.69	0.81
RMSE	1.74	1.26	1.11	103.01	90.25	40.38	1.90	1.76	0.92	2.05	2.42	1.00
MNB	0.51	0.28	0.48	Inf	1.21	0.56	NaN	-0.08	0.54	Inf	-2.71	-5.31
MNGE	0.63	0.47	0.52	Inf	1.43	0.66	Inf	0.11	0.26	Inf	1.69	8.25
FB	0.25	0.14	0.31	0.09	0.04	-0.01	-0.17	0.18	-0.10	-0.44	-0.29	0.50
FGE	0.41	0.38	0.36	0.40	0.36	0.12	-0.21	0.72	-0.65	0.01	-0.38	-0.11
NMFB	0.24	0.10	0.25	0.06	0.00	0.01	0.48	0.12	0.13	1.51	55.92	-0.55
NMFGE	0.37	0.34	0.31	0.30	0.26	0.07	1.05	3.18	0.56	7.05	158.54	3.94
MNFB	0.44	0.20	0.47	Inf	-4.76	-0.75	Inf	1.06	0.46	Inf	-0.16	1.83
MNGFE	0.71	0.56	0.53	Inf	7.40	1.96	Inf	3.32	0.80	Inf	2.61	2.31
NMBF	0.28	0.10	0.29	0.06	0.00	0.01	0.63	0.13	0.14	6.23	-2.07	-0.76
NMEF	0.43	0.36	0.36	0.31	0.26	0.07	1.39	3.39	0.60	29.00	-5.88	5.43

Obs: Observations, **Mod:** Model, **NMB:** Normalized Mean Bias, **NME:** Normalized Mean Error, **corr:** Correlation, **MB:** Mean Bias, **MAGE:** Mean Absolute Gross Error, **RMSE:** Root Mean Square Error, **MNB:** Mean Normalized Bias, **MNGE:** Mean Normalized Gross Error, **FB:** Fractional Bias, **FGE:** Fractional Gross Error, **NMFB:** Normalized Mean Fractional Bias, **NMFGE:** Normalized Mean Fractional Gross Error, **MNFB:** Mean Normalized Fractional Bias, **MNGFE:** Mean Normalized Gross Fractional Error, **NMBF:** Normalized Mean Bias Factor, **NMEF:** Normalized Mean Error Factor, **T2:** Temperature at 2-m, **RH2:** Relative Humidity at 2-m, **Precip:** Precipitation, **WSP10:** Wind Speed at 10-m, **WDR10:** Wind Direction at 10-m, **CAST:** CASTNET - Clean Air Status and Trends Network, **STN:** Speciation Trends Network, **SEARCH:** Southeastern Aerosol Research Characterization, **SCO:** NC State Climate Office.

Table 4.2. Performance statistics for meteorological variables for July 2002.

Variable	T2 (°C)				RH2 (%)		Precip (mm)
	CAST	STN	SEARCH	SCO	CAST	SEARCH	NADP
Number	7410	134	1393	744	6741	1164	84
MeanObs	23.40	26.03	28.54	26.25	76.38	75.14	30.11
MeanMod	24.42	25.58	26.02	25.99	70.73	71.78	75.69
NMB	0.04	-0.02	-0.09	-0.01	-0.07	-0.05	1.51
NME	0.07	0.04	0.10	0.03	0.14	0.12	2.03
corr	0.89	0.87	0.86	0.98	0.73	0.74	0.34
MB	1.02	-0.45	-2.51	-0.26	-5.65	-3.36	45.58
MAGE	1.64	1.03	2.83	0.76	10.45	9.22	61.10
RMSE	2.14	1.42	3.33	0.94	13.57	12.35	96.24
MNB	0.05	-0.02	-0.08	-0.01	Inf	-0.03	Inf
MNGE	0.07	0.04	0.10	0.03	Inf	0.13	Inf
FB	0.05	-0.02	-0.09	-0.01	-0.08	-0.05	0.54
FGE	0.07	0.04	0.10	0.03	0.15	0.13	1.18
NMFB	0.04	-0.02	-0.09	-0.01	-0.08	-0.05	0.86
NMGFE	0.07	0.04	0.10	0.03	0.14	0.13	1.16
MNFB	0.05	-0.02	-0.10	-0.01	Inf	-0.06	NaN
MNGFE	0.08	0.04	0.11	0.03	Inf	0.15	Inf
NMBF	0.04	-0.02	-0.10	-0.01	-0.08	-0.05	1.51
NMEF	0.07	0.04	0.11	0.03	0.15	0.13	2.03

Inf (Infinity) and **NaN** (Not a Number) are a result of a small denominator compared to the numerator and mean observation (Seigneur et al., 2000) in the following equations (from Zhang et al., 2006a):

$$MNB = \frac{1}{N} \sum_{i=1}^N \frac{M_i}{O_i} - 1$$

$$MNGE = \frac{1}{N} \sum_{i=1}^N \frac{|M_i - O_i|}{O_i}$$

$$MNFB = \frac{1}{N} \sum_{i=1}^N F_i \text{ where } F_i = \frac{M_i}{O_i} - 1 \text{ for } M_i \geq O_i, \text{ or } F_i = 1 - \frac{O_i}{M_i} \text{ for } M_i < O_i$$

$$MNGFE = \frac{1}{N} \sum_{i=1}^N |F_i| \text{ where } F_i = \frac{M_i}{O_i} - 1 \text{ for } M_i \geq O_i, \text{ or } F_i = 1 - \frac{O_i}{M_i} \text{ for } M_i < O_i$$

Table 4.2. Continued.

Variable	WSP10 (m s ⁻¹)			WDR10 (°)			U-component (m s ⁻¹)			V-component (m s ⁻¹)		
	CAST	SEARCH	SCO	CAST	SEARCH	SCO	CAST	SEARCH	SCO	CAST	SEARCH	SCO
Number	5425	946	697	7140	1182	744	5425	949	703	5425	949	703
MeanObs	1.95	1.95	2.13	183.54	222.84	197.46	0.30	0.58	0.52	0.20	0.39	0.42
MeanMod	2.89	2.58	2.91	184.47	216.38	186.12	0.47	0.75	0.39	0.57	0.32	0.76
NMB	0.48	0.32	0.37	0.01	-0.03	-0.06	0.58	0.31	-0.25	1.87	-0.18	0.83
NME	0.63	0.53	0.40	0.41	0.20	0.16	4.41	1.80	1.35	6.35	2.43	1.70
corr	0.51	0.34	0.73	0.30	0.61	0.61	0.68	0.81	0.92	0.67	0.63	0.93
MB	0.94	0.63	0.79	0.94	-6.45	-11.34	0.17	0.18	-0.13	0.37	-0.07	0.35
MAGE	1.23	1.03	0.85	75.87	43.49	31.24	1.32	1.03	0.70	1.26	0.94	0.71
RMSE	1.53	1.27	0.99	116.37	74.28	79.65	1.69	1.29	0.88	1.64	1.22	0.88
MNB	0.65	0.50	0.54	Inf	0.43	1.63	NaN	1.03	0.40	Inf	3.26	0.24
MNGE	0.79	0.65	0.56	Inf	0.64	1.79	Inf	0.32	0.04	Inf	-0.99	0.31
FB	0.34	0.27	0.36	0.06	-0.04	-0.05	0.46	0.61	0.26	0.31	0.74	0.22
FGE	0.52	0.47	0.38	0.50	0.26	0.20	-0.63	0.15	-0.16	1.29	-0.90	-0.11
NMFB	0.39	0.28	0.31	0.01	-0.03	-0.06	0.45	0.27	-0.29	0.97	-0.19	0.59
NMFGE	0.51	0.45	0.34	0.41	0.20	0.16	3.43	1.56	1.54	3.28	2.67	1.20
MNFB	0.52	0.33	0.53	Inf	-0.50	-1.02	Inf	0.61	Inf	Inf	0.63	0.28
MNGFE	0.92	0.82	0.56	Inf	1.57	4.43	Inf	2.00	Inf	Inf	4.32	0.98
NMBF	0.48	0.32	0.37	0.01	-0.03	-0.06	0.58	0.31	-0.33	1.87	-0.21	0.83
NMEF	0.63	0.53	0.40	0.41	0.20	0.17	4.41	1.80	1.80	6.35	2.96	1.70

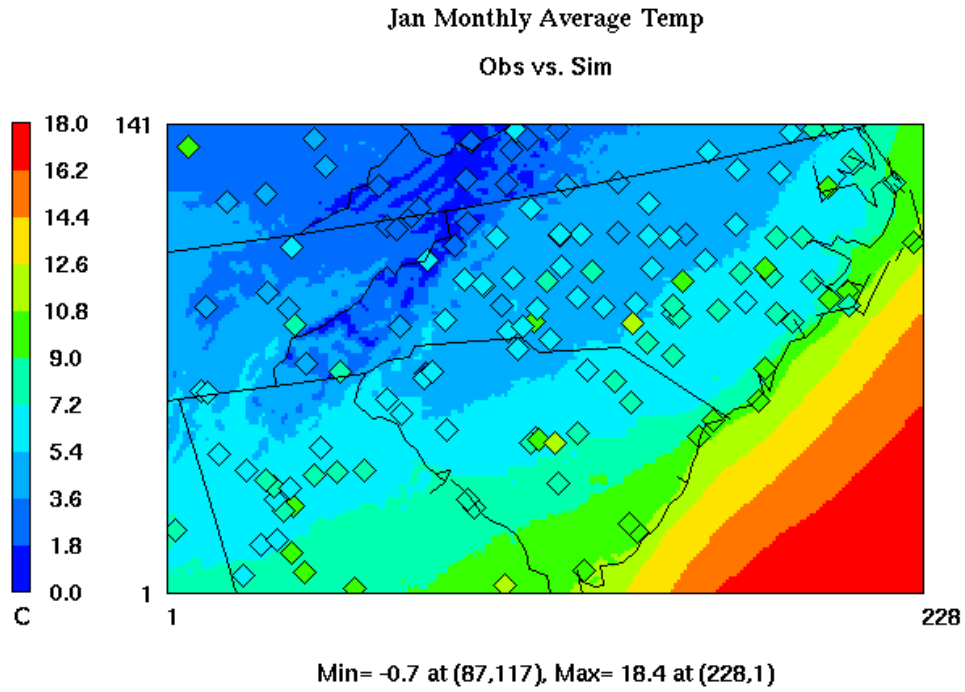
Obs: Observations, **Mod:** Model, **NMB:** Normalized Mean Bias, **NME:** Normalized Mean Error, **corr:** Correlation, **MB:** Mean Bias, **MAGE:** Mean Absolute Gross Error, **RMSE:** Root Mean Square Error, **MNB:** Mean Normalized Bias, **MNGE:** Mean Normalized Gross Error, **FB:** Fractional Bias, **FGE:** Fractional Gross Error, **NMFB:** Normalized Mean Fractional Bias, **NMFGE:** Normalized Mean Fractional Gross Error, **MNFB:** Mean Normalized Fractional Bias, **MNGFE:** Mean Normalized Gross Fractional Error, **NMBF:** Normalized Mean Bias Factor, **NMEF:** Normalized Mean Error Factor, **T2:** Temperature at 2-m, **RH2:** Relative Humidity at 2-m, **Precip:** Precipitation, **WSP10:** Wind Speed at 10-m, **WDR10:** Wind Direction at 10-m, **CAST:** CASTNET - Clean Air Status and Trends Network, **STN:** Speciation Trends Network, **SEARCH:** Southeastern Aerosol Research Characterization, **SCO:** NC State Climate Office.

u component at the NC SCO sites and the v component at the SEARCH sites in July, consistent with the model performance in wind speed and direction. Despite providing additional information on the model performance, using the u and v components has the disadvantage of including negative numbers, which can be cancelled out by positive numbers and give misleading NMB and NME (i.e., v-component at the SEARCH sites in January) consistent with the findings of Zhang et al. (2006a). When the simulated value is positive and the observed value is negative (an overprediction), the numerator of the NMB or NME is positive and the denominator is negative resulting in a negative NMB/NME despite the overprediction by the model. The final variable analyzed through statistics is precipitation. The model significantly overpredicts precipitation in July, with a better performance in January. The large overprediction in July may be partially influenced by the fact that the weather in the southeast U.S. in 2002 was drier than the historical average for the region. The overprediction in precipitation also plays an important role in the removal of pollutants through wet deposition.

Figure 4.1 shows the monthly-mean spatial distributions of T2 in January and July overlaid with observations from CASTNET, STN, and NC SCO. Generally, the spatial distributions in both months are captured, with cooler temperatures in the mountains in the western NC and warmer temperatures along the coastline. However, in January, an underprediction is visible between these two regions. In July, the model captures T2 better near the mountains than the surrounding areas and an underprediction is noticeable in the central and eastern NC and eastern GA, particularly around Atlanta. The statistics for July temperatures at the SEARCH sites (Yorkville and downtown Atlanta), shown in Table 4.2 also indicate the underprediction near Atlanta, with the largest NMB and NME of -8.8 and 9.9, respectively.

Similar plots are made for RH2 in Figure 4.2. There is a general overprediction of RH2 in January across the whole domain, consistent with the domain wide statistics. In July, however, an underprediction is visible in the western part of the domain, while the model overpredicts RH2 in the eastern half of the domain and performs relatively well in the leeward side of the mountains. This variation across the domain is not discernable from the

(a)



(b)

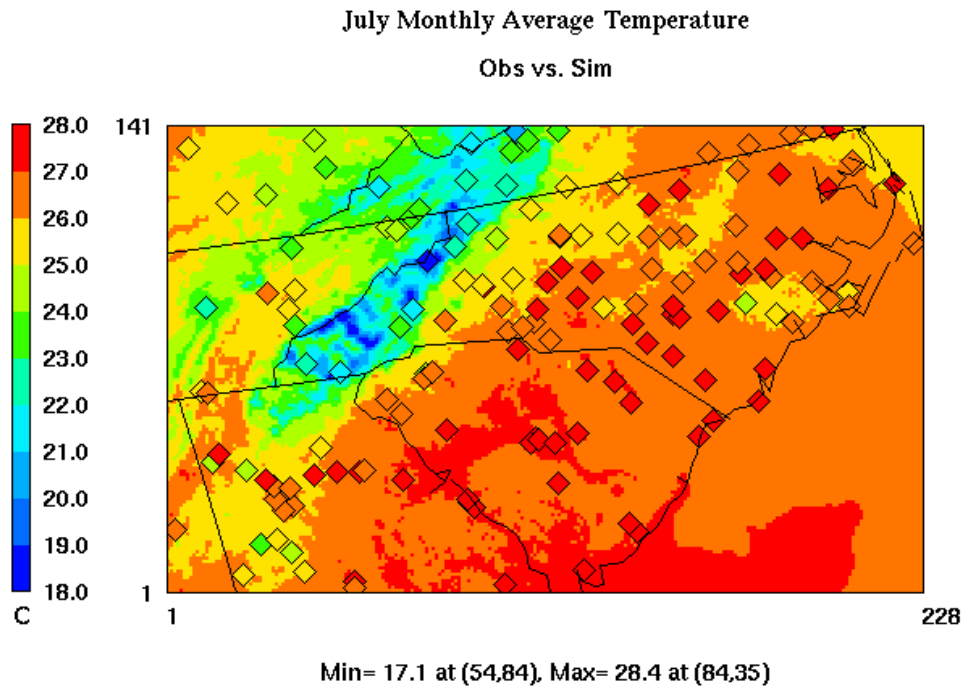
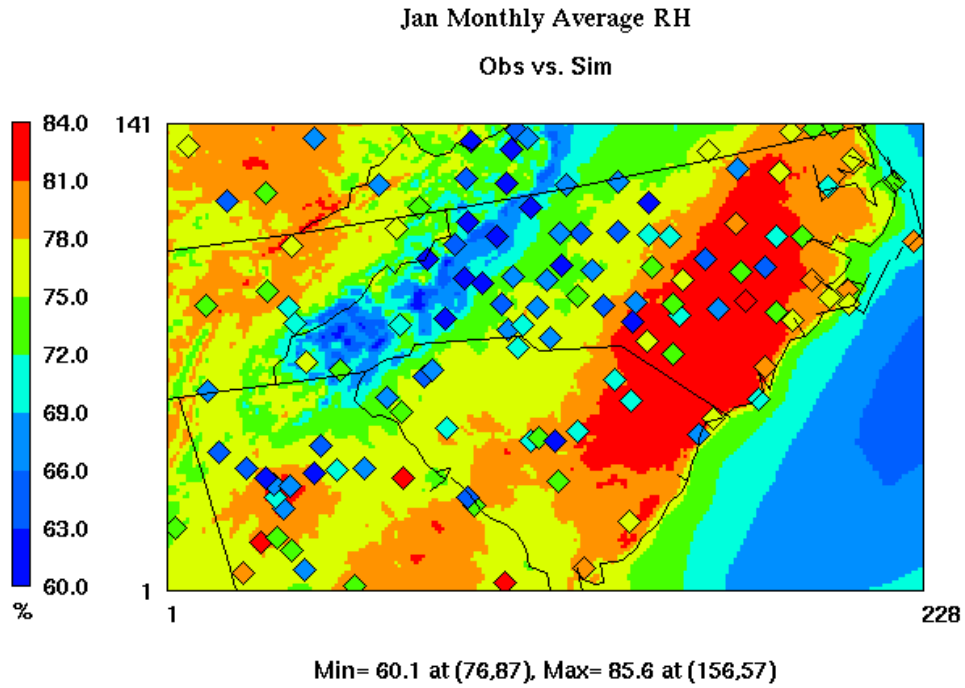


Figure 4.1. The spatial distribution of monthly-mean temperatures at 2-m in (a) January and (b) July as simulated by MM5 (background color) overlaid with observations (diamonds) from CASTNET, STN, and NC SCO.

(a)



(b)

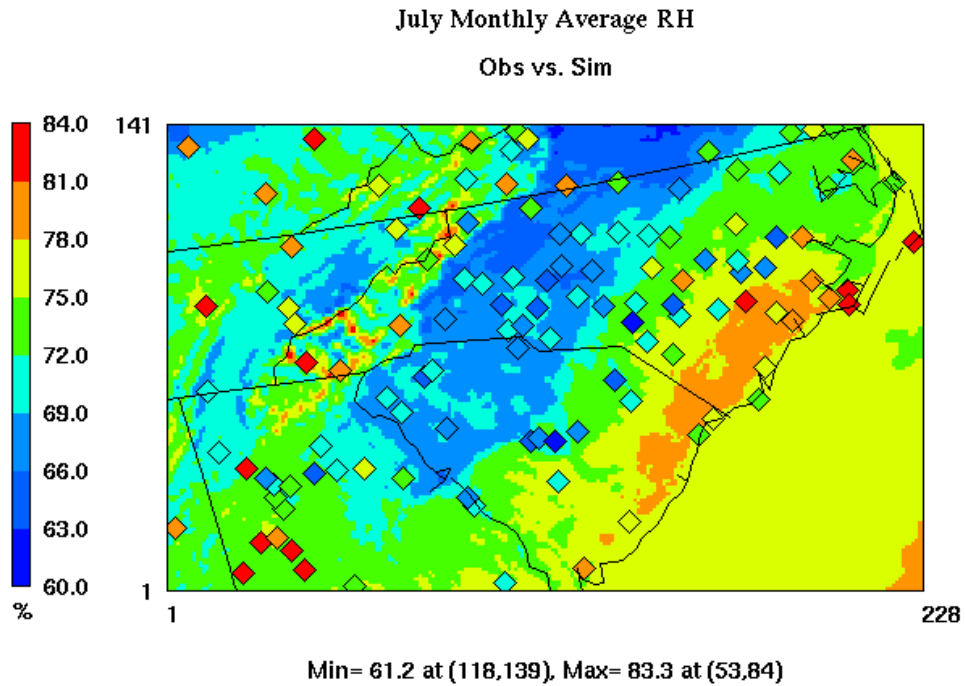


Figure 4.2. The spatial distribution of monthly-mean relative humidities at 2-m in (a) January and (b) July as simulated by MM5 (background color) overlaid with observations (diamonds) from CASTNET, STN, and NC SCO.

domain-wide statistics, which just show a general underprediction by the model.

The third form of evaluation completed for meteorological variables is temporal analysis. Figure 4.3 shows the temporal variations for temperature in January at four sites in the 4-km domain: Beaufort, NC along the coast, Kinston, NC in the eastern, agricultural region of NC, Great Smoky Mountains, TN, and Raleigh, NC. Generally, the diurnal variation is captured at all four sites. The temperature in Kinston and Raleigh, NC from January 6th to 11th is largely underpredicted by the model. This is likely due to MM5's incapability in accurately representing snow cover associated with the early January snowstorm. On some dates at some sites, an underprediction of maximum temperature is shown, i.e., the middle and end of the month at Beaufort, Kinston, and Raleigh. While the statistics and spatial distributions show that the monthly-mean temperature is generally underpredicted, the time series does show that occasionally the minimum temperature at night is overpredicted (i.e., January 12th, 13th, 16th, 27th, and 28th at Beaufort, January 12th, 14th, 26th, and 27th at Kinston and Raleigh). The ability of the model to capture diurnal variations in July (Figure 4.4) appears better than that in January. Occasionally the maximum temperature at Beaufort, Kinston, and Raleigh is underpredicted, however, at the Great Smoky Mountain site, maximum temperature is overpredicted throughout the month. MM5 with FDDA is generally able to capture the seasonal and diurnal variations in temperature in the southeast U.S., with better performance in July, as indicated through statistics, spatial distribution, and temporal analysis.

The statistics and spatial distribution for relative humidity at 2-m in January indicate an overprediction by MM5 across the domain. As shown in Figure 4.5, at three of the four sites, the overprediction resulted from an inaccurate representation of the low relative humidity during some time periods. The model appears to more accurately capture the diurnal variations of relative humidity in July (Figure 4.6) than in January. Maximum relative humidity in July at the Beaufort and Kinston site is generally underpredicted, while the minimum relative humidity at the Raleigh site is overpredicted. The geography of the region plays an important role in meteorological variables, particularly relative humidity. Higher relative humidity is expected along the coast; however a sharp gradient develops to

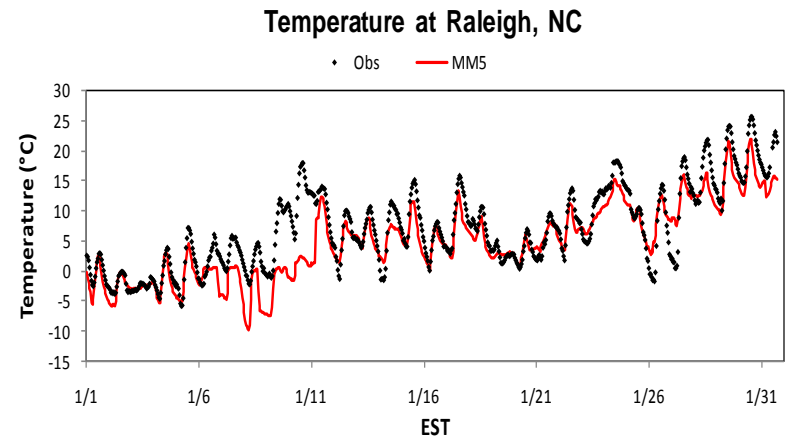
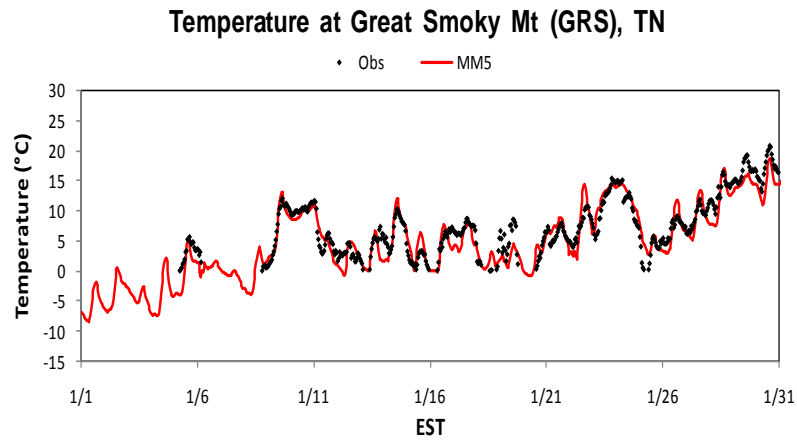
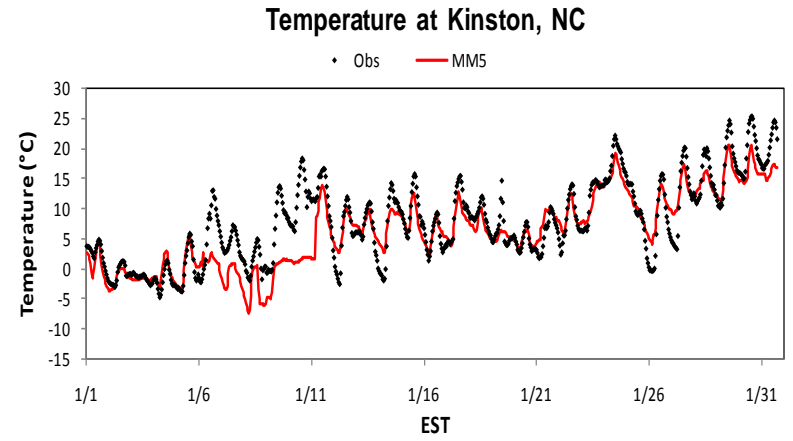
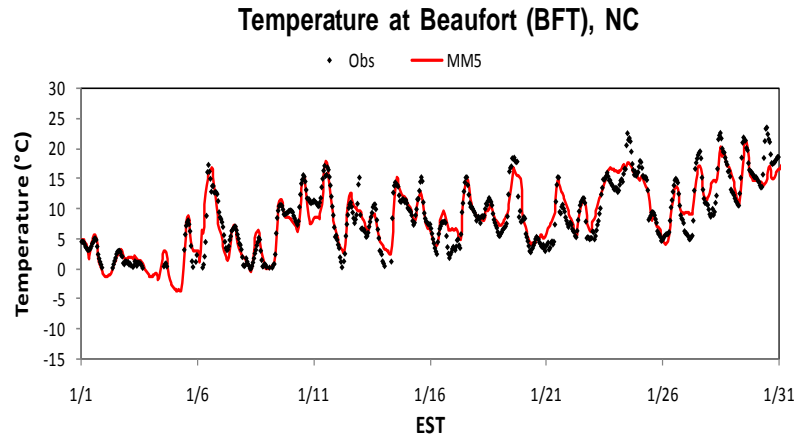


Figure 4.3. Temporal variation of temperatures in January at Beaufort, NC (coastal), Kinston, NC (central), Great Smoky Mountains (mountain), TN, and Raleigh, NC (urban).

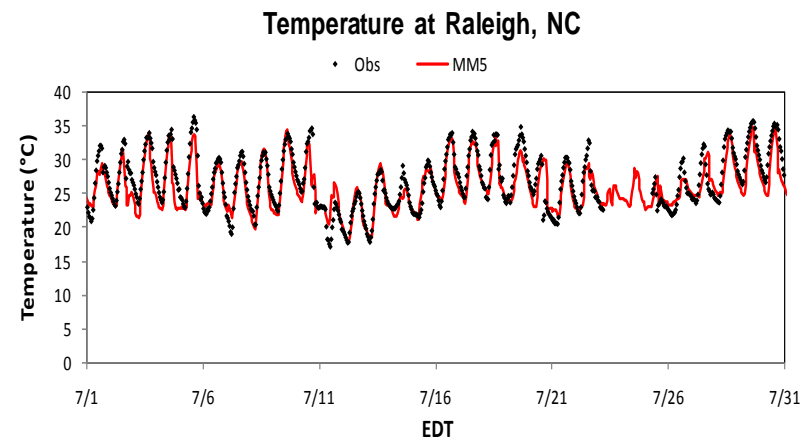
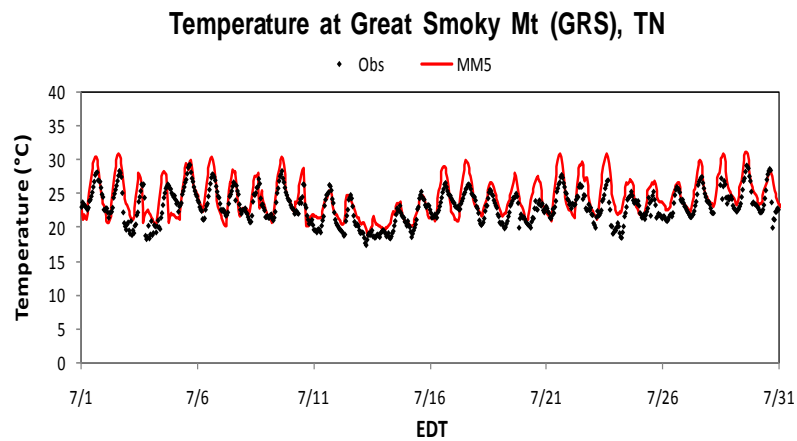
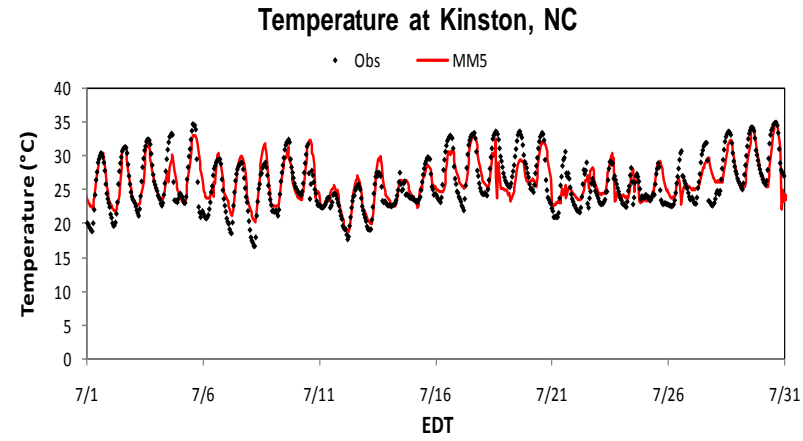
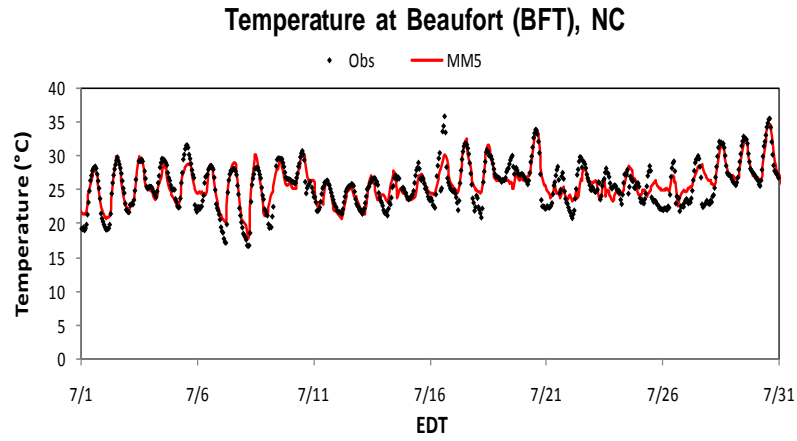


Figure 4.4. Temporal variation of temperatures at 2-m in July at Beaufort, NC (coastal), Kinston, NC (central), Great Smoky Mountains (mountain), TN, and Raleigh, NC (urban).

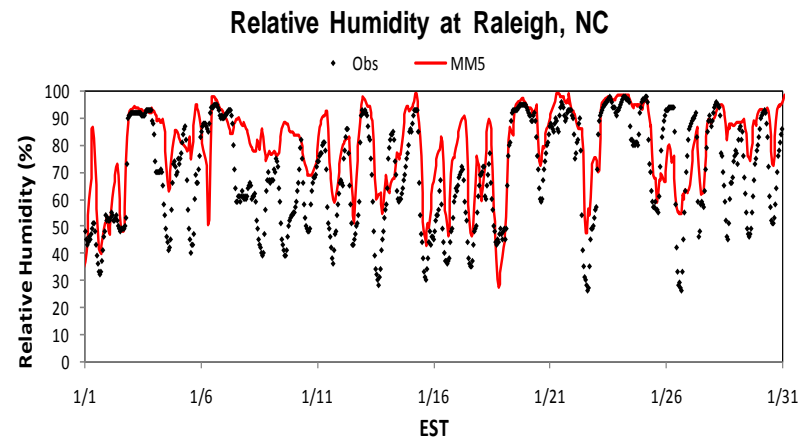
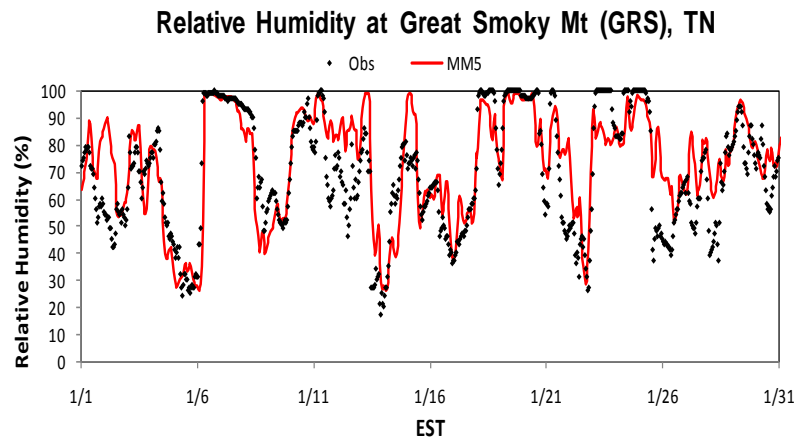
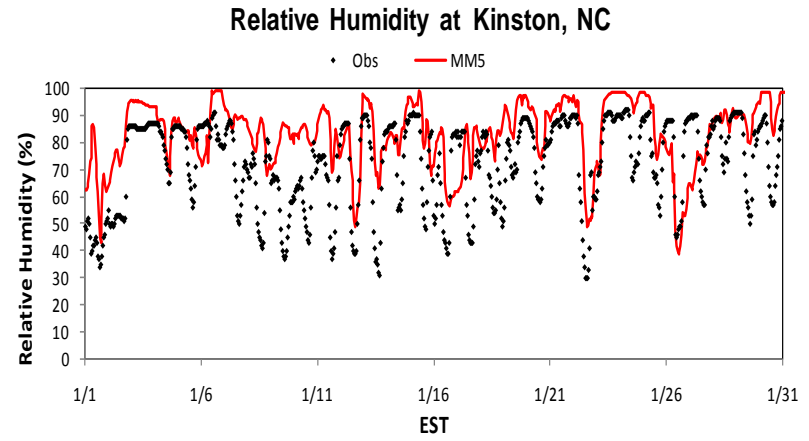
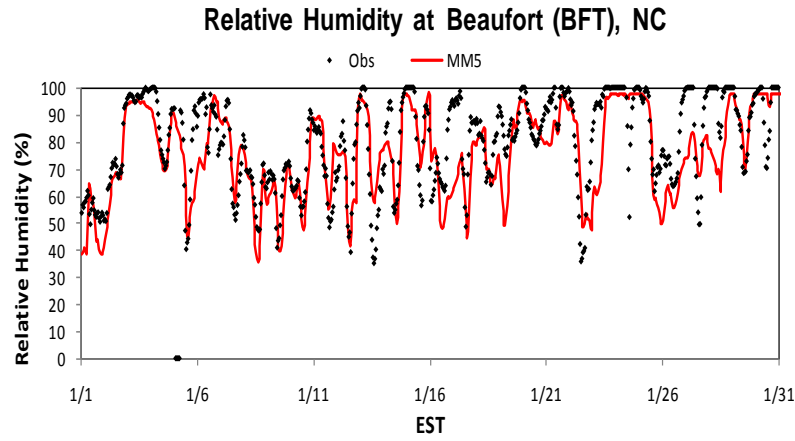


Figure 4.5. Temporal variation of relative humidity at 2-m in January at Beaufort, NC (coastal), Kinston, NC (central), Great Smoky Mountains (mountain), TN, and Raleigh, NC (urban).

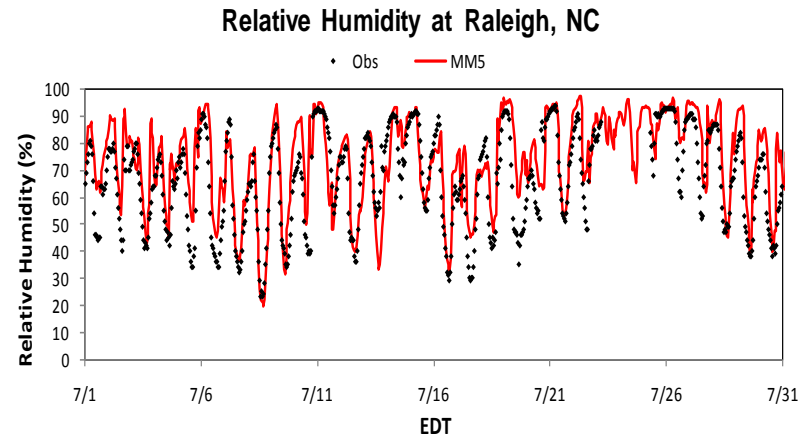
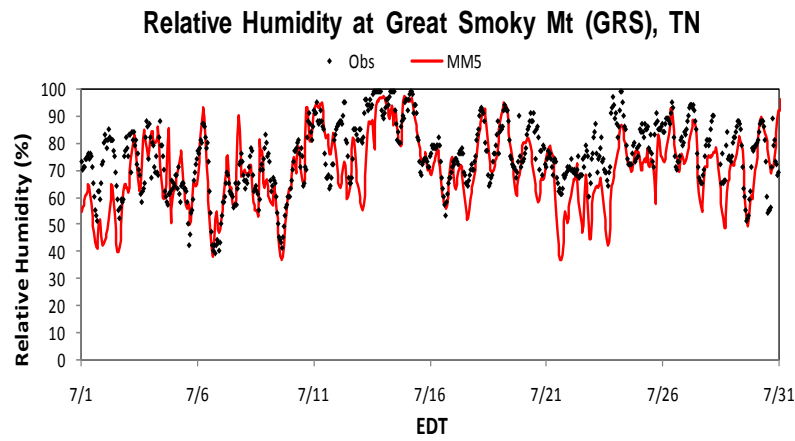
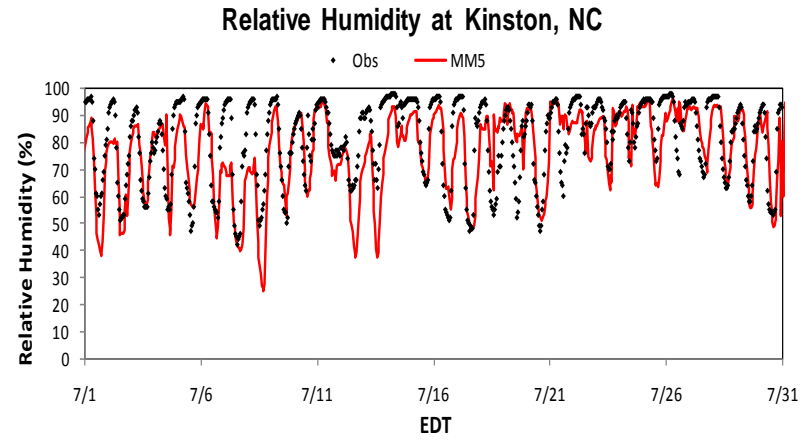
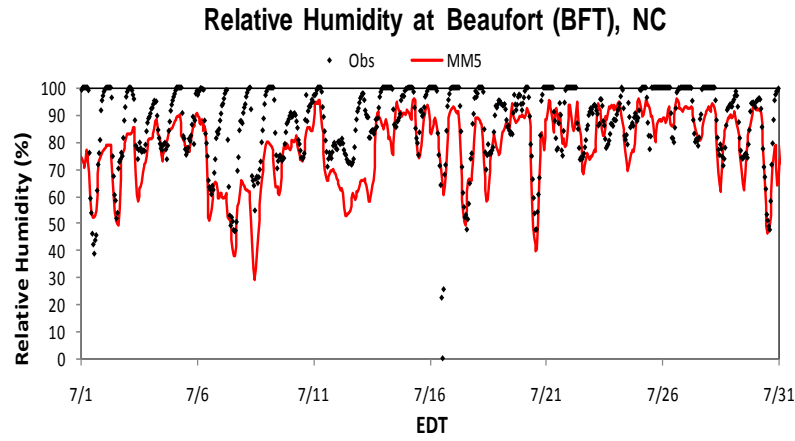


Figure 4.6. Temporal variation of relative humidity at 2-m in July at Beaufort, NC (coastal), Kinston, NC (central), Great Smoky Mountains (mountain), TN, and Raleigh, NC (urban).

the west because subsidence on the leeward side of the mountains creates a region of drier air. Raleigh is essentially in this transition zone, which can impact the model's performance.

The high variability of wind speed and direction makes it difficult for the model to reproduce the observations, as indicated in Figures 4.7 - 4.10. While the statistics indicate an overprediction of wind speed, Figures 4.7 and 4.8 show periods of over and underpredictions. In July (Figure 4.8), the peak wind speeds at Beaufort and Raleigh are overpredicted, while the calm winds at Kinston are underpredicted. Figure 4.9 shows relatively good agreement between the modeled and observed wind direction, particularly when there is a consistent wind pattern for the region (i.e., land-sea breeze at Beaufort; mountain-valley breeze at the Great Smoky Mountain site). In July (Figure 4.10) however, there is significantly more variation in the wind direction that the model is not able to accurately model. These variations will influence the transport of pollutants from their emission sources and are thus an important variable to be evaluated.

4.2 Chemical Concentrations of Gaseous and PM Species

The air quality models are also evaluated following the evaluation protocol discussed in Chapter 3. Tables 4.3 and 4.4 provide the statistics for several gaseous (i.e., O_3 , HNO_3 , SO_2 , CO , NO , and NO_2) and PM species (i.e., $PM_{2.5}$, NH_4^+ , SO_4^{2-} , NO_3^- , BC , OC , and total carbon ($TC = BC + OC$)) for January and July, respectively, for both CMAQ and CAMx. Maximum O_3 (1-hour and 8-hour) in January is overpredicted by both models ranging from +4.6% by CMAQ at the AIRS-AQS sites to +15.8% by CAMx at the CASTNET sites, with CAMx predicting higher values at both networks. One of the likely reasons for the overprediction in O_3 by both models is weaker vertical mixing and diffusion of the precursor species. As discussed in Chapter 2, the vertical mixing simulated by the models can be assessed by the model's ability to simulate slow-reacting species such as CO . The overprediction of CO by both models in Table 4.3 indicates that both CMAQ and CAMx may be simulating weaker vertical mixing than what is observed. The statistics also indicate that CAMx has weaker vertical mixing than CMAQ, with a much larger overprediction of CO . As mentioned, the weaker vertical mixing can trap the precursor species in the lower

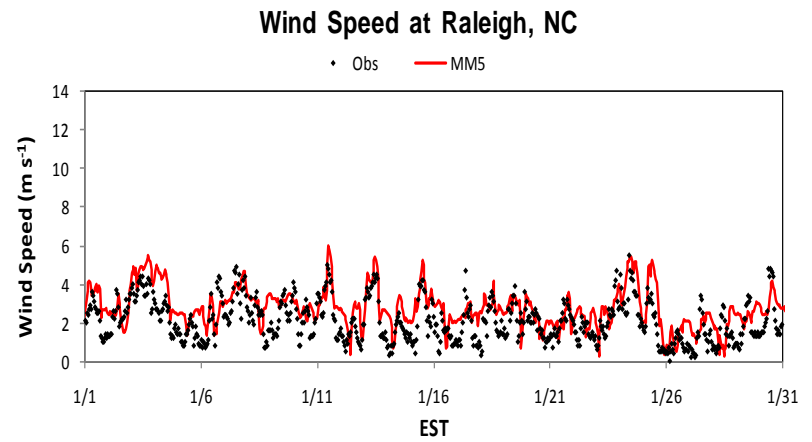
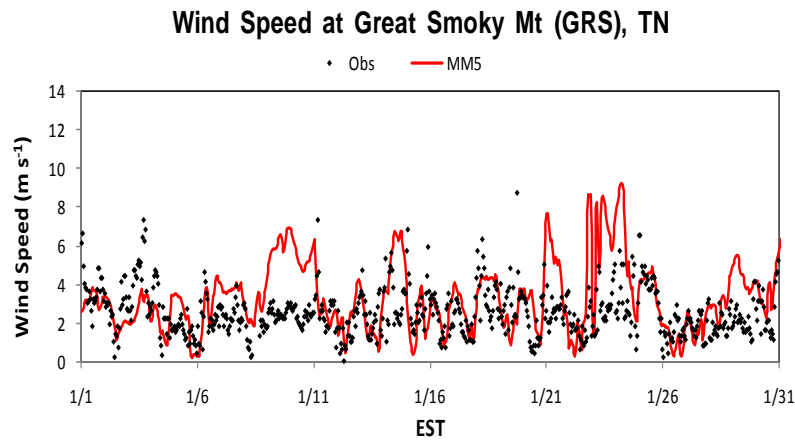
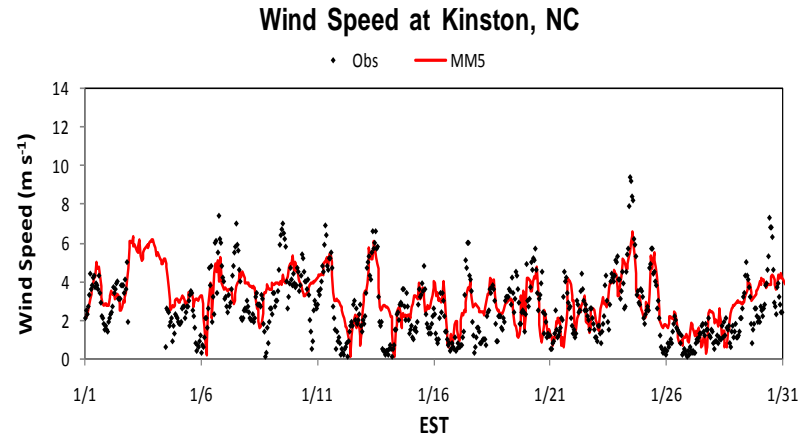
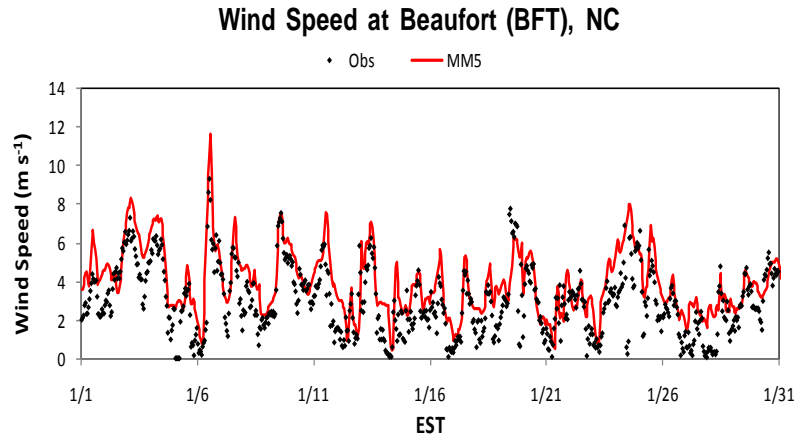


Figure 4.7. Temporal variation of wind speeds at 10-m in January at Beaufort, NC (coastal), Kinston, NC (central), Great Smoky Mountains (mountain), TN, and Raleigh, NC (urban).

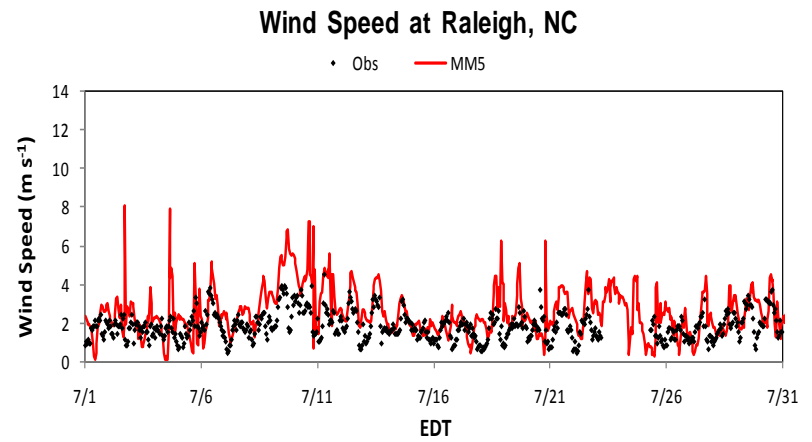
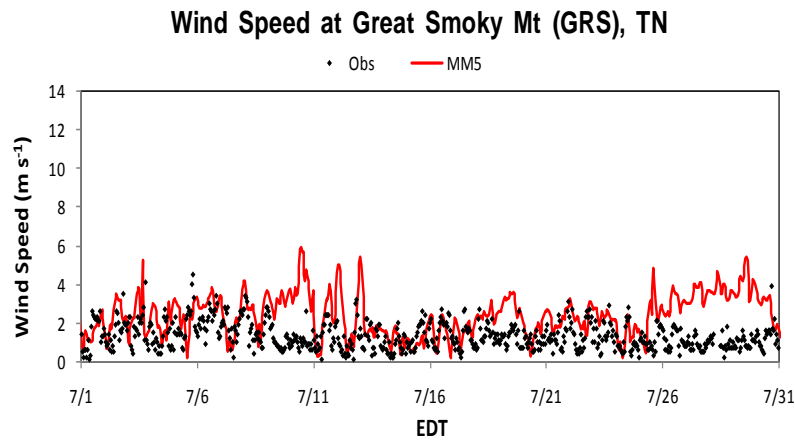
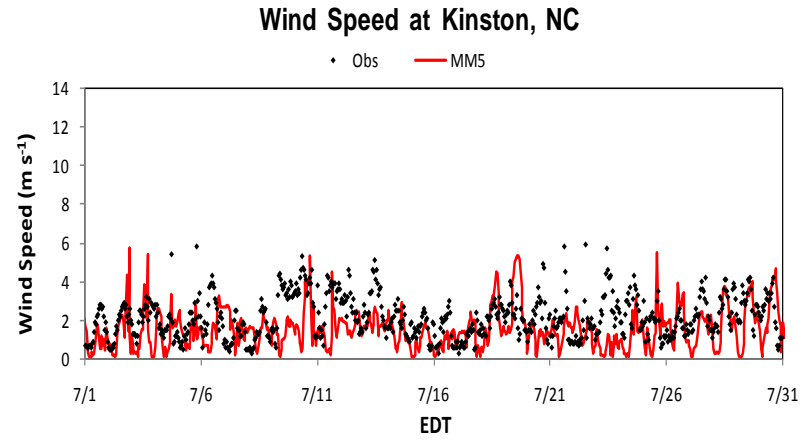
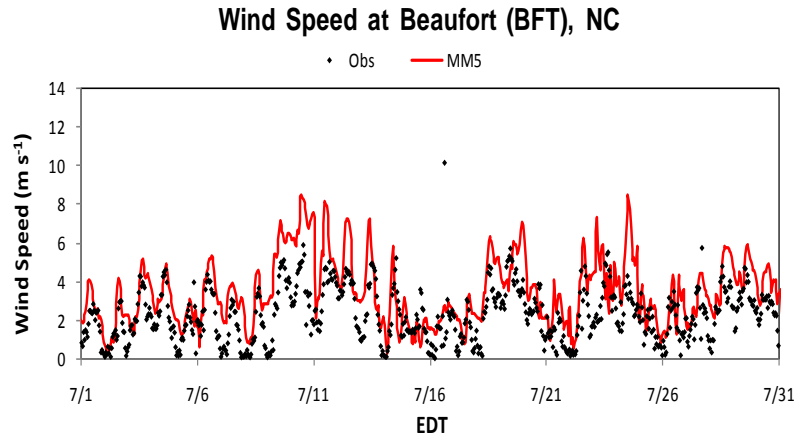


Figure 4.8. Temporal variation of wind speeds at 10-m in July at Beaufort, NC (coastal), Kinston, NC (central), Great Smoky Mountains (mountain), TN, and Raleigh, NC (urban).

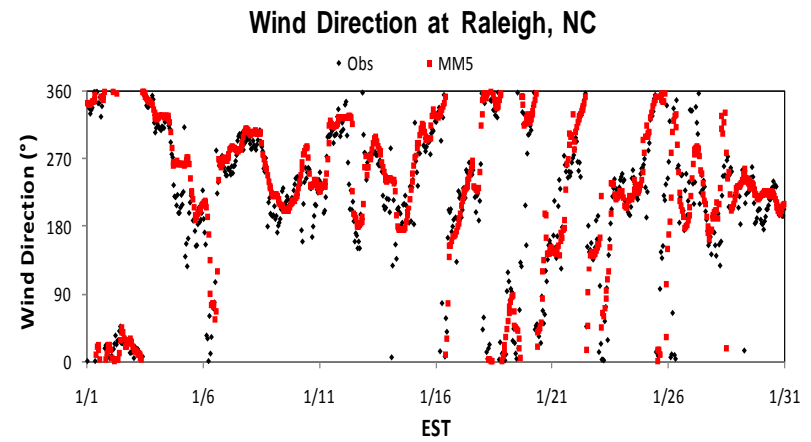
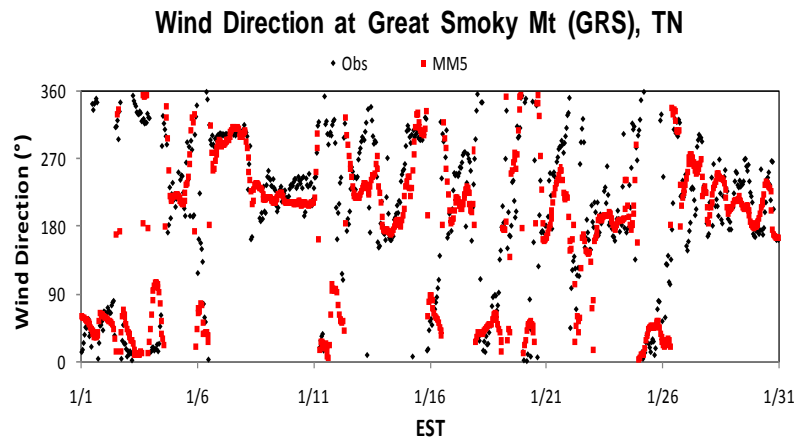
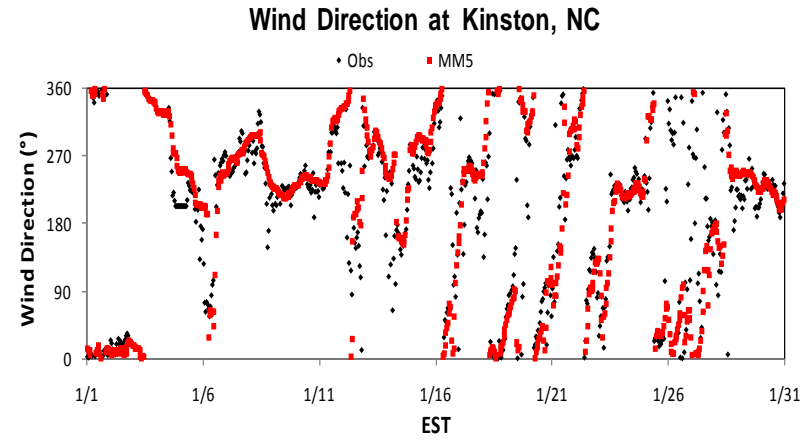
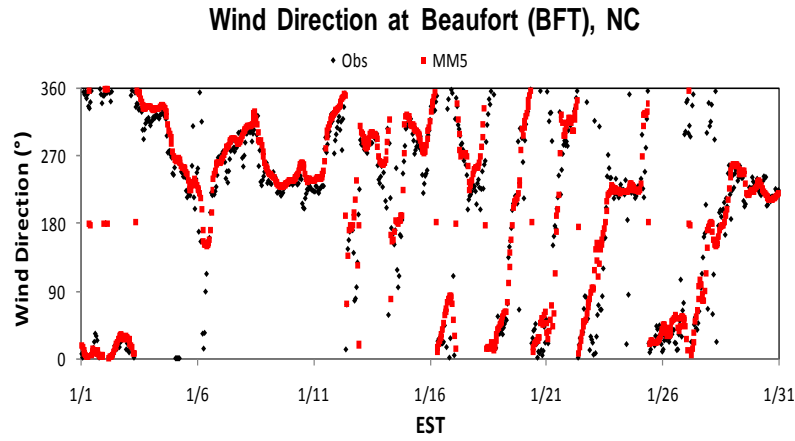


Figure 4.9. Temporal variation of wind direction at 10-m in January at Beaufort, NC (coastal), Kinston, NC (central), Great Smoky Mountains (mountain), TN, and Raleigh, NC (urban).

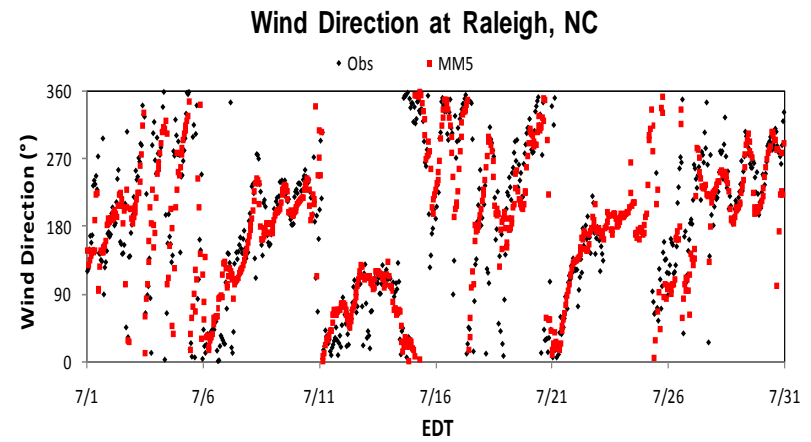
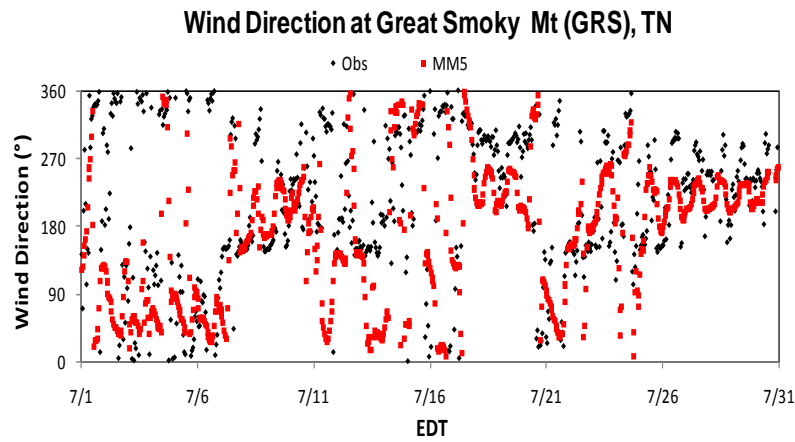
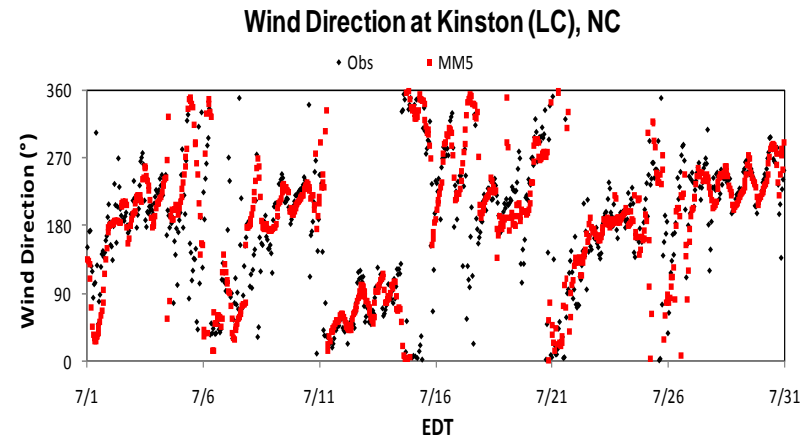
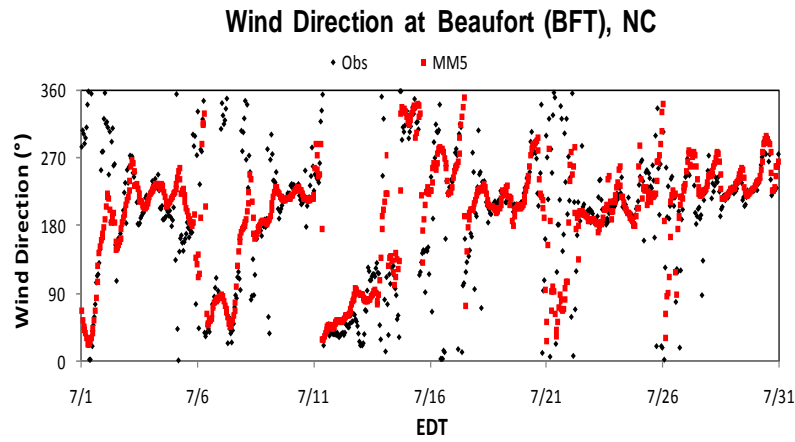


Figure 4.10. Temporal variation of wind direction at 10-m in July at Beaufort, NC (coastal), Kinston, NC (central), Great Smoky Mountains (mountain), TN, and Raleigh, NC (urban).

Table 4.3. Performance statistics for gaseous and PM species in January 2002.

Variable	1-hour max O ₃ (ppb)				8-hour max O ₃ (ppb)			
	AIRS-AQS		CASTNET		AIRS-AQS		CASTNET	
Network	CMAQ	CAMx	CMAQ	CAMx	CMAQ	CAMx	CMAQ	CAMx
Model	CMAQ	CAMx	CMAQ	CAMx	CMAQ	CAMx	CMAQ	CAMx
Number	384		301		384		301	
MeanObs	37.00		37.00		32.00		34.00	
MeanMod	39.00	41.00	41.00	42.00	35.00	36.00	38.00	39.00
NMB	0.05	0.10	0.09	0.12	0.09	0.12	0.13	0.16
NME	0.18	0.21	0.15	0.18	0.21	0.23	0.19	0.21
corr	0.53	0.54	0.66	0.66	0.56	0.58	0.63	0.64
MB	0.00	0.00	0.00	0.01	0.00	0.00	0.00	0.01
MAGE	0.01	0.01	0.01	0.01	0.01	0.01	0.01	0.01
RMSE	0.01	0.01	0.01	0.01	0.01	0.01	0.01	0.01
MNB	0.10	0.15	0.11	0.14	0.16	0.18	0.17	0.20
MNGE	0.22	0.25	0.17	0.19	0.26	0.28	0.23	0.25
FB	0.05	0.09	0.08	0.11	0.10	0.11	0.12	0.14
FGE	0.19	0.21	0.15	0.17	0.21	0.24	0.19	0.20
NMFB	0.05	0.10	0.09	0.12	0.09	0.11	0.12	0.15
NMFGE	0.18	0.20	0.15	0.17	0.20	0.22	0.18	0.19
MNFB	0.08	0.11	0.10	0.13	0.14	0.13	0.17	0.19
MNGFE	0.25	0.29	0.18	0.20	0.28	0.32	0.24	0.26
NMBF	0.05	0.10	0.09	0.12	0.09	0.12	0.13	0.16
NMEF	0.18	0.21	0.15	0.18	0.21	0.23	0.19	0.21
Variable	CO (ppb)		NO (ppb)		NO ₂ (ppb)			
Network	SEARCH		SEARCH		SEARCH			
Model	CMAQ	CAMx	CMAQ	CAMx	CMAQ	CAMx		
Number	1377		1408		1343			
MeanObs	416.09		20.55		12.1			
MeanMod	502.55	775.74	7.99	20.12	19.05	21.77		
NMB	0.21	0.86	-0.61	-0.02	0.58	0.80		
NME	0.64	1.01	0.93	1.06	0.73	0.92		
corr	0.47	0.57	0.2	0.38	0.68	0.69		
MB	86.46	359.66	-12.56	-0.43	6.95	9.67		
MAGE	264.47	421.77	19.16	21.71	8.78	11.14		
RMSE	498.41	744.26	53.22	53.00	12.99	16.79		
MNB	0.56	1.11	1.01	2.95	1.19	1.37		
MNGE	0.68	1.14	1.76	3.95	1.31	1.48		
FB	0.28	0.52	-0.28	-0.58	0.41	0.48		
FGE	0.43	0.55	0.94	1.27	0.57	0.62		
NMFB	0.19	0.60	-0.88	-0.02	0.45	0.57		
NMFGE	0.58	0.71	1.34	1.07	0.56	0.66		
MNFB	0.50	1.10	-7.34	Inf	1.13	1.32		
MNGFE	0.74	1.15	10.11	Inf	1.37	1.53		
NMBF	0.21	0.86	-1.57	-0.02	0.58	0.80		
NMEF	0.64	1.01	2.40	1.08	0.73	0.92		

Table 4.3. Continued.

Variable	HNO ₃ (µg m ⁻³)				SO ₂ (µg m ⁻³)			
	CAST		SEARCH		CAST		SEARCH	
Model	CMAQ	CAMx	CMAQ	CAMx	CMAQ	CAMx	CMAQ	CAMx
Number	39		1390		39		1340	
MeanObs	1.64		0.63		6.80		5.24	
MeanMod	2.38	1.64	0.75	0.52	9.01	9.66	5.62	6.84
NMB	0.45	0.00	0.19	-0.18	0.33	0.42	0.07	0.31
NME	0.51	0.37	0.96	0.80	0.33	0.42	0.70	0.82
corr	0.23	0.18	0.24	0.22	0.92	0.91	0.51	0.47
MB	0.74	0.00	0.12	-0.11	2.21	2.86	0.37	1.60
MAGE	0.83	0.61	0.61	0.50	2.25	2.86	3.66	4.31
RMSE	1.12	0.76	0.83	0.67	2.85	3.34	6.28	7.20
MNB	0.74	0.22	2.4	1.40	0.55	0.76	7.25	10.97
MNGE	0.78	0.49	2.96	2.03	0.56	0.76	7.54	11.20
FB	0.40	0.06	0.06	-0.07	0.35	0.44	0.30	0.44
FGE	0.44	0.38	0.99	0.94	0.35	0.44	0.72	0.77
NMFB	0.37	0.00	0.17	-0.19	0.28	0.35	0.07	0.27
NMFGE	0.41	0.37	0.88	0.87	0.29	0.35	0.67	0.71
MNFB	0.74	0.15	Inf	-1.30	0.55	0.76	6.80	10.70
MNGFE	0.78	0.56	Inf	4.73	0.56	0.76	7.99	11.48
NMBF	0.45	0.00	0.19	-0.21	0.33	0.42	0.07	0.31
NMEF	0.51	0.37	0.96	0.97	0.33	0.42	0.70	0.82
Variable	PM _{2.5} (µg m ⁻³)				NH ₄ ⁺ (µg m ⁻³)			
Network	IMPROVE		STN		CASTNET		STN	
Model	CMAQ	CAMx	CMAQ	CAMx	CMAQ	CAMx	CMAQ	CAMx
Number	49		76		39		79	
MeanObs	6.08		12.44		0.99		1.11	
MeanMod	6.91	7.23	14.80	16.52	0.92	0.91	1.76	1.75
NMB	0.14	0.19	0.19	0.33	-0.07	-0.08	0.59	0.58
NME	0.30	0.29	0.38	0.48	0.25	0.25	0.81	0.77
corr	0.80	0.68	0.35	0.23	0.75	0.74	0.02	-0.05
MB	0.84	1.16	2.36	4.08	-0.07	-0.08	0.66	0.65
MAGE	1.80	1.78	4.67	6.02	0.25	0.24	0.89	0.85
RMSE	2.41	3.03	5.86	8.05	0.31	0.31	1.08	1.12
MNB	0.24	0.34	0.25	0.42	-0.04	-0.04	0.89	0.91
MNGE	0.42	0.43	0.41	0.55	0.26	0.25	1.02	1.02
FB	0.10	0.17	0.14	0.23	-0.08	-0.08	0.43	0.41
FGE	0.32	0.27	0.34	0.39	0.25	0.25	0.60	0.56
NMFB	0.13	0.17	0.17	0.28	-0.07	-0.08	0.46	0.45
NMFGE	0.28	0.27	0.34	0.42	0.26	0.26	0.62	0.60
MNFB	0.17	0.33	0.20	0.39	-0.09	-0.09	0.83	0.86
MNGFE	0.49	0.44	0.47	0.59	0.31	0.30	1.08	1.07
NMBF	0.14	0.19	0.19	0.33	-0.07	-0.09	0.59	0.58
NMEF	0.30	0.29	0.38	0.48	0.27	0.27	0.81	0.77

Table 4.3. Continued.

Variable	SO ₄ ²⁻ (µg m ⁻³)					
Network	IMPROVE		CASTNET		STN	
Model	CMAQ	CAMx	CMAQ	CAMx	CMAQ	CAMx
Number	49		39		79	
MeanObs	2.11		2.28		2.87	
MeanMod	2.22	2.81	1.86	2.30	2.58	3.27
NMB	0.05	0.33	-0.18	0.01	-0.10	0.14
NME	0.32	0.48	0.23	0.24	0.39	0.47
corr	0.69	0.55	0.58	0.34	0.29	0.20
MB	0.11	0.70	-0.41	0.02	-0.30	0.39
MAGE	0.68	1.01	0.52	0.54	1.13	1.36
RMSE	1.00	1.77	0.66	0.68	1.56	2.11
MNB	0.17	0.51	-0.14	0.07	-0.01	0.27
MNGE	0.41	0.64	0.21	0.25	0.39	0.53
FB	0.04	0.23	-0.18	0.03	-0.12	0.08
FGE	0.33	0.38	0.24	0.23	0.38	0.39
NMFB	0.05	0.29	-0.20	0.01	-0.11	0.13
NMFGE	0.31	0.41	0.25	0.23	0.41	0.44
MNFB	0.10	0.48	-0.23	0.04	-0.16	0.20
MNGFE	0.48	0.66	0.29	0.29	0.54	0.61
NMBF	0.05	0.33	-0.22	0.01	-0.12	0.14
NMEF	0.32	0.48	0.28	0.24	0.44	0.47
Variable	NO ₃ ⁻ (µg m ⁻³)					
Network	IMPROVE		IMPROVE		IMPROVE	
Model	CMAQ	CMAQ	CMAQ	CMAQ	CMAQ	CMAQ
Number	49		39		79	
MeanObs	0.55		1.30		1.55	
MeanMod	0.80	0.43	1.32	1.02	3.15	2.40
NMB	0.46	-0.21	0.02	-0.22	1.04	0.55
NME	1.05	0.68	0.55	0.53	1.27	0.95
corr	0.75	0.75	0.62	0.66	0.30	0.25
MB	0.25	-0.12	0.02	-0.28	1.60	0.86
MAGE	0.57	0.37	0.71	0.69	1.97	1.48
RMSE	0.94	0.48	0.99	0.95	2.62	1.97
MNB	0.53	-0.11	0.49	0.05	1.38	0.81
MNGE	1.31	0.98	0.84	0.63	1.61	1.22
FB	-0.33	-0.78	0.12	-0.23	0.46	0.14
FGE	1.04	1.15	0.59	0.63	0.78	0.79
NMFB	0.37	-0.24	0.02	-0.24	0.68	0.43
NMFGE	0.86	0.76	0.54	0.59	0.84	0.75
MNFB	Inf	-450.96	0.30	-0.62	0.40	-69.53
MNGFE	Inf	451.83	1.03	1.30	2.59	71.56
NMBF	0.46	-0.27	0.02	-0.28	1.04	0.55
NMEF	1.05	0.87	0.55	1.30	1.27	1.55

Table 4.3. Continued.

Variable	BC ($\mu\text{g m}^{-3}$)		OC ($\mu\text{g m}^{-3}$)		TC ($\mu\text{g m}^{-3}$)	
Network	IMPROVE		IMPROVE		STN	
Model	CMAQ	CAMx	CMAQ	CAMx	CMAQ	CAMx
Number	49		49		79	
MeanObs	0.33		1.42		6.92	
MeanMod	0.30	0.34	1.21	1.17	3.48	4.25
NMB	-0.09	0.05	-0.15	-0.18	-0.50	-0.39
NME	0.33	0.36	0.31	0.33	0.52	0.49
corr	0.70	0.69	0.81	0.77	0.49	0.43
MB	-0.03	0.02	-0.21	-0.25	-3.44	-2.67
MAGE	0.11	0.12	0.44	0.47	3.63	3.40
RMSE	0.14	0.16	0.59	0.65	4.55	4.20
MNB	-0.01	0.15	0.00	-0.02	-0.40	-0.28
MNGE	0.42	0.43	0.43	0.40	0.47	0.47
FB	-0.17	0.01	-0.17	-0.15	-0.60	-0.46
FGE	0.41	0.34	0.41	0.37	0.65	0.61
NMFB	-0.10	0.04	-0.16	-0.20	-0.66	-0.48
NMFGE	0.35	0.35	0.34	0.36	0.70	0.61
MNFB	-0.36	0.07	-0.26	-0.16	-1.24	-0.93
MNGFE	0.77	0.51	0.69	0.55	1.30	1.13
NMBF	-0.10	0.05	-0.18	-0.22	-0.99	-0.63
NMEF	0.37	0.36	0.36	0.40	1.04	0.80

TC: Total Carbon = BC + OC

Table 4.4. Performance statistics for gaseous and PM species in July 2002.

Variable	1-hour max O ₃ (ppb)				8-hour max O ₃ (ppb)			
	AIRS-AQS		CASTNET		AIRS-AQS		CASTNET	
Network	CMAQ	CAMx	CMAQ	CAMx	CMAQ	CAMx	CMAQ	CAMx
Model	CMAQ	CAMx	CMAQ	CAMx	CMAQ	CAMx	CMAQ	CAMx
Number	3216		300		3215		300	
MeanObs	71.05		65.54		62.65		58.39	
MeanMod	62.08	68.79	59.79	64.90	56.33	62.97	55.66	60.61
NMB	-0.13	-0.03	-0.09	-0.01	-0.10	0.01	-0.05	0.04
NME	0.17	0.16	0.15	0.14	0.16	0.17	0.15	0.15
corr	0.70	0.57	0.69	0.64	0.70	0.56	0.69	0.64
MB	-8.97	-2.26	-5.75	-0.64	-6.32	0.33	-2.73	2.23
MAGE	12.20	11.55	9.49	8.96	10.17	10.42	8.46	8.98
RMSE	15.60	16.53	12.49	12.04	13.07	14.90	11.10	11.76
MNB	Inf	Inf	-0.07	0.02	-0.07	0.04	-0.01	0.08
MNGE	Inf	Inf	0.14	0.14	0.16	0.18	0.15	0.18
FB	-0.12	-0.04	-0.08	0.00	-0.09	0.00	-0.03	0.05
FGE	0.18	0.18	0.15	0.14	0.17	0.19	0.15	0.16
NMFB	-0.14	-0.03	-0.09	-0.01	-0.11	0.01	-0.05	0.04
NMFGE	0.18	0.17	0.15	0.14	0.17	0.17	0.15	0.15
MNFB	Inf	NaN	-0.09	0.00	-0.11	Inf	-0.03	0.07
MNGFE	Inf	Inf	0.17	0.16	0.20	Inf	0.17	0.19
NMBF	-0.15	-0.03	-0.10	-0.01	-0.11	0.01	-0.05	0.04
NMEF	0.20	0.17	0.16	0.14	0.18	0.17	0.15	0.15
Variable	CO (ppb)		NO (ppb)		NO ₂ (ppb)			
Network	SEARCH		SEARCH		SEARCH			
Model	CMAQ	CAMx	CMAQ	CAMx	CMAQ	CAMx		
Number	1374		1351		1088			
MeanObs	259.82		3.89		10.17			
MeanMod	308.83	441.41	1.72	4.58	14.19	17.03		
NMB	0.19	0.70	-0.56	0.18	0.40	0.67		
NME	0.44	0.78	0.82	1.04	0.66	0.83		
corr	0.67	0.73	0.55	0.61	0.71	0.79		
MB	49.02	181.50	-2.17	0.69	4.02	6.86		
MAGE	114.39	203.19	3.21	4.07	6.74	8.42		
RMSE	174.19	369.86	10.25	10.90	10.66	14.60		
MNB	0.21	0.60	1.04	13.10	2.08	1.97		
MNGE	0.47	0.69	1.89	14.03	2.29	2.16		
FB	0.06	0.31	-0.42	-0.50	0.32	0.36		
FGE	0.38	0.41	1.09	1.18	0.60	0.61		
NMFB	0.17	0.52	-0.77	0.16	0.33	0.50		
NMFGE	0.40	0.58	1.14	0.96	0.55	0.62		
MNFB	Inf	0.58	Inf	Inf	Inf	1.85		
MNGFE	Inf	0.71	Inf	Inf	Inf	2.27		
NMBF	0.19	0.70	-1.26	0.18	0.40	0.67		
NMEF	0.44	0.78	1.86	1.04	0.66	0.83		

Table 4.4. Continued.

Variable	HNO ₃ (µg m ⁻³)				SO ₂ (µg m ⁻³)			
	CAST		SEARCH		CAST		SEARCH	
Model	CMAQ	CAMx	CMAQ	CAMx	CMAQ	CAMx	CMAQ	CAMx
Number	40		1365		40		1368	
MeanObs	2.10		1.27		2.95		2.96	
MeanMod	2.16	1.75	1.00	1.01	4.19	4.18	4.16	4.52
NMB	0.03	-0.17	-0.21	-0.21	0.42	0.42	0.41	0.53
NME	0.27	0.29	0.56	0.58	0.58	0.56	1.11	1.22
corr	0.78	0.76	0.53	0.55	0.82	0.83	0.36	0.32
MB	0.06	-0.35	-0.27	-0.26	1.25	1.23	1.20	1.56
MAGE	0.56	0.61	0.71	0.74	1.70	1.65	3.27	3.62
RMSE	0.77	0.73	1.08	1.11	2.10	2.05	6.19	6.50
MNB	0.10	-0.09	0.24	0.21	1.34	1.24	3.49	3.81
MNGE	0.33	0.32	0.87	0.88	1.40	1.30	3.73	4.03
FB	0.02	-0.17	-0.25	-0.30	0.55	0.55	0.54	0.59
FGE	0.28	0.34	0.67	0.71	0.63	0.62	0.90	0.93
NMFB	0.03	-0.18	-0.24	-0.23	0.35	0.35	0.34	0.42
NMFGE	0.27	0.32	0.62	0.65	0.48	0.46	0.92	0.97
MNFB	0.06	-0.22	Inf	-0.74	1.32	1.22	Inf	3.26
MNGFE	0.37	0.45	Inf	1.83	1.42	1.32	Inf	4.58
NMBF	0.03	-0.20	-0.27	-0.26	0.42	0.42	0.41	0.53
NMEF	0.27	0.35	0.71	0.74	0.58	0.56	1.11	1.22
Variable	PM _{2.5} (µg m ⁻³)							
Network	IMPROVE		STN					
Model	CMAQ	CAMx	CMAQ	CAMx				
Number	55		127					
MeanObs	15.77		19.26					
MeanMod	6.66	9.91	9.71	13.09				
NMB	-0.58	-0.37	-0.50	-0.32				
NME	0.60	0.46	0.51	0.37				
corr	0.45	0.51	0.48	0.66				
MB	-9.11	-5.86	-9.55	-6.17				
MAGE	9.46	7.28	9.85	7.17				
RMSE	11.84	9.47	11.79	8.51				
MNB	-0.52	-0.29	-0.45	-0.28				
MNGE	0.56	0.45	0.48	0.36				
FB	-0.80	-0.45	-0.66	-0.38				
FGE	0.83	0.57	0.68	0.44				
NMFB	-0.81	-0.46	-0.66	-0.38				
NMFGE	0.84	0.57	0.68	0.44				
MNFB	-2.04	-0.82	-1.67	-0.55				
MNGFE	2.07	0.98	1.69	0.63				
NMBF	-1.37	-0.59	-0.98	-0.47				
NMEF	1.42	0.73	1.01	0.55				

Table 4.4. Continued.

Variable	NH_4^+ ($\mu\text{g m}^{-3}$)					
Network	IMPROVE		CASTNET		STN	
Model	CMAQ	CAMx	CMAQ	CAMx	CMAQ	CAMx
Number	9		40		135	
MeanObs	1.67		2.29		2.01	
MeanMod	0.71	0.87	1.09	1.27	1.18	1.49
NMB	-0.57	-0.48	-0.52	-0.45	-0.41	-0.26
NME	0.60	0.52	0.52	0.46	0.50	0.36
corr	0.58	0.90	0.73	0.71	0.39	0.63
MB	-0.95	-0.79	-1.20	-1.02	-0.83	-0.51
MAGE	1.00	0.87	1.20	1.05	1.00	0.72
RMSE	1.20	1.05	1.37	1.21	1.35	1.02
MNB	-0.43	-0.29	-0.49	-0.40	-0.28	-0.15
MNGE	0.54	0.46	0.49	0.43	0.47	0.35
FB	-0.66	-0.45	-0.52	-0.54	-0.48	-0.25
FGE	0.75	0.59	0.52	0.57	0.61	0.41
NMFB	-0.80	-0.62	-0.68	-0.58	-0.52	-0.29
NMFGE	0.85	0.68	0.68	0.59	0.63	0.41
MNFB	-1.34	-0.77	-0.71	-0.86	-1.61	-0.44
MNGFE	1.45	0.94	0.71	0.89	1.79	0.65
NMBF	-1.34	-0.90	-1.17	-0.81	-0.70	-0.34
NMEF	1.41	0.99	1.17	0.83	0.85	0.48
Variable	SO_4^{2-} ($\mu\text{g m}^{-3}$)					
Network	IMPROVE		CASTNET		STN	
Model	CMAQ	CAMx	CMAQ	CAMx	CMAQ	CAMx
Number	56		40		135	
MeanObs	7.12		8.32		7.16	
MeanMod	4.34	6.51	6.33	8.27	4.70	6.85
NMB	-0.39	-0.09	-0.24	-0.01	-0.34	-0.04
NME	0.50	0.40	0.27	0.18	0.44	0.30
corr	0.49	0.56	0.70	0.75	0.54	0.68
MB	-2.78	-0.61	-1.99	-0.05	-2.46	-0.31
MAGE	3.57	2.86	2.24	1.52	3.18	2.18
RMSE	4.99	4.35	2.91	1.91	4.24	3.12
MNB	-0.31	0.03	-0.23	0.04	-0.29	0.00
MNGE	0.45	0.44	0.26	0.20	0.43	0.32
FB	-0.39	-0.09	-0.24	-0.01	-0.34	-0.04
FGE	0.50	0.40	0.27	0.18	0.44	0.30
NMFB	-0.50	-0.11	-0.29	0.01	-0.46	-0.08
NMFGE	0.61	0.42	0.33	0.20	0.56	0.31
MNFB	-0.49	-0.09	-0.27	-0.01	-0.41	-0.04
MNGFE	0.62	0.42	0.31	0.18	0.54	0.31
NMBF	-1.19	-0.18	-0.43	0.00	-1.48	-0.10
NMEF	1.33	0.64	0.46	0.24	1.61	0.42

Table 4.4. Continued.

Variable	NO₃⁻ (µg m⁻³)					
Network	IMPROVE		CASTNET		STN	
Model	CMAQ	CAMx	CMAQ	CAMx	CMAQ	CAMx
Number	56		40		135	
MeanObs	0.23		0.22		0.69	
MeanMod	0.09	0.05	0.06	0.03	0.09	0.05
NMB	-0.62	-0.80	-0.73	-0.89	-0.87	-0.93
NME	1.07	0.99	0.90	0.93	0.87	0.93
corr	0.19	0.18	0.02	-0.10	0.14	0.30
MB	-0.14	-0.18	-0.16	-0.19	-0.60	-0.64
MAGE	0.24	0.23	0.19	0.20	0.60	0.64
RMSE	0.34	0.28	0.35	0.37	0.74	0.76
MNB	-0.69	-0.85	-0.39	-0.71	-0.85	-0.93
MNGE	1.03	0.99	0.91	0.85	0.85	0.93
FB	-1.59	-1.74	-1.03	-1.40	-1.56	-1.76
FGE	1.73	1.79	1.29	1.49	1.56	1.76
NMFB	-0.89	-1.34	-1.16	-1.59	-1.54	-1.73
NMFGE	1.55	1.66	1.42	1.66	1.54	1.73
MNFB	Inf	-3192.27	-29.86	-67.86	Inf	-544.48
MNGFE	Inf	3192.41	30.38	68.00	Inf	544.48
NMBF	-1.62	-4.07	-2.77	-7.74	-6.62	-13.06
NMEF	2.80	5.04	3.38	8.09	6.62	13.06
Variable	BC (µg m⁻³)		OC (µg m⁻³)		TC (µg m⁻³)	
Network	IMPROVE		IMPROVE		STN	
Model	CMAQ	CAMx	CMAQ	CAMx	CMAQ	CAMx
Number	43		43		134	
MeanObs	0.29		2.27		7.15	
MeanMod	0.16	0.20	0.62	1.22	1.91	2.85
NMB	-0.47	-0.33	-0.73	-0.47	-0.73	-0.60
NME	0.63	0.58	0.76	0.52	0.75	0.63
corr	0.39	0.35	0.73	0.70	0.37	0.41
MB	-0.14	-0.10	-1.65	-1.06	-5.24	-4.30
MAGE	0.18	0.17	1.72	1.19	5.33	4.48
RMSE	0.22	0.21	2.10	1.71	6.07	5.24
MNB	0.09	0.30	-0.69	-0.37	-0.62	-0.42
MNGE	1.08	1.08	0.77	0.50	0.77	0.69
FB	-0.66	-0.44	-1.20	-0.57	-1.11	-0.78
FGE	0.81	0.67	1.25	0.67	1.18	0.88
NMFB	-0.61	-0.39	-1.14	-0.61	-1.16	-0.86
NMFGE	0.82	0.70	1.19	0.68	1.18	0.90
MNFB	-1.13	-0.38	-4.68	-1.21	-4.81	-1.69
MNGFE	2.30	1.76	4.76	1.34	4.97	1.97
NMBF	-0.87	-0.49	-2.64	-0.87	-2.75	-1.51
NMEF	1.18	0.86	2.76	0.98	2.80	1.57

layers, making them more readily available for secondary pollutant formation. This effect also influences the formation of $PM_{2.5}$. Table 4.3 shows an overprediction of $PM_{2.5}$ by both models in January, ranging from +13.8% by CMAQ at the IMPROVE sites to +32.8% by CAMx at the STN sites. While some of the overprediction of $PM_{2.5}$ may be influenced by the weaker vertical mixing, the statistics of the individual species show varying performance ability by both models. For example, while SO_4^{2-} is underpredicted by CMAQ at the CASTNET and STN sites, it is overpredicted by CAMx, and just the opposite is true for NO_3^- at the IMPROVE and CASTNET sites. This varying performance of $PM_{2.5}$ species may indicate that other differences between the models, such as removal through wet and dry deposition, are more influential than vertical mixing alone. The performance of carbon species (i.e., BC, OC, and total carbon (TC = BC + OC)) is kept separate by networks because of the different methods used to distinguish OC and BC. STN uses a Thermal Optical Transmittance (TOT) method (U.S. EPA, 1999), while IMPROVE and SEARCH use a Thermal Optical Reflectance (TOR) method (Hansen et al., 2003; Yu et al., 2004, 2007). The results for January and July indicate that CAMx predicts higher BC, OC, and TC than CMAQ. This may be due to the weaker vertical mixing in CAMx or the additional formation of SOA from condensable gases that is not simulated in CMAQ. Additionally, while observational data are not available for the wet or dry deposition of carbon species, the removal of inorganic species is overpredicted by CMAQ and underpredicted by CAMx (to be discussed in detail in Section 4.3) which may indicate that the differences in OC performance between the models may also be due to removal processes.

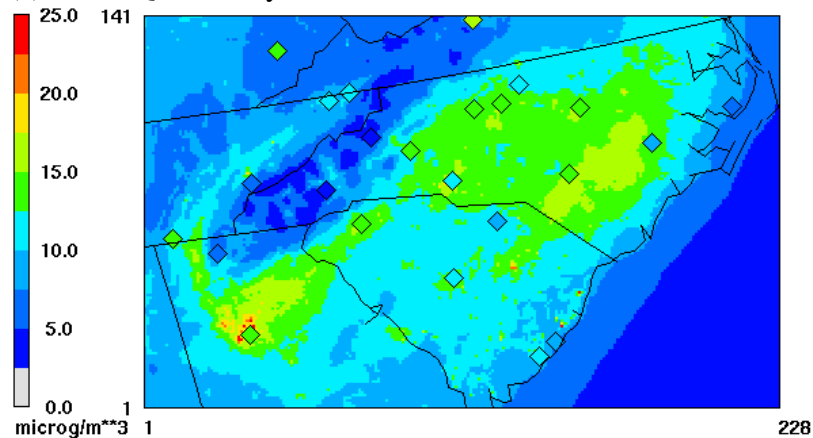
In July, when O_3 and $PM_{2.5}$ levels are more of a concern, both models underpredict both pollutants (Table 4.4). CO is again overpredicted by both models; however, the weaker vertical mixing has much less impact in July than it does in January. In July, all $PM_{2.5}$ components are underpredicted at all sites by both models. This underprediction can be due to wet and/or dry deposition (to be discussed in Section 4.3) and uncertainties in emissions. While both models underpredict SO_4^{2-} , the precursor, SO_2 , is overpredicted by both models, indicating that the oxidation of SO_2 to SO_4^{2-} may be underpredicted. The worst performance in July is for NO_3^- because of uncertainties in the emissions of its precursors and the

complexity of NO_3^- formation due to its volatility (Zhang et al., 2006c). However, NO_3^- is also the smallest component of $\text{PM}_{2.5}$ in the summer, so the underpredicted NO_3^- mass has little impact on the underprediction of total $\text{PM}_{2.5}$.

Figure 4.11 shows the spatial distribution of $\text{PM}_{2.5}$ as simulated by CMAQ and CAMx in January and July overlaid with observations. The spatial distributions in both months show that CAMx predicts higher values than CMAQ, as also indicated in the statistical tables, due to the weaker vertical mixing in CAMx. The spatial distributions also show that, in some regions, particularly the eastern half of the domain, and Atlanta, GA, the models predict higher monthly-mean $\text{PM}_{2.5}$ in January than in July. This can be attributed partly to the removal of more pollutants through wet deposition in July than in January. The largest underpredictions in July appear in the western NC and northwestern GA, while in January, Atlanta, GA is a region of significant overprediction. The overprediction in January may be attributed to high SO_2 emissions from the Bowen power plant in Bartow, GA, which had been ranked among the 50 power plants with the highest SO_2 emissions (see <http://www.environmentalintegrity.org/pubs/2007%20Dirty%20Kilowatts.pdf>). As mentioned earlier, statistically, both models show an overprediction of SO_2 , and CAMx, which shows higher $\text{PM}_{2.5}$ near Atlanta in Figure 4.11, also overpredicts SO_4^{2-} in January.

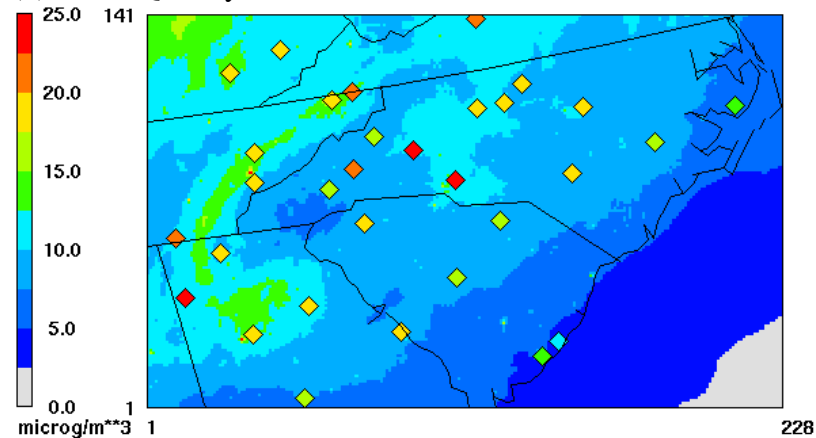
Figures 4.12 and 4.13 show hourly O_3 observations plotted with hourly simulated values by both models in January and July, respectively. Observations are only available for the Kinston and Raleigh sites from April through October, so only observations at the Beaufort and the Great Smoky Mountain sites can be shown for January. The performance of both models at both sites is relatively good at the beginning of January; however at the end of the month, the overprediction of maximum O_3 occurs, which is consistent with the statistics reported in the Table 4.3. This may be a result of weaker vertical mixing in both models, as mentioned earlier. Additionally, in Beaufort, nighttime O_3 is overpredicted in both models, which may be a result of insufficient NO in the region to consume O_3 at night. The only observations of NO used in this study are from the sites near Atlanta, GA in the SEARCH network and both models underpredict NO mixing ratios at these sites in January. Figure 4.13 shows the hourly O_3 mixing ratios at all four sites for July. The underprediction

(a) CMAQ - January



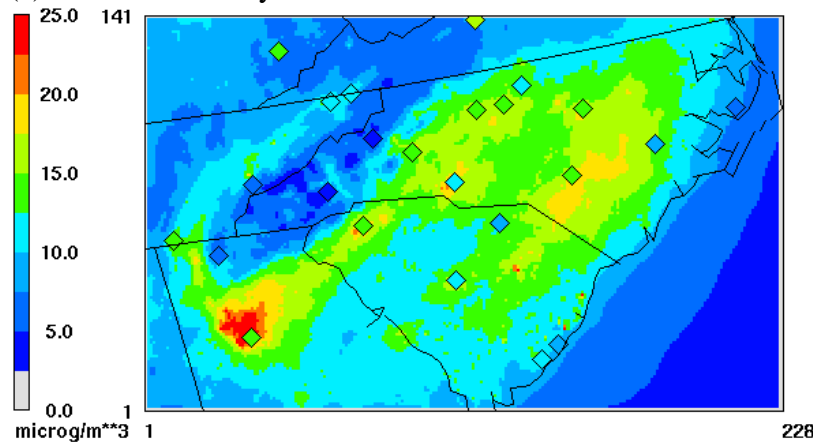
Min= 3.1 at (54,85), Max= 44.2 at (35,25)

(b) CMAQ - July



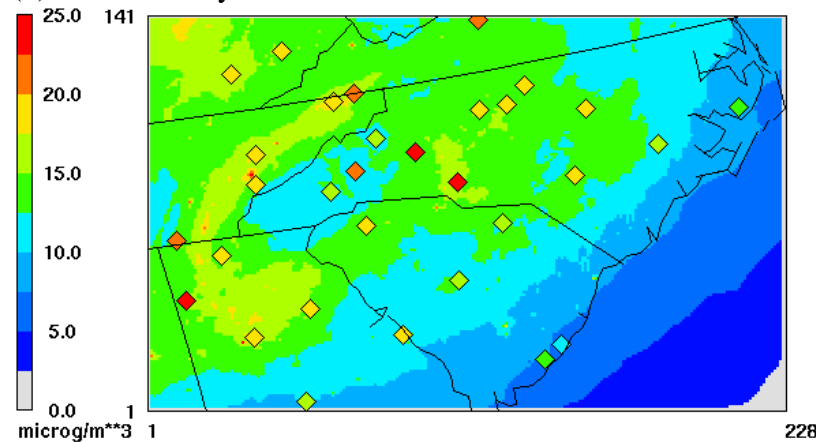
Min= 1.7 at (228,3), Max= 37.7 at (35,25)

(c) CAMx - January



Min= 0.0 at (1,1), Max= 50.7 at (35,25)

(d) CAMx - July



Min= 0.0 at (1,1), Max= 30.1 at (66,111)

Figure 4.11. Spatial distribution of the monthly-mean $PM_{2.5}$ concentrations as simulated by CMAQ (top) and CAMx (bottom) in January (left) and July (right) overlaid with observations (diamonds) from IMPROVE and STN.

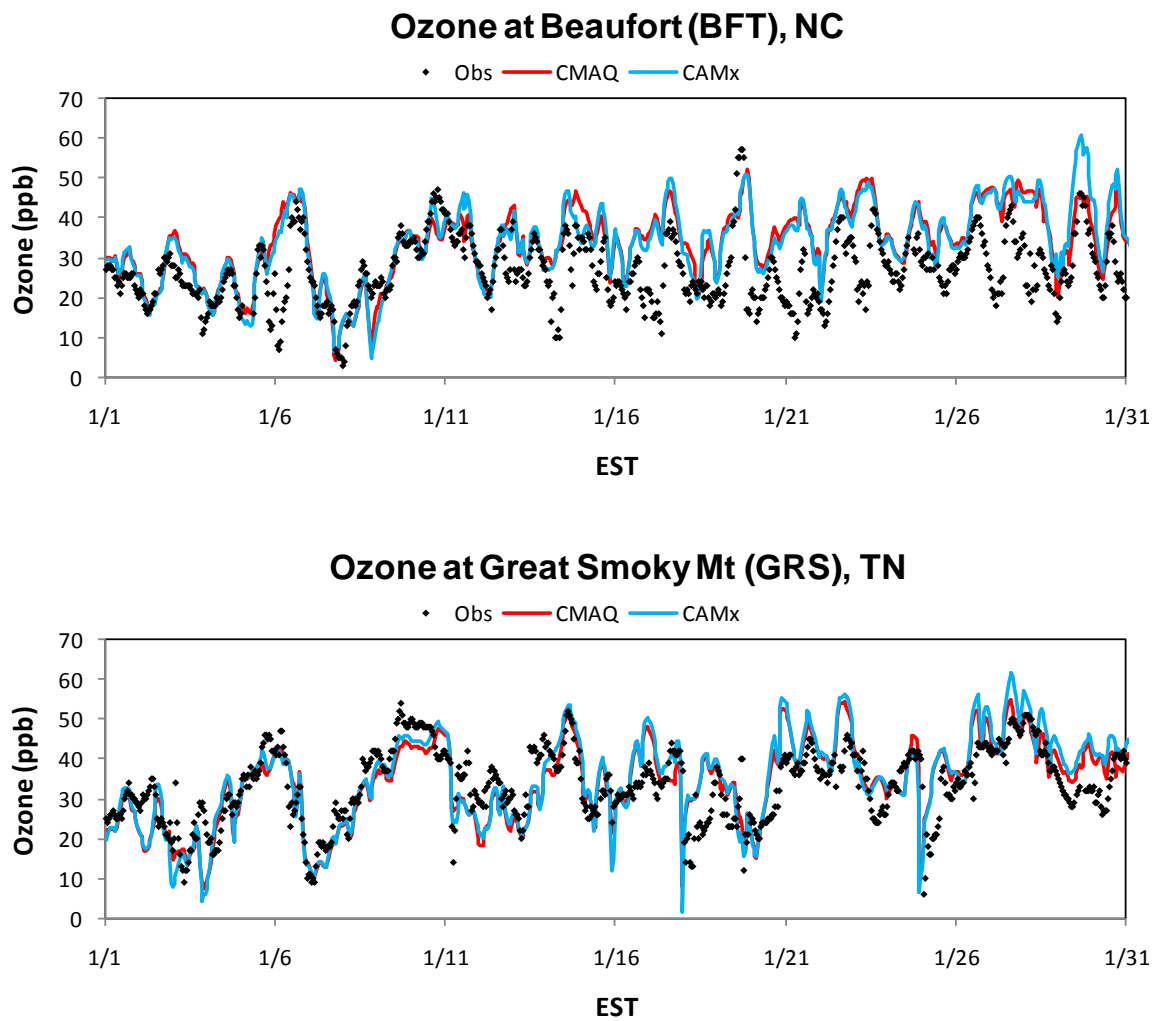


Figure 4.12. Hourly O₃ mixing ratios as simulated by CMAQ and CAMx, compared to observations at Beaufort, NC and Great Smoky Mountains, TN (no observations available at Kinston or Raleigh, NC).

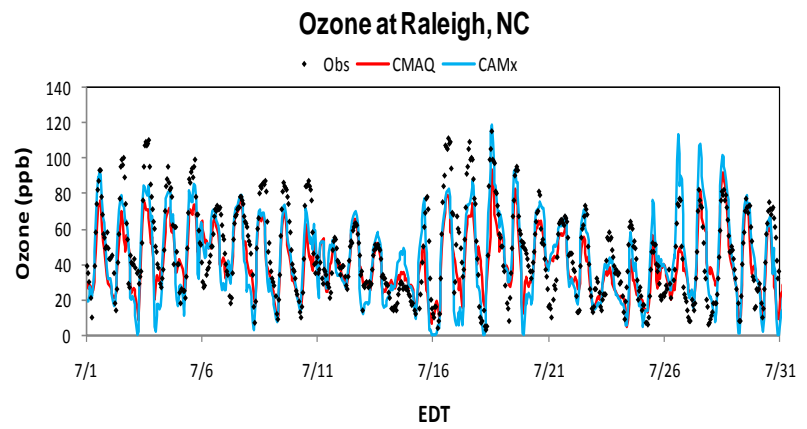
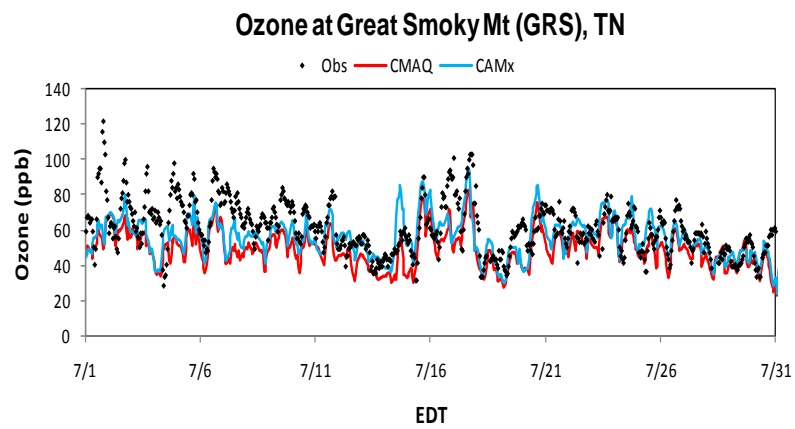
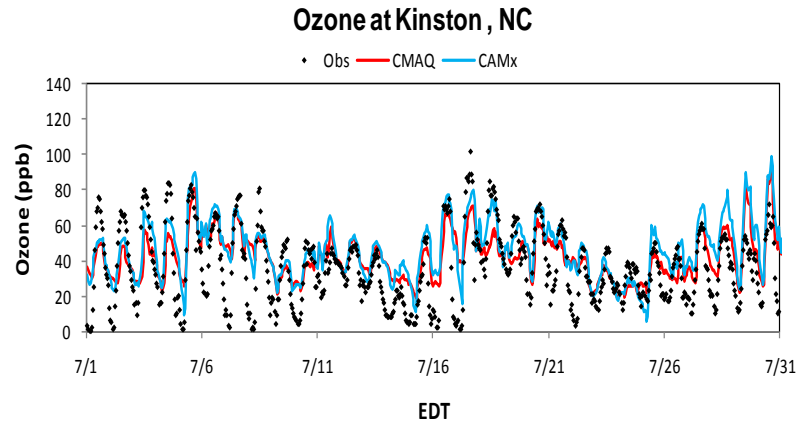
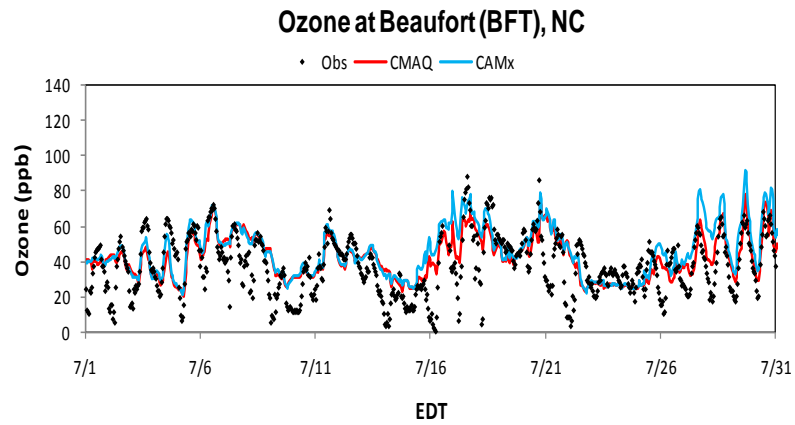


Figure 4.13. Hourly O₃ as simulated by CMAQ and CAMx, compared to observed hourly O₃ mixing ratios, at Beaufort, NC, Kinston, NC, Great Smoky Mountains, TN, and Raleigh, NC.

of maximum O₃ is observable at all four sites. The models also overpredict the minimum O₃ at the Beaufort and Kinston sites. Both models seem to better capture the diurnal variations at the urban site in Raleigh, NC where the O₃ diurnal pattern is more consistent day to day and the O₃ cycle is better understood and represented in the models.

Figure 4.14 shows the temporal variations of PM_{2.5} at Raleigh and Kinston, NC in January and July. No observations are available at the Beaufort or Great Smoky Mountain sites, and only 24-hour average observations are available once every three days at the Kinston site. The models show very little agreement with the diurnal patterns of the observations in both months, however, the long term trends are somewhat reproduced (i.e., the increase and decrease in PM_{2.5} in Raleigh from July 15th to 20th and the three peaks throughout July in Kinston). Similar to the statistics and spatial distributions, January PM_{2.5} is overpredicted throughout the month, while July is generally underpredicted. The relatively significant underprediction at both sites in the beginning of July is most likely due to the advection of PM mass into the area from the wildfires in Quebec (see Section 3.2). While emissions from wildfires are included in the emission inventory, many assumptions are made (Barnard and Brewer, 2004) in estimating the emissions thus introducing possible error into the inventory.

To look at the results in more detail, particularly the effects of NH₃, the spatial distributions of NH₄⁺/NH_x and the AdjGR are shown in Figures 4.15 and 4.16, respectively. One way to assess the fate and transport of NH₃ in the atmosphere is to look at the ratio of NH₄⁺/NH_x, where the reduced nitrogen, NH_x, is defined as a sum of molar fractions of NH₃ and NH₄⁺, i.e., NH_x = NH₃ + NH₄⁺. This ratio gives information as to the amount of NH₃ that has been converted to NH₄⁺ and its spatial distribution (Figure 4.15) shows the distance from the source where the conversion has occurred. Both models give similar conversion rates and their spatial distributions in January. CAMx gives a higher conversion rate of NH₃ to NH₄⁺ near the source of NH₃ (i.e., eastern NC, northeastern GA) than CMAQ in July. A possible explanation for the similarities between the models in January, but the differences in July is the simulated aqueous-phase concentrations of hydrogen peroxide (H₂O₂) in both models. H₂O₂ is one of the major species responsible for the conversion of SO₂ to SO₄²⁻

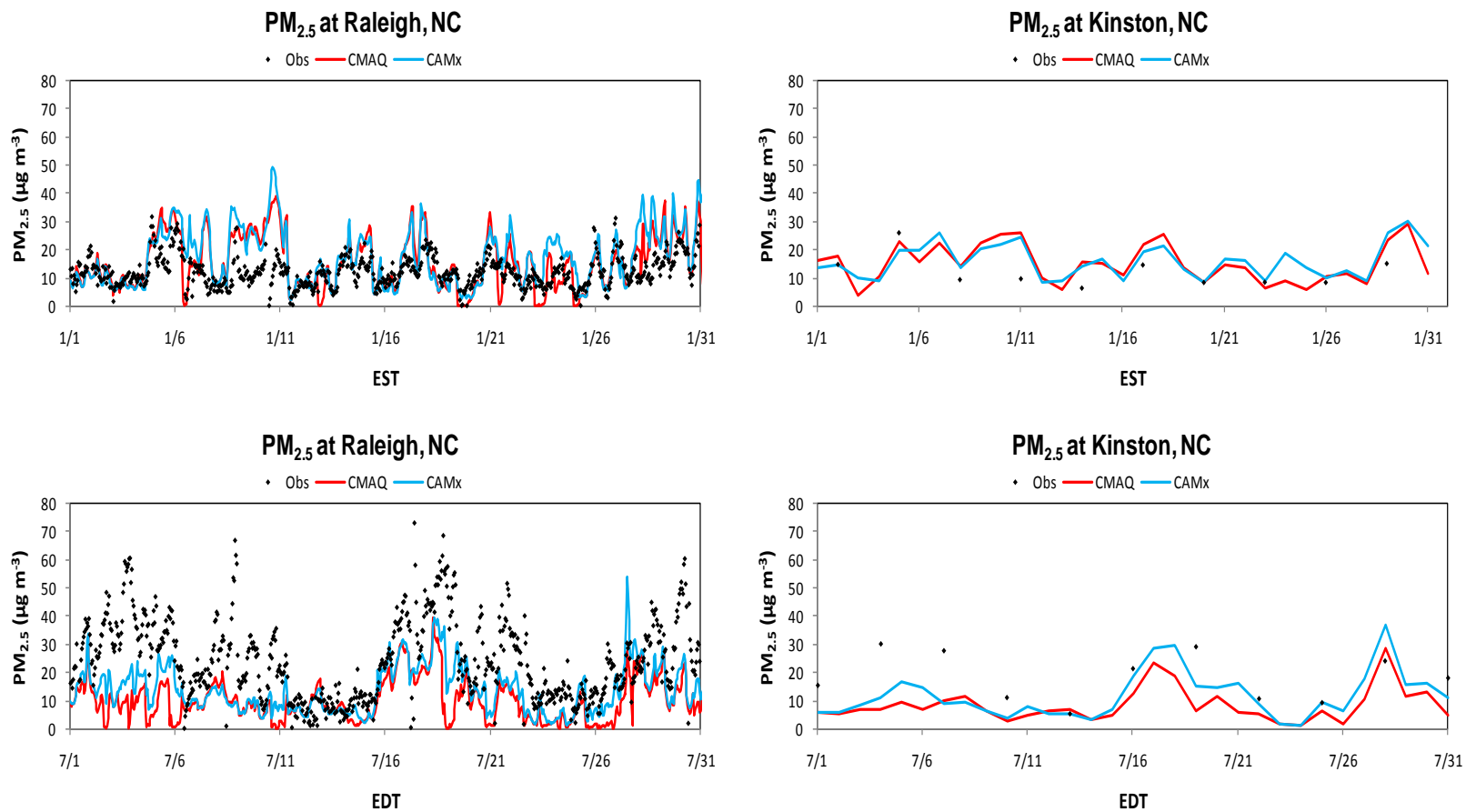
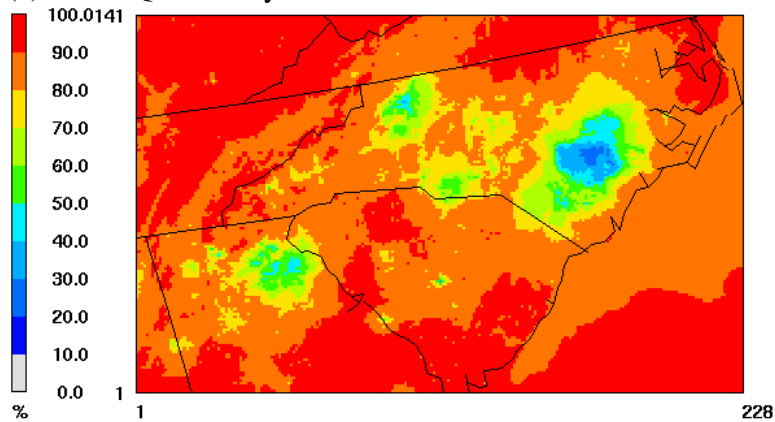


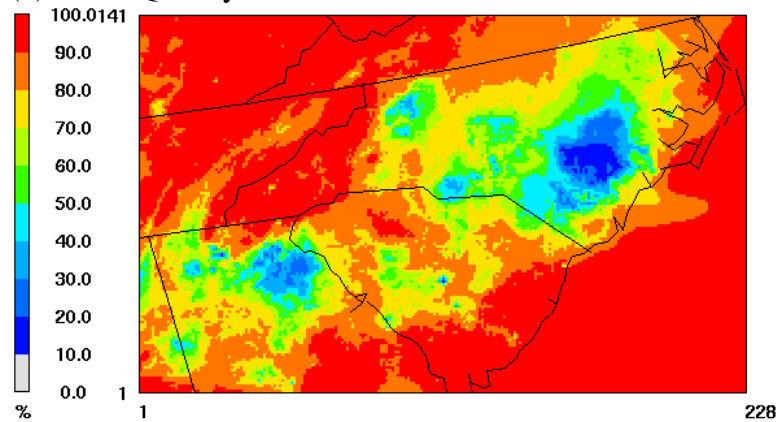
Figure 4.14. Observed PM_{2.5} concentrations compared to modeled PM_{2.5} concentrations in January (left) and July (right) at Raleigh (top) and Kinston (bottom). Only 24-hour average observations are available at Kinston, NC, not hourly. No observations of PM_{2.5} are available at the Beaufort or Great Smoky Mountain sites.

(a) CMAQ - January



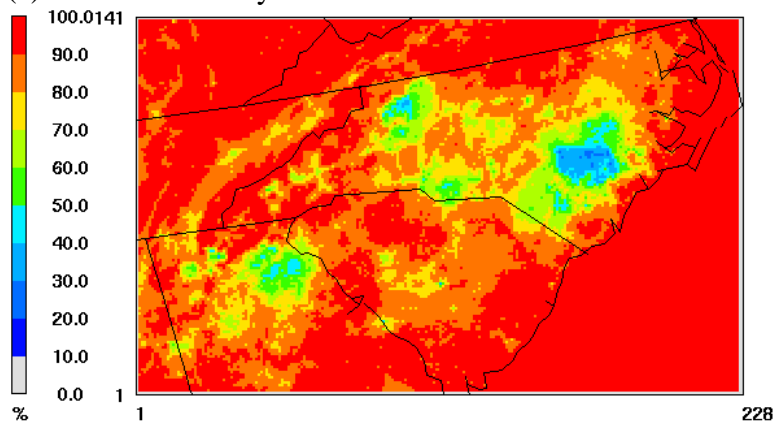
Min= 23.1 at (171,91), Max= 98.0 at (74,131)

(b) CMAQ - July



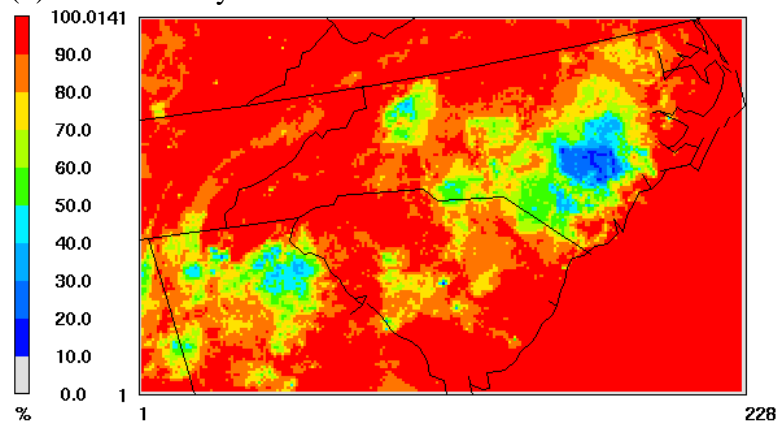
Min= 11.0 at (171,91), Max= 99.5 at (54,84)

(c) CAMx - January



Min= 0.0 at (1,1), Max= 98.6 at (56,119)

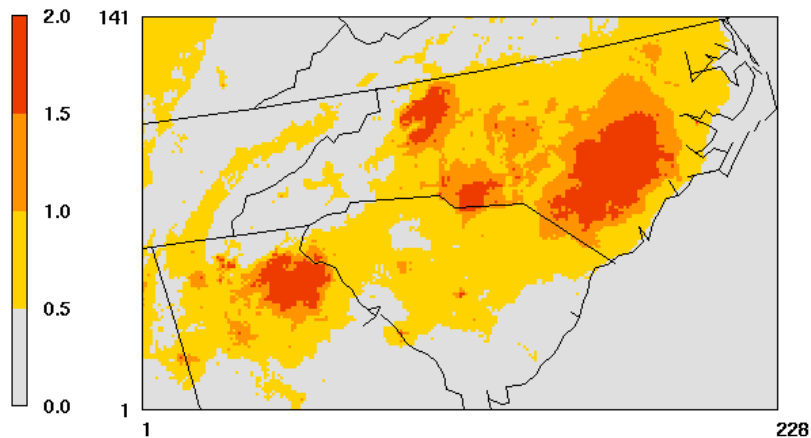
(d) CAMx - July



Min= 0.0 at (1,1), Max= 99.8 at (56,84)

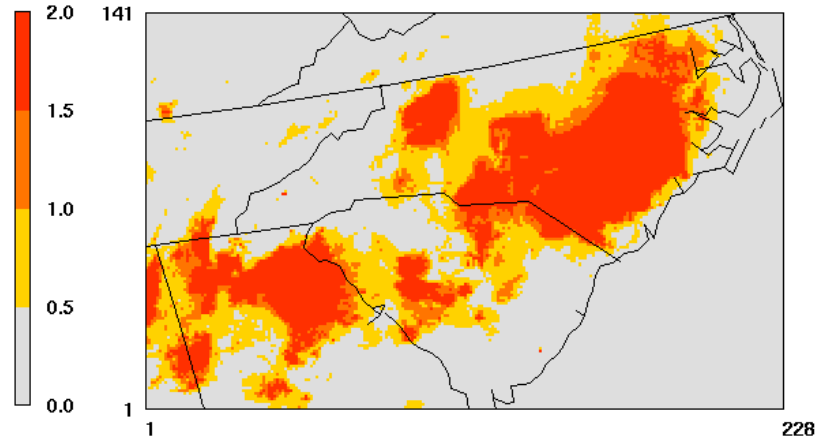
Figure 4.15. Monthly-mean spatial distribution of the ratio $\text{NH}_4^+/\text{NH}_x$ (in percentage) as simulated by (a) CMAQ in January, (b) CMAQ in July, (c) CAMx in January, and (d) CAMx in July.

(a) CMAQ - January



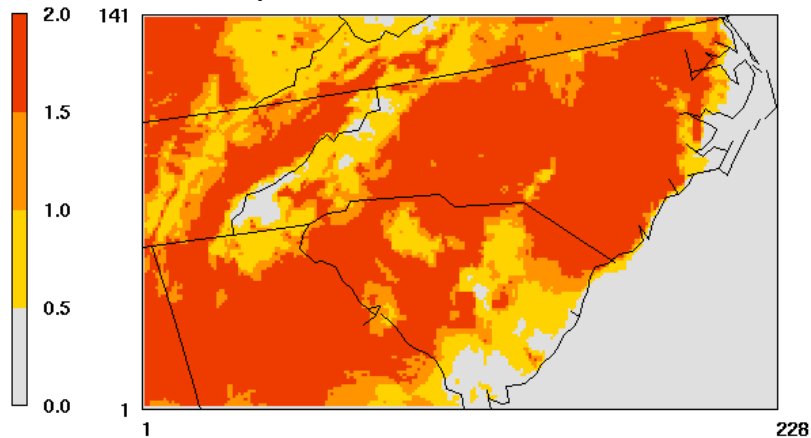
Min= 0.0 at (228,1), Max= 6.1 at (171,91)

(b) CMAQ - July



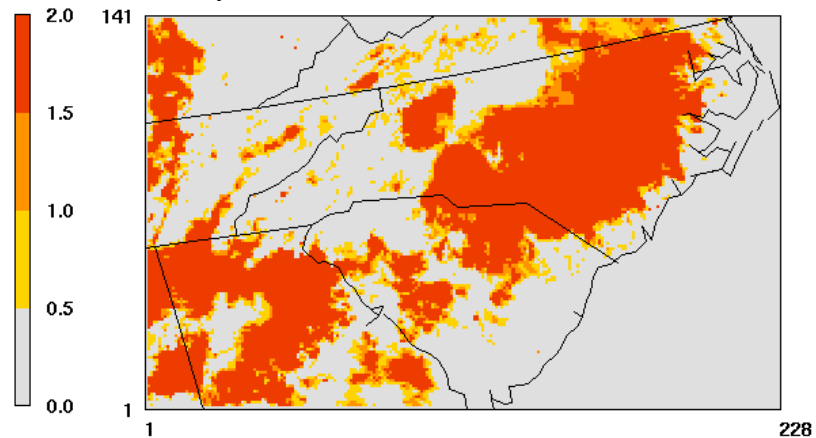
Min= 0.0 at (171,1), Max= 30.8 at (115,42)

(a) CAMx - January



Min= 0.0 at (1,1), Max= 24.1 at (172,85)

(b) CAMx - July



Min= 0.0 at (1,1), Max=176.3 at (170,91)

Figure 4.16. Monthly-mean spatial distribution of AdjGR as simulated by (a) CMAQ in January, (b) CMAQ in July, (c) CAMx in January, and (d) CAMx in July.

through aqueous-phase oxidation. NH_4^+ is more likely to enter particles that contain SO_4^{2-} or NO_3^- in order to neutralize the aerosol. In January, both models simulate similar gas-phase concentrations of H_2O_2 (and thus similar aqueous-phase concentrations of H_2O_2) resulting in similar concentrations of SO_4^{2-} and NH_4^+ . In July, however, CAMx simulates up to 60% more H_2O_2 in the gas-phase than CMAQ, which would result in more aqueous-phase H_2O_2 , and thus more SO_4^{2-} and NH_4^+ through the aqueous-phase oxidation reactions. The higher H_2O_2 , SO_4^{2-} , and NH_4^+ in CAMx may be a result of weaker vertical mixing, and different aerosol representation and microphysics treatments. The conversion to NH_4^+ is important because NH_4^+ has a longer atmospheric lifetime than NH_3 , so the faster conversion could result in deposition of NH_x at locations further from the source. Wu et al. (2008a) found similar results for the fate and transport of NH_x over NC in August and December 2002 using CMAQ. They reported a conversion rate of 10-40% in August and 20-50% in December at or near the source. There are limited observations of NH_3 and NH_4^+ available for comparison, however, Robarge et al. (2002) measured concentrations from October 1998 to September 1999 in Sampson County, NC and found that NH_4^+ accounts for ~18% and ~27% of NH_x in summer and winter, respectively, which are also comparable to the results found in this research.

Figure 4.16 shows the calculated AdjGR for both months based on simulated values from both models. There is a significant difference between the models in January. Based on the CMAQ simulation for January, the NH_3 -rich regions ($\text{AdjGR} \gg 1$) are only found near the NH_3 sources in the eastern NC and northeastern GA. The AdjGR based on the CAMx simulation shows the majority of the domain is NH_3 -rich. Recall equation 2.2, the formula for AdjGR as defined by Pinder et al. (2008), contains $\text{TN} = \text{NO}_3^- + \text{HNO}_3$ in the denominator. The statistics from Table 4.2 indicate that CAMx predicted much lower values for NO_3^- and HNO_3 , which would result in a smaller denominator and thus a larger AdjGR. The lower NO_3^- and HNO_3 concentrations in CAMx may be due to inaccurate oxidation of NO_2 , as CAMx gives a larger overprediction of NO_2 . In July, CAMx simulates a slightly larger NH_3 -rich region than CMAQ, with very little in the transition region. The reason for higher AdjGR by CAMx in July is again likely due to lower NO_3^- and HNO_3 ; however the

differences between CMAQ and CAMx are much smaller in July than in January. The high NH₃ emissions in the eastern NC and northern GA do result in large regions of NH₃-rich conditions, mainly in July. This indicates that reducing NO_x and SO₂ would act to reduce PM in those regions, but would also free up additional NH₃ that could be deposited closer to the source. Thus reducing NH₃ in addition to SO₂ and NO_x could provide additional environmental benefits besides reducing PM.

4.3 Dry and Wet Deposition Fluxes

Dry and wet deposition are major pollutant removal processes. As discussed in Chapter 3, weekly precipitation is collected at the NADP sites and analyzed for PM components, while the dry deposition flux and velocity of some species are calculated using the MLM, which is based on concentrations and vegetation data collected at the CASTNET sites. The statistical evaluations of CMAQ and CAMx against the NADP measurements and the MLM simulation are presented in Tables 4.5 (January) and 4.6 (July), along with precipitation statistics. When compared to the MLM, the M3Dry deposition module in CMAQ does show an improvement over Wesely's deposition module in CAMx, with the exception of SO₂ in both months. While a statistical comparison is completed between the air quality models and the MLM, the performance of MLM must also be considered because it, too, is a model. The MLM estimates the dry deposition velocity for O₃, SO₂, and HNO₃ by dividing the canopy into 20 layers and calculating individual stomatal and boundary layer resistances in each layer (Meyers et al., 1998). This is significantly more detailed than the dry deposition modules used in the AQMs that treat the canopy as one layer. Finkelstein et al. (2000) evaluated the MLM using data collected from a two field experiments (Pennsylvania and New York) and found that the MLM underestimates the dry deposition velocity of SO₂ by an average of 35%. Meyers et al. (1998) also found an underestimation of SO₂ dry deposition velocity at sites in Illinois and Alabama by an average of 10.6% and 6.9%, respectively. An average overestimation of 18.3% for SO₂ dry deposition velocity was reported by Meyers et al. (1998) at a site in Nashville, TN. Meyers et al. (1998) also evaluated the dry deposition of HNO₃ and found it was overestimated at all three sites

Table 4.5. Performance statistics for dry and wet deposition in January 2002.

Variable	DD_NH ₄ ⁺ (g ha ⁻¹)		DD_SO ₄ ²⁻ (g ha ⁻¹)		DD_NO ₃ ⁻ (g ha ⁻¹)	
	CASTNET		CASTNET		CASTNET	
Model	CMAQ	CAMx	CMAQ	CAMx	CMAQ	CAMx
Number	6450		6450		6450	
MeanObs ¹	0.03		0.08		0.04	
MeanMod	0.01	0.01	0.04	0.01	0.02	0.01
NMB	-0.68	-0.86	-0.56	-0.82	-0.63	-0.89
NME	0.87	0.88	0.97	0.86	1.02	0.92
corr	0.12	0.25	0.05	0.19	0.03	0.22
MB	-0.02	-0.03	-0.04	-0.07	-0.03	-0.04
MAGE	0.03	0.03	0.08	0.07	0.04	0.04
RMSE	0.06	0.05	0.19	0.12	0.14	0.08
MNB	Inf	Inf	Inf	Inf	Inf	Inf
MNGE	Inf	Inf	Inf	Inf	Inf	Inf
FB	-0.78	-0.98	-0.79	-0.91	-1.00	-1.33
FGE	1.09	1.19	1.10	1.15	1.37	1.52
NMFB	-1.03	-1.50	-0.77	-1.39	-0.93	-1.60
NMFGE	1.32	1.53	1.34	1.46	1.49	1.66
MNFB	Inf	Inf	Inf	Inf	Inf	Inf
MNGFE	Inf	Inf	Inf	Inf	Inf	Inf
NMBF	-2.13	-5.93	-1.26	-4.58	-1.72	-8.06
NMEF	2.71	6.08	2.18	4.79	2.78	8.36

Inf (Infinity) and **NaN** (Not a Number) are a result of a small denominator compared to the numerator and mean observation (Seigneur et al., 2000) in the following equations (from Zhang et al., 2006a):

$$MNB = \frac{1}{N} \sum_{i=1}^N \frac{M_i}{O_i} - 1$$

$$MNGE = \frac{1}{N} \sum_{i=1}^N \frac{|M_i - O_i|}{O_i}$$

$$MNFB = \frac{1}{N} \sum_{i=1}^N F_i \text{ where } F_i = \frac{M_i}{O_i} - 1 \text{ for } M_i \geq O_i, \text{ or } F_i = 1 - \frac{O_i}{M_i} \text{ for } M_i < O_i$$

$$MNGFE = \frac{1}{N} \sum_{i=1}^N |F_i| \text{ where } F_i = \frac{M_i}{O_i} - 1 \text{ for } M_i \geq O_i, \text{ or } F_i = 1 - \frac{O_i}{M_i} \text{ for } M_i < O_i$$

Table 4.5. Continued.

Variable	DD_SO ₂ (g ha ⁻¹)		DD_HNO ₃ (g ha ⁻¹)		DV_SO ₂ (cm s ⁻¹)		DV_HNO ₃ (cm s ⁻¹)	
	CASTNET		CASTNET		CASTNET		CASTNET	
Model	CMAQ	CAMx	CMAQ	CAMx	CMAQ	CAMx	CMAQ	CAMx
Number	6450		6450		6455		6455	
MeanObs ¹	0.80		0.73		0.30		1.12	
MeanMod	1.26	0.63	1.85	2.16	0.77	0.24	2.27	3.54
NMB	0.58	-0.21	1.51	1.94	1.59	-0.21	1.03	2.17
NME	1.31	0.82	1.88	2.31	2.19	0.77	1.17	2.30
corr	0.18	0.19	0.30	0.21	0.21	0.16	0.55	0.47
MB	0.46	-0.16	1.11	1.42	0.47	-0.06	1.15	2.42
MAGE	1.05	0.65	1.38	1.69	0.65	0.23	1.31	2.57
RMSE	2.00	0.99	2.15	2.80	1.15	0.30	1.74	3.33
MNB	Inf	Inf	Inf	Inf	Inf	Inf	Inf	Inf
MNGE	Inf	Inf	Inf	Inf	Inf	Inf	Inf	Inf
FB	0.09	-0.32	0.58	0.65	0.24	-0.35	0.58	0.88
FGE	0.89	0.89	1.04	1.06	0.88	0.83	0.81	1.05
NMFB	0.45	-0.23	0.86	0.99	0.89	-0.23	0.68	1.04
NMFGE	1.02	0.91	1.07	1.17	1.22	0.86	0.77	1.10
MNFB	Inf	Inf	Inf	Inf	Inf	Inf	Inf	Inf
MNGFE	Inf	Inf	Inf	Inf	Inf	Inf	Inf	Inf
NMBF	0.58	-0.26	1.51	1.94	1.59	-0.26	1.03	2.17
NMEF	1.31	1.03	1.88	2.31	2.19	0.97	1.17	2.30

Table 4.5. Continued.

Variable	Precip ² (mm)	WD_NH ₄ ⁺ (kg ha ⁻¹)		WD_SO ₄ ²⁻ (kg ha ⁻¹)		WD_NO ₃ ⁻ (kg ha ⁻¹)	
Network	NADP	NADP		NADP		NADP	
Model	MM5	CMAQ	CAMx	CMAQ	CAMx	CMAQ	CAMx
Number	72	62		62		62	
MeanObs ¹	29.30	0.17		1.20		0.91	
MeanMod	26.09	0.22	0.10	1.66	0.99	1.66	0.06
NMB	-0.11	0.24	-0.45	0.38	-0.18	0.83	-0.93
NME	0.40	0.63	0.84	0.54	0.82	0.98	0.93
corr	0.79	0.59	-0.21	0.66	-0.26	0.68	-0.05
MB	-3.22	0.04	-0.08	0.46	-0.21	0.75	-0.84
MAGE	11.73	0.11	0.15	0.65	0.99	0.89	0.85
RMSE	17.71	0.20	0.24	0.93	1.38	1.31	1.21
MNB	0.49	0.87	0.24	0.55	0.26	1.28	-0.89
MNGE	0.93	1.12	1.06	0.66	0.98	1.36	0.89
NMB	-0.11	0.24	-0.45	0.38	-0.18	0.83	-0.93
NME	0.40	0.63	0.84	0.54	0.82	0.98	0.93
FB	-0.07	0.19	-0.42	0.30	-0.32	0.54	-1.68
FGE	0.52	0.53	0.98	0.44	0.87	0.67	1.69
NMFB	-0.12	0.21	-0.57	0.32	-0.19	0.59	-1.74
NMFGE	0.42	0.57	1.08	0.46	0.90	0.69	1.75
MNFB	0.20	0.35	Inf	0.35	Inf	1.06	Inf
MNGFE	1.22	1.64	Inf	0.86	Inf	1.58	Inf
NMBF	-0.12	0.24	-0.80	0.38	-0.21	0.83	-13.42
NMEF	0.45	0.63	1.52	0.54	0.99	0.98	13.47

¹ Dry deposition fluxes and dry deposition velocities are not observed measurements, but calculated from measurements using the Multilayer Model (MLM) (Meyers et al., 1998; Finkelstein et al., 2000).

² Precip (weekly) is predicted by MM5, so it is the same in both CMAQ and CAMx

WD: Wet Deposition

DD: Dry Deposition

DV: Deposition Velocity

Table 4.6. Performance statistics for dry and wet deposition in July 2002.

Variable	DD_NH ₄ ⁺ (g ha ⁻¹)		DD_SO ₄ ²⁻ (g ha ⁻¹)		DD_NO ₃ ⁻ (g ha ⁻¹)	
	CASTNET		CASTNET		CASTNET	
Model	CMAQ	CAMx	CMAQ	CAMx	CMAQ	CAMx
Number	6239		6239		6239	
MeanObs ²	0.10		0.36		0.01	
MeanMod	0.01	0.01	0.07	0.04	0.00	0.00
NMB	-0.89	-0.94	-0.80	-0.89	-0.98	-0.99
NME	0.96	0.95	0.97	0.91	1.00	1.00
corr	-0.03	0.27	-0.04	0.42	-0.02	-0.05
MB	-0.09	-0.09	-0.28	-0.32	-0.01	-0.01
MAGE	0.10	0.10	0.34	0.32	0.01	0.01
RMSE	0.16	0.16	0.56	0.56	0.03	0.03
MNB	Inf	Inf	Inf	Inf	Inf	Inf
MNGE	Inf	Inf	Inf	Inf	Inf	Inf
FB	-0.95	-1.12	-0.76	-0.92	-1.68	-1.83
FGE	1.40	1.33	1.36	1.23	1.82	1.89
NMFB	-1.60	-1.77	-1.34	-1.60	-1.92	-1.98
NMFGE	1.73	1.79	1.61	1.64	1.95	1.98
MNFB	Inf	Inf	Inf	Inf	Inf	Inf
MNGFE	Inf	Inf	Inf	Inf	Inf	Inf
NMBF	-8.10	-15.45	-4.02	-7.87	-48.98	-158.80
NMEF	8.76	15.62	4.86	8.11	49.81	159.47

Inf (Infinity) and **NaN** (Not a Number) are a result of a small denominator compared to the numerator and mean observation (Seigneur et al., 2000) in the following equations (from Zhang et al., 2006a):

$$MNB = \frac{1}{N} \sum_{i=1}^N \frac{M_i}{O_i} - 1$$

$$MNGE = \frac{1}{N} \sum_{i=1}^N \frac{|M_i - O_i|}{O_i}$$

$$MNFB = \frac{1}{N} \sum_{i=1}^N F_i \text{ where } F_i = \frac{M_i}{O_i} - 1 \text{ for } M_i \geq O_i, \text{ or } F_i = 1 - \frac{O_i}{M_i} \text{ for } M_i < O_i$$

$$MNGFE = \frac{1}{N} \sum_{i=1}^N |F_i| \text{ where } F_i = \frac{M_i}{O_i} - 1 \text{ for } M_i \geq O_i, \text{ or } F_i = 1 - \frac{O_i}{M_i} \text{ for } M_i < O_i$$

Table 4.6. Continued.

Variable	DD_SO₂ (g ha⁻¹)		DD_HNO₃ (g ha⁻¹)		DV_SO₂ (cm s⁻¹)		DV_HNO₃ (cm s⁻¹)	
Network	CASTNET		CASTNET		CASTNET		CASTNET	
Model	CMAQ	CAMx	CMAQ	CAMx	CMAQ	CAMx	CMAQ	CAMx
Number	6239		6239		6285		6284	
MeanObs²	0.46		1.11		0.34		1.41	
MeanMod	0.72	0.54	1.76	2.50	0.64	0.33	2.28	3.72
NMB	0.56	0.16	0.59	1.25	0.91	-0.01	0.62	1.64
NME	1.59	1.01	1.57	1.60	1.49	0.73	1.27	2.05
corr	-0.03	0.39	-0.03	0.57	-0.04	0.06	-0.02	0.07
MB	0.26	0.07	0.65	1.38	0.31	0.00	0.87	2.31
MAGE	0.73	0.46	1.75	1.77	0.50	0.24	1.79	2.88
RMSE	1.43	0.91	2.80	3.55	0.78	0.31	2.24	3.76
MNB	Inf	Inf	Inf	Inf	Inf	Inf	Inf	Inf
MNGE	Inf	Inf	Inf	Inf	Inf	Inf	Inf	Inf
FB	0.07	-0.12	0.15	0.48	0.41	0.06	0.43	0.75
FGE	1.12	0.96	1.20	0.95	0.93	0.79	1.07	1.13
NMFB	0.44	0.15	0.45	0.77	0.63	-0.01	0.47	0.90
NMFE	1.24	0.93	1.22	0.98	1.03	0.73	0.97	1.13
MNFB	Inf	Inf	Inf	Inf	Inf	Inf	Inf	Inf
MNGFE	Inf	Inf	Inf	Inf	Inf	Inf	Inf	Inf
NMBF	0.56	0.16	0.59	1.25	0.91	-0.01	0.62	1.64
NMEF	1.59	1.01	1.57	1.60	1.49	0.73	1.27	2.05

Table 4.6. Continued.

Variable	Precip ¹ (mm)	WD_NH ₄ ⁺ (kg ha ⁻¹)		WD_SO ₄ ²⁻ (kg ha ⁻¹)		WD_NO ₃ ⁻ (kg ha ⁻¹)	
Network	NADP	NADP		NADP		NADP	
Model	MM5	CMAQ	CAMx	CMAQ	CAMx	CMAQ	CAMx
Number	84	68		68		68	
MeanObs	30.11	0.32		2.16		1.58	
MeanMod	75.69	0.24	0.42	2.98	4.67	0.89	0.04
NMB	1.51	-0.23	0.31	0.38	1.17	-0.44	-0.98
NME	2.03	0.77	1.05	1.13	1.73	0.81	0.98
corr	0.34	0.28	0.29	0.15	0.06	0.23	0.30
MB	45.58	-0.07	0.10	0.83	2.52	-0.69	-1.54
MAGE	61.10	0.25	0.33	2.43	3.73	1.29	1.54
RMSE	96.24	0.35	0.50	5.63	5.73	1.85	1.79
MNB	Inf	Inf	Inf	Inf	Inf	Inf	Inf
MNGE	Inf	Inf	Inf	Inf	Inf	Inf	Inf
FB	0.54	-0.46	-0.06	-0.20	0.23	-0.83	-1.80
FGE	1.18	0.92	0.97	0.77	1.01	1.09	1.92
NMFB	0.86	-0.26	0.27	0.32	0.74	-0.56	-1.91
NMFGE	1.16	0.87	0.91	0.95	1.09	1.04	1.91
MNFB	NaN	Inf	NaN	Inf	NaN	Inf	NaN
MNGFE	Inf	Inf	Inf	Inf	Inf	Inf	Inf
NMBF	1.51	-0.30	0.31	0.38	1.17	-0.77	-40.24
NMEF	2.03	1.00	1.05	1.13	1.73	1.44	40.28

¹ Precip (weekly) is predicted by MM5, so it is the same in both CMAQ and CAMx

² Dry deposition fluxes and dry deposition velocities are not observed measurements, but calculated from measurements using the Multilayer Model (MLM) (Meyers et al., 1998; Finkelstein et al., 2000).

WD: Wet Deposition

DD: Dry Deposition

DV: Deposition Velocity

(Illinois, Alabama, and Tennessee), by 3.6%, 14.7%, and 7.8%. Limited studies on the observed dry deposition velocity make evaluation of the MLM difficult. However, the biases reported by Finkelstein et al. (2000) and Meyers et al. (1998) provided guidance as to the magnitude of over or underestimation by the MLM. If the bias of the AQMs is around the same value as the bias of the MLM to observations, the AQM may be considered comparable to the MLM and observed dry deposition. If the AQM bias is significantly different from the bias of the MLM compared to observed values, then the simulation of dry deposition by the AQM may be considered less accurate.

Table 4.5 shows that CMAQ underpredicts the dry deposition (DD) of all three PM species (i.e., NH_4^+ , SO_4^{2-} , NO_3^-) when compared to MLM and overpredicts their wet deposition (WD) in January. The overestimation of the dry deposition velocity (DV) of the gaseous species SO_2 and HNO_3 results in an overestimation of the dry deposition flux of those species and also limits the amount of gaseous species available for gas-to-particle conversion. This may contribute partially to the underestimation of the dry deposition flux of the secondary aerosol species. Additionally, despite underpredicted precipitation, wet deposition of the aerosol species is overpredicted, suggesting that it is a more efficient removal process than dry deposition and thus limits the aerosol mass available for dry deposition. While CMAQ overestimates wet deposition, CAMx underestimates both wet and dry deposition. The differences between the models may be due to the PM size representation, as well as the treatment of wet deposition. The underestimation of the removal of PM through wet and dry deposition by CAMx would also be contributing to the higher $\text{PM}_{2.5}$ ambient concentrations compared to CMAQ.

In July (Table 4.6), the underprediction of ambient PM concentrations contributes to an underprediction of all three PM species (i.e., NH_4^+ , SO_4^{2-} , NO_3^-) by both models. Additionally, while a significant overprediction of precipitation occurs, the wet deposition of NH_4^+ by CMAQ and of NO_3^- by both models is underpredicted. The underprediction of NO_3^- wet deposition is likely due to limited NO_3^- in the summer months in the southeast, so that no matter how much precipitation occurs, there is simply not enough NO_3^- mass for removal. The differences in performance of NH_4^+ between the air quality models may be attributed to

differences in wet deposition processes or PM size representation, as well as weaker vertical mixing in CAMx resulting in higher ambient NH_4^+ concentrations available for removal through wet deposition. Both models overpredict the wet deposition of SO_4^{2-} , despite an underprediction of SO_4^{2-} ambient concentrations, because precipitation is largely overpredicted and there is sufficient SO_4^{2-} available for removal.

Figure 4.17 shows the time series of the modeled SO_2 dry deposition velocity at Beaufort, NC and Great Smoky Mountains, TN in January and July. CAMx is nearly identical to the MLM, especially at the Great Smoky Mountain site in July. CMAQ generally gives a higher SO_2 dry deposition velocity throughout both months, with larger differences in January. Despite dry deposition velocities similar to MLM, both CMAQ and CAMx show high variability in estimating the dry deposition flux of SO_2 (Figure 4.18), generating much larger diurnal variations than what the MLM predicted. CMAQ and CAMx give similar diurnal patterns for HNO_3 dry deposition velocity (Figure 4.19); however, CAMx gives slightly higher velocities in both months at Beaufort and in January at the Great Smoky Mountain site. The similarities of the HNO_3 dry deposition velocities by CMAQ and CAMx do result in some similarities in HNO_3 dry deposition flux (Figure 4.20), especially in January at Beaufort. In July, at both sites, the improved performance by M3Dry in MCIP/CMAQ is observable.

The time series for the dry deposition flux of the PM species are shown in Figures 4.21, 4.22, and 4.23. Because NH_4^+ is often associated with SO_4^{2-} , the dry deposition fluxes of the two species are very similar (Figures 4.21 and 4.22). However, the model inter-comparison shows large differences between all three models (CMAQ, CAMx, and MLM). Both CMAQ and CAMx fail to capture the same maximum flux values as the MLM at both sites, during both months. CMAQ tends to have larger diurnal variations than both the MLM and CAMx, while CAMx simulates much less diurnal variation (e.g., at the beginning of July at the Great Smoky Mountain site). The largest variations in dry deposition, however, are in the NO_3^- dry deposition flux (Figure 4.23), which also displays some of the poorest performance in ambient concentration predictions that affects the amount of mass available for dry deposition. These combined results indicate that the dry deposition may not be

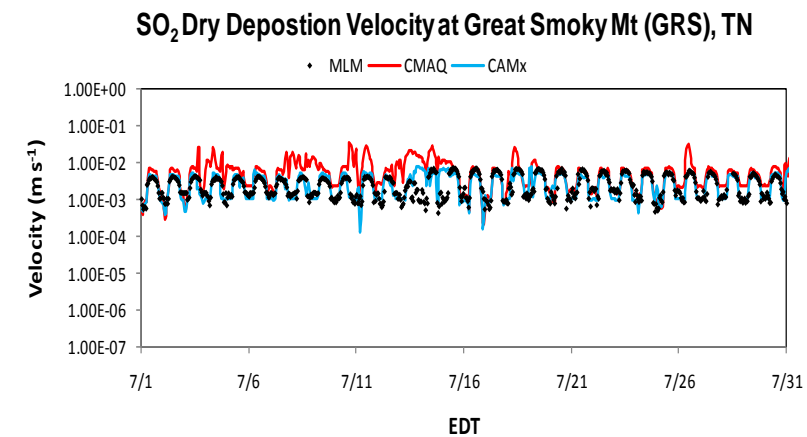
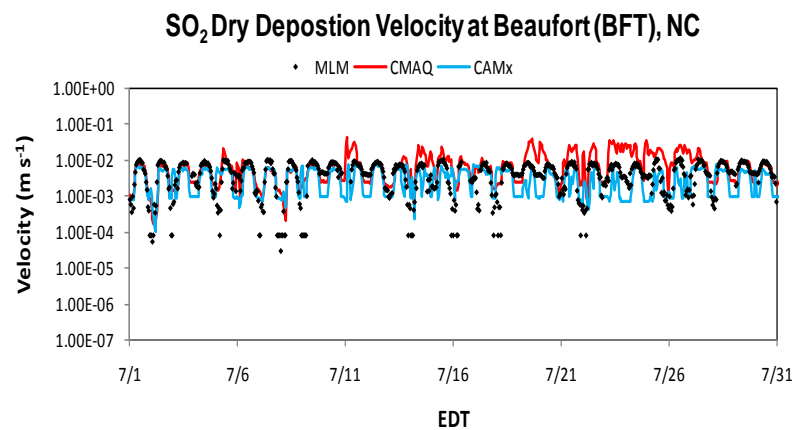
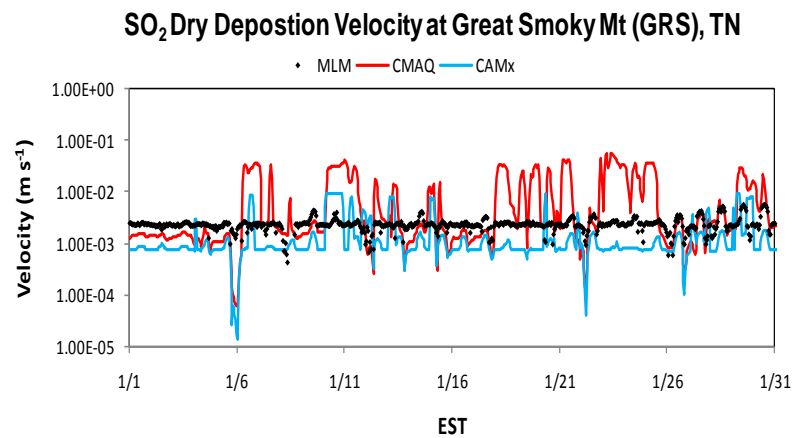
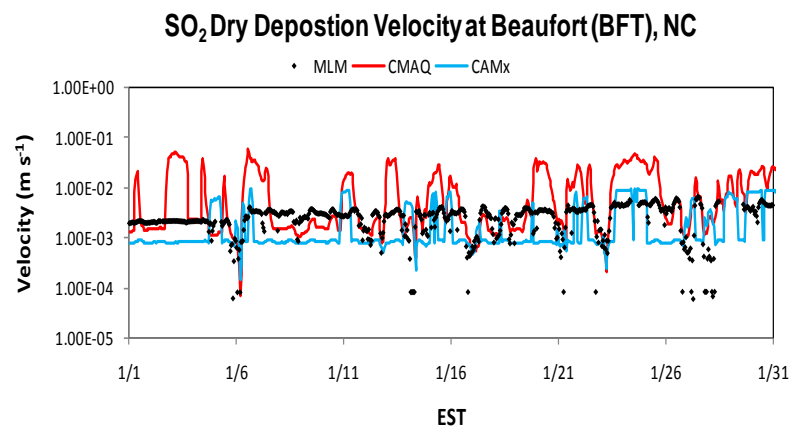


Figure 4.17. SO₂ dry deposition velocity in January (top) and July (bottom) as simulated by MLM, CMAQ, and CAMx at Beaufort, NC (left) and Great Smoky Mountains, TN (right).

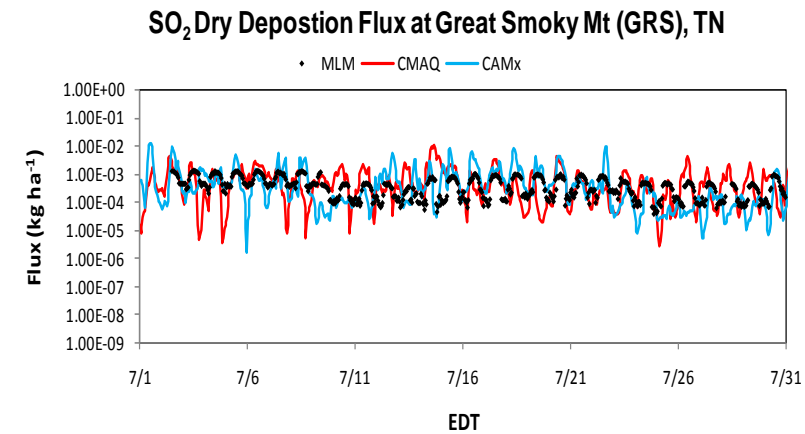
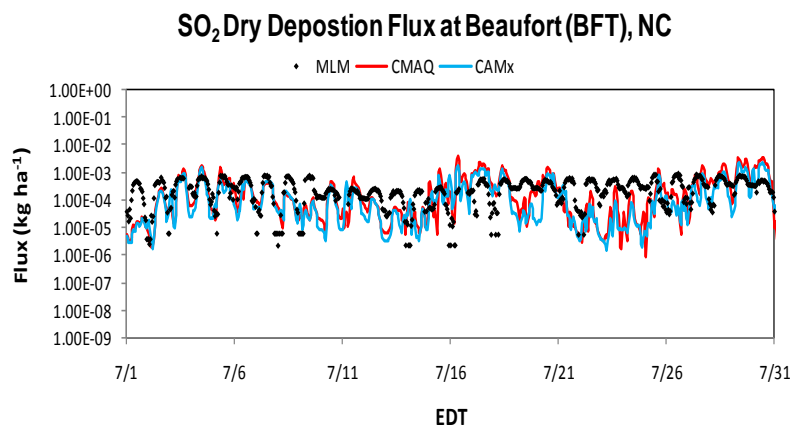
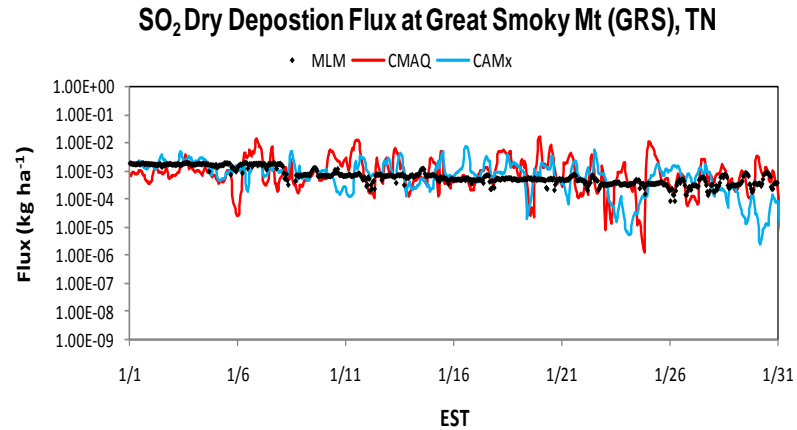
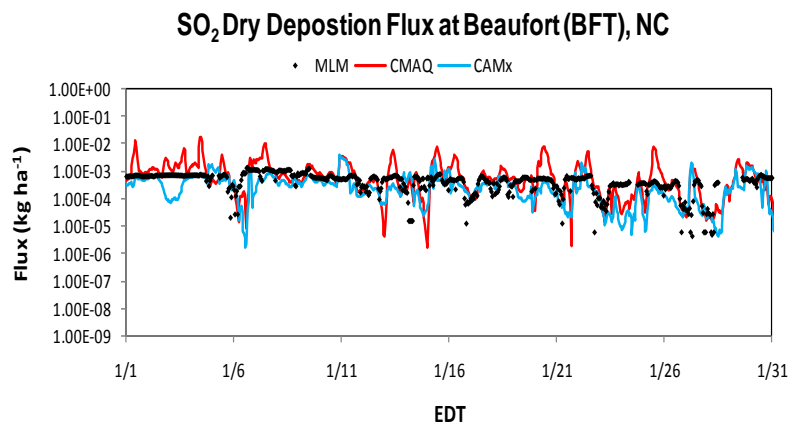


Figure 4.18. SO₂ dry deposition flux in January (top) and July (bottom) as simulated by MLM, CMAQ, and CAMx at Beaufort, NC (left) and Great Smoky Mountains, TN (right).

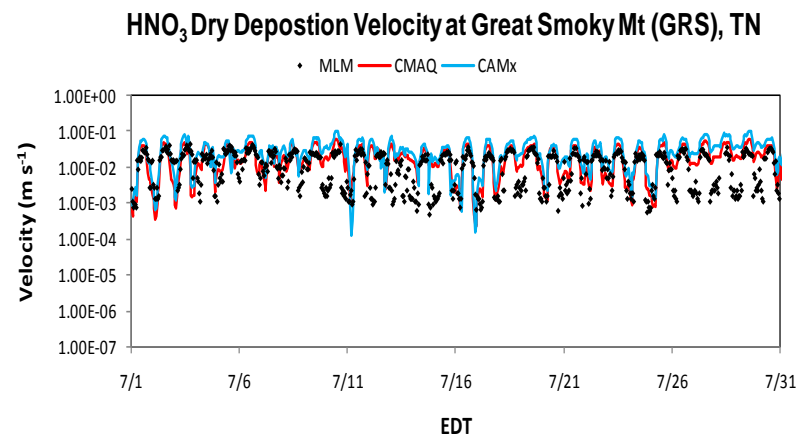
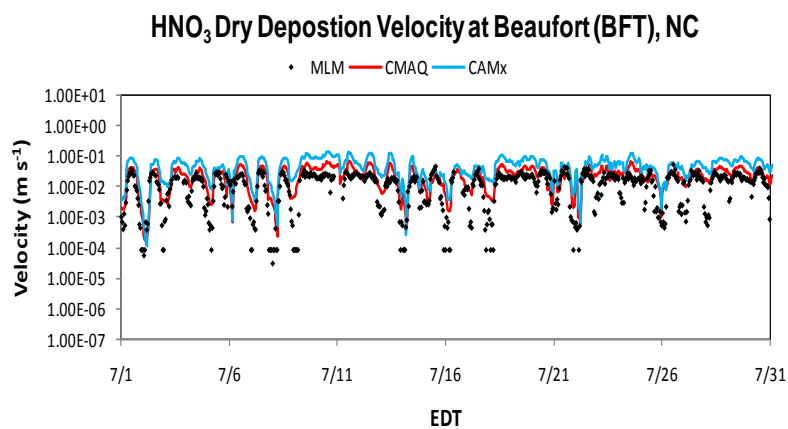
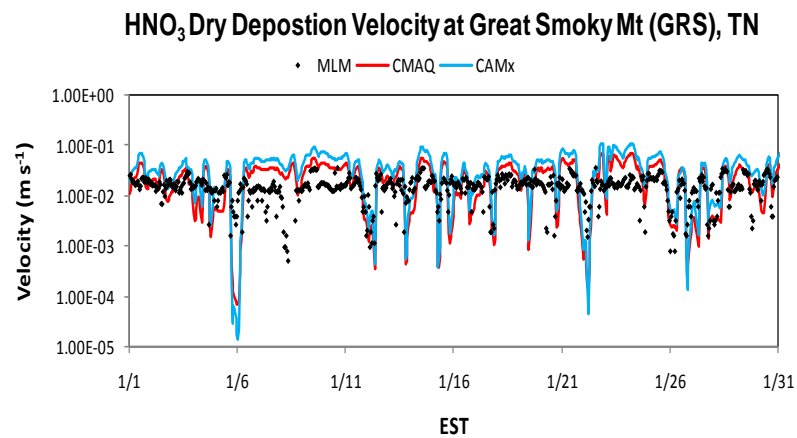
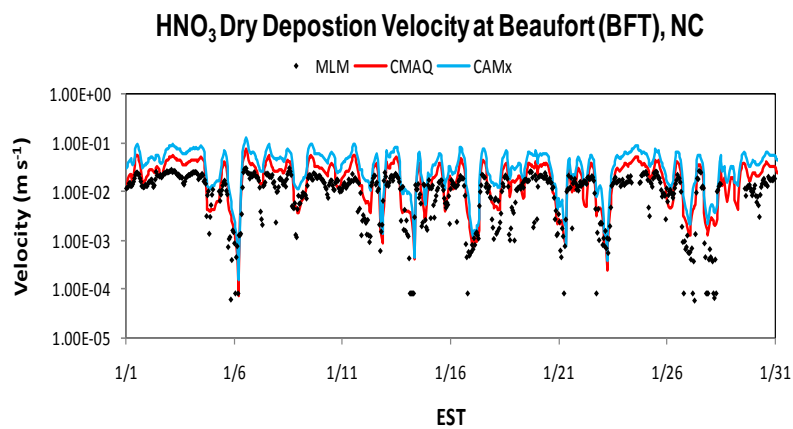


Figure 4.19. HNO₃ dry deposition velocity in January (top) and July (bottom) as simulated by MLM, CMAQ, and CAMx at Beaufort, NC (left) and Great Smoky Mountains, TN (right).

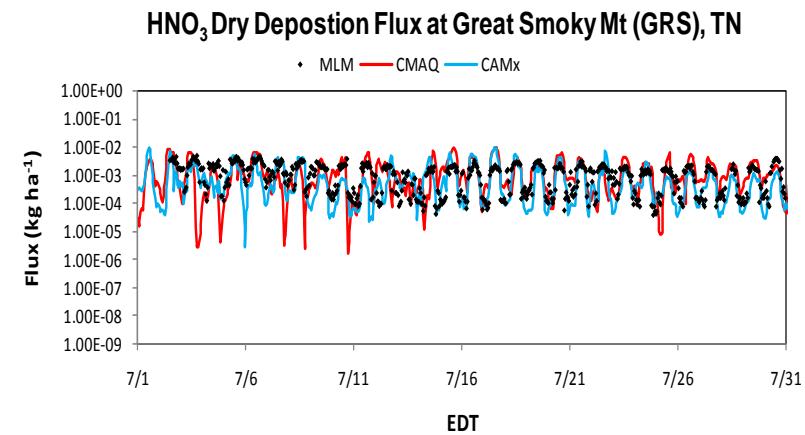
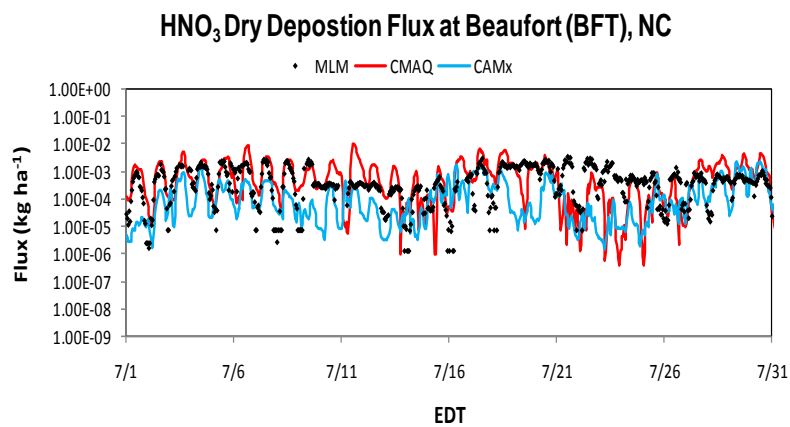
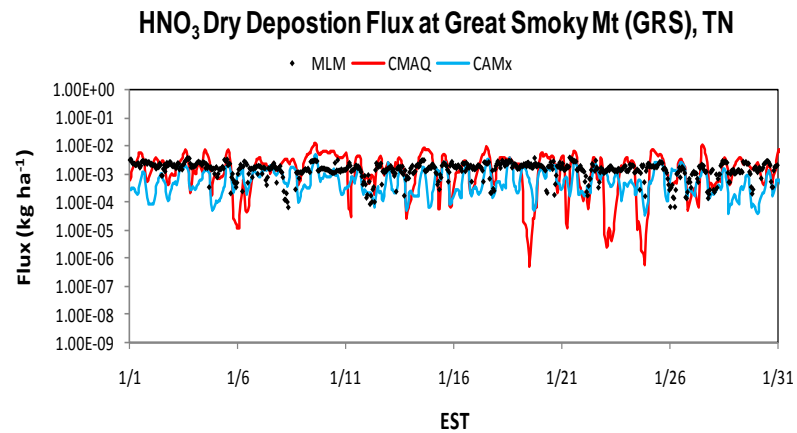
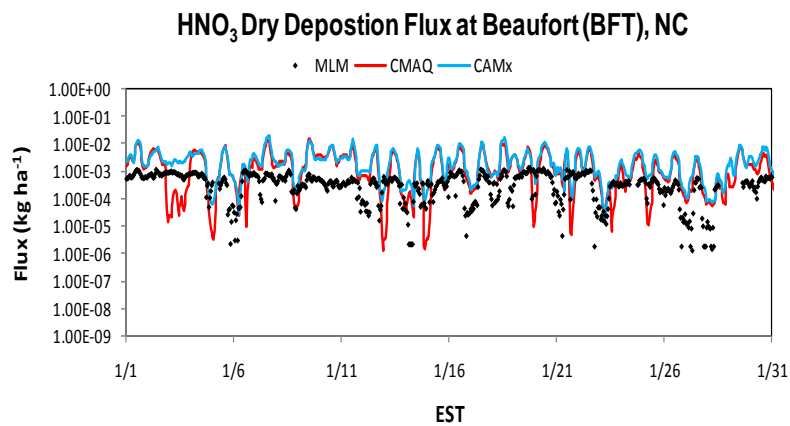


Figure 4.20. HNO_3 dry deposition flux in January (top) and July (bottom) as simulated by MLM, CMAQ, and CAMx at Beaufort, NC (left) and Great Smoky Mountains, TN (right).

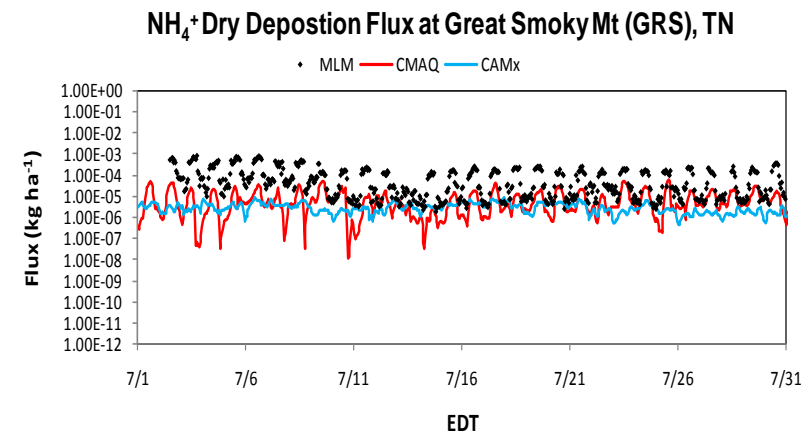
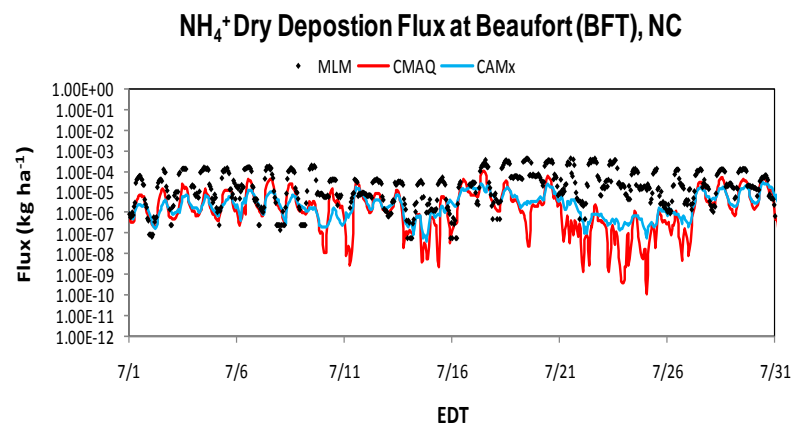
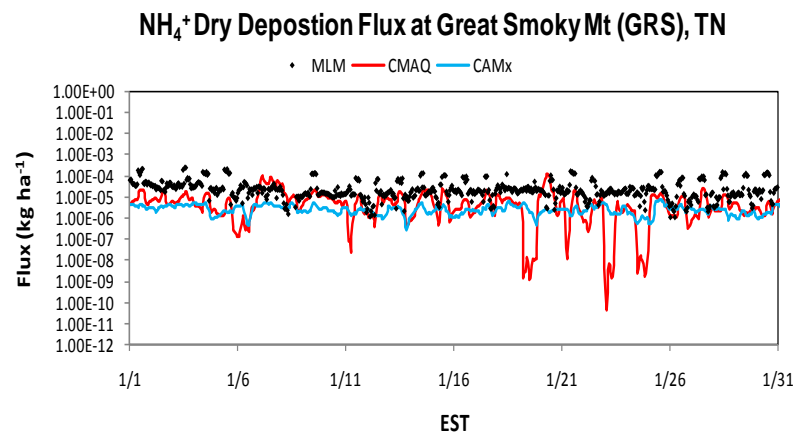
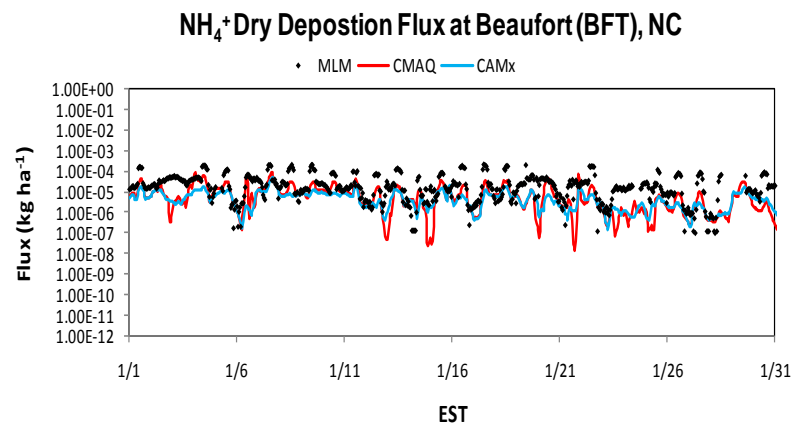


Figure 4.21. NH_4^+ dry deposition velocity in January (top) and July (bottom) as simulated by MLM, CMAQ, and CAMx at Beaufort, NC (left) and Great Smoky Mountains, TN (right).

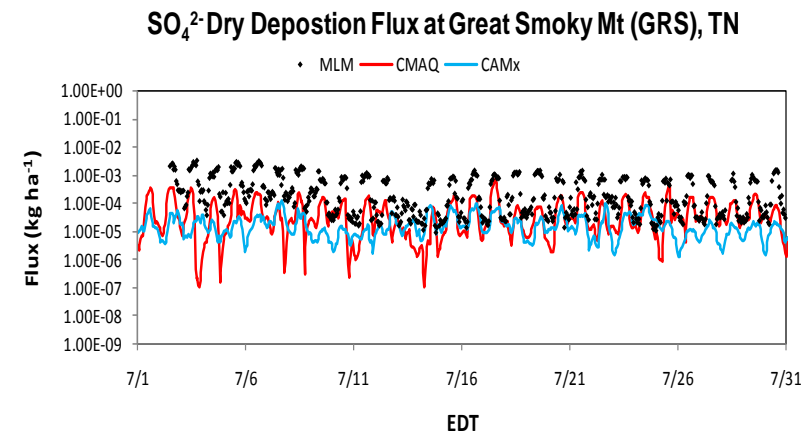
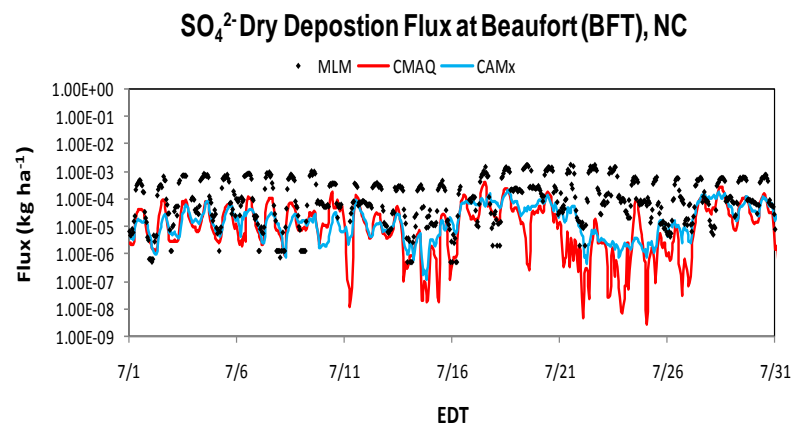
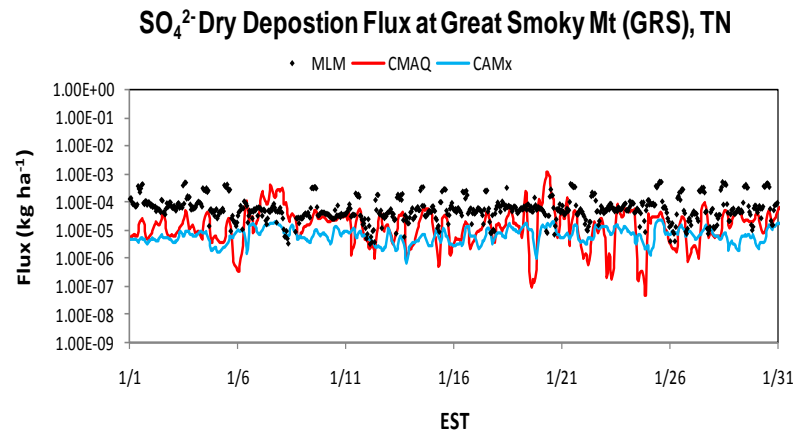
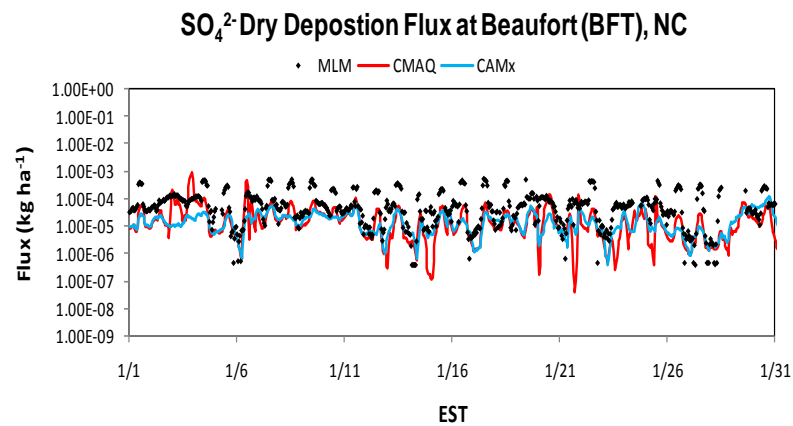


Figure 4.22. SO₄²⁻ dry deposition flux in January (top) and July (bottom) as simulated by MLM, CMAQ, and CAMx at Beaufort, NC (left) and Great Smoky Mountains, TN (right).

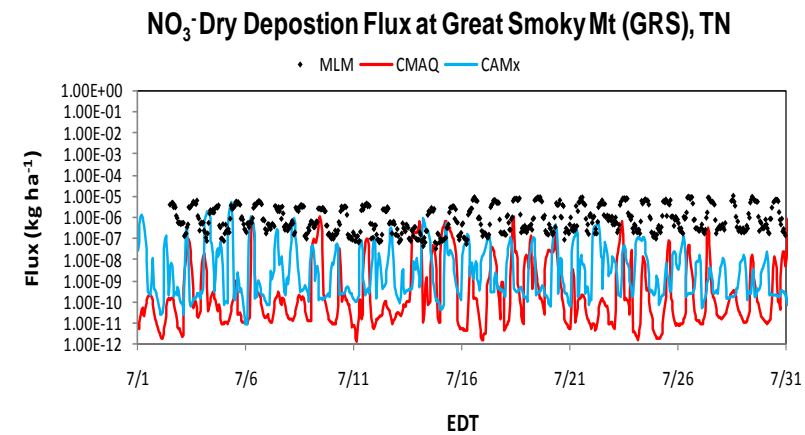
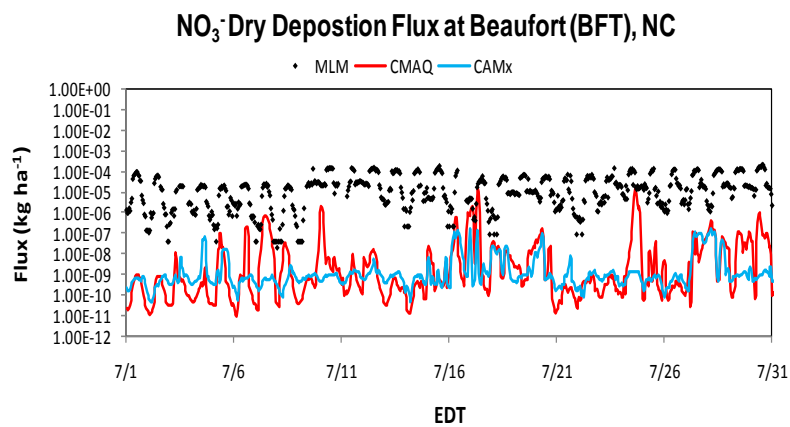
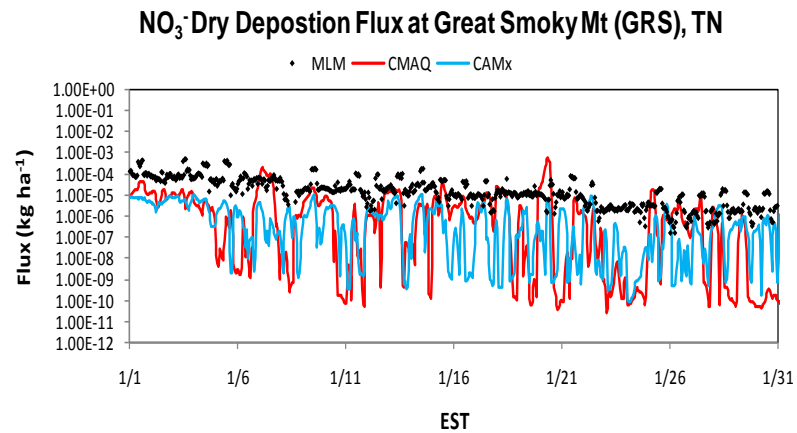
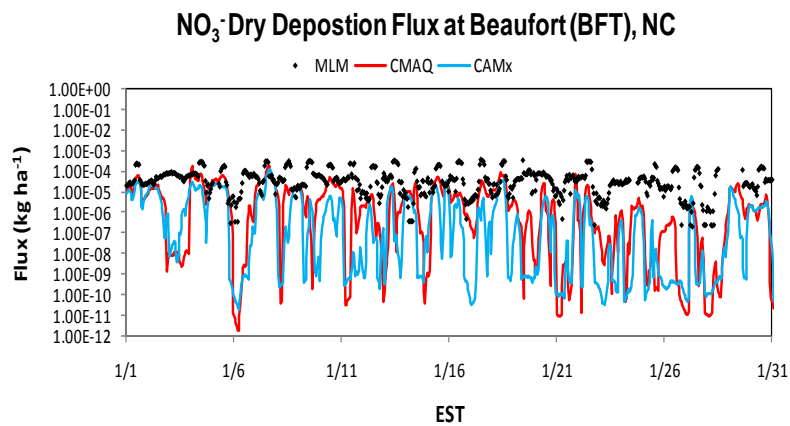


Figure 4.23. NO₃⁻ dry deposition velocity in January (top) and July (bottom) as simulated by MLM, CMAQ, and CAMx at Beaufort, NC (left) and Great Smoky Mountains, TN (right).

accurately modeled in the 3-D air quality models using the single-layer, bulk approaches; however M3Dry in CMAQ does result in some improvement of HNO₃.

4.4 Column Mass of Chemical Species

The performance of CMAQ through the depth of the troposphere is evaluated using satellite observations of CO, NO₂, O₃, and AOD. AOD is calculated from CMAQ simulated PM_{2.5} values using the following equation from Chameides et al. (2002):

$$\tau = \sum_{i=1}^N (\sigma_{sp} + \sigma_{ap})_i \times \Delta z_i \quad (4.1)$$

where σ_{sp} (m⁻¹) is the scattering coefficient and σ_{ap} is the specific absorption coefficient (m⁻¹), Δz is the layer thickness (m), and N is the total number of layers (19 for this simulation). Tables 4.7 and 4.8 provide the performance statistics for January and July, respectively. When compared to satellite observations, tropospheric CO is underpredicted by 4% in January. At the surface, CO is overpredicted, which is used as an indicator that there is weaker vertical mixing in the model. With weaker vertical mixing, less CO would be transported into the upper layers of the model, thus contributing to the underprediction of CO through the depth of the troposphere. Column CO was also underpredicted in July, again likely due to weaker vertical mixing in the model, as surface CO was overpredicted (Table 4.4). Column NO₂ was overpredicted in both months, as was surface NO₂. The overprediction at the surface could allow for excess transport into the upper troposphere, where the lifetime of NO₂ is longer (Seinfeld and Pandis, 2006), contributing to the overprediction of column NO₂.

In January, AOD and O₃ are overpredicted by 29% and 60%, respectively. Engel-Cox et al. (2004a) reported that MODIS AOD correlates well with ground-based PM_{2.5} measurements in the eastern U.S. so the overprediction of surface PM_{2.5} reported in Table 4.3 helps to explain the overprediction of AOD. In July, the AOD and O₃ are both underpredicted, again agreeing with the statistics for the surface evaluation. The underprediction of PM_{2.5} at the surface associated with the early July wildfire contributes the

Table 4.7. Performance statistics for satellite derived variables in January 2002.

Variable	CO (1×10^{17} molecules cm^{-2})	NO₂ (1×10^{15} molecules cm^{-2})	O₃ (DU)	AOD
Satellite	MOPITT	GOME	TOMS	MODIS
Number	32148	32147	32148	32148
MeanObs	20.32	6.60	25.39	0.07
MeanMod¹	19.56	7.49	40.51	0.09
NMB	-0.04	0.14	0.60	0.29
NME	0.07	0.28	0.60	0.36
corr	0.01	0.53	0.23	0.21
MB	-0.75	0.89	15.12	0.02
MAGE	1.51	1.86	15.12	0.03
RMSE	2.26	2.41	15.20	0.03
MNB	-0.02	0.14	0.60	0.37
MNGE	0.08	0.29	0.60	0.42
FB	-0.03	0.08	0.46	0.28
FGE	0.08	0.26	0.46	0.33
NMFB	-0.04	0.13	0.46	0.26
NMFGE	0.08	0.26	0.46	0.31
MNFB	-0.03	0.10	0.60	0.37
MNGFE	0.09	0.33	0.60	0.42
NMBF	-0.04	0.14	0.60	0.29
NMEF	0.08	0.28	0.60	0.36

AOD: Aerosol Optical Depth

MOPITT: Measurements of Pollution in the Troposphere

GOME: Global Ozone Monitoring Experiment

TOMS: Total Ozone Mapping Spectrometer

MODIS: Moderate Resolution Imaging Spectrometer

¹ Simulated values from CMAQ

Table 4.8. Performance statistics for satellite derived variables in July 2002.

Variable	CO (1×10^{17} molecules cm^{-2})	NO₂ (1×10^{15} molecules cm^{-2})	O₃ (DU)	AOD
Satellite	MOPITT	GOME	TOMS	MODIS
Number	32148	31986	32148	32148
MeanObs	20.64	2.70	53.53	0.51
MeanMod	17.81	2.88	37.67	0.26
NMB	-0.14	0.07	-0.30	-0.48
NME	0.16	0.40	0.30	0.49
corr	0.22	0.47	0.70	0.21
MB	-2.82	0.18	-15.86	-0.25
MAGE	3.25	1.07	15.86	0.25
RMSE	3.55	1.76	15.99	0.26
MNB	-0.13	0.04	-0.30	-0.47
MNGE	0.16	0.40	0.30	0.48
FB	-0.14	-0.09	-0.35	-0.63
FGE	0.17	0.37	0.35	0.64
NMFB	-0.15	0.06	-0.35	-0.64
NMFGE	0.17	0.38	0.35	0.64
MNFB	-0.16	-0.10	-0.42	-0.99
MNGFE	0.19	0.54	0.42	1.00
NMBF	-0.16	0.07	-0.42	-0.94
NMEF	0.18	0.40	0.42	0.94

AOD: Aerosol Optical Depth

MOPITT: Measurements of Pollution in the Troposphere

GOME: Global Ozone Monitoring Experiment

TOMS: Total Ozone Mapping Spectrometer

MODIS: Moderate Resolution Imaging Spectrometer

¹ Simulated values from CMAQ

underprediction of the AOD. It is also important to note, however, that the AOD algorithm used in MODIS may have removed high AOD values associated with the wildfire (Engel-Cox et al., 2004a) which would act to reduce the bias between the satellite AOD and the AQM AOD. The overprediction in O_3 at the surface could contribute to the overprediction through the column.

The monthly-mean spatial distributions of the satellite derived variables are displayed in Figures 4.24 – 4.27. Figure 4.24 shows the spatial distribution of column CO in both months. The performance of CMAQ in January appears better than the performance in July, as also indicated by the statistics. In January, the special distribution of higher values in the eastern NC and lower values near the mountains is captured by both the satellite data and CMAQ, despite the coarser resolution of the satellite data. In July, the underprediction is observed throughout the whole domain, with less agreement on the spatial variability than in January. As mentioned, the underprediction of column CO may be due to weaker vertical mixing by the model, resulting in higher CO concentrations at the surface (Tables 4.3 and 4.4) but preventing CO from mixing vertically.

The statistics for column NO_2 indicate an overprediction in both months. The spatial distribution in Figure 4.25 indicates that significant overprediction occurs near the major cities, such as Winston-Salem and Charlotte, NC and Atlanta, GA. The statistics for surface NO_2 at the SEARCH sites near Atlanta, GA also indicate an overprediction in both months. NO_2 has a relatively short lifetime near the surface (Seinfeld and Pandis, 2006), limiting horizontal or vertical transport away from the source. However, if NO_2 does get transported vertically into the upper troposphere, the longer lifetime allows for transport further from the source. Because the overprediction by CMAQ in column NO_2 is localized near the major sources (i.e., cities and roadways), it is likely that the overprediction of NO_2 at the surface is contributing to the overprediction of the column NO_2 .

The O_3 data from TOMS (Figure 4.26) also has a coarse resolution, however, the spatial distribution in January, although overpredicted by CMAQ, is generally captured (i.e., lower O_3 in the western NC and the western GA). In July, column O_3 is significantly underpredicted by CMAQ and shows very little spatial variation, whereas the satellite

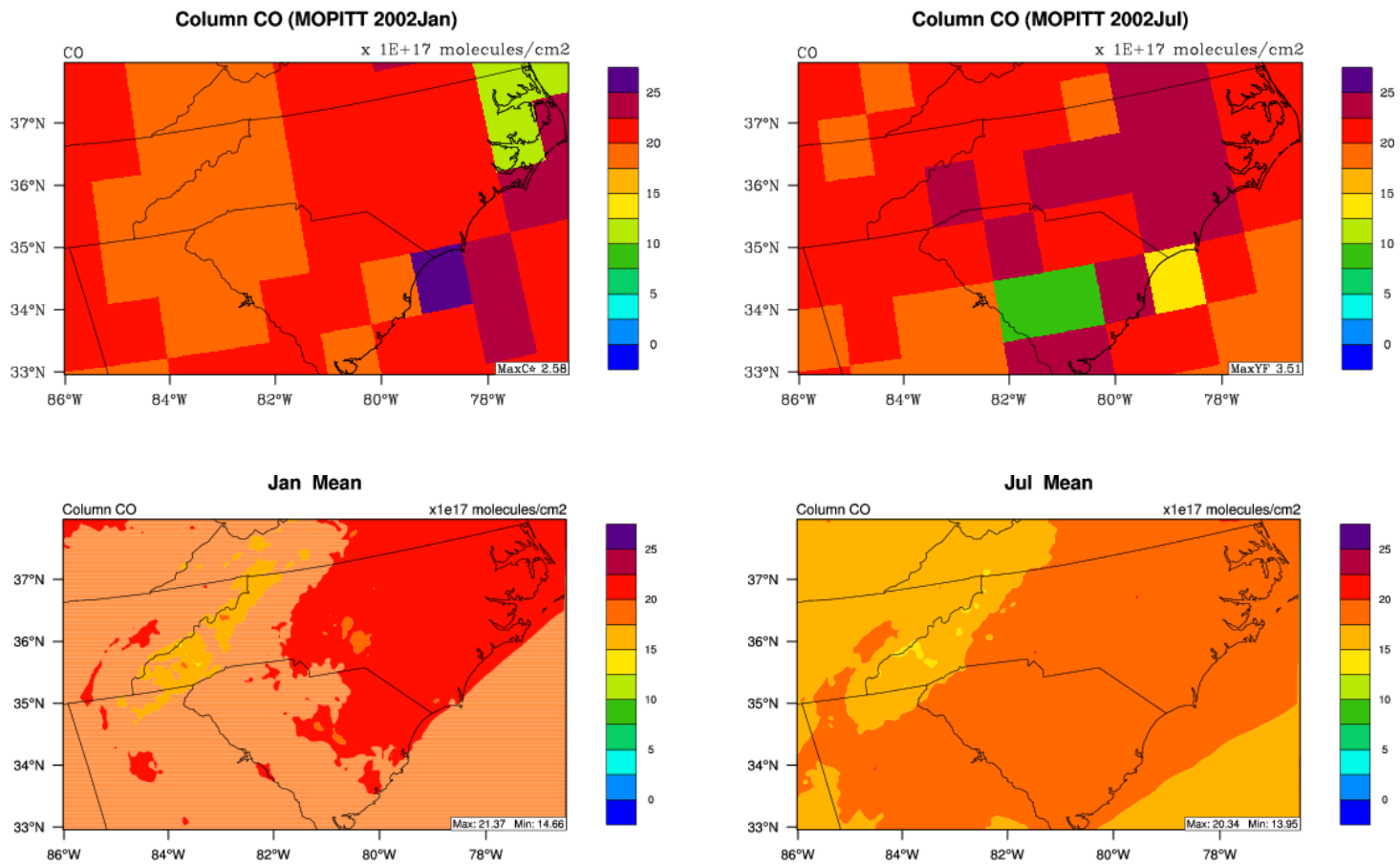


Figure 4.24. Monthly-mean column CO as derived from MOPITT (top) and from the CMAQ simulation (bottom) for January (left) and July (right).

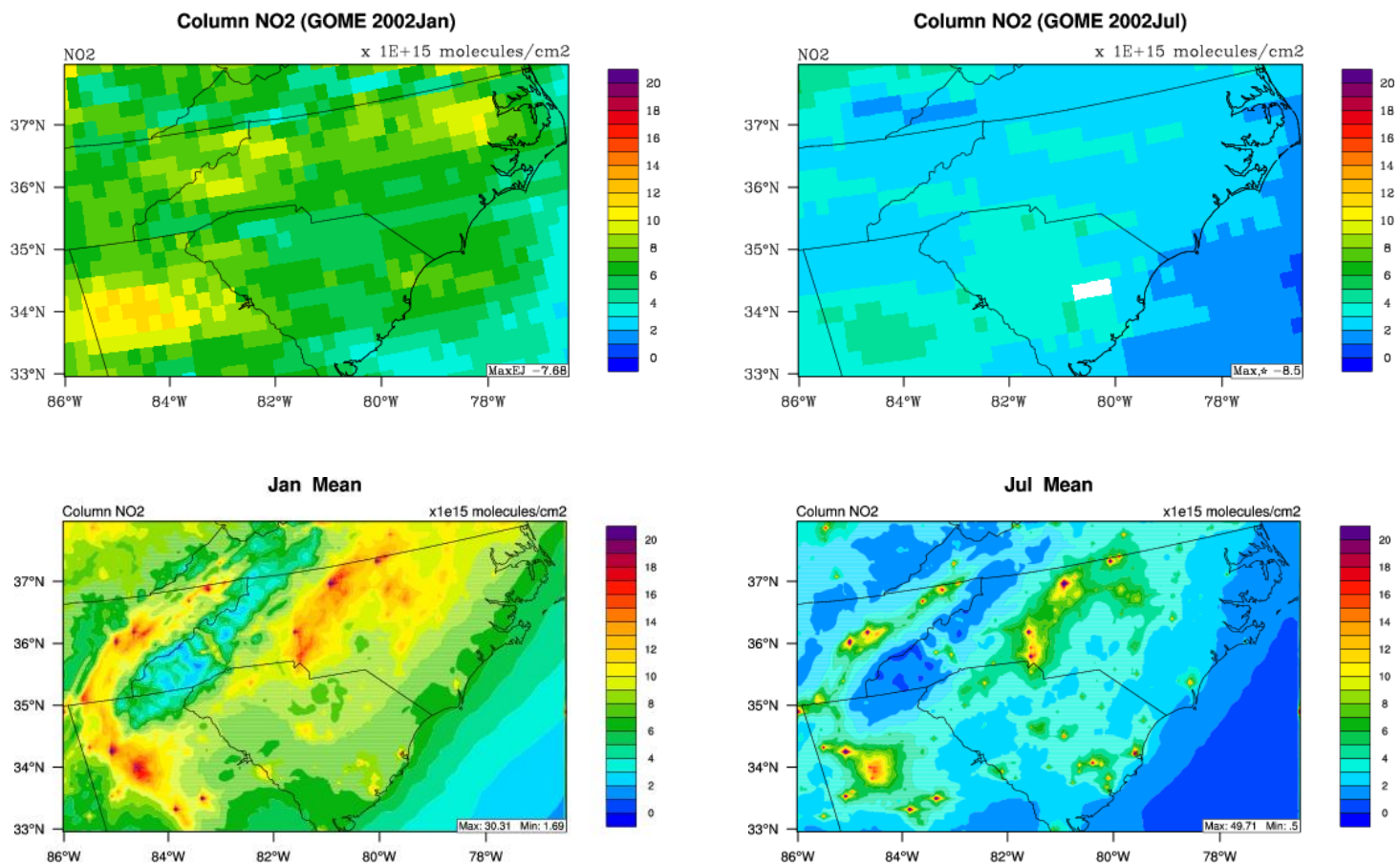


Figure 4.25. Monthly-mean column NO₂ as derived from GOME (top) and from the CMAQ simulation (bottom) for January (left) and July (right).

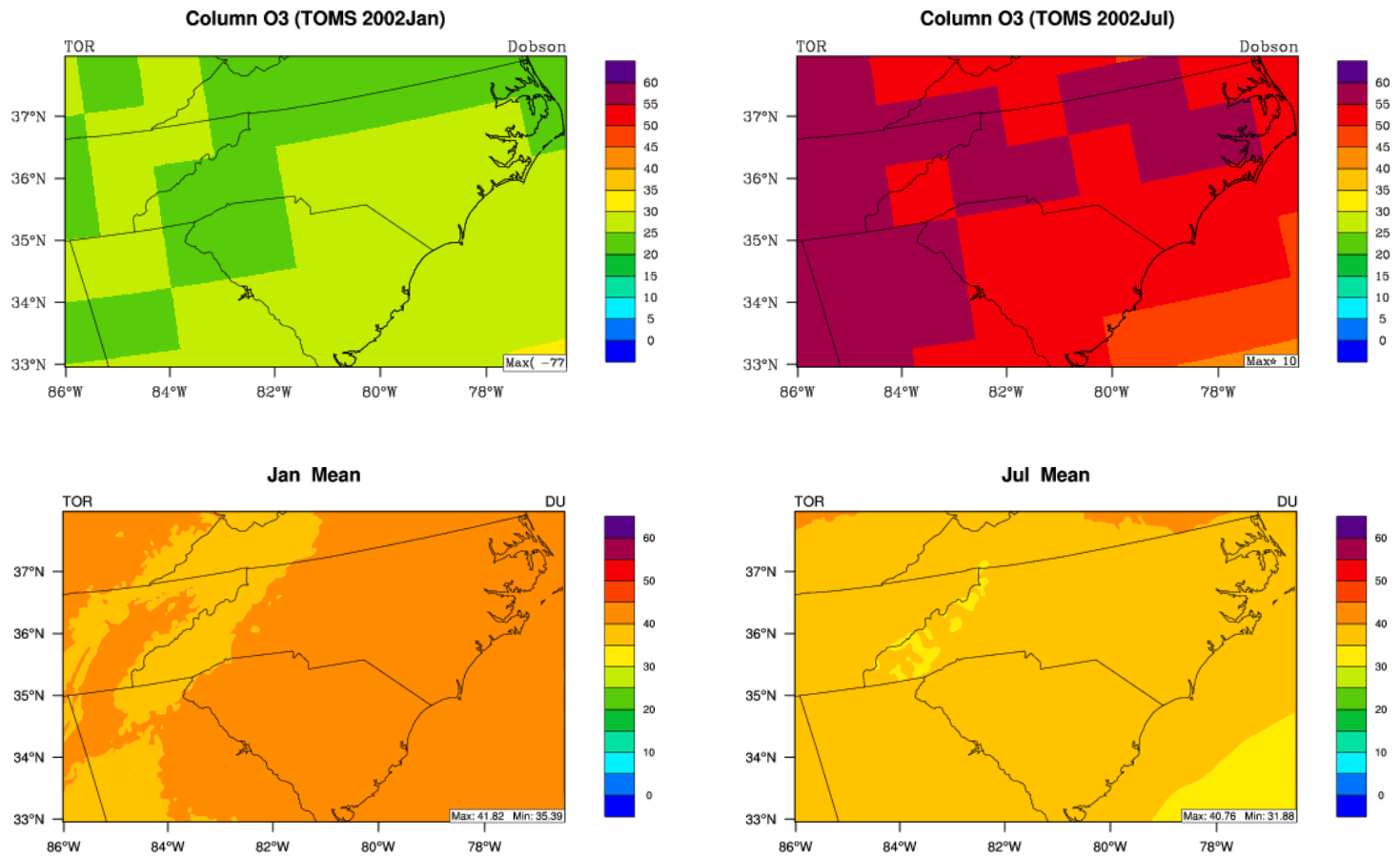


Figure 4.26. Monthly-mean column O₃ as derived from TOMS (top) and from the CMAQ simulation (bottom) for January (left) and July (right).

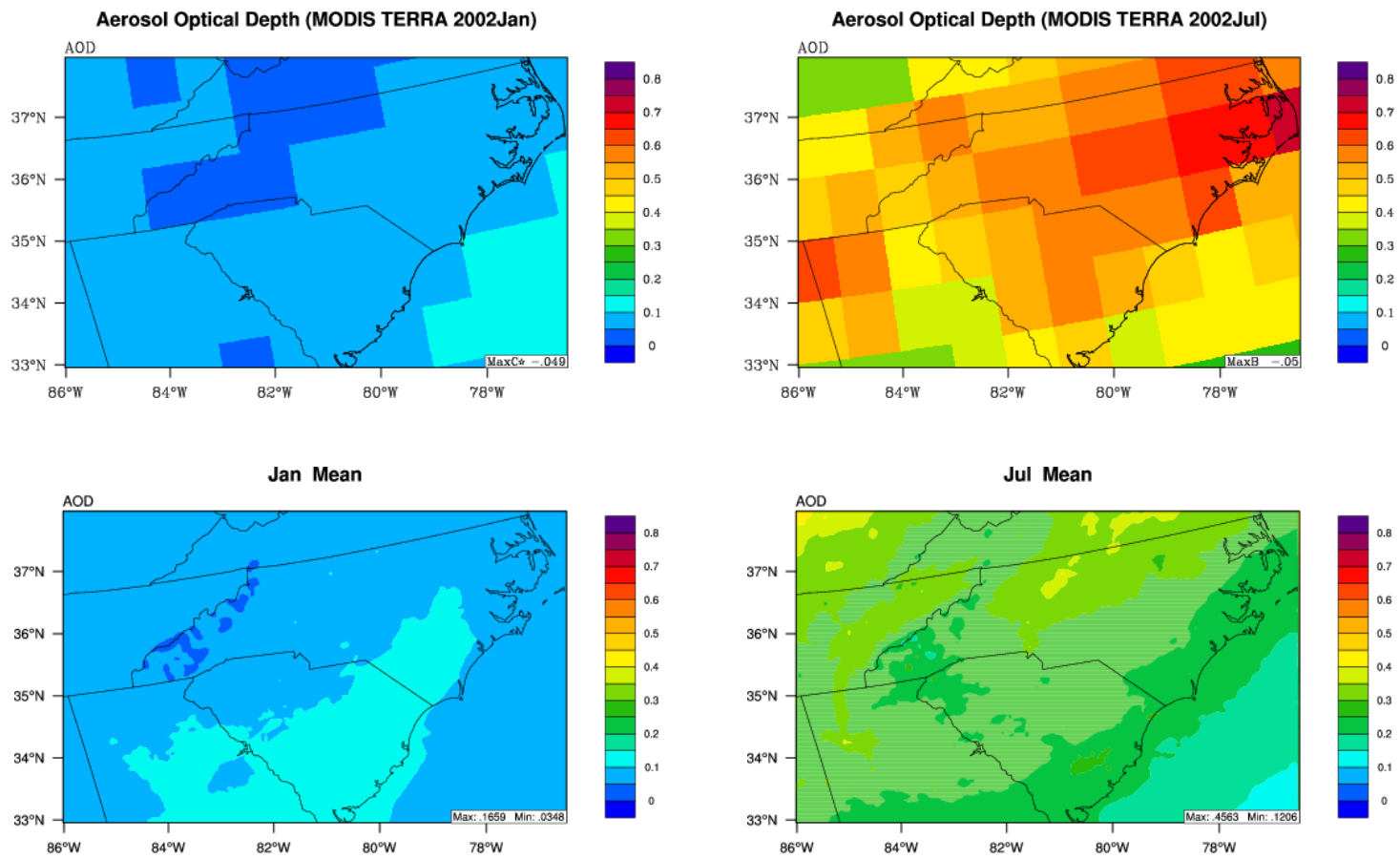


Figure 4.27. Monthly-mean aerosol optical depth (AOD) as derived from MODIS (top) and from the CMAQ simulation (bottom) for January (left) and July (right).

derived O₃ shows regions of higher O₃ in the western half of the domain. The AOD (Figure 4.27) in January is overpredicted by the model throughout most of the domain, but both the observed and modeled AOD values are low, given that PM_{2.5} concentrations in January are low. In July, a significant underprediction is observed, particularly in the eastern NC. As previously mentioned, the satellite-derived AOD can be correlated well with the surface PM_{2.5} measurements in the eastern U.S. (Engel-Cox et al., 2004a), however the coarse resolution of the AOD satellite data makes it difficult to identify fine scale features and variability, such as the lower AOD values over the mountains. Discrepancies between the model simulations and satellite data of tropospheric O₃ and AOD may arise from uncertainties in the BCONs in the upper layers. In the model, there is limited transport of pollutants from the boundary layer into the upper layers, so the derived column O₃ and AOD are significantly impacted by the BCONs in the upper layers (Wang et al., 2009). The BCON for O₃ has an average value of 58 ppb and 54 ppb in January and July, respectively, in the upper layers, which is significantly lower than those used in other models that give closer agreement to TOMS O₃ (e.g., Zhang et al, 2009a).

4.5 Visibility

The general public may not directly notice health impacts of PM_{2.5}, but they may notice the impact on visibility. As mentioned in Chapter 3, the IMPROVE network was established to protect visibility in Federal Class I areas (national parks and woodlands) and some of the sites report optical properties, such as the beta extinction coefficient (β_{ext}) and the haziness index (HI). Additionally, the calculation of optical properties has been incorporated in CMAQ (Binkowski and Roselle, 2003; Mebust et al., 2003). One method that CMAQ uses to calculate β_{ext} is based on the aerosol size distribution. The second method, and the calculation used in this thesis, is based on aerosol species mass concentrations and is similar to the calculation used by IMPROVE:

$$\begin{aligned} \beta_{\text{ext}} \text{ (km}^{-1}\text{)} &= 0.003 \times f(\text{RH}) \times [\text{ammonium} + \text{sulfate} + \text{nitrate}] \\ &+ 0.004 \times [\text{all organic species}] \\ &+ 0.01 \times [\text{elemental carbon}] \end{aligned}$$

$$\begin{aligned}
& + 0.001 \times [\text{unspeciated PM}_{2.5}] \\
& + 0.01
\end{aligned}
\tag{4.2}$$

where $f(\text{RH})$ is a relative humidity factor obtained from a lookup table based on Malm et al. (1994), the brackets are the mass concentration of the species in $\mu\text{g m}^{-3}$ and the coefficients are the scattering efficiencies. The final term in equation 4.2 (0.01) represents Mie scattering, the scattering of light by gas molecules alone. In a pristine environment, where there are no particles scattering light, $\beta_{\text{ext}} = 0.01 \text{ km}^{-1}$ (Mebust et al., 2003). The HI is then calculated by CMAQ using equation 3.2. In pristine conditions, the HI is equal to 0. Because CAMx does not internally calculate any optical properties, the mass concentrations of species at the IMPROVE sites are used in equation 4.2 with a relative humidity factor, $f(\text{RH})$, calculated for each IMPROVE site and explained in Appendix A of the Guidance for Estimating Natural Visibility Conditions Under the Regional Haze Rule (U.S. EPA, 2003). The values used for January and July at the sites within the 4-km domain of this thesis are provided in Table 4.9. For CAMx, β_{ext} is only calculated at the IMPROVE sites, not across the whole domain, so the evaluation is only completed statistically. As mentioned, β_{ext} can be used to calculate the HI, but it can also be used to calculate the visual range (VR) using the following equation (Seinfeld and Pandis, 2006):

$$\text{VR (km)} = 3.912 / \beta_{\text{ext}}
\tag{4.3}$$

The statistics for β_{ext} and HI, as compared to values reported from IMPROVE, are provided in Tables 4.10 and 4.11 for January and July, respectively. VR is not reported by IMPROVE and is not statistically evaluated, however, the spatial distribution by the model will be discussed later. Recall in January, $\text{PM}_{2.5}$ is overpredicted by both models. One would then expect the models to simulate optical properties worse than those observed which means higher β_{ext} and HI. While the statistics show that both models do overpredict β_{ext} , the CAMx value indicates that CAMx simulates a cleaner environment than CMAQ, where in fact Table 4.2 indicates that CAMx predicts higher $\text{PM}_{2.5}$. This may be a result of using different $f(\text{RH})$ values than what CMAQ selected from the look-up table. Table 4.10 also shows that the HI is slightly underpredicted by both models, or closer to pristine conditions than observed, instead of predicting worse visibility. This may indicate that, despite

Table 4.9. Values of $f(\text{RH})$ used to calculate β_{ext} for CAMx at the IMPROVE sites within the 4-km domain (U.S. EPA, 2003).

Area	Site ID	$f(\text{RH})$	
		January	July
Cape Romain, SC	ROMA1	3.2	3.3
Cohutta, GA	COHU1	3.4	3.6
Great Smoky Mountains, TN	GRSM1	3.6	3.6
Linville Gorge, NC	LIGO1	3.2	3.6
Shining Rock, NC	SHRO1	3.3	3.6
Swanquarter, NC	SWAN1	2.9	3.1

Table 4.10. Statistics for visibility parameters in January 2002.

Variable	β_{ext} (Mm⁻¹)		HI (dev)	
Network	IMPROVE		IMPROVE	
Model	CMAQ	CAMx	CMAQ	CAMx
Number	42		42	
MeanObs	52.37		17.72	
MeanMod	102.64	63.04	16.94	17.40
NMB	0.96	0.20	-0.04	-0.02
NME	1.20	0.30	0.27	0.13
corr	0.32	0.60	0.58	0.71
MB	50.27	10.67	-0.78	-0.32
MAGE	62.63	15.60	4.84	2.27
RMSE	135.78	27.34	6.07	3.11
MNB	0.97	0.27	-0.05	-0.01
MNGE	1.18	0.35	0.27	0.14
FB	0.27	0.16	-0.11	-0.03
FGE	0.52	0.25	0.28	0.13
NMFB	0.65	0.19	-0.05	-0.02
NMFGE	0.81	0.27	0.28	0.13
MNFB	0.91	0.27	-0.14	-0.03
MNGFE	1.24	0.36	0.36	0.15
NMBF	0.96	0.20	-0.05	-0.02
NMEF	1.20	0.30	0.29	0.13

Note: Mm = 1,000 km

Table 4.11. Statistics for visibility parameters in July 2002.

Variable	β_{ext} (Mm⁻¹)		HI (dev)	
Network	IMPROVE		IMPROVE	
Model	CMAQ	CAMx	CMAQ	CAMx
Number	32		32	
MeanObs	107.86		23.51	
MeanMod	53.63	80.75	14.04	19.22
NMB	-0.50	-0.25	0.41	-0.18
NME	0.58	0.41	-0.54	0.22
corr	0.33	0.56	29.82	0.70
MB	-54.23	-27.12	9.64	-4.30
MAGE	62.40	44.29	10.66	5.25
RMSE	76.34	54.68	-0.40	6.08
MNB	-0.43	-0.19	0.41	-0.18
MNGE	0.53	0.40	-0.40	0.23
FB	-0.65	-0.30	0.54	-0.23
FGE	0.73	0.46	-0.51	0.27
NMFB	-0.67	-0.29	0.51	-0.20
NMFGE	0.77	0.47	-0.86	0.25
MNFB	-1.27	-0.47	0.86	-0.31
MNGFE	1.38	0.68	-0.68	0.35
NMBF	-1.01	-0.34	0.69	-0.22
NMEF	1.16	0.55	0.53	0.27

Note: Mm = 1,000 km

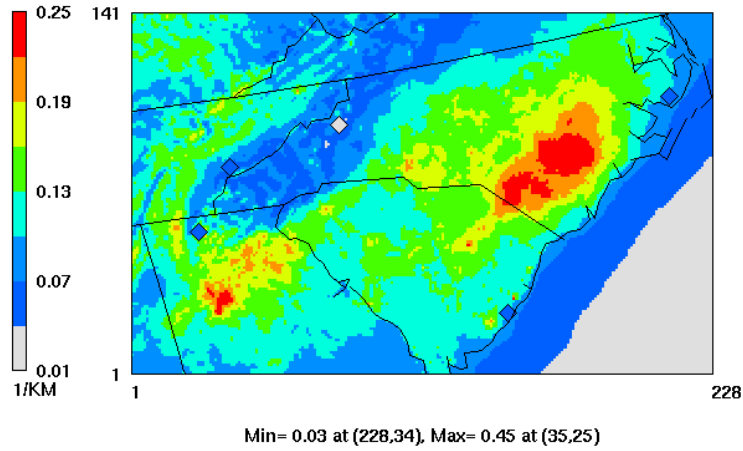
overpredicted $PM_{2.5}$ at the IMPROVE sites, the perceived change in visibility due to the particles is negligible in January. The simulated optical properties in July perform as expected. $PM_{2.5}$ is underpredicted at the IMPROVE sites in July, so one would expect an improved visibility performance. Table 4.11 does show lower β_{ext} and HI, with the more pristine environment simulated by CMAQ, as shown in the $PM_{2.5}$ statistics.

Figure 4.28 and 4.29 show the spatial distribution of the three optical properties, extinction coefficient, haziness index, and visual range, as simulated by CMAQ in January and July, respectively. Because the extinction coefficient calculated for CAMx is site specific, not domain-wide, no spatial distribution is provided for CAMx. The spatial distributions for January (Figure 4.28) show that the worse visibility (high β_{ext} and HI, low VR) are in the eastern NC and northern GA, the same locations as the highest NH_3 emissions. The spatial distributions also confirm that the best visibility is over the ocean and in the mountains, resulting in large variations of visibility throughout the domain. In July, there is not much change in visibility throughout the domain as there is in January. While the eastern NC and northern GA do show some visibility degradation, the regions of the poorest visibility in July are generally to the west of the mountains. This seasonal variation indicates that NH_3 may play a significant role in visibility degradation in January and less of a role in July.

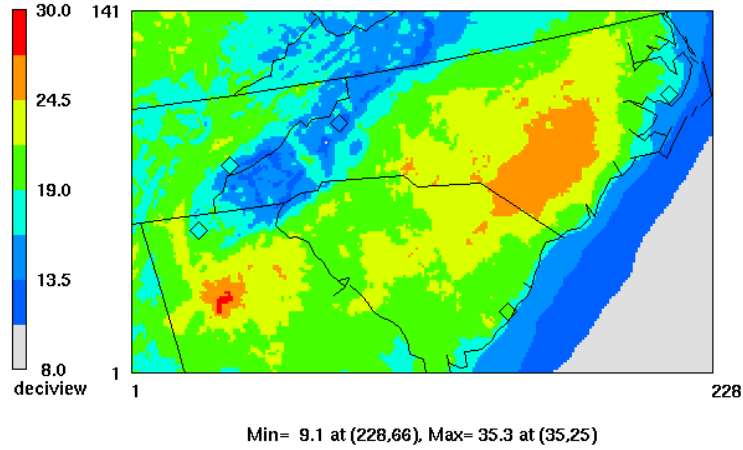
4.6 Summary

This chapter evaluates the performance of two commonly-used air quality modeling systems, MM5/CMAQ and MM5/CAMx, in January and July, 2002 at a horizontal grid spacing of 4-km using numerous observational networks. Simulated 2-m temperature and relative humidity using MM5 are generally within $\pm 10\%$ of the observed values. Precipitation in July is significantly overpredicted, which impacts the removal of pollutants through wet deposition. Both models overpredict $PM_{2.5}$ and maximum O_3 in the surface layer in January, with CAMx predicting higher values. This is likely due to weaker vertical mixing simulated by the models, particularly CAMx, as indicated by an overprediction in CO. Although CO is also overpredicted in July by both models, $PM_{2.5}$ and O_3 are

(a) CMAQ – January – Extinction Coefficient



(b) CMAQ – January – Haze Index



(c) CMAQ – January – Visual Range

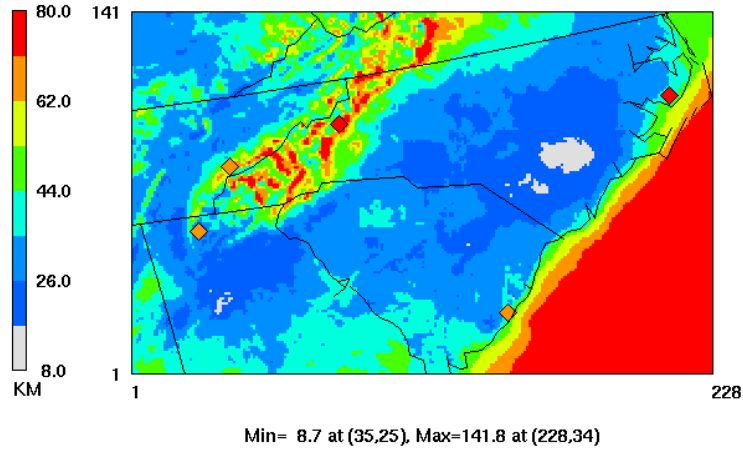
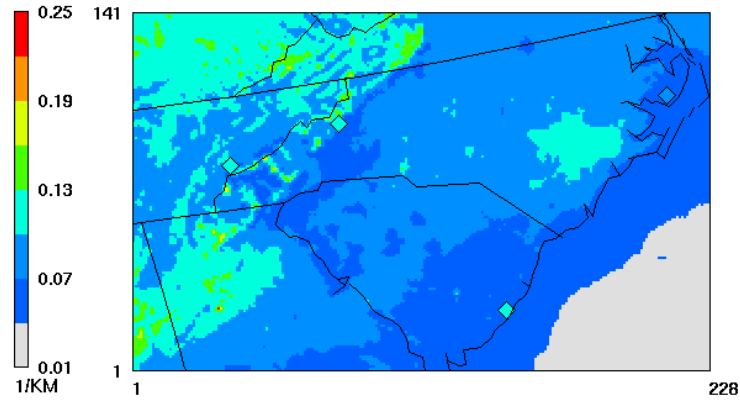


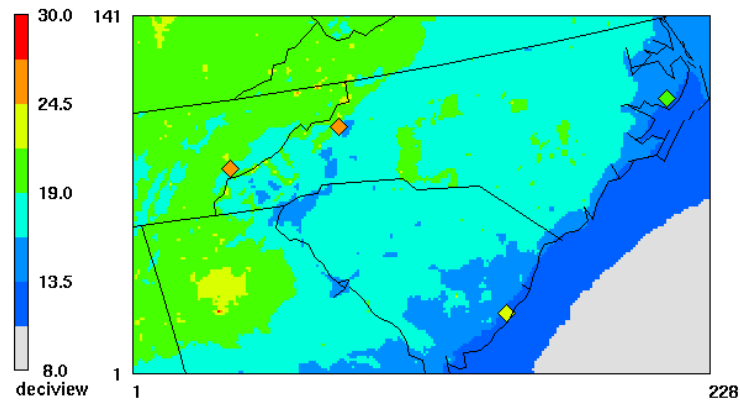
Figure 4.28. The monthly-mean (a) extinction coefficient, (b) haze index, and (c) visual range in January, based on the CMAQ simulation, overlaid with observations from IMPROVE (diamonds).

(a) CMAQ – July – Extinction Coefficient



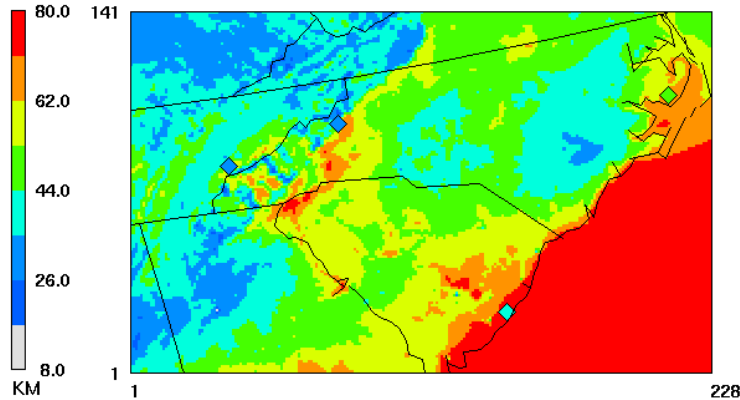
Min= 0.03 at (228,3), Max= 0.33 at (35,25)

(b) CMAQ – July – Haziness Index



Min= 7.1 at (228,3), Max= 33.2 at (35,25)

(c) CMAQ – July – Visual Range



Min= 11.8 at (35,25), Max=154.3 at (228,3)

Figure 4.29. The monthly-mean (a) extinction coefficient, (b) haziness index, and (c) visual range in July, based on the CMAQ simulation, overlaid with observations from IMRPOVE (diamonds).

underpredicted. This is partly due to excess removal of pollutants through wet deposition (i.e., SO_4^{2-}), but may also indicate an underestimation of emissions of PM precursor species. The diurnal variations of O_3 are simulated better than the diurnal variations of $\text{PM}_{2.5}$ because the formation mechanisms of O_3 are better understood and represented in the models. Difficulties in simulating $\text{PM}_{2.5}$ arise from the volatility of some species (i.e., NO_3^-) and lack of information in the formation mechanisms (i.e. SOA). Differences between CMAQ and CAMx simulation results can be attributed to model differences, such as the treatment of vertical mixing and SOA formation, PM size representation (i.e., modal vs. sectional), and wet and dry deposition modules.

The spatial distribution of the AdjGR indicates that the eastern NC and northeastern GA are NH_3 -rich regions and reducing NH_3 will result in little change in $\text{PM}_{2.5}$ concentrations. The NH_3 -rich regions as simulated by CAMx are larger in both months than the regions simulated by CMAQ, likely due to lower NO_3^- and HNO_3 concentrations.

5. SENSITIVITY TO HORIZONTAL GRID SPACING AND EMISSION REDUCTIONS

Two types of sensitivity evaluations have been completed. The first one to be discussed in section 5.1 is the sensitivity of MM5/CMAQ to horizontal grid resolution. The performance of MM5/CMAQ at 4- and 1.33-km horizontal grid spacing is evaluated against observations and inter-compared, along with the performance of VISTAS simulation at a horizontal grid spacing of 12-km. The second sensitivity study completed (Section 5.2) is the sensitivity of CMAQ at a 4-km horizontal grid spacing to reductions in emissions, specifically a 50% reduction in AL-NH₃, SO₂, and NO_x (Section 5.2). The objectives of these sensitivity simulations are to assess model performance at finer grid spacings and to determine if reductions in AL-NH₃ can aid in reducing PM_{2.5} concentrations in the southeastern U.S when combined with projected SO₂ and NO_x emission reductions.

5.1 Sensitivity to Horizontal Grid Spacing

Advancements in technology have allowed for continuous improvements to 3-D air quality models, including the ability to complete simulations at increasingly finer grid spacing. The following sections evaluate and compare MM5/CMAQ simulations completed at horizontal grid spacings of 12-, 4-, and 1.33-km. The evaluation is only completed for the domain common to all three grid spacings, which limits the observational sites from some networks (see Table 3.3).

5.1.1 Meteorology

Prior to evaluating the sensitivity of the air quality model, the performance and sensitivity of the meteorology model at the three grid spacings is evaluated. Table 5.1 provides the statistics for the meteorological variables in January for the central and eastern NC at all three grid spacings. In January, the use of 1.33-km horizontal grid spacing does not improve the model performance at the CASTNET or STN sites. However, it is important to note that the observations are limited to one CASTNET site and nine STN sites within the domain. The statistics for July (Table 5.2) temperature, wind speed, wind direction and

Table 5.1. Mean biases and NMBs of meteorological variables for January at 12-, 4-, and 1.33-km horizontal grid spacing. Bold numbers indicate the lowest NMBs for the corresponding variables.

Variable	Network	Data #	Mean Obs	Mean Bias			NMB (%)		
				12-km	4-km	1.33-km	12-km	4-km	1.33-km
T2 (°C)	CASTNET	549	7.0	-1.2	-2.0	-1.9	-15.2	-28.2	-27.4
	STN	21	6.3	0.7	0.7	0.7	11.4	10.8	11.1
RH2 (%)	CASTNET	739	63.7	7.2	14.3	14.9	11.3	22.5	23.4
WSP10 (m s ⁻¹)	CASTNET	442	2.2	0.4	0.6	0.6	15.8	23.2	22.6
WDR10 (°)	CASTNET	644	168.2	9.7	14.4	15.5	11.1	8.5	9.2
Precip (mm)	NADP	15	32.9	-4.3	-7.1	-9.9	-13.1	-21.5	-30.3

NMB: Normalized Mean Bias

T2: Temperature at 2-m

RH2: Relative Humidity at 2-m

WSP10: Wind Speed at 10-m

WDR10: Wind Direction at 10-m

Precip: Precipitation (weekly)

CASTNET: Clean Air Status and Trends Network

STN: Speciation Trends Network

NADP: National Atmospheric Deposition Program

precipitation do show improvement when using the finer grid spacing, emphasizing the importance of sensitivity analysis to grid resolution when selecting a domain and episode.

The spatial distribution of monthly-mean temperature in January (Figure 5.1) shows very similar performance between the 4- and 1.33-km simulations, however, all three simulations show an underprediction of temperatures throughout central NC. In July (Figure 5.2), the 12-km simulation more accurately captures the regions of central NC with higher monthly-mean temperatures; however, it fails to capture the regions of lower temperatures. More detail is simulated by the 4- and 1.33-km simulations, which are able to capture the regions of lower monthly-mean temperature that the 12-km simulation was not able to capture. Figure 5.3 shows the spatial distribution of monthly-mean relative humidity within the domain. The 4- and 1.33-km simulations predicted much higher relative humidity along the coast, likely due to an inaccurate representation of the snow cover from the early January snow event. The 12-km simulation also shows a significant overprediction of monthly-mean relative humidity in the eastern half of the domain. While the topography of the mountains in the western half of the domain is more detailed at the finer resolutions, this appears to be more detrimental than beneficial for January monthly-mean relative humidity. In July (Figure 5.4), the eastern half is again overpredicted at all three grid spacings, while the simulations at the finer grid spacings of 4- and 1.33-km appear to perform slightly better than the 12-km simulation near the mountains.

Figures 5.5 and 5.6 show the times series in January and July, respectively, for the meteorological variables at the CASTNET site in Candor, NC (central). All three grid spacings show similar performance temporally for all variables. The simulations at 4- and 1.33-km horizontal grid spacing give colder temperatures and higher relative humidity associated with the early January snow storm compared to the 12-km simulation. The 12-km simulation also predicts lower relative humidity at the middle and end of January than the 4- and 1.33-km. The simulation of wind speed and wind direction in January is nearly identical among all three simulations, indicating that these variables may be less sensitive to horizontal grid resolution in January than the other variables. In July (Figure 5.6), the 12-km simulation

Table 5.2. Mean biases and NMBs of meteorological variables for July at 12-, 4-, and 1.33-km horizontal grid spacing. Bold numbers indicate the lowest NMBs for the corresponding variables.

Variable	Network	Data #	Mean Obs	Mean Bias			NMB (%)		
				12-km	4-km	1.33-km	12-km	4-km	1.33-km
T2 (°C)	CASTNET	740	25.8	1.1	0.4	-0.1	4.1	1.4	-0.4
	STN	38	26.7	-0.6	-0.9	-1.3	-2.1	-3.5	-5.0
RH2 (%)	CASTNET	744	66.2	2.1	4.9	5.9	3.2	7.5	9.0
WSP10 (m s ⁻¹)	CASTNET	344	1.8	0.5	0.8	0.3	23.5	34.2	16.2
WDR10 (°)	CASTNET	659	149.4	26.6	20.2	16.2	17.8	13.5	10.9
Precip (mm)	NADP	20	30.2	34.8	62.5	26.2	115.1	206.1	86.7

NMB: Normalized Mean Bias

T2: Temperature at 2-m

RH2: Relative Humidity at 2-m

WSP10: Wind Speed at 10-m

WDR10: Wind Direction at 10-m

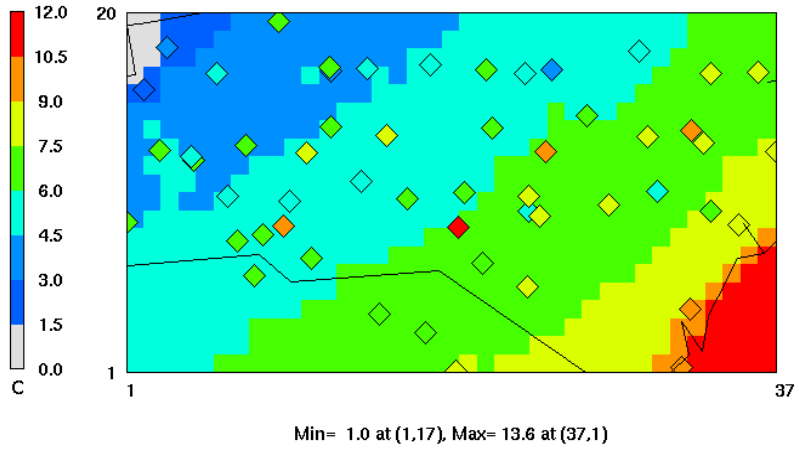
Precip: Precipitation (weekly)

CASTNET: Clean Air Status and Trends Network

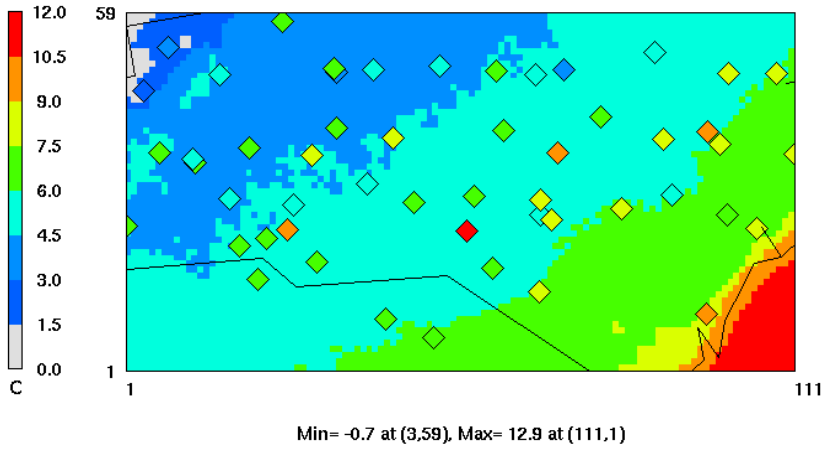
STN: Speciation Trends Network

NADP: National Atmospheric Deposition Program

(a)



(b)



(c)

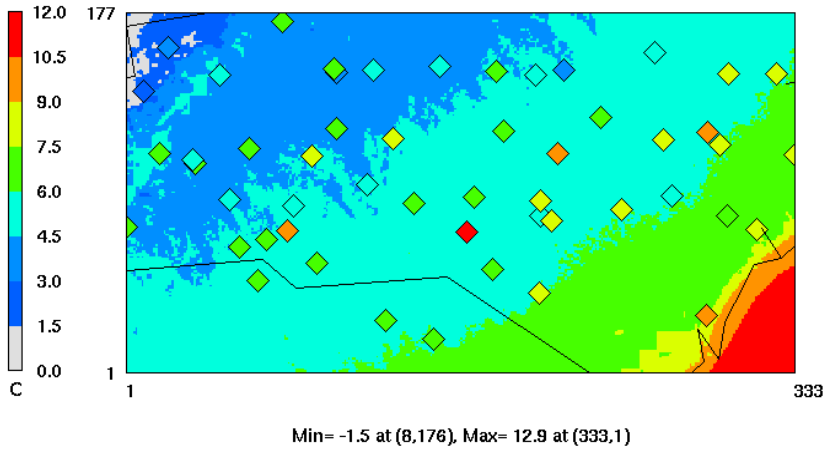
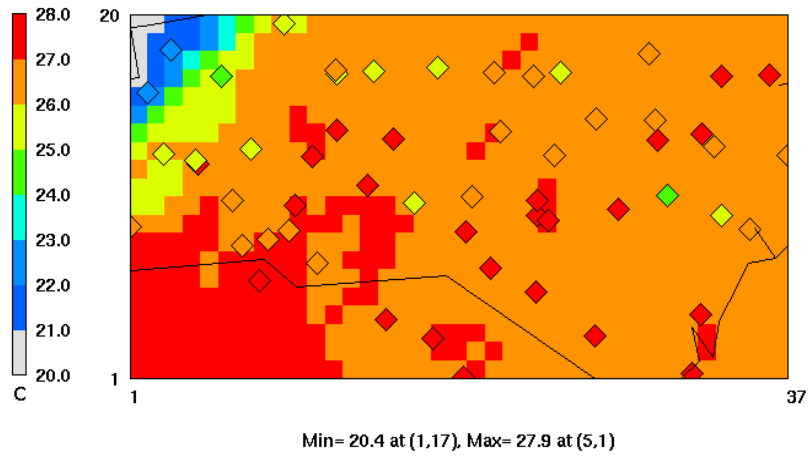
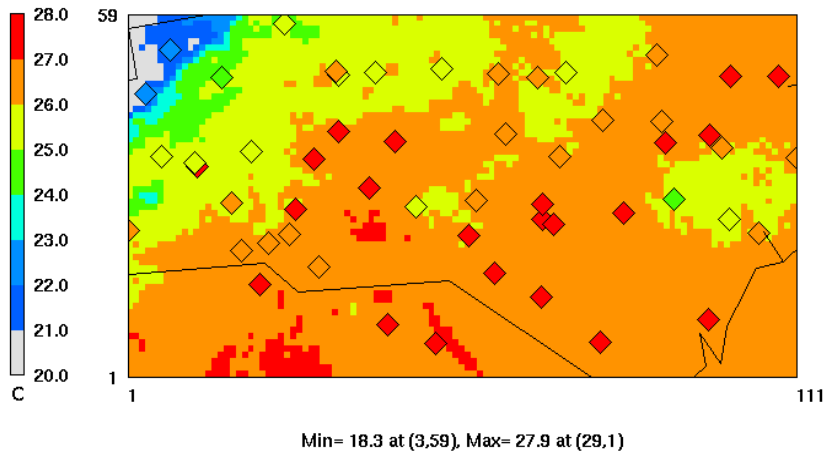


Figure 5.1. Spatial distribution of monthly-mean temperature in January at a grid spacing of (a) 12-km, (b) 4-km, and (c) 1.33-km, all overlaid with observations from CASTNET, STN, and NC SCO.

(a)



(b)



(c)

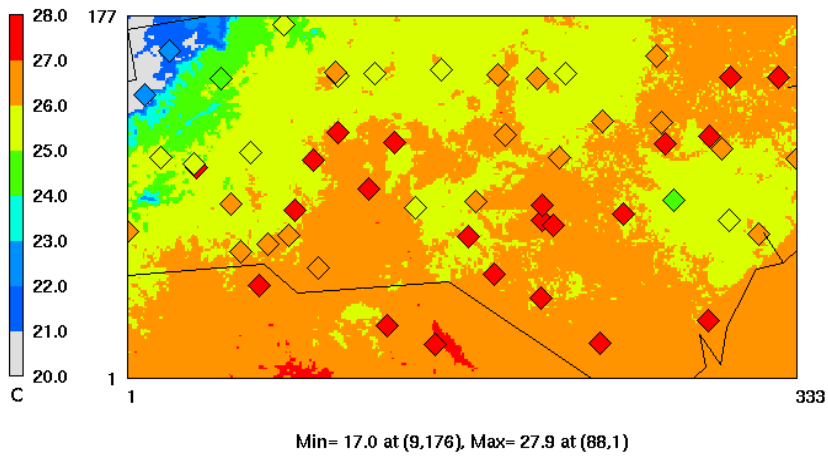
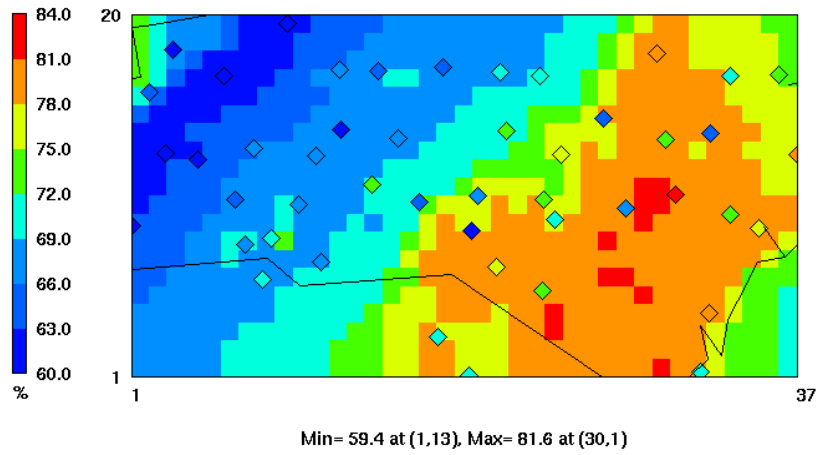
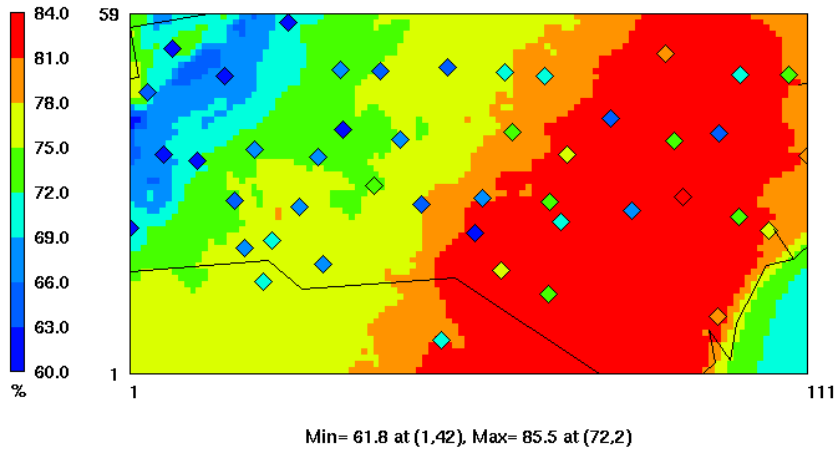


Figure 5.2. Spatial distribution of monthly-mean temperature in July at a grid spacing of (a) 12-km, (b) 4-km, and (c) 1.33-km, all overlaid with observations from CASTNET, STN, and NC SCO.

(a)



(b)



(c)

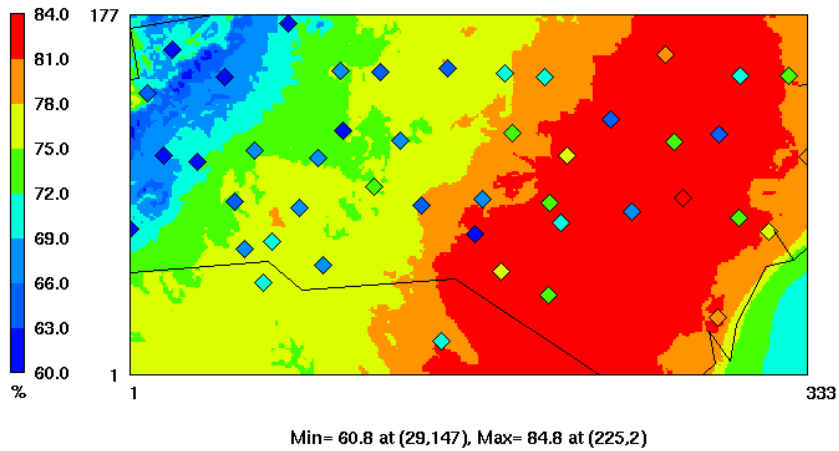


Figure 5.3. Spatial distribution of monthly-mean relative humidity in January at a grid spacing of (a) 12-km, (b) 4-km, and (c) 1.33-km, all overlaid with observations from CASTNET and NC SCO.

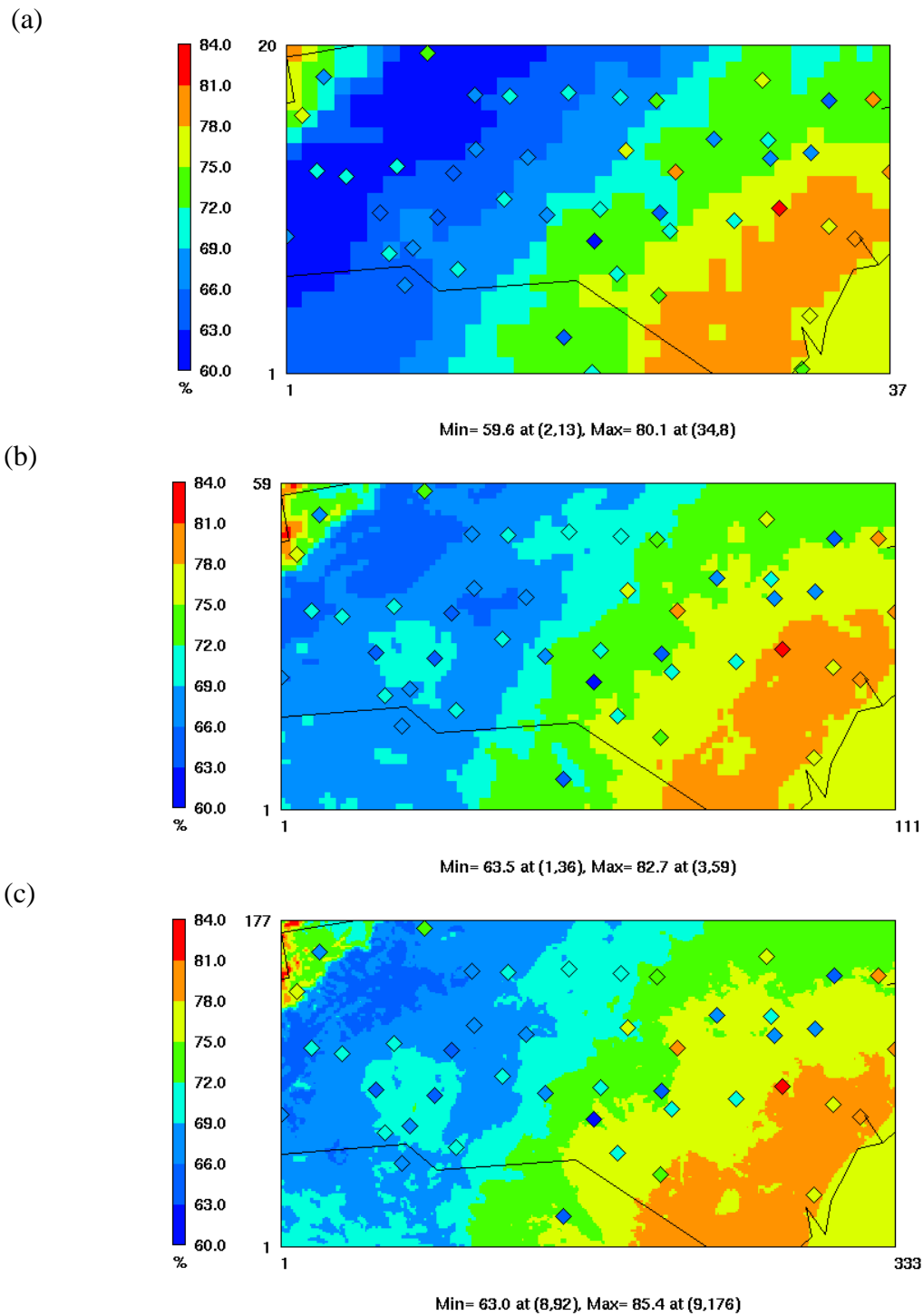


Figure 5.4. Spatial distribution of monthly-mean relative humidity in July at a grid spacing of (a) 12-km, (b) 4-km, and (c) 1.33-km, all overlaid with observations from CASTNET and NC SCO.

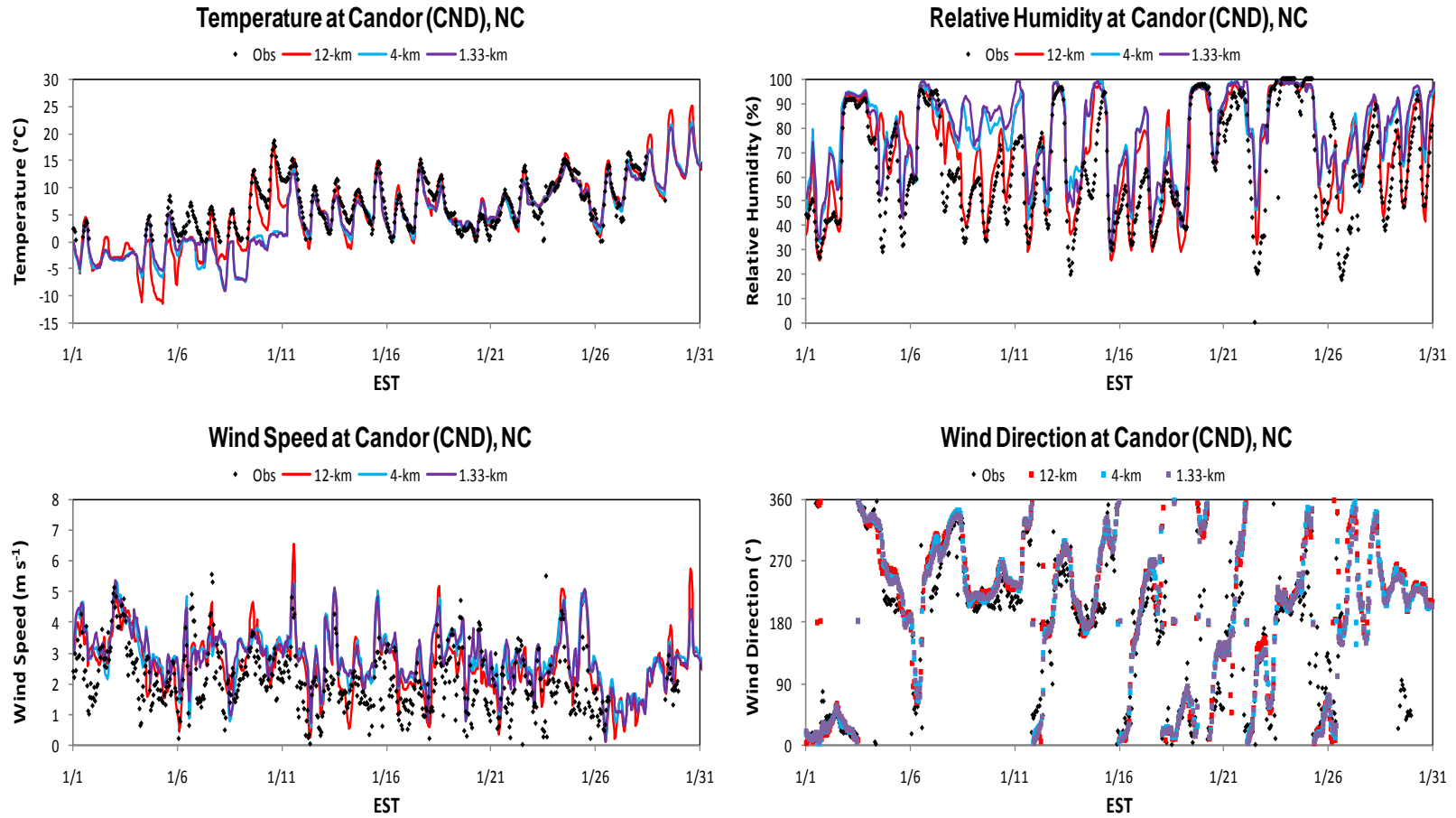


Figure 5.5. Time series for meteorological variables at Candor, NC in January at 12-, 4-, 1.33-km horizontal grid spacing.

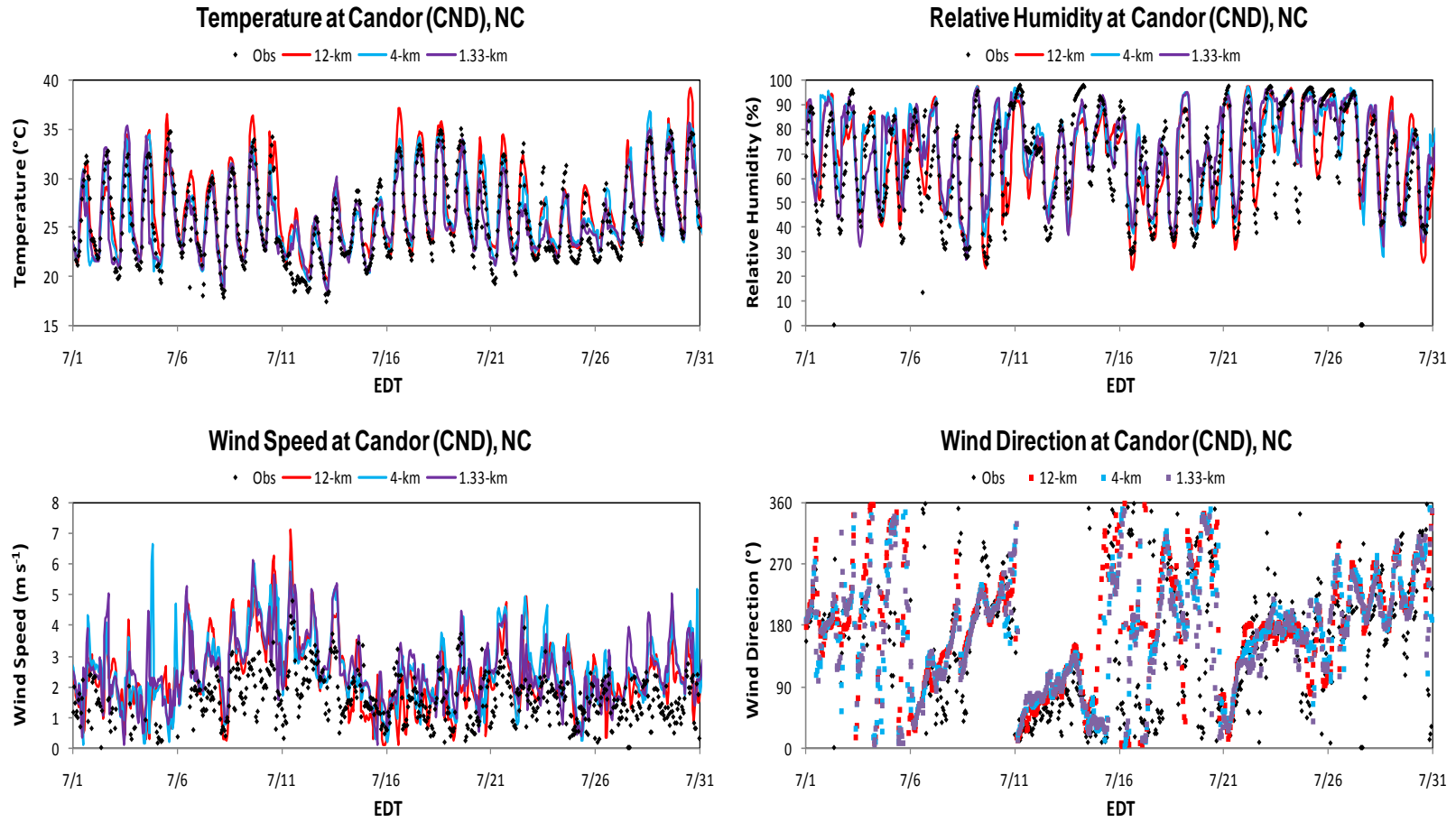


Figure 5.6. Time series for meteorological variables at Candor, NC in July at 12-, 4-, 1.33-km horizontal grid spacing.

predicts higher daytime temperatures and lower nighttime relative humidity than the finer grid spacing at the Candor site, which agrees with the spatial distribution and statistics.

5.1.2 Emissions

In addition to meteorology, differences in emissions at various grid spacings can also influence the performance of the air quality model. Figures 5.7 through 5.13 show the spatial distribution of the percentage difference of the monthly-mean emissions of gaseous precursors (i.e., NH₃, SO₂, NO₂, NO) and primary PM (i.e., PM_{2.5}, SO₄²⁻ and NO₃⁻) in January and July 2002 as simulated by SMOKE. The percentage differences are calculated by subtracting the coarse grid emissions from the 1.33-km emissions and dividing that value by the coarse grid emissions (i.e., $\{(1.33\text{-km} \times 9) - (4\text{-km})\} / (4\text{-km})$ and $\{(1.33\text{-km} \times 81) - (12\text{-km})\} / (12\text{-km})$, where the constants 9 and 81 are the number of fine grid cells in one coarser grid cell). Overall, the largest differences in emissions occur between the 1.33-km and the 12-km as would be expected. The differences in NH₃ emissions (Figure 5.7) show that the AL-NH₃ emissions in the eastern NC are the same among all three grid spacings. The small regions of differences in NH₃ emissions that do exist between grid spacings occur mainly in the central NC near cities (i.e., Raleigh, Durham, and Charlotte). The differences in SO₂ (Figure 5.8), NO₂ (Figure 5.9), and NO (Figure 5.10) occur throughout the domain, mainly along roadways, and are similar between January and July. The differences in primary PM emissions (including PM_{2.5} (Figure 5.11), SO₄²⁻ (Figure 5.12), and NO₃⁻ (Figure 5.13)) indicate some seasonal sensitivity to horizontal grid spacing with larger differences and more regions of differences in July than January. Although the differences for NO₃⁻ are larger in July than January, the actual emissions are less so even small differences can result in larger percentage differences. All of these differences can be attributed to the smoothing out of emissions in the coarser grid spacing. The coarse grid spacing may require a wide range of emissions be simulated as more of an average value, distributing high emissions uniformly throughout a larger grid compared to the emissions confined to smaller grid cells.

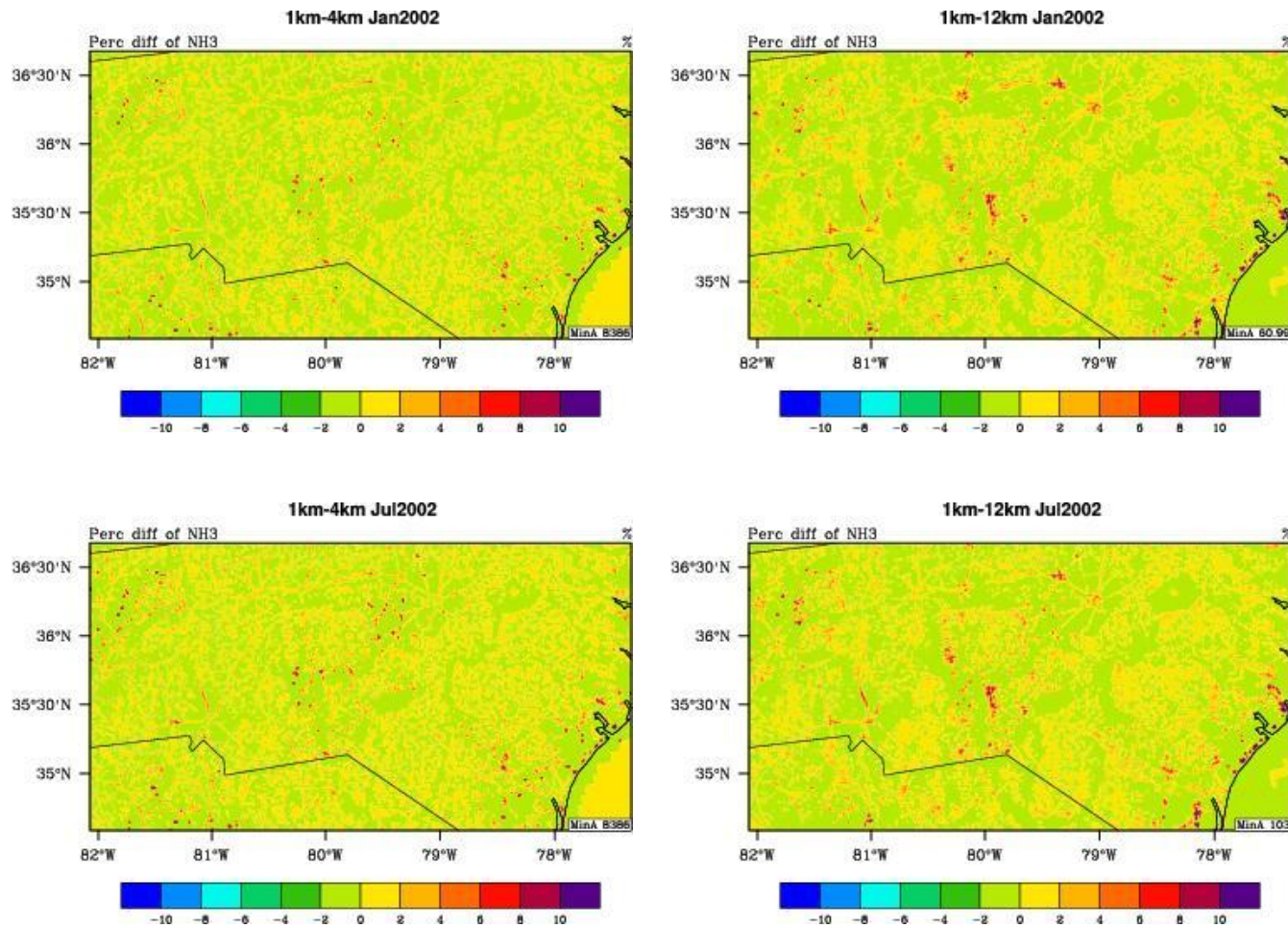


Figure 5.7. Spatial distributions of the percentage difference of monthly-mean NH₃ emissions at 1.33-km compared to 4-km (left) and 12-km (right) in January (top) and July (bottom).

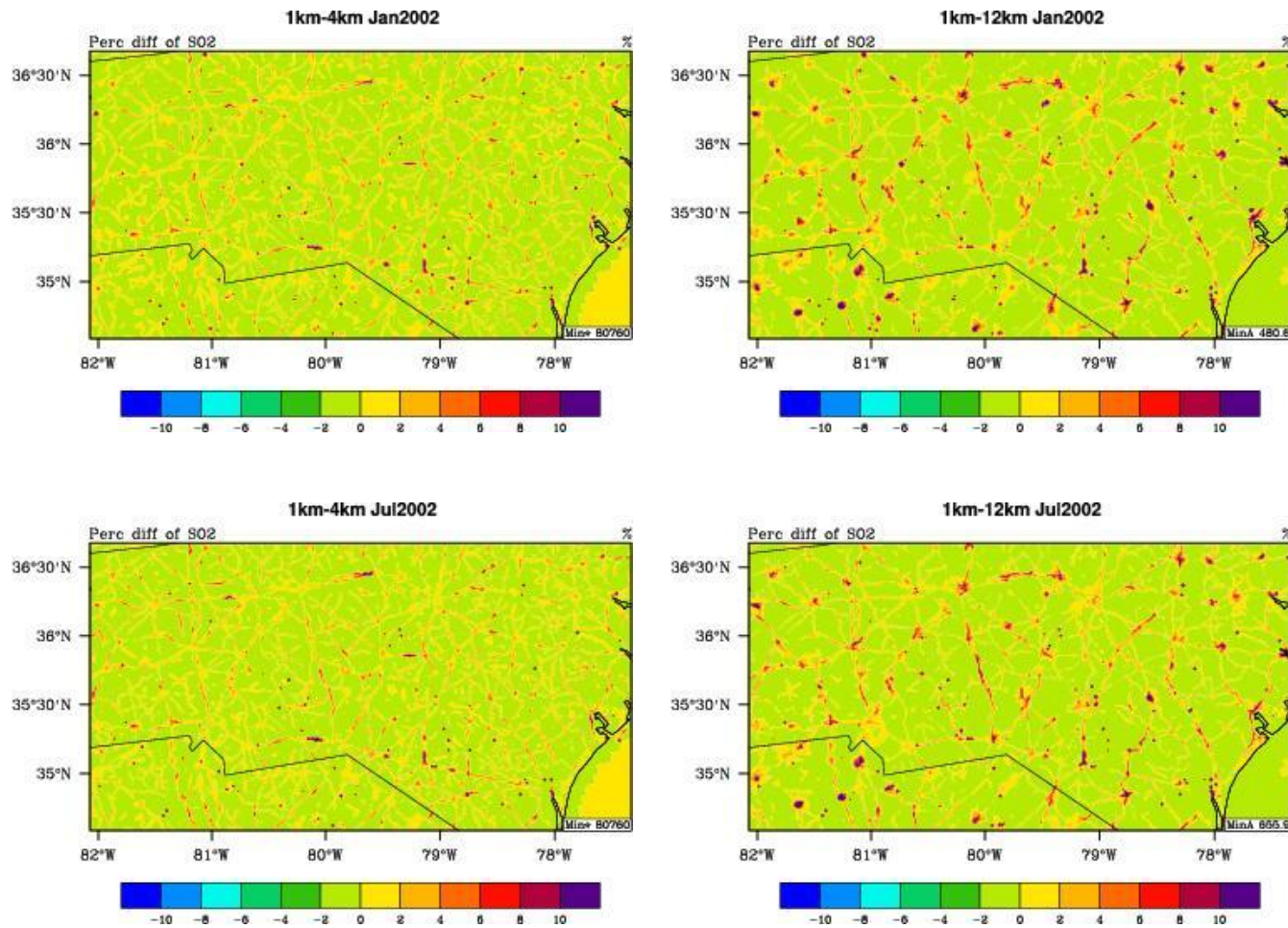


Figure 5.8. Spatial distributions of the percentage difference of monthly-mean SO₂ emissions at 1.33-km compared to 4-km (left) and 12-km (right) in January (top) and July (bottom).

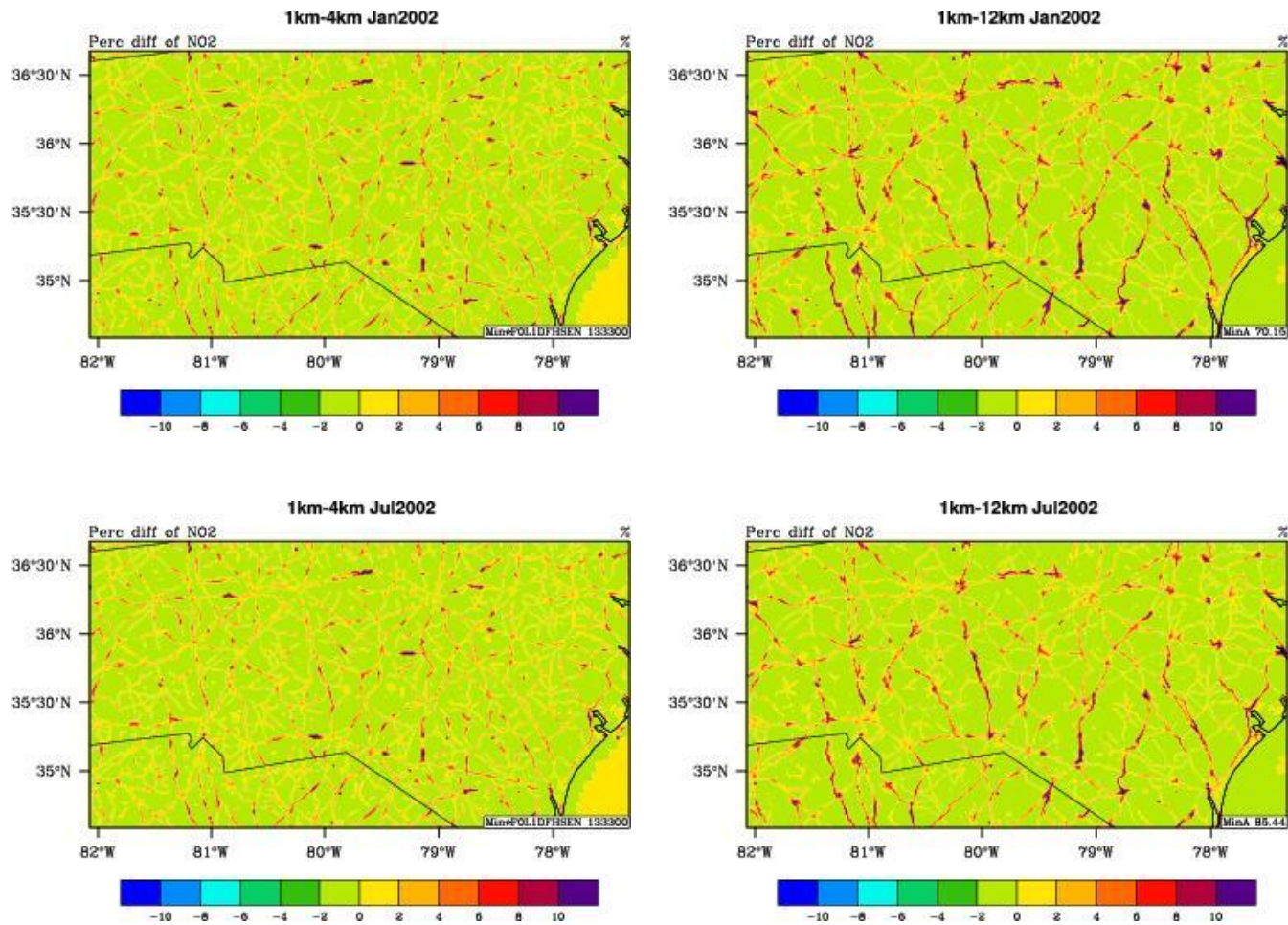


Figure 5.9. Spatial distributions of the percentage difference of monthly-mean NO₂ emissions at 1.33-km compared to 4-km (left) and 12-km (right) in January (top) and July (bottom).

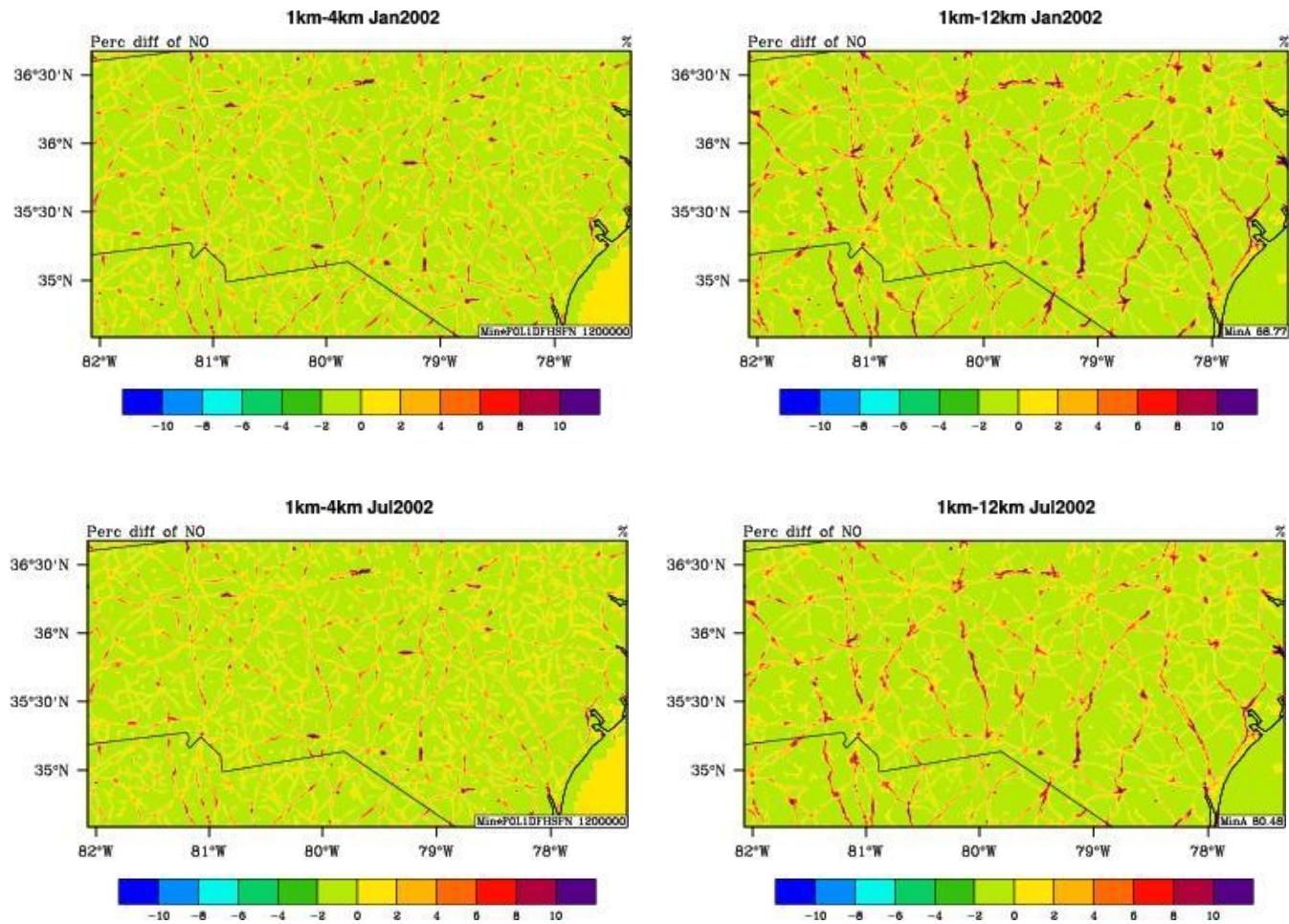


Figure 5.10. Spatial distributions of the percentage difference of monthly-mean NO emissions at 1.33-km compared to 4-km (left) and 12-km (right) in January (top) and July (bottom).

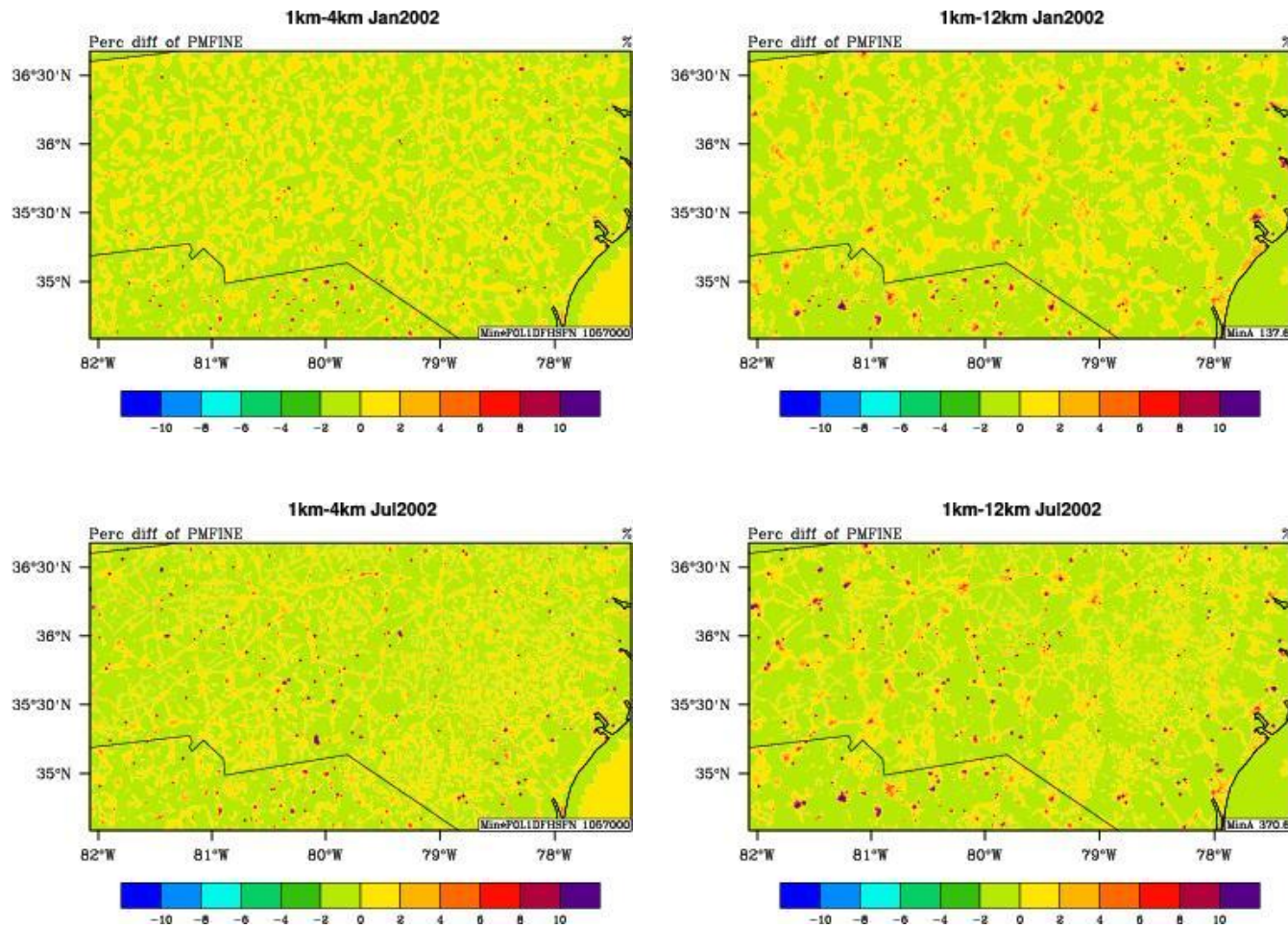


Figure 5.11. Spatial distributions of the percentage difference of monthly-mean PM_{2.5} emissions at 1.33-km compared to 4-km (left) and 12-km (right) in January (top) and July (bottom).

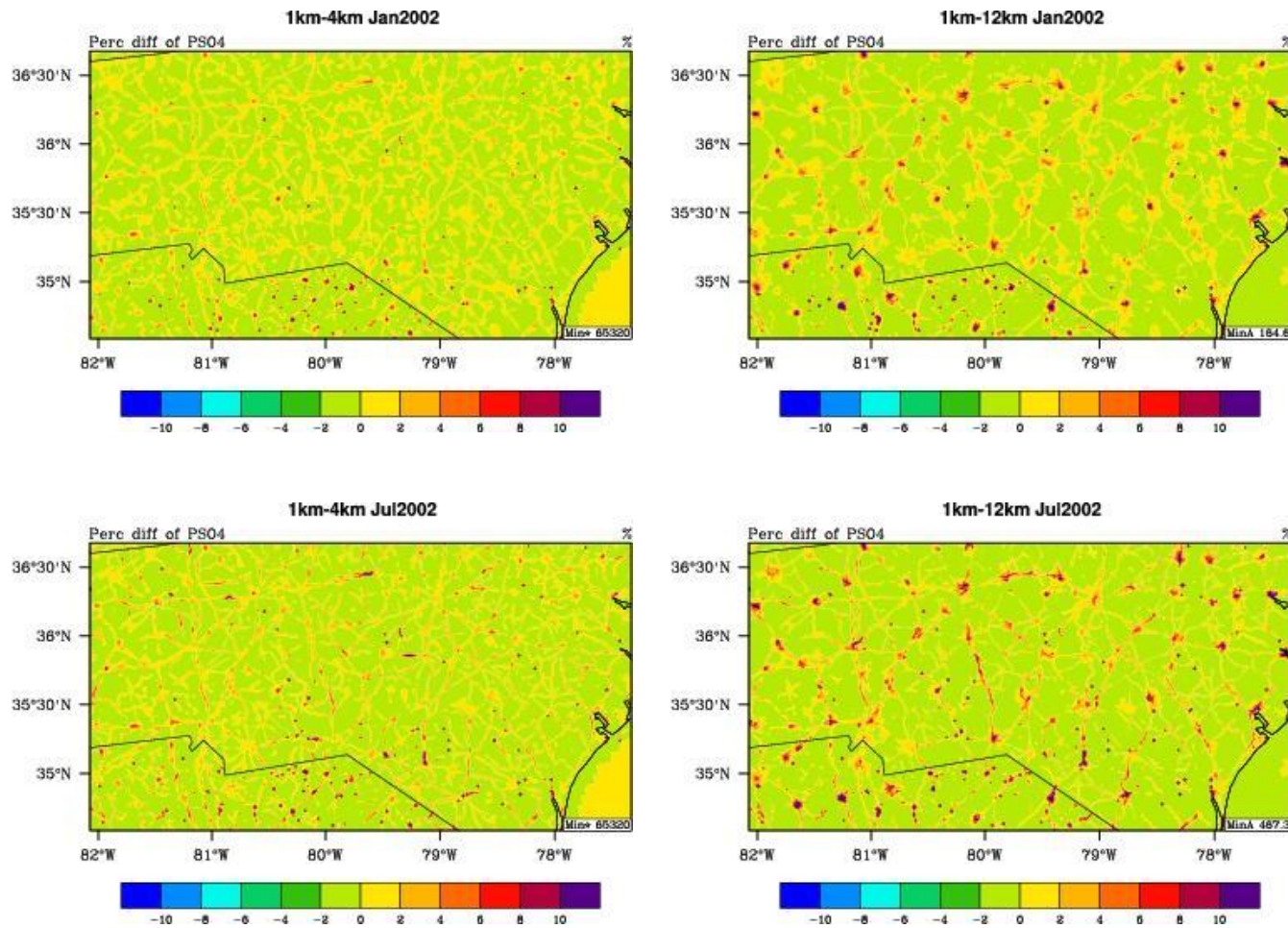


Figure 5.12. Spatial distributions of the percentage difference of monthly-mean SO_4^{2-} emissions at 1.33-km compared to 4-km (left) and 12-km (right) in January (top) and July (bottom).

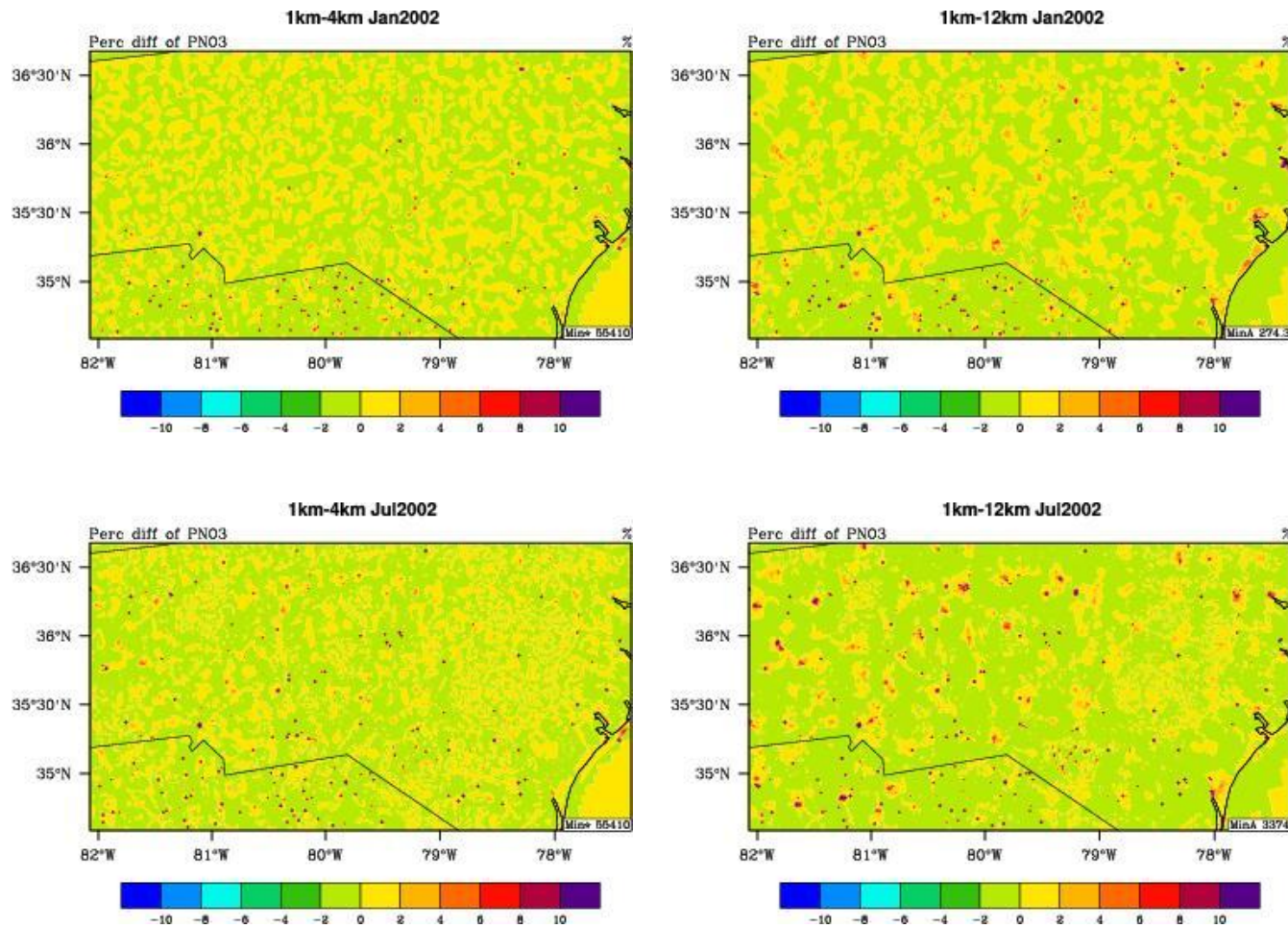


Figure 5.13. Spatial distributions of the percentage difference of monthly-mean NO_3^- emissions at 1.33-km compared to 4-km (left) and 12-km (right) in January (top) and July (bottom).

5.1.3 Chemical Concentrations of Gaseous and PM Species

The next step is to evaluate the air quality simulations completed at all three horizontal grid spacings. Similar to the meteorological evaluation, only the sites within the 1.33-km domain are used to evaluate all three simulations. This limits the availability of observations. There is only one CASTNET site in the domain, with weekly average chemical observations, providing only four values for evaluation, with a few additional observations from AIRS and STN. Table 5.3 provides the statistics for January. Maximum O₃ is overpredicted by all three simulations with the 4-km simulation generally performing the best. The higher emissions of NO_x at 1.33-km (see Section 5.1.2), combined with less dispersion of the emissions through the grid cell may have increased the O₃ production in comparison to the 4-km simulation. The two gaseous precursors to PM, HNO₃ and SO₂, are overpredicted with the finer resolutions performing better than the 12-km simulation. With the exception of TC, the performance for PM_{2.5} and its components is the best simulated by the 1.33-km simulation. One explanation for this is more mass removed through wet deposition (explained in Section 5.1.4) resulting in less mass in the ambient air, reducing the overprediction. For some species (i.e., SO₄²⁻, TC, total PM_{2.5}), the differences in performance between the simulations is relatively small, within 4%. As shown in Section 5.1.1, MM5 did not show any improvement using the finer grid spacing in January, however, CMAQ does, indicating other factors such as the differences in emissions and wet deposition are more influential than meteorology on the sensitivity of CMAQ to horizontal grid spacing.

Table 5.4 provides the statistics for July at all three horizontal grid spacings. The results indicate the 12-km simulation performs the best for all species. Similar to January, more PM mass is removed through wet deposition at the finer grid spacings. In July, this results in a larger underprediction of ambient concentrations at the finer grid spacing. The differences in performance between the simulations are much larger in July than in January, with some species having a range of NMBs of more than 10%.

While the spatial distribution of PM_{2.5} among all three simulations is similar in January (Figure 5.14), the 12-km simulation predicts higher PM_{2.5} concentrations in the central NC, which may be a result of the diffusion of precursor species into larger grid cells,

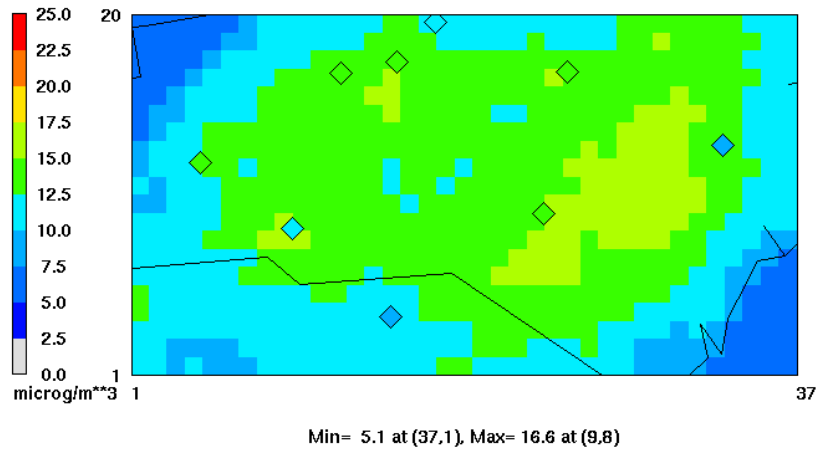
Table 5.3. Statistics for gaseous and PM species in January at 12-, 4-, and 1.33-km horizontal grid spacing. Bold numbers indicate the lowest NMBs for the corresponding variables.

Variable	Network	Data #	Mean Obs	Mean Sim			NMB (%)		
				12-km	4-km	1.33-km	12-km	4-km	1.33-km
1-hour max O ₃ (ppb)	AIRS-AQS	91	32.8	36.2	34.5	36.0	10.3	5.3	9.8
	CASTNET	30	35.2	37.6	37.2	38.7	6.9	7.6	10.0
8-hour max O ₃ (ppb)	AIRS-AQS	91	27.7	31.9	30.9	32.4	14.8	11.2	16.9
	CASTNET	30	32.1	34.5	34.1	36.0	7.7	6.4	12.3
HNO ₃ (µg m ⁻³)	CASTNET	4	1.6	2.0	1.9	2.0	25.3	20.6	25.1
SO ₂ (µg m ⁻³)	CASTNET	4	7.4	9.4	8.8	8.5	27.8	19.4	14.6
PM _{2.5} (µg m ⁻³)	STN	33	12.5	14.8	15.4	14.8	22.9	27.8	23.2
NH ₄ ⁺ (µg m ⁻³)	CASTNET	4	1.2	1.7	1.7	1.5	41.1	42.6	31.9
	STN	35	1.1	2.1	2.2	2.1	99.3	102.6	92.4
SO ₄ ²⁻ (µg m ⁻³)	CASTNET	4	2.3	1.9	2.0	2.0	-17.3	-14.3	-14.4
	STN	35	2.8	2.2	2.3	2.4	-21.5	-16.6	-15.7
NO ₃ ⁻ (µg m ⁻³)	CASTNET	4	1.5	3.4	3.4	3.1	124.5	123.6	104.5
	STN	35	1.6	4.6	4.7	4.3	182.4	185.3	163.8
TC (µg m ⁻³)	STN	35	7.1	3.1	3.1	2.9	-55.1	-55.9	-58.7

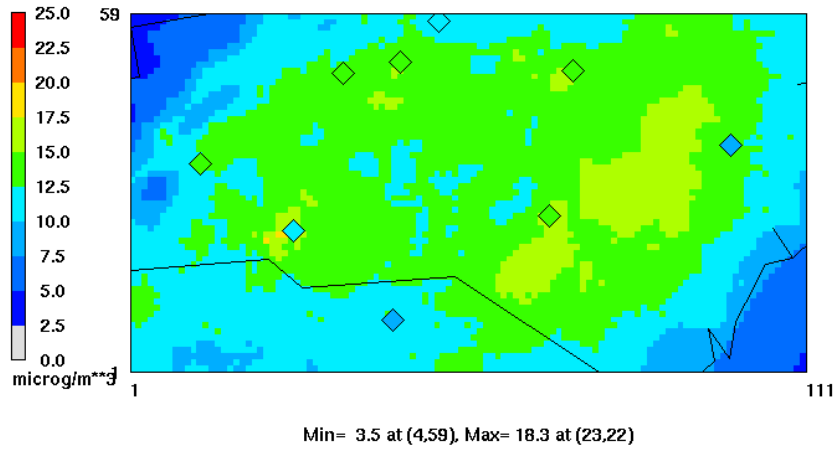
Table 5.4. Statistics for gaseous and PM species in July at 12-, 4-, and 1.33-km horizontal grid spacing. Bold numbers indicate the lowest NMBs for the corresponding variables.

Variable	Network	Data #	Mean Obs	Mean Sim			NMB (%)		
				12-km	4-km	1.33-km	12-km	4-km	1.33-km
1-hour max O ₃ (ppb)	AIRS-AQS	1229	75.2	67.0	63.0	61.0	-10.9	-16.3	-18.5
	CASTNET	30	67.7	64.0	59.6	58.0	-5.5	-12.0	-14.4
8-hour max O ₃ (ppb)	AIRS-AQS	1228	66.8	62.4	57.0	56.0	-6.5	-14.6	-16.3
	CASTNET	30	60.9	60.5	55.1	54.0	-0.7	-9.6	-11.2
HNO ₃ (μg m ⁻³)	CASTNET	4	2.4	1.9	1.7	1.6	-22.1	-32.6	-32.8
SO ₂ (μg m ⁻³)	CASTNET	4	2.4	2.9	4.0	3.7	25.0	68.4	57.8
PM _{2.5} (μg m ⁻³)	STN	48	20.0	10.3	9.1	8.8	-48.8	-54.4	-56.2
NH ₄ ⁺ (μg m ⁻³)	CASTNET	4	2.5	1.7	1.5	1.4	-31.7	-40.2	-44.5
	STN	49	2.1	1.3	1.2	1.1	-37.3	-43.9	-47.5
SO ₄ ²⁻ (μg m ⁻³)	CASTNET	4	8.0	5.9	4.6	4.3	-26.1	-42.2	-45.8
	STN	49	7.5	5.4	4.0	3.8	-28.6	-46.2	-49.4
NO ₃ ⁻ (μg m ⁻³)	CASTNET	4	0.1	0.1	0.2	0.2	-19.4	77.9	66.6
	STN	49	0.8	0.1	0.1	0.1	-88.1	-84.7	-84.2
TC (μg m ⁻³)	STN	49	7.8	2.1	2.2	2.1	-73.6	-72.0	-73.8

(a)



(b)



(c)

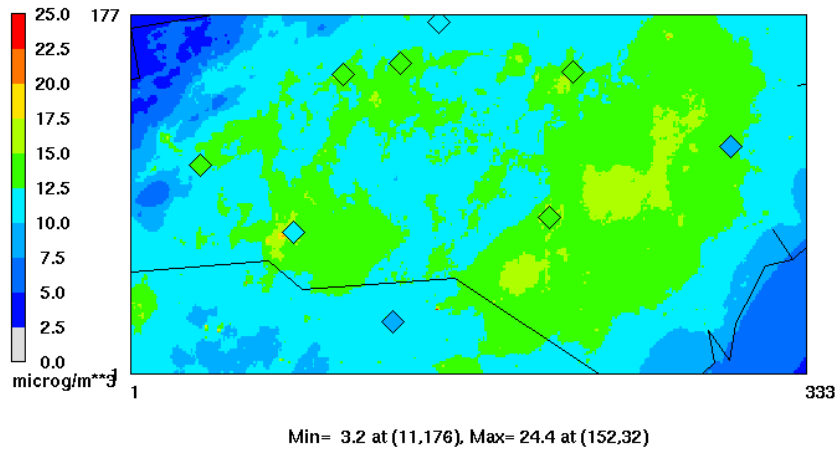


Figure 5.14. Spatial distribution of monthly-mean PM_{2.5} as simulated in January by CMAQ at (a) 12-km, (b) 4-km, and (c) 1.33-km overlaid with observations (diamonds) from STN and CASTNET.

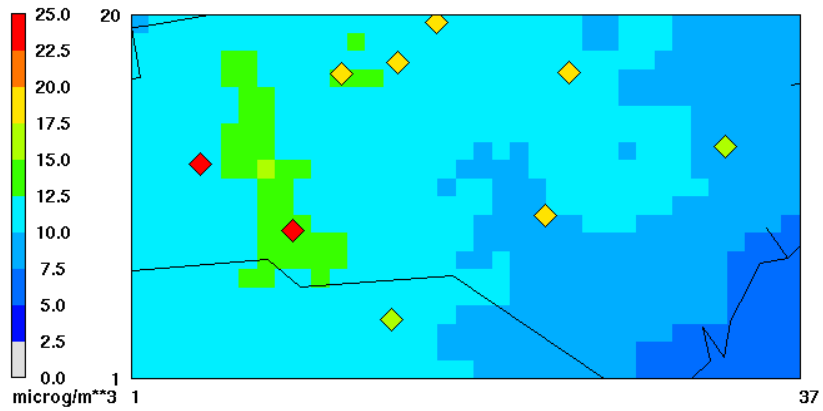
as opposed to being confined near the source. The highest PM concentrations in January occur near the major cities of Raleigh, Durham, Winston-Salem, and Charlotte, as well as the eastern NC in the region of high AL-NH₃ emissions.

In July (Figure 5.15), the 12-km simulation again predicts much higher PM_{2.5} than the finer grid simulations, particularly in the central and western NC. However, both the 4- and 1.33-km simulations capture regions of higher PM_{2.5} concentrations near some of the observational sites (i.e., Raleigh, Winston-Salem, and Charlotte). This may again be attributed to more mass being removed through wet deposition and the diffusion of emissions into larger grid cells, rather than being confined closer to the source (i.e., roadways).

Figure 5.16 shows the time series for O₃ at Candor, NC as simulated by CMAQ at the three horizontal grid spacings. In January, there are a few days (i.e., January 4th, 5th, 13th, 29th and 30th) when the 4- and 1.33-km simulations more accurately predict the maximum O₃ compared to the 12-km, but overall, there is little improvement in predicting the diurnal variations of O₃ at this site in January. In July, the simulations are again nearly identical, with the 12-km simulation predicting higher O₃ mixing ratios in the middle of the month. The higher O₃ predictions by the 12-km simulation may be a result of the diffusion of the emissions into the larger grid cell, as reported by Mathur et al. (2005) and Cohan et al. (2006).

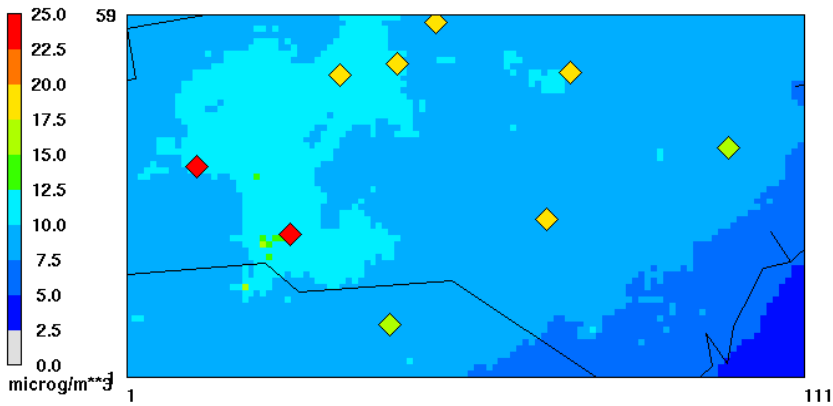
The time series for PM_{2.5} at Raleigh and Kinston NC are presented in Figure 5.17. Similar to O₃, there is no improvement in capturing the diurnal variations of hourly PM_{2.5} at the Raleigh site using finer grid spacing. All three simulations give nearly identical predictions in both months. At the site in Kinston, however, some improvement in predicting the 24-hour average PM_{2.5} at the finer grid spacing in January is noticeable, especially at the middle and end of the month. The spatial distribution for January monthly-mean PM_{2.5} (Figure 5.14) does show regions in the eastern NC where the finer grid spacing gives lower PM_{2.5}. As stated, this may be a result of the emissions being confined to the small grid cells, and not being diffused into larger grid cells which could result in an overprediction of PM_{2.5} in some regions. In July at the Kinston site, all three simulations give similar 24-hour average PM_{2.5}, which also occurs in some of the far eastern regions of the July spatial

(a)



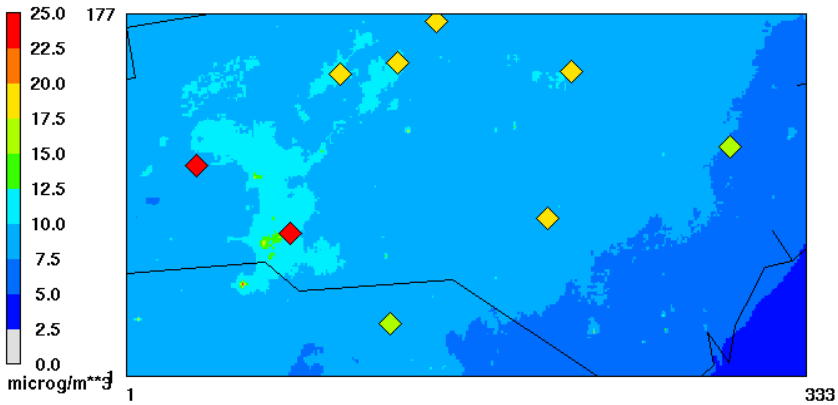
Min= 5.2 at (37,1), Max= 15.1 at (8,12)

(b)



Min= 4.1 at (111,1), Max= 16.7 at (20,15)

(c)



Min= 4.0 at (333,1), Max= 37.2 at (58,45)

Figure 5.15. Spatial distribution of monthly-mean PM_{2.5} as simulated in January by CMAQ at (a) 12-km, (b) 4-km, and (c) 1.33-km overlaid with observations (diamonds) from STN and CASTNET.

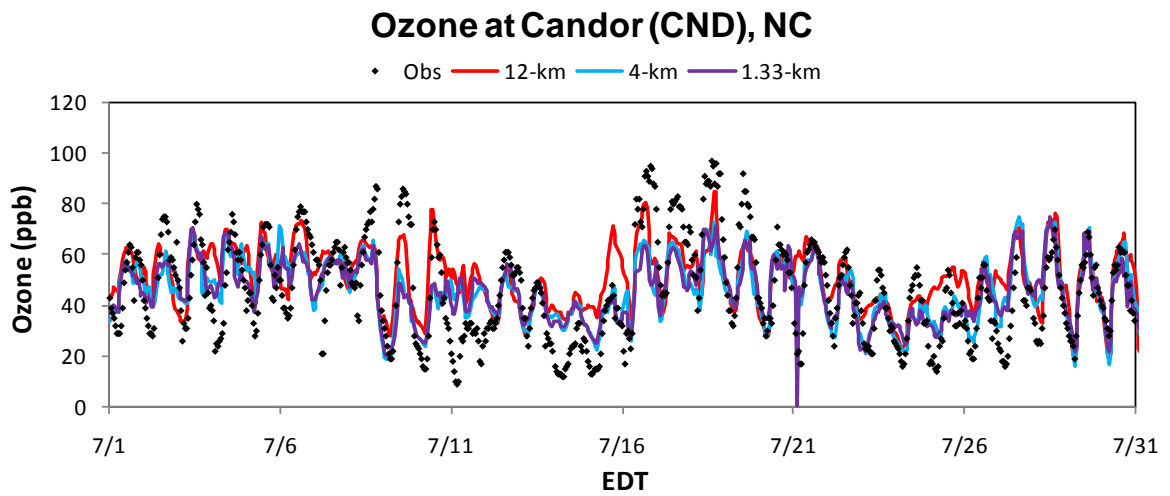
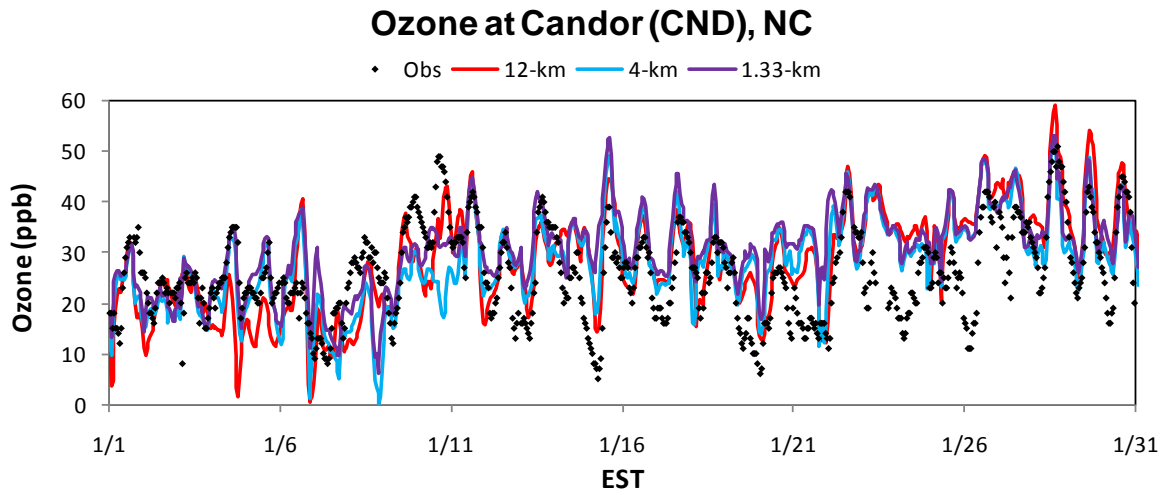


Figure 5.16. Time series for O₃ at the CASTNET site in Candor, NC as simulated at 12-, 4-, and 1.33-km horizontal grid spacings.

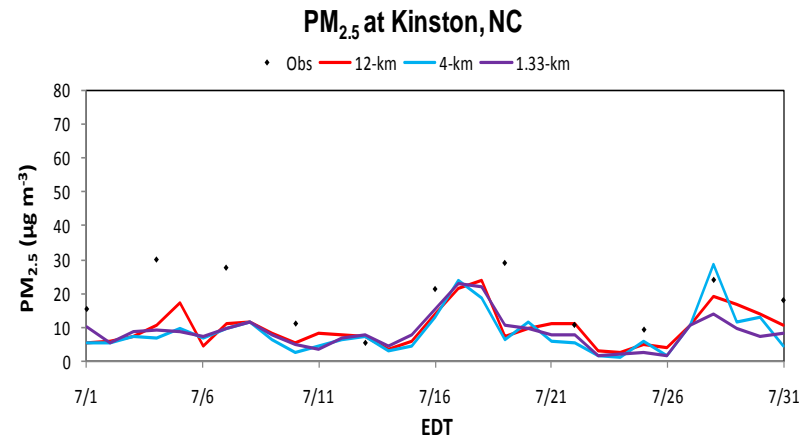
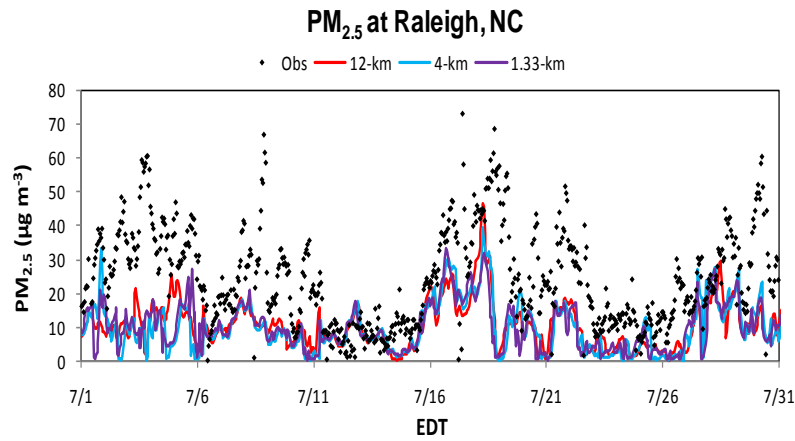
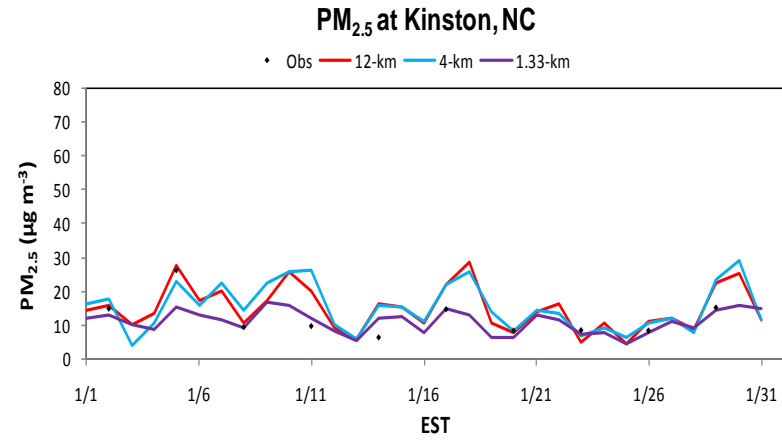
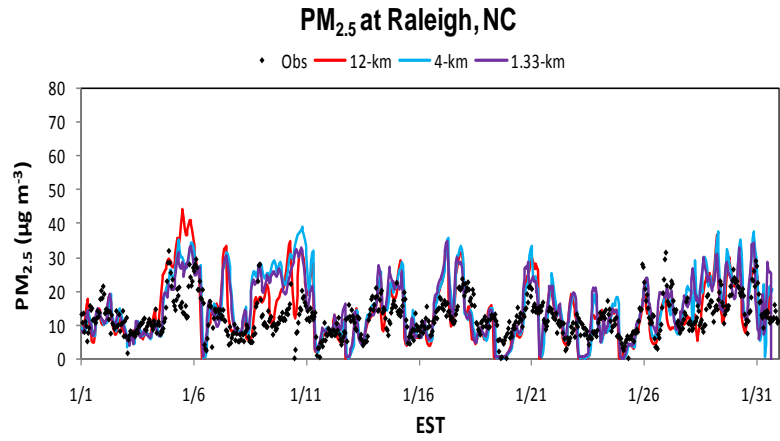


Figure 5.17. Time series for PM_{2.5} at Raleigh, NC (hourly) and Kinston, NC (24-hour average) as simulated at 12-, 4-, and 1.33-km horizontal grid spacings.

distribution (Figure 5.15). Despite the 12-km simulation predicting some higher monthly-mean $PM_{2.5}$ that extends into eastern NC, it does not seem to impact Kinston.

5.1.4 Dry and Wet Deposition Fluxes

As mentioned in Section 5.1.3, more PM mass was removed at the finer grid spacings than the coarser grid spacings in both months. The statistics for January and July are provided in Tables 5.5 and 5.6, respectively. In January, the removal of more PM mass results in a larger overprediction of wet deposition so that, statistically, the simulation completed at 12-km has a better performance. However, the mean bias of mass removed in January is relatively low, with the largest difference occurring for the wet deposition of NO_3^- (mean bias $< 0.6 \text{ kg ha}^{-1}$). In July, the removal of more PM mass at the finer grid spacing results in a shift from a relatively large underprediction at 12-km to an overprediction at 1.33-km. The worst performance in wet deposition for both months is NO_3^- . In both January and July, the sensitivity of precipitation to horizontal grid spacing affects the sensitivity of wet deposition, which in turn affects the ambient PM concentrations. For example, in January, the 12-km simulation performed the best in simulating precipitation and the wet deposition of NH_4^+ and NO_3^- ; however the underprediction in wet deposition contributed to the overprediction in ambient PM concentrations. This emphasizes the importance of simulating and evaluating as many processes as possible in order to determine if the model can accurately simulate ambient concentrations for the right reasons.

Dry deposition is also evaluated at all three horizontal grid spacings at the CASTNET site in Candor, NC using the results from the MLM for comparison. For $PM_{2.5}$ components, little sensitivity to horizontal grid spacing is observed. The NMBs in January (Table 5.5) and July (Table 5.6) generally vary by less than 4% between the different horizontal grid spacings and are all largely underpredicted. Figures 5.18 through 5.20 show the time series of NH_4^+ , SO_4^{2-} , and NO_3^- dry deposition flux in January and July at the site in Candor, NC as simulated by CMAQ at 12-, 4-, and 1.33-km and compared to the MLM simulation. These figures show how the dry deposition module in CMAQ fails to capture the maximum flux of

Table 5.5. Statistics for wet and dry deposition in January at 12-, 4-, and 1.33-km horizontal grid spacings. Bold numbers indicate the lowest NMBs for the corresponding variables.

Variable	Network	Data #	Mean Obs ¹	Mean Sim			NMB (%)		
				12-km	4-km	1.33-km	12-km	4-km	1.33-km
Precip (mm)	NADP	15	32.9	28.6	25.8	23.0	-13.1	-21.5	-30.3
WD_NH ₄ ⁺ (kg ha ⁻¹)	NADP	14	0.2	0.2	0.2	0.2	-3.1	11.2	18.7
WD_SO ₄ ²⁻ (kg ha ⁻¹)	NADP	14	1.2	1.1	1.3	1.4	-9.3	3.7	16.4
WD_NO ₃ ⁻ (kg ha ⁻¹)	NADP	14	0.9	1.1	1.2	1.5	34.0	46.7	70.4
DD_NH ₄ ⁺ (g ha ⁻¹)	CASTNET	629	0.04	0.01	0.01	0.01	-69.5	-69.5	-71.8
DD_SO ₄ ²⁻ (g ha ⁻¹)	CASTNET	629	0.07	0.02	0.02	0.02	-77.4	-76.9	-76.9
DD_NO ₃ ⁻ (g ha ⁻¹)	CASTNET	629	0.05	0.02	0.02	0.02	-58.2	-57.7	-61.4
DD_SO ₂ (g ha ⁻¹)	CASTNET	629	0.33	1.49	1.37	1.44	352.8	316.7	338.4
DD_HNO ₃ (g ha ⁻¹)	CASTNET	629	0.47	1.36	1.26	1.33	191.7	169.2	184.7

¹ Dry deposition fluxes and dry deposition velocities are not observed measurements, but calculated from measurements using the Multilayer Model (MLM) (Meyers et al., 1998; Finkelstein et al., 2000).

Table 5.6. Statistics for wet and dry deposition in July at 12-, 4-, and 1.33-km horizontal grid spacings. Bold numbers indicate the lowest NMBs for the corresponding variables.

Variable	Network	Data #	Mean Obs ¹	Mean Sim			NMB (%)		
				12-km	4-km	1.33-km	12-km	4-km	1.33-km
Precip (mm)	NADP	20	30.2	65.0	92.7	56.43	115.1	206.1	86.7
WD_NH ₄ ⁺ (kg ha ⁻¹)	NADP	16	0.4	0.3	0.3	0.5	-42.0	-34.5	3.7
WD_SO ₄ ²⁻ (kg ha ⁻¹)	NADP	16	2.4	1.4	2.1	2.9	-41.2	-10.1	21.7
WD_NO ₃ ⁻ (kg ha ⁻¹)	NADP	16	1.9	0.4	0.8	1.0	-78.7	-59.6	-47.0
DD_NH ₄ ⁺ (g ha ⁻¹)	CASTNET	645	0.12	0.02	0.02	0.01	-85.1	-86.8	-88.9
DD_SO ₄ ²⁻ (g ha ⁻¹)	CASTNET	645	0.40	0.08	0.06	0.05	-80.6	-85.2	-88.1
DD_NO ₃ ⁻ (g ha ⁻¹)	CASTNET	645	0.01	0.00	0.00	0.00	-93.7	-89.5	-89.1
DD_SO ₂ (g ha ⁻¹)	CASTNET	645	0.25	0.47	0.67	0.63	85.9	166.3	150.6
DD_HNO ₃ (g ha ⁻¹)	CASTNET	645	1.32	1.71	1.46	1.34	30.1	10.8	1.7

¹ Dry deposition fluxes and dry deposition velocities are not observed measurements, but calculated from measurements using the Multilayer Model (MLM) (Meyers et al., 1998; Finkelstein et al., 2000).

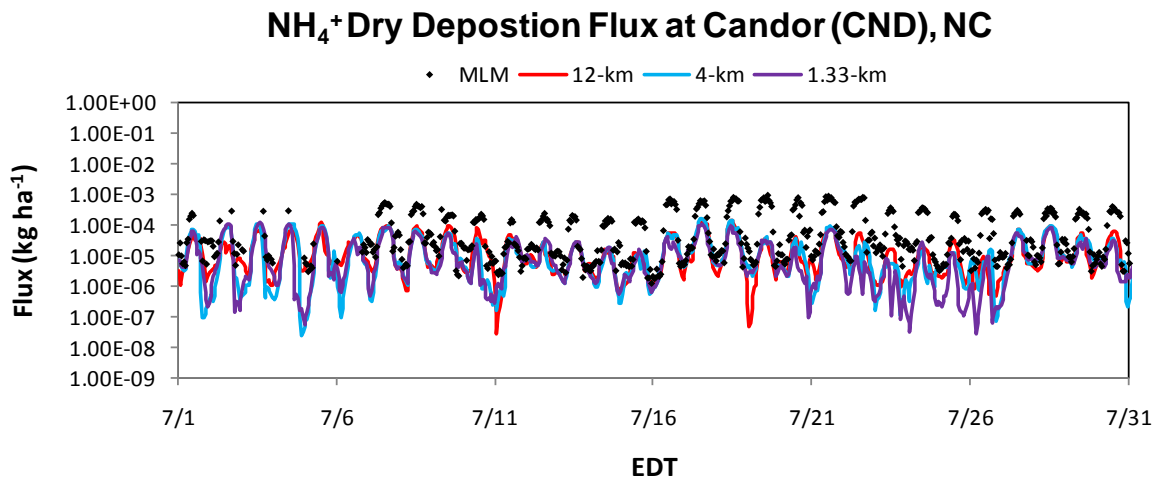
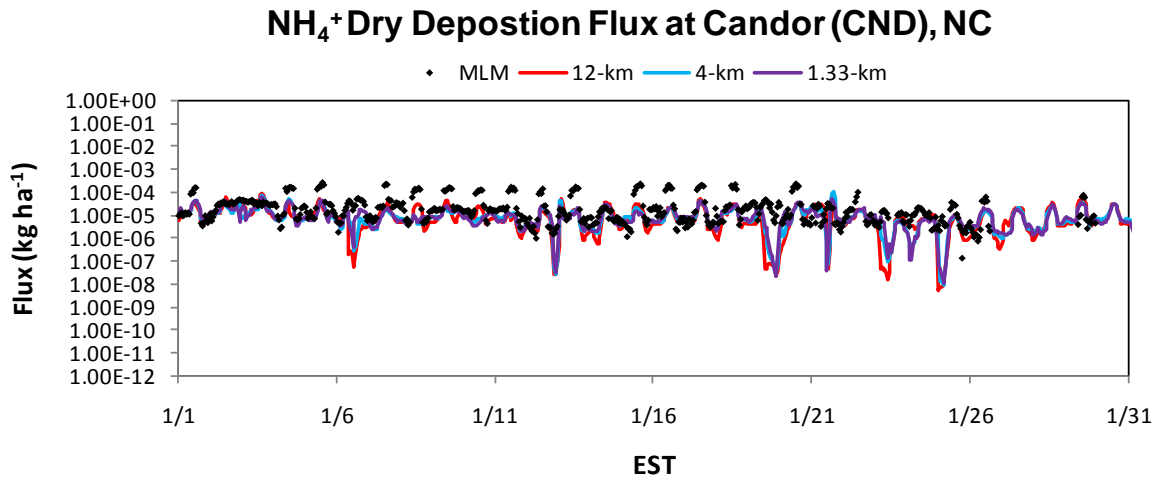


Figure 5.18. Time series of NH₄⁺ dry deposition flux at Candor, NC in January and July as simulated by CMAQ at 12-, 4-, and 1.33-km and compared to the MLM.

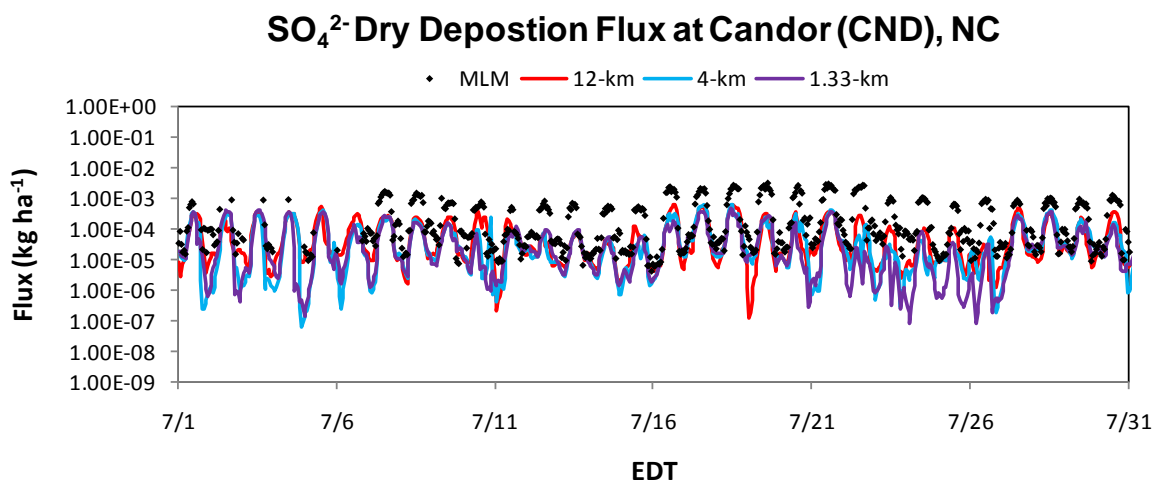
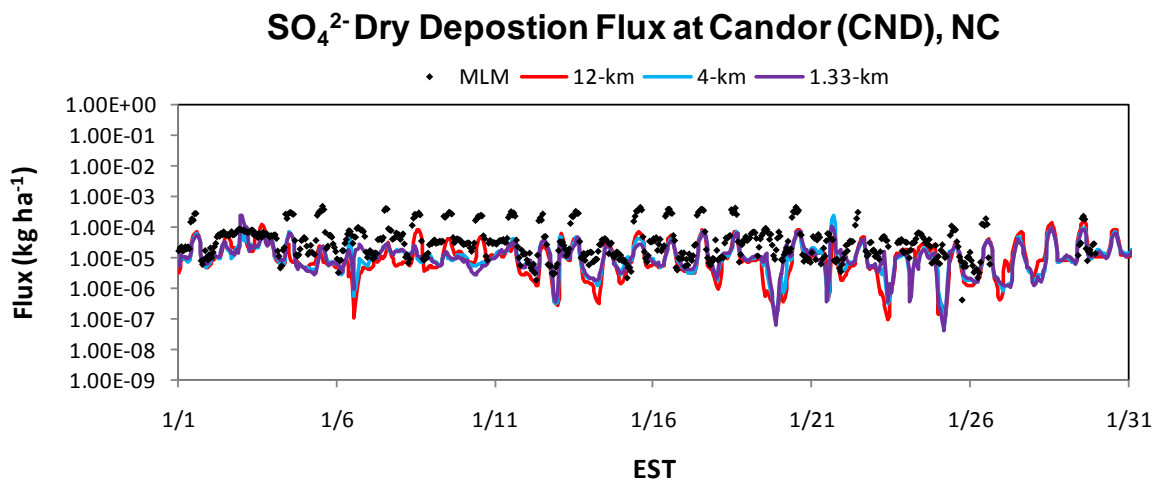


Figure 5.19. Time series of SO₄²⁻ dry deposition flux at Candor, NC in January and July as simulated by CMAQ at 12-, 4-, and 1.33-km and compared to the MLM.

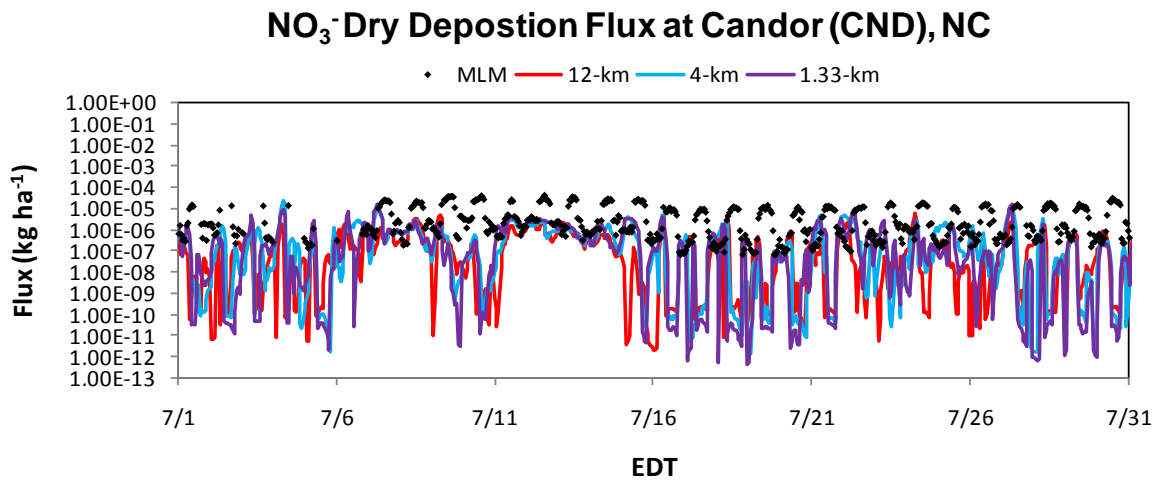
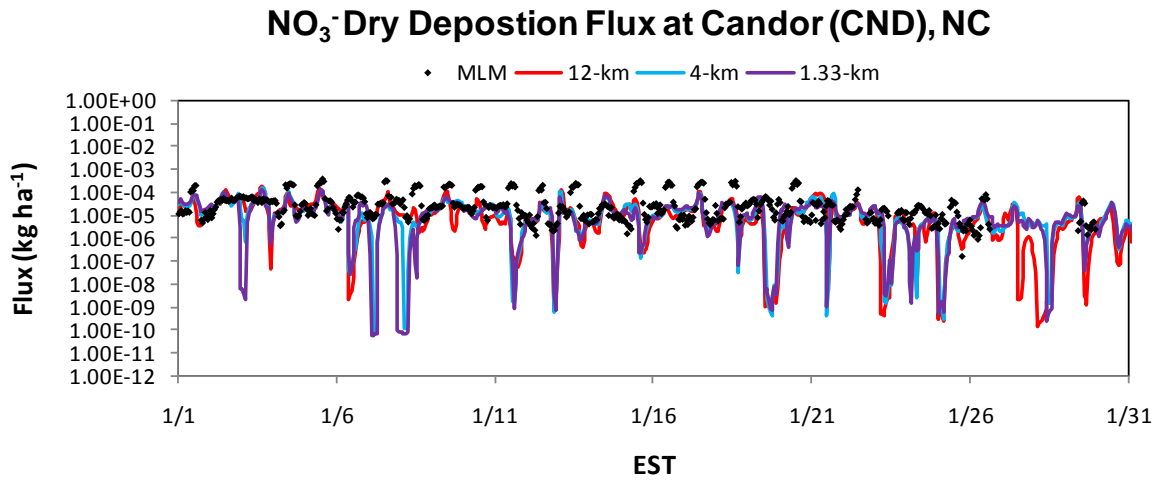


Figure 5.20. Time series of NO₃⁻ dry deposition flux at Candor, NC in January and July as simulated by CMAQ at 12-, 4-, and 1.33-km and compared to the MLM.

all three species and underpredicts low flux during some periods. The underpredictions are also larger in July, as indicated by the statistics.

The dry deposition of gaseous SO₂ and HNO₃ is largely overpredicted at all three horizontal grid spacings in January as indicated both statistically and in the time series (Figures 5.21 and 5.22). The best performance for the dry deposition of these two gaseous species is for HNO₃ in July. While the time series does not indicate much sensitivity to horizontal grid resolution, the statistics indicate a significant improvement for HNO₃ in July by the simulation completed at a 1.33-km horizontal grid spacing.

5.1.5 Visibility

The last variable evaluated for sensitivity to horizontal grid resolution is the HI; however, there are no IMPROVE sites within the 1.33-km domain so only a spatial comparison can be completed. Figure 5.23 shows the spatial distribution of the HI in January at all three horizontal grid spacings. The regions with higher HI in the eastern NC are associated with the regions of higher PM_{2.5} (Figure 5.14). While Figure 5.14 shows defined areas of higher ambient PM_{2.5} at the 1.33-km horizontal grid spacing surrounded by lower PM_{2.5}, Figure 5.23 shows higher HI throughout the eastern NC. This may be a result of the higher RH simulated at the finer grid spacing causing CMAQ to select a higher $f(\text{RH})$ from the lookup table.

In July (Figure 5.24), the western half of the domain resembles the PM_{2.5} distribution in Figure 5.15 with the higher HI values associated with higher PM_{2.5} concentrations. The 12-km simulation predicts higher HI values than the 4-km or 1.33-km across the whole domain. The HI values in the eastern half of the domain in all three simulations are similar to the western half, despite PM_{2.5} concentrations being lower in the eastern half than the western half. This may again be due to higher simulated RH values in the eastern NC compared to the simulated RH in the western NC.

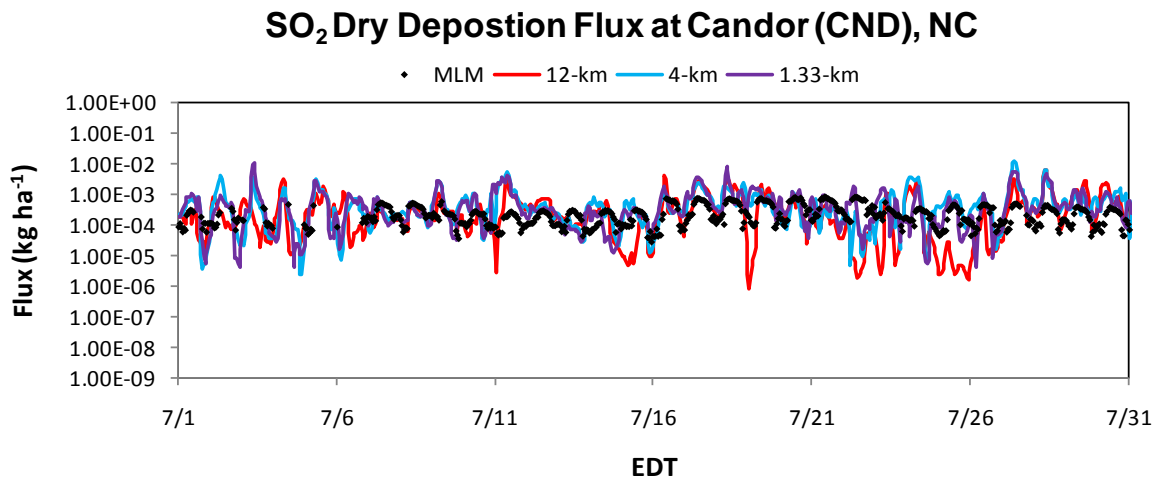
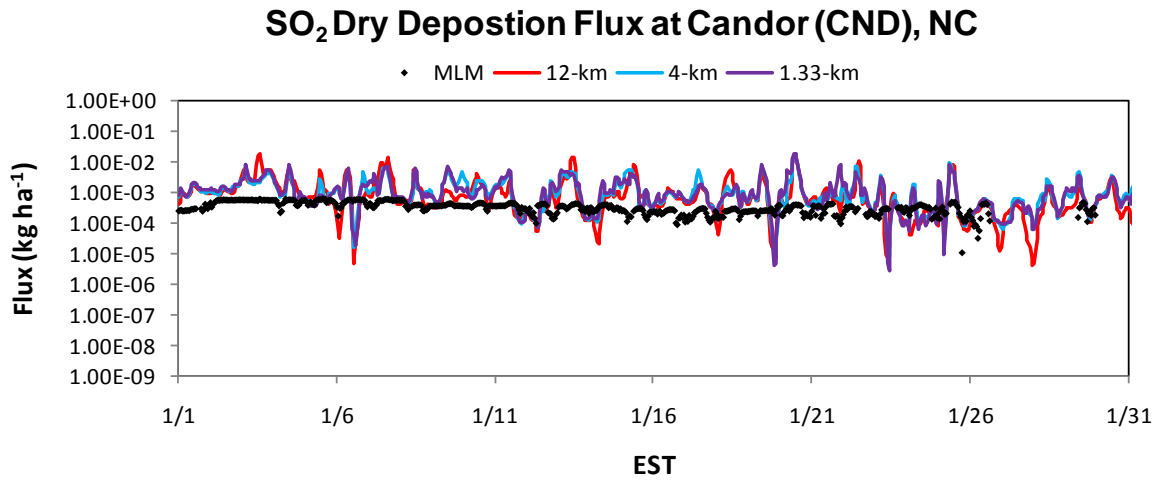


Figure 5.21. Time series of SO₂ dry deposition flux at Candor, NC in January and July as simulated by CMAQ at 12-, 4-, and 1.33-km and compared to the MLM.

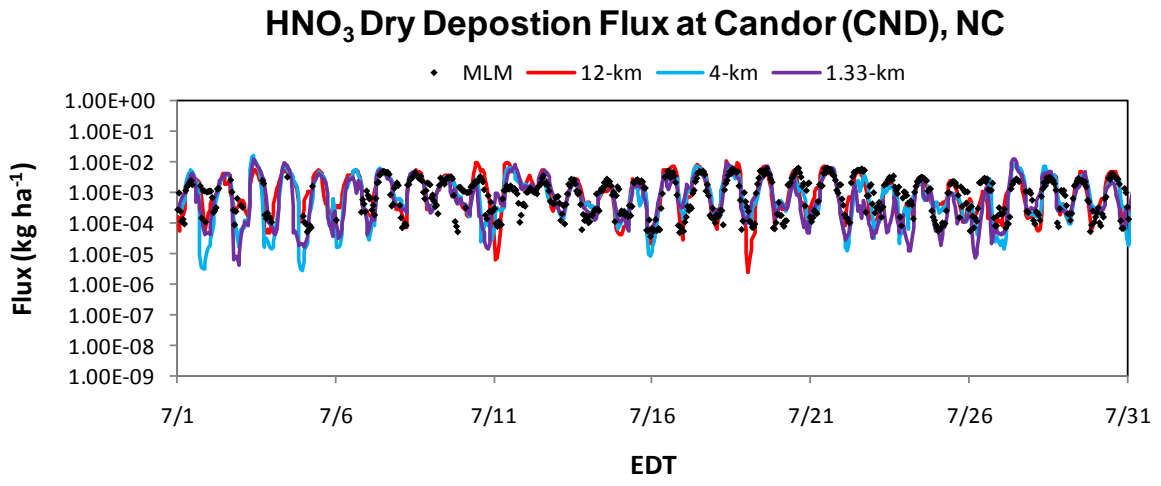
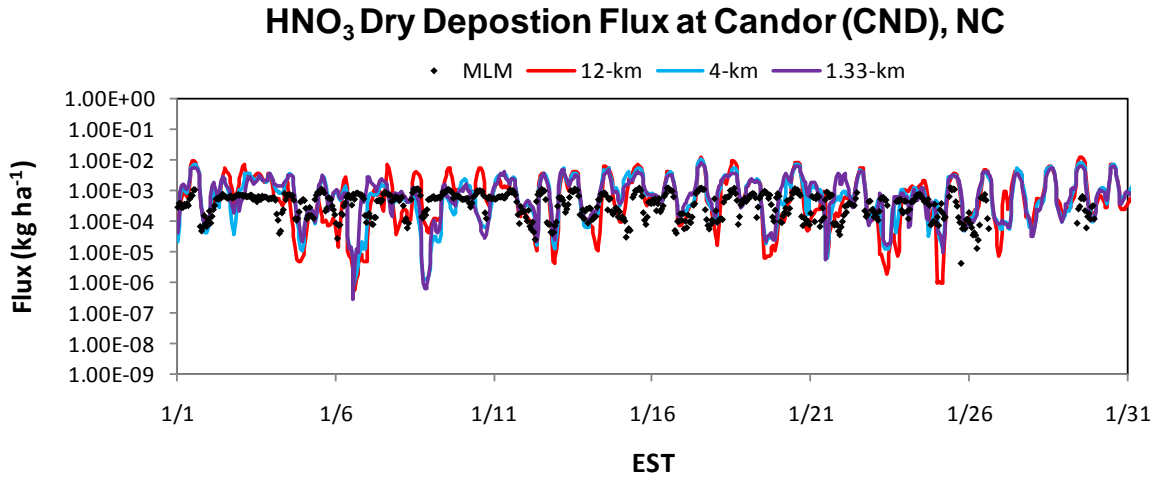
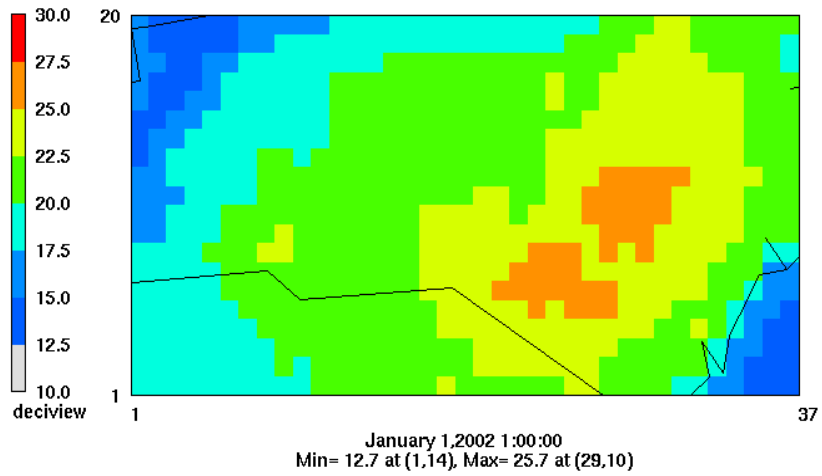
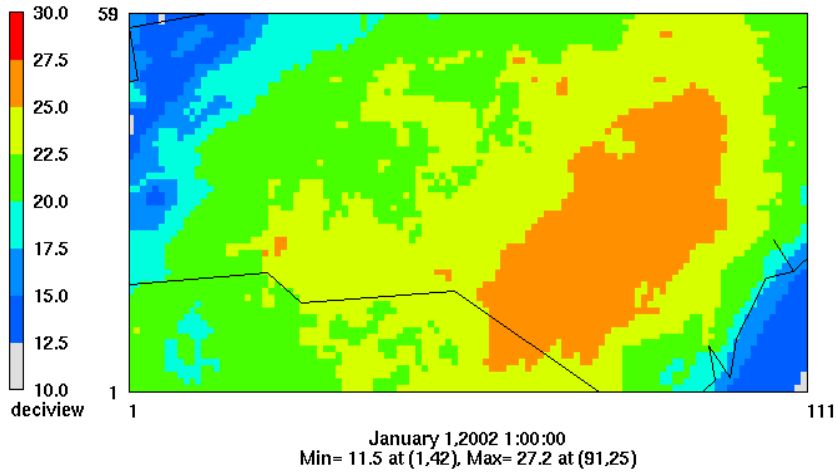


Figure 5.22. Time series of HNO₃ dry deposition flux at Candor, NC in January and July as simulated by CMAQ at 12-, 4-, and 1.33-km and compared to the MLM.

(a)



(b)



(c)

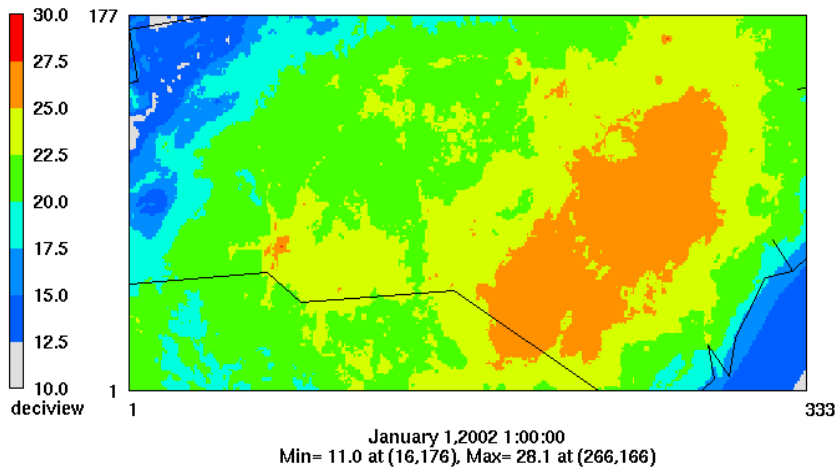
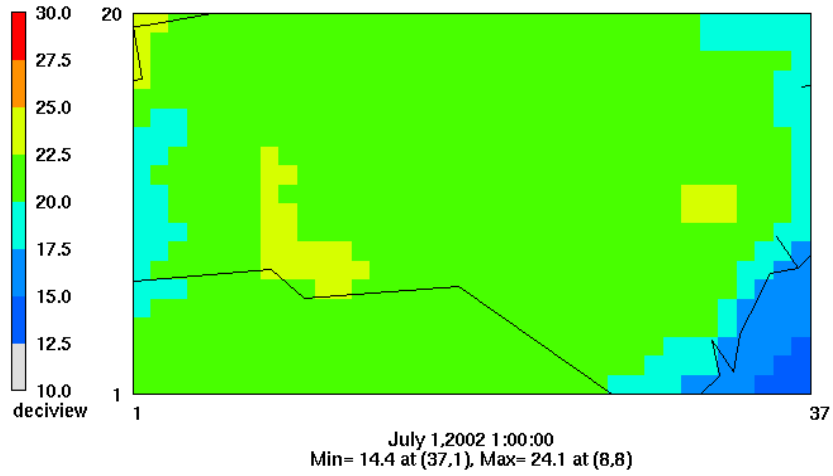
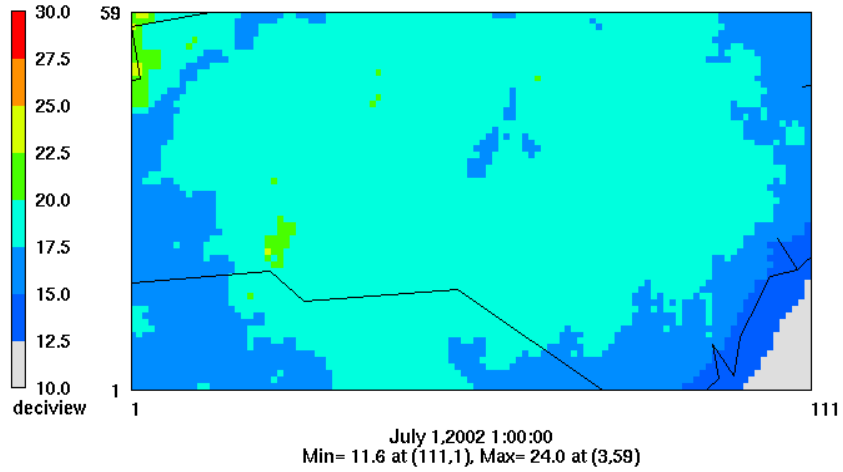


Figure 5.23. Spatial distribution of the haziness index in January as simulated by CMAQ at horizontal grid spacings of (a) 12-km, (b) 4-km, and (c) 1.33-km.

(a)



(b)



(c)

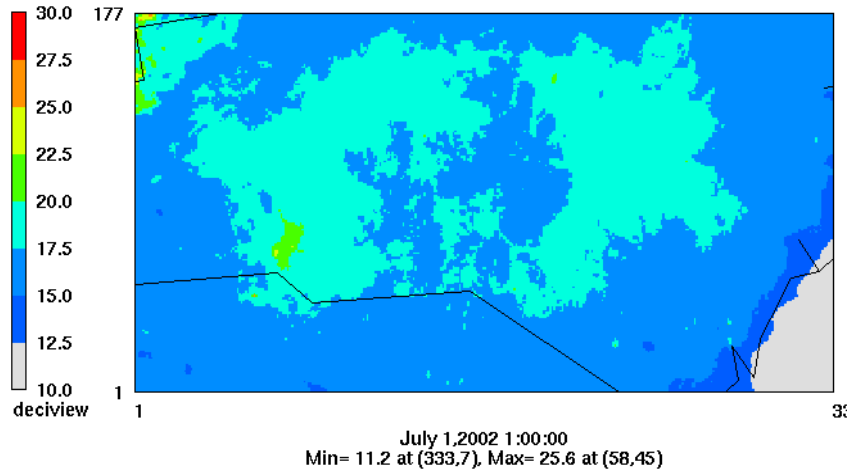


Figure 5.24. Spatial distribution of the haziness index in July as simulated by CMAQ at horizontal grid spacings of (a) 12-km, (b) 4-km, and (c) 1.33-km.

5.2 Sensitivity to Emission Reductions

The second sensitivity study conducted in this thesis is the sensitivity of CMAQ predictions to emission reductions in AL-NH₃, SO₂, and NO_x. A simulation is completed in which all AL-NH₃ emissions within the domain are reduced by 50% from the baseline emissions in both January and July. Tsimpidi et al. (2007) reported that lower NH₃ reductions (e.g., 25%) are less effective in reducing PM mass in regions of high NH₃ concentrations in July than higher reductions (e.g., 50%). A 50% reduction in AL-NH₃ is selected for the simulation over the southeastern U.S. because it is a region with high NH₃ concentrations. The results of this simulation are discussed in Section 5.2.1. Three additional sensitivity simulations are completed for each month, which include:

- (a) reducing NO_x from electric generating units (EGUs) and mobile sources by 50% (Section 5.2.2);
- (b) reducing SO₂ from EGUs, mobile, and non-road (NR) sources by 50% (Section 5.2.3);
- (c) and combining reduced AL-NH₃, NO_x, SO₂ emissions (Section 5.2.4).

The selection of EGU, mobile, and NR sources for reduction of SO₂ and NO_x is made based on VISTAS projected emission reductions for 2009 and 2018 (MACTEC, Inc., 2008). MACTEC, Inc. (2008) provides a table of annual NO_x and SO₂ emissions from each source type within each state for 2002, 2009, and 2018. The percentage difference in emissions is calculated based on these values and are presented in Tables 5.7 (NO_x) and 5.8 (SO₂). The values in red indicate when the percentage decrease in emissions is projected to be at least 50%. By 2018 in most of the states within the 4-km domain, NO_x and SO₂ emissions are projected to be reduced by more than 50% from EGU and mobile sources. SO₂ will also be significantly reduced from non-road sources, such as construction equipment and farm machinery. Based on this data, NO_x was reduced by 50% from EGU and mobile sources, while SO₂ was reduced by 50% from EGU, mobile, and non-road sources for the sensitivity simulations. The results of the sensitivity simulations are illustrated using absolute and percentage difference plots. It should be noted that the percent change in PM_{2.5} and SO₄²⁻ was generally smaller than the percentage change in NH₄⁺ and NO₃⁻ and so the scales used in

Table 5.7. Percent change in annual NO_x emissions from each source type in each state contained in the 4-km domain, based on projected annual emissions reported by MACTEC, Inc. (2008). Bold values indicate when the percentage decrease in emissions is greater than or equal to 50%.

State	Year	Percentage Change in NO _x from 2002					
		EGU	NEGU	Mobile	NR	Area	Fire
GA	2009	-33.23	2.24	-31.97	-12.48	4.39	0.28
	2018	-52.65	13.35	-66.80	-34.08	14.36	0.28
KY	2009	-51.08	-1.65	-35.31	-9.39	6.53	264.71
	2018	-67.62	6.88	-66.59	-24.08	12.25	281.82
NC	2009	-56.19	-22.62	-38.41	-15.76	9.31	179.05
	2018	-59.76	-15.86	-73.18	-41.79	20.01	222.57
SC	2009	-44.85	-6.61	-34.16	-13.96	0.14	19.61
	2018	-41.35	2.79	-69.04	-36.80	6.52	19.61
TN	2009	-57.79	-10.61	-36.33	-10.52	3.67	305.43
	2018	-79.84	-2.84	-70.92	-27.47	9.82	340.22
VA	2009	-25.93	-15.58	-39.64	-13.01	2.33	35.22
	2018	-25.94	-7.75	-71.52	-36.11	9.22	72.54
WV	2009	-62.99	-18.43	-39.60	-9.34	5.93	-41.38
	2018	-77.71	-7.15	-70.77	-22.65	16.88	-25.52

Table 5.8. Percent change in annual NO_x emissions from each source type in each state contained in the 4-km domain, based on projected annual emissions reported by MACTEC, Inc. (2008). Bold values indicate when the percentage decrease in emissions is greater than or equal to 50%.

State	Year	Percentage Change in SO ₂ from 2002					
		EGU	NEGU	Mobile	NR	Area	Fire
GA	2009	-20.64	0.39	-86.99	-69.74	0.24	-13.58
	2018	-86.69	10.36	-88.04	-81.02	3.77	-13.58
KY	2009	-43.88	7.02	-87.97	-34.63	3.07	266.67
	2018	-54.12	19.55	-87.90	-38.82	5.70	284.31
NC	2009	-49.31	-3.60	-87.90	-75.41	6.26	178.82
	2018	-74.86	4.97	-88.08	-88.24	12.44	222.66
SC	2009	-37.44	-11.82	-87.93	-65.04	1.17	6.09
	2018	-53.79	-2.07	-89.23	-75.38	4.32	6.09
TN	2009	-23.56	-18.39	-88.34	-45.88	2.21	308.00
	2018	-66.28	-28.80	-89.72	-50.13	6.84	344.00
VA	2009	-27.54	-9.18	-86.99	-80.30	0.09	34.78
	2018	-58.96	-9.57	-87.42	-94.15	3.30	71.74
WV	2009	-47.89	2.83	-88.68	-83.00	5.29	-42.50
	2018	-79.42	14.12	-89.73	-97.35	10.13	-27.50

the figures for $\text{PM}_{2.5}$ and SO_4^{2-} are different than the scales used for NH_4^+ and NO_3^- in order to clearly show the spatial distributions of all species.

5.2.1 Agricultural Livestock Ammonia (AL-NH₃) Reduction

As described in Section 4.2, the AdjGR based on simulated concentrations from CMAQ indicates that the eastern NC and northeastern GA are NH_3 -rich in both January and July, with a larger NH_3 -rich region in July. This would suggest that reducing NH_3 will have less impact on reducing $\text{PM}_{2.5}$ than reducing SO_2 and NO_x . This section evaluates the impact of reducing AL- NH_3 emissions without any influence from reduced SO_2 or NO_x .

Figure 5.25 shows the absolute and percentage difference in $\text{PM}_{2.5}$, NH_4^+ , SO_4^{2-} , and NO_3^- in January when AL- NH_3 emissions are reduced by 50%. $\text{PM}_{2.5}$ shows a maximum reduction of 16.2% with the largest reductions occurring near the AL- NH_3 source locations. The decrease in $\text{PM}_{2.5}$ is due to a decrease in NH_4NO_3 , as NO_3^- is also significantly reduced. As expected, there is sufficient NH_3 to neutralize SO_4^{2-} and some NO_3^- so that when NH_3 is reduced, it eliminates NO_3^- first and has little impact on SO_4^{2-} . In July (Figure 5.26), while NH_4NO_3 is again reduced, there is less NO_3^- in July than January (as indicated by the absolute difference of NO_3^-), so the reduction of AL- NH_3 only results in a maximum reduction of $\text{PM}_{2.5}$ of 7.4%. The reduction of NH_3 and NH_4^+ acts to decrease the pH of the aerosols, where oxidation of SO_2 to SO_4^{2-} is highly dominated by reaction with abundant H_2O_2 (Seinfeld and Pandis, 2006) and results in an increase of SO_4^{2-} in some regions. Wu et al. (2008b) completed a sensitivity simulation that eliminated AL- NH_3 in NC in August 2002 and found a decrease of 10-20% in $\text{PM}_{2.5}$ concentrations, mainly due to a decrease in NH_4^+ and NO_3^- . While the reduction of NH_4^+ nearly doubles from the 50% reduction of AL- NH_3 emissions to 100% reduction, the decrease in NO_3^- and SO_4^{2-} are similar between the studies, so there is only a slightly larger decrease in $\text{PM}_{2.5}$ when all AL- NH_3 emissions are removed compared to a 50% reduction.

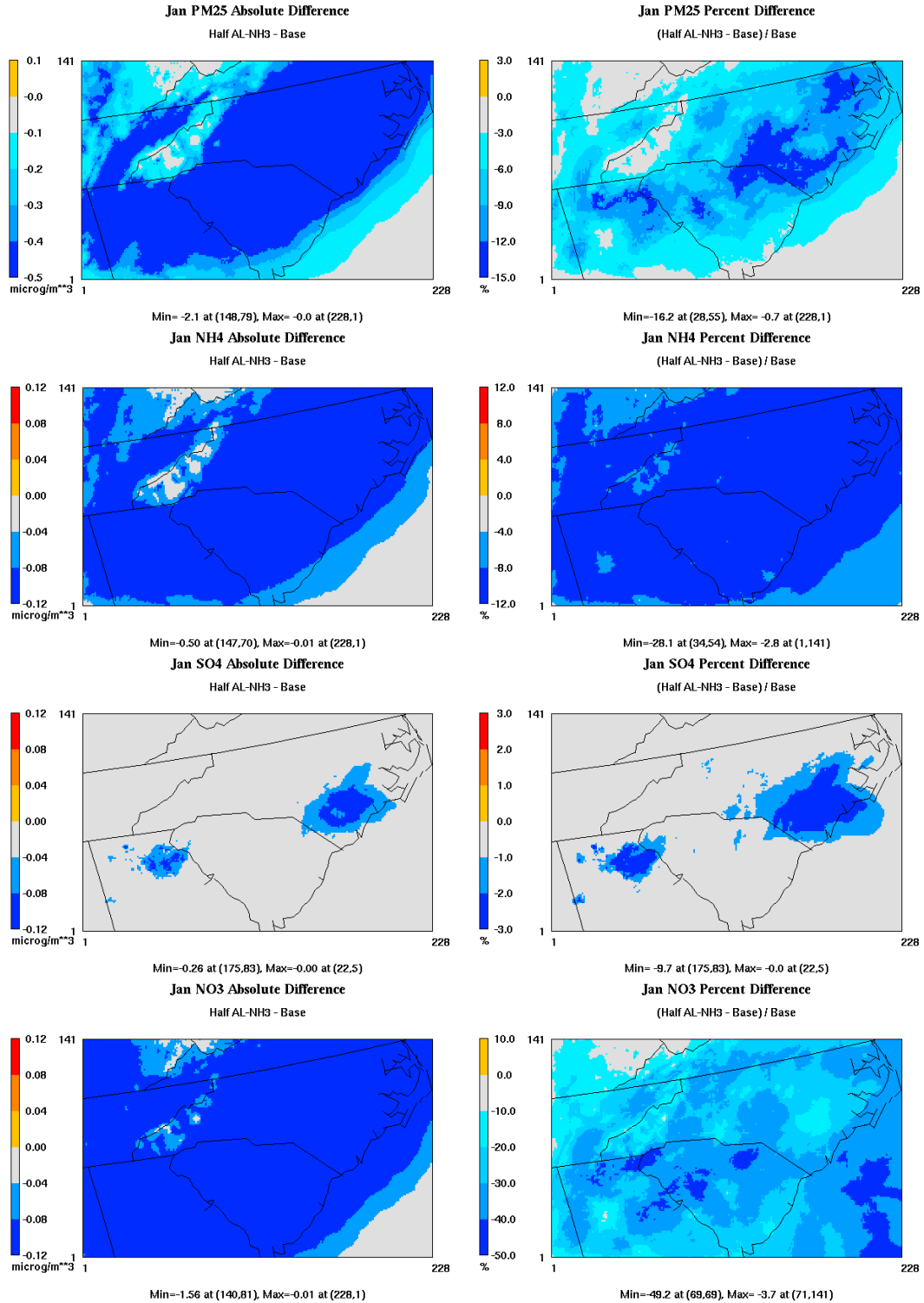


Figure 5.25. The absolute (left) and percentage (right) difference in $PM_{2.5}$, NH_4^+ , SO_4^{2-} , and NO_3^- in January when AL- NH_3 emissions are reduced by 50%.

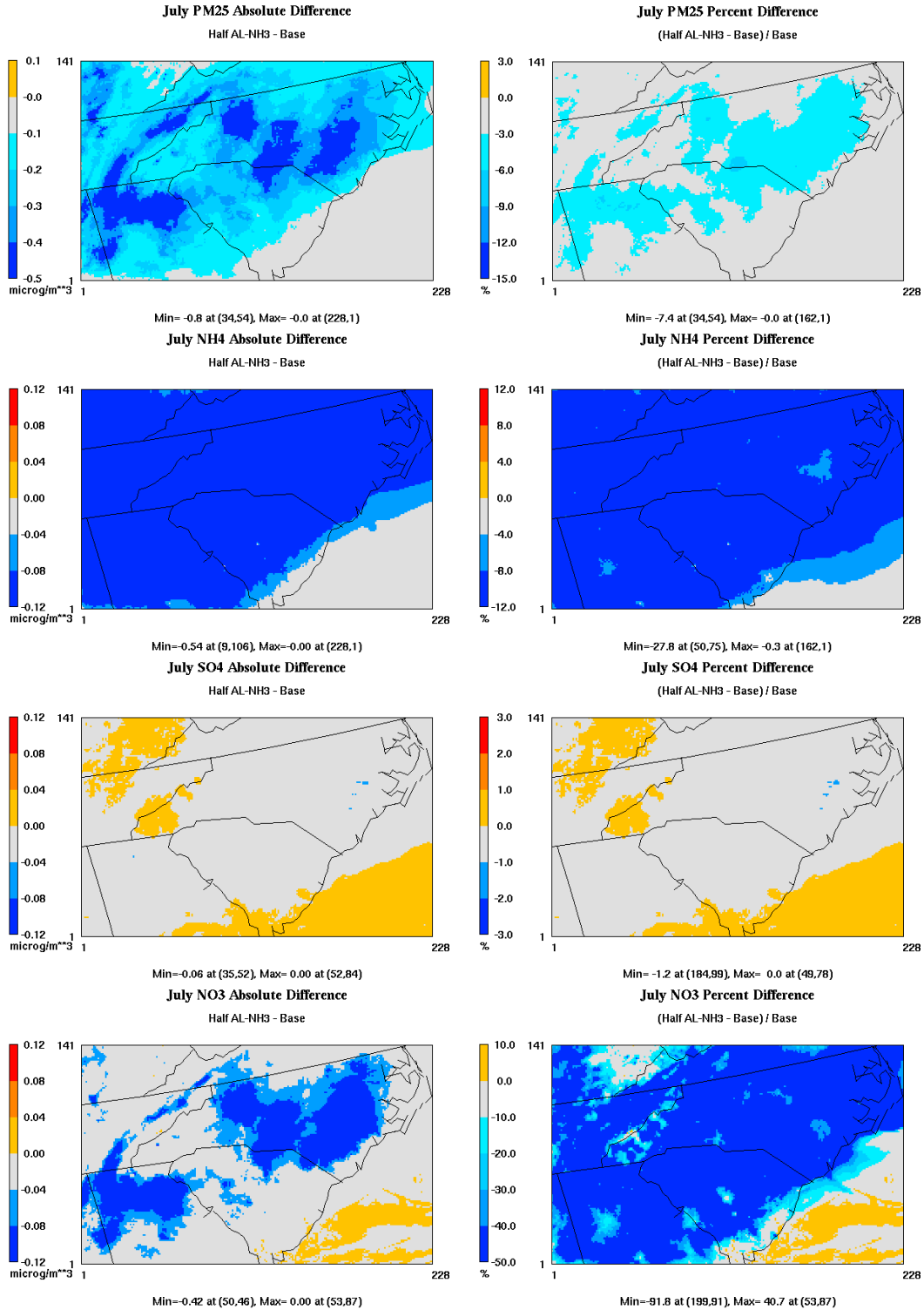


Figure 5.26. The absolute (left) and percentage (right) difference in PM_{2.5}, NH₄⁺, SO₄²⁻, and NO₃⁻ in July when AL-NH₃ emissions are reduced by 50%.

5.2.2 NO_x Reduction

Figures 5.27 and 5.28 show the absolute and percentage change in January and July, respectively, of PM_{2.5}, NH₄⁺, SO₄²⁻, and NO₃⁻ when NO_x is reduced by 50% from EGU and mobile sources. Reducing NO_x in January decreases NO₃⁻ slightly, particularly in the regions of high NH₃ emissions, which results in a decrease of PM_{2.5} by up to 6% in those regions. However, all the NH₄⁺ released from NH₄NO₃ is consumed by SO₄²⁻, resulting in an increase of SO₄²⁻ throughout the domain and an increase in PM_{2.5} by up to almost 1% at locations further from the NH₃ sources. A similar situation occurs in July, however, to a lesser extent because less NH₄NO₃ exists in the summer and thus less NH₄⁺ is released with the reduction of NO_x. These results suggest that reducing NO_x alone in the southeast by 50% does not result in a significant decrease in PM_{2.5} in January or July and is not an effective control strategy.

5.2.3 SO₂ Reduction

Figures 5.29 and 5.30 show the results of the sensitivity simulations in January and July, respectively, when SO₂ is reduced by 50% from EGU, mobile, and non-road sources. The reduction of SO₂ in January (Figure 5.29) does reduce SO₄²⁻ (by up to 10.5%); however the released NH₄⁺ is consumed by NO₃⁻. The increase in NO₃⁻ cancels out the reduced SO₄²⁻, resulting in less than 3% decrease in PM_{2.5}. In July (Figure 5.30), there is a larger decrease in SO₄²⁻ but less NO₃⁻ available to consume the NH₄⁺. This results in some decrease in NH₄⁺, particularly in regions of high NH₃ emissions, and a larger decrease in PM_{2.5} than January throughout the domain (up to 11.7%). While SO₂ reductions had little impact on PM_{2.5} in January, it is more effective in reducing PM_{2.5} in July than the individual reductions of NO_x or NH₃, consistent with the research conducted by Tsimpidi et al. (2007) and Pinder et al. (2007).

5.2.4 Combination of NH₃, NO_x, and SO₂ Emission Reductions

The final sensitivity simulations are conducted with AL-NH₃, NO_x, and SO₂ emissions each reduced by 50%. Figure 5.31 shows the results for the PM_{2.5} components in

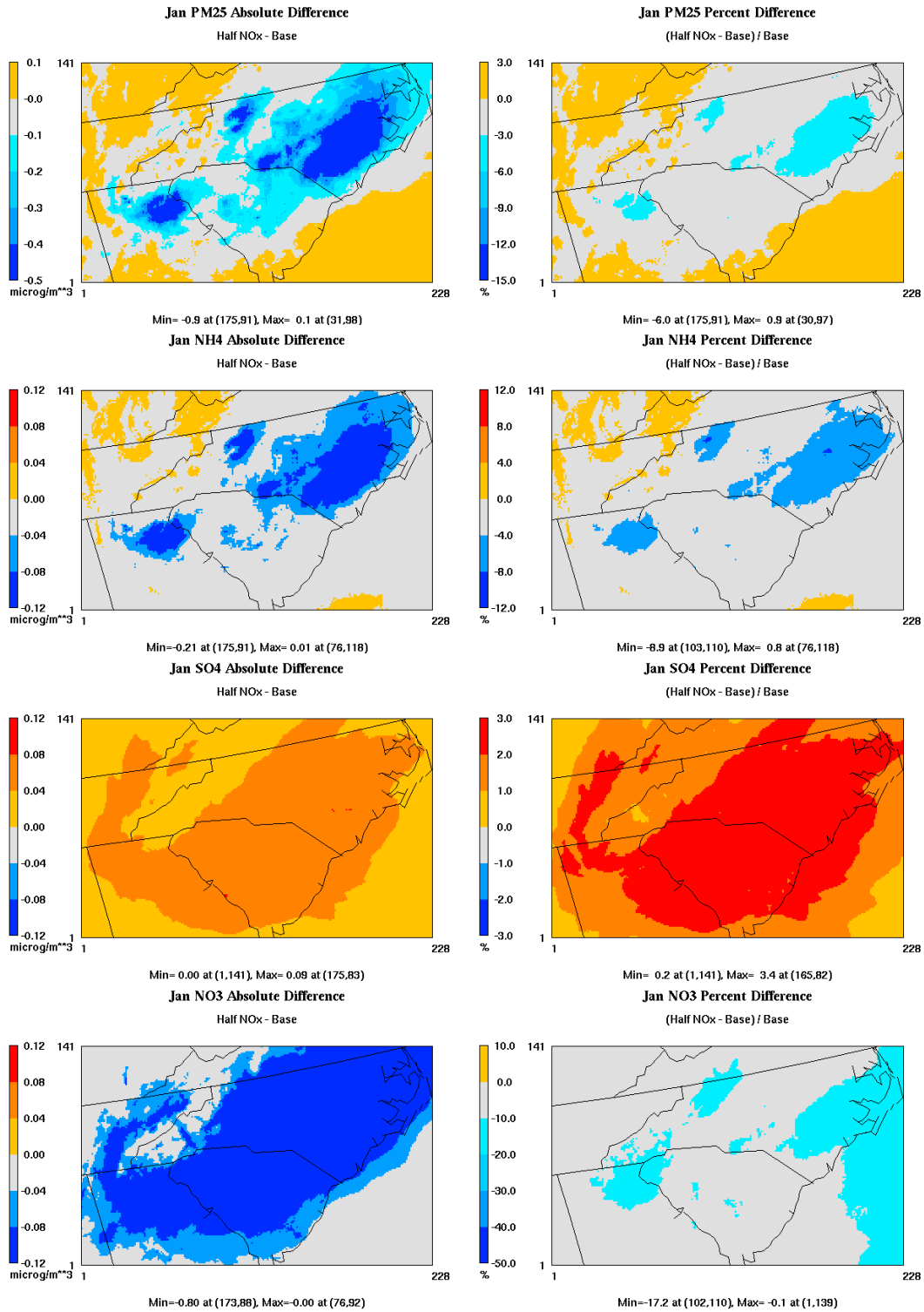


Figure 5.27. The absolute (left) and percentage (right) difference in PM_{2.5}, NH₄⁺, SO₄²⁻, and NO₃⁻ in January when NO_x is reduced by 50%.

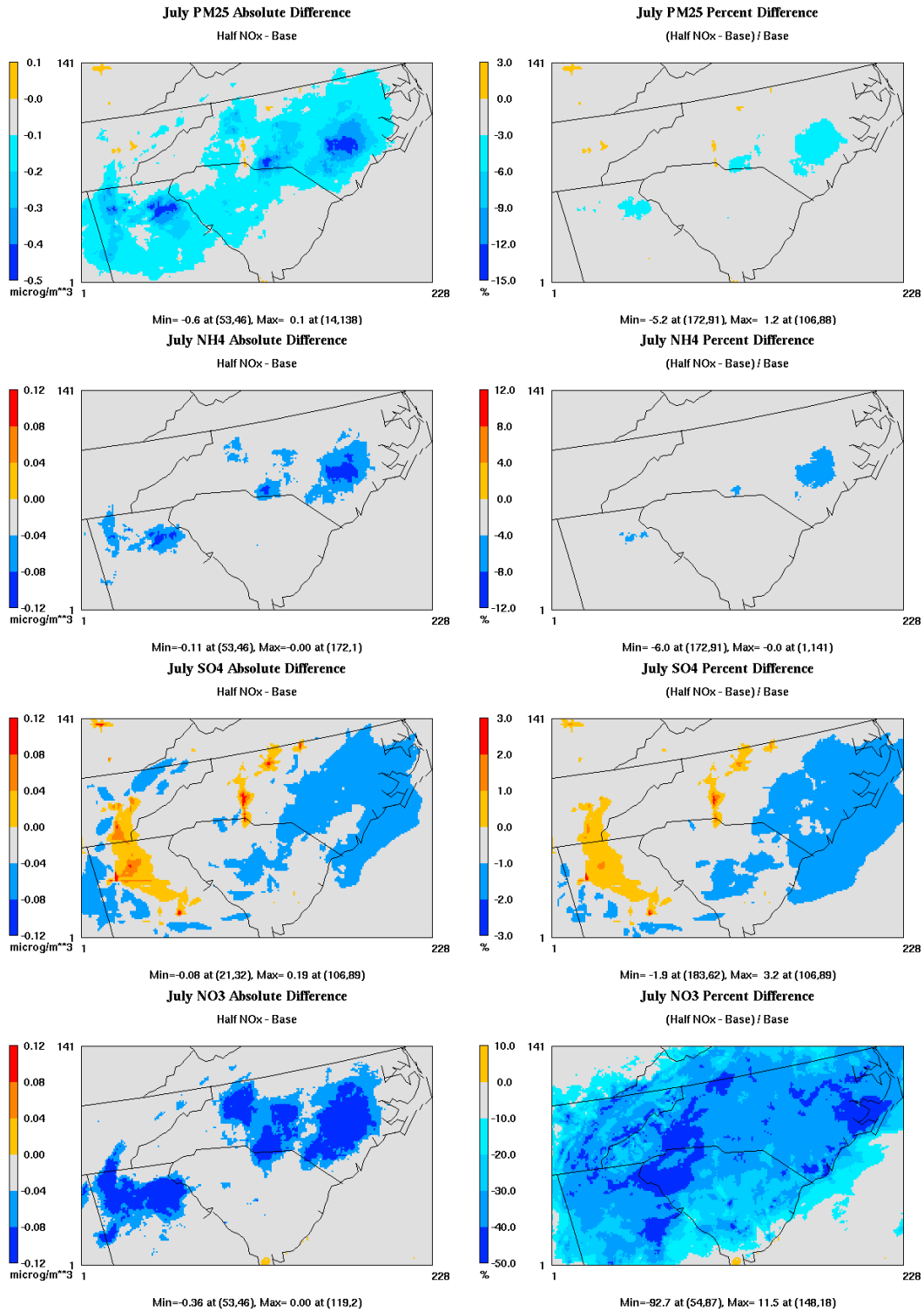


Figure 5.28. The absolute (left) and percentage (right) difference in PM_{2.5}, NH₄⁺, SO₄²⁻, and NO₃⁻ in July when NO_x emissions are reduced by 50%.

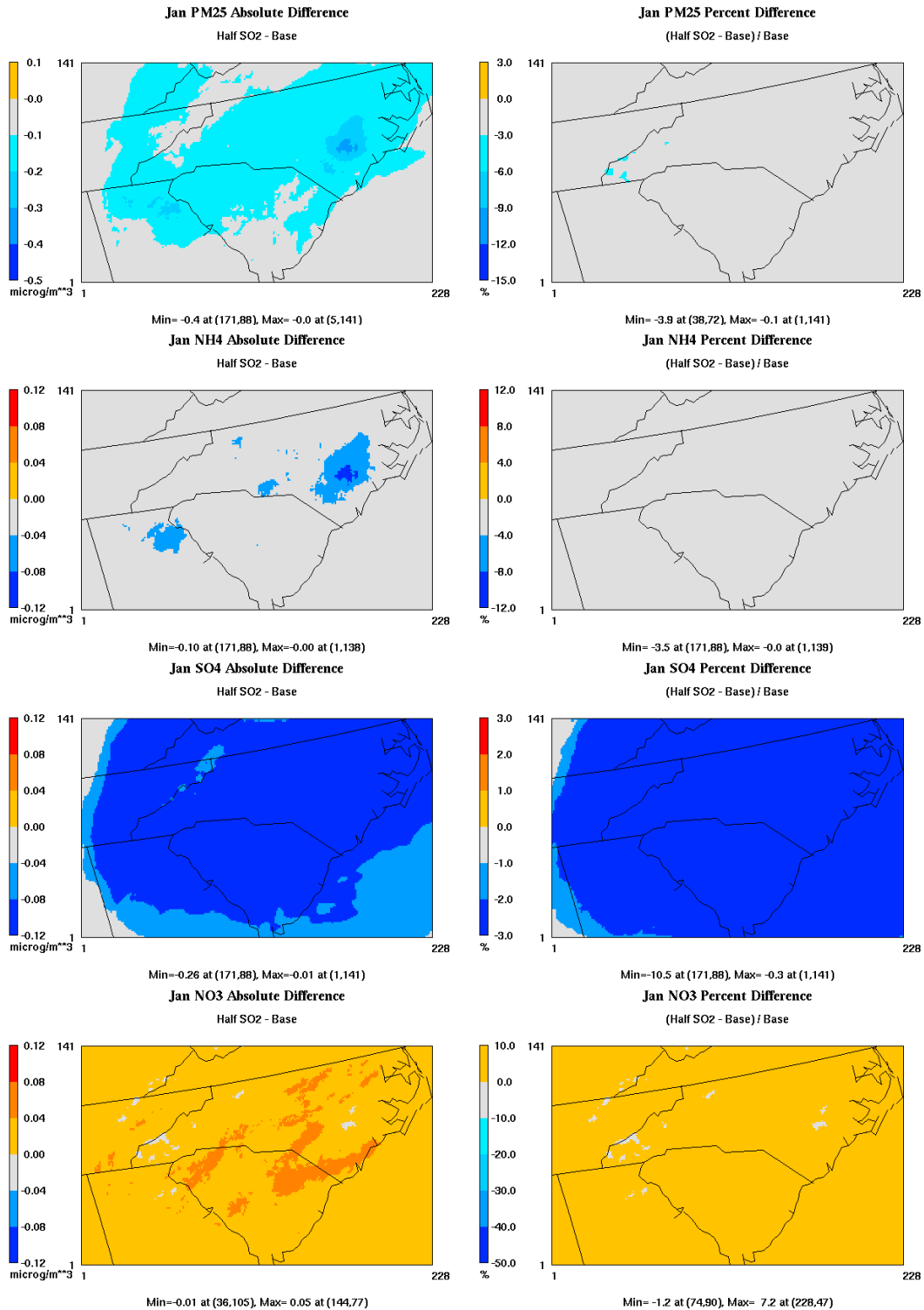


Figure 5.29. The absolute (left) and percentage (right) difference in PM_{2.5}, NH₄⁺, SO₄²⁻, and NO₃⁻ in January when SO₂ emissions are reduced by 50%.

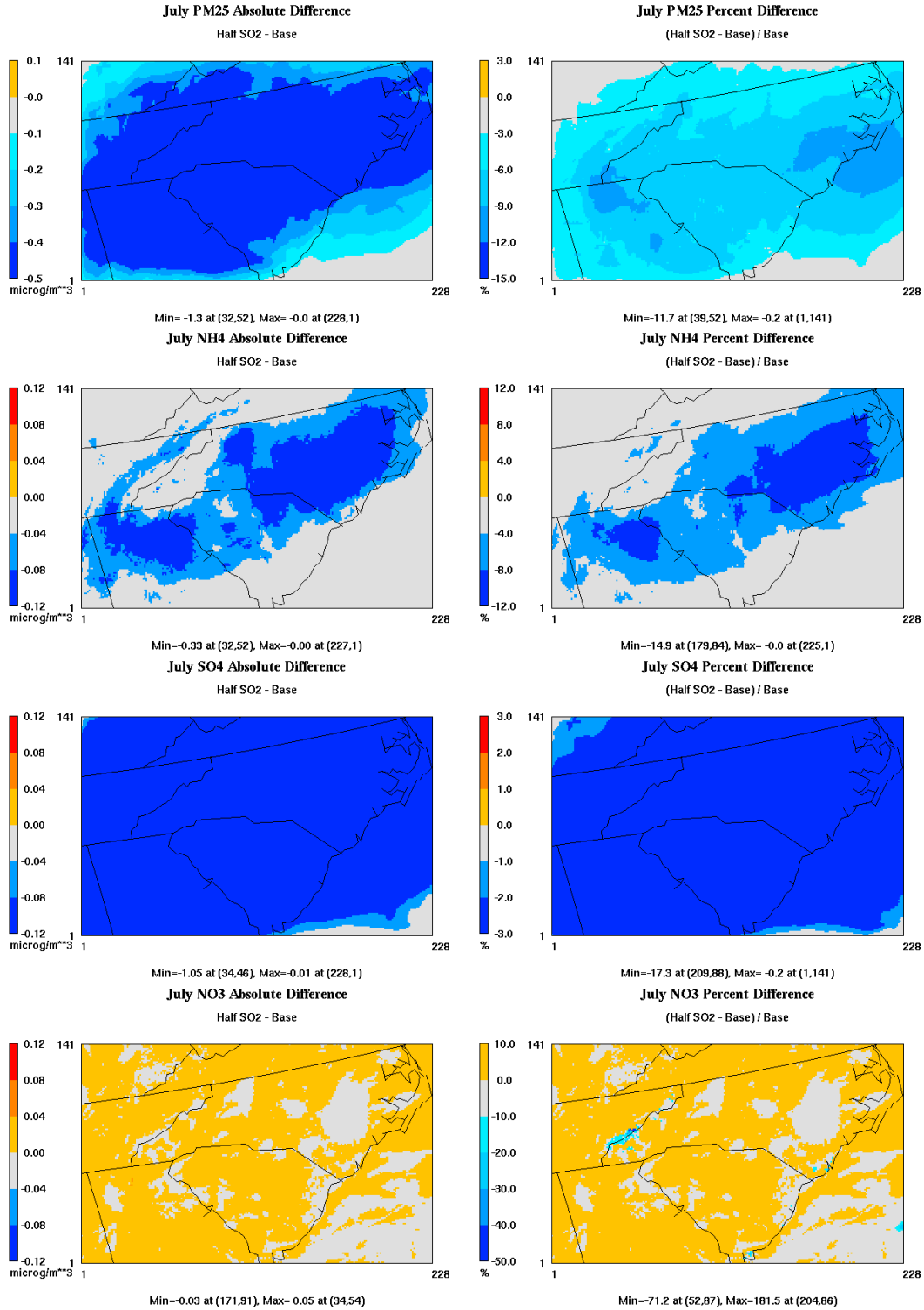


Figure 5.30. The absolute (left) and percentage (right) difference in PM_{2.5}, NH₄⁺, SO₄²⁻, and NO₃⁻ in July when SO₂ emissions are reduced by 50%.

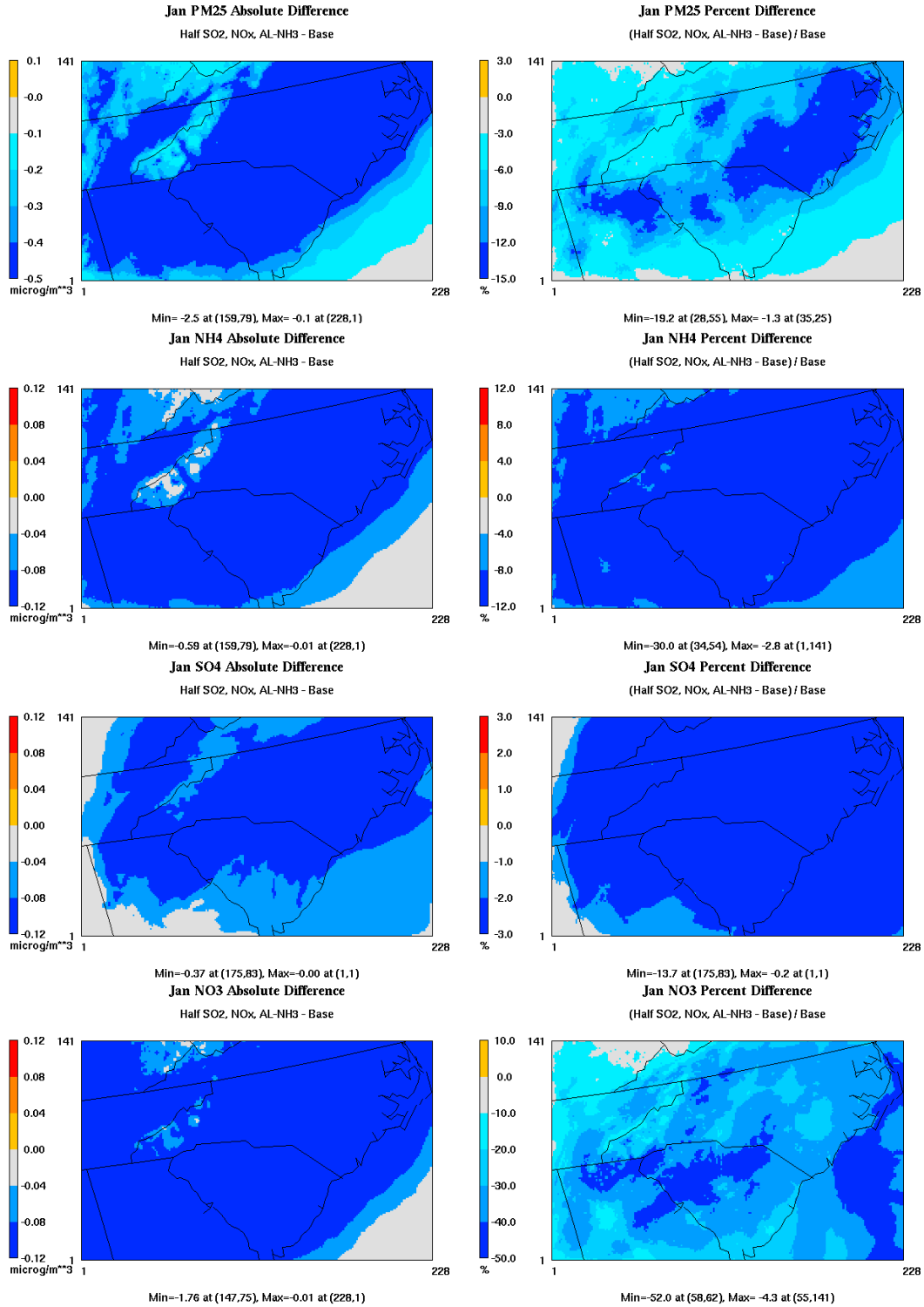


Figure 5.31. The absolute (left) and percentage (right) difference in PM_{2.5}, NH₄⁺, SO₄²⁻, and NO₃⁻ in January when AL-NH₃, NO_x, and SO₂ emissions are reduced by 50%.

January. The combined reductions result in a decrease of all three components (NH_4^+ , SO_4^{2-} , and NO_3^-) throughout the domain, with larger reductions of NH_4^+ and SO_4^{2-} in the regions of high NH_3 emissions. $\text{PM}_{2.5}$ was reduced by up to 19.2%, the largest reduction among all the sensitivity simulations, with the largest reductions occurring throughout the eastern NC and in the northeastern GA, in the same regions as reduced NH_4^+ . The reduction of $\text{PM}_{2.5}$ in January is dominated by a reduction in NH_4NO_3 resulting from the reduced NH_3 emissions as indicated in Section 5.2.1 and Figure 5.25. In July (Figure 5.32), similar results to January are found in the reduction of $\text{PM}_{2.5}$ and NH_4^+ . The region of SO_4^{2-} reductions is significantly larger in July than it was in January. While the percentage change in NO_3^- is very large in July, the concentration is small resulting in little effect on $\text{PM}_{2.5}$. The decrease in $\text{PM}_{2.5}$ is dominated by the reduction in NH_4^+ and SO_4^{2-} , which is a result of combined reductions in SO_2 and NH_3 emissions. The results of the sensitivity simulations indicate that combined reductions of AL- NH_3 , NO_x , and SO_2 emissions reduce $\text{PM}_{2.5}$ more than reducing any of them individually, with the reduction of NH_3 being the most effective control strategy in January and the reduction of NH_3 and SO_2 being the most effective control strategy in July. This indicates, in terms of air quality policy in the southeastern U.S., reducing NH_3 emissions in July could be beneficial in reducing $\text{PM}_{2.5}$ in the region. Additionally, Pinder et al. (2007) reported that, for regions that may require additional controls beyond initial SO_2 and NO_x reductions to meet the NAAQS, reducing NH_3 may be more cost effective than implementing further reductions in SO_2 and NO_x .

5.2.5 Summary

Table 5.9 summarizes the domain-wide average reductions in $\text{PM}_{2.5}$, NH_4^+ , SO_4^{2-} , and NO_3^- for each emission control scenario. Reducing AL- NH_3 emissions results in a domain-wide average decrease of $\text{PM}_{2.5}$ of 7.06% and 2.59% in January and July, respectively, due to reduced NH_4NO_3 . Reducing NO_x or SO_2 in January results in little change in domain-wide average $\text{PM}_{2.5}$ concentrations because of an increase in SO_4^{2-} or NO_3^- , respectively. The increase in SO_4^{2-} or NO_3^- is due to the release of NH_4^+ , which is then consumed by available SO_4^{2-} or NO_3^- . This also happens in July when SO_2 emissions are reduced; however the

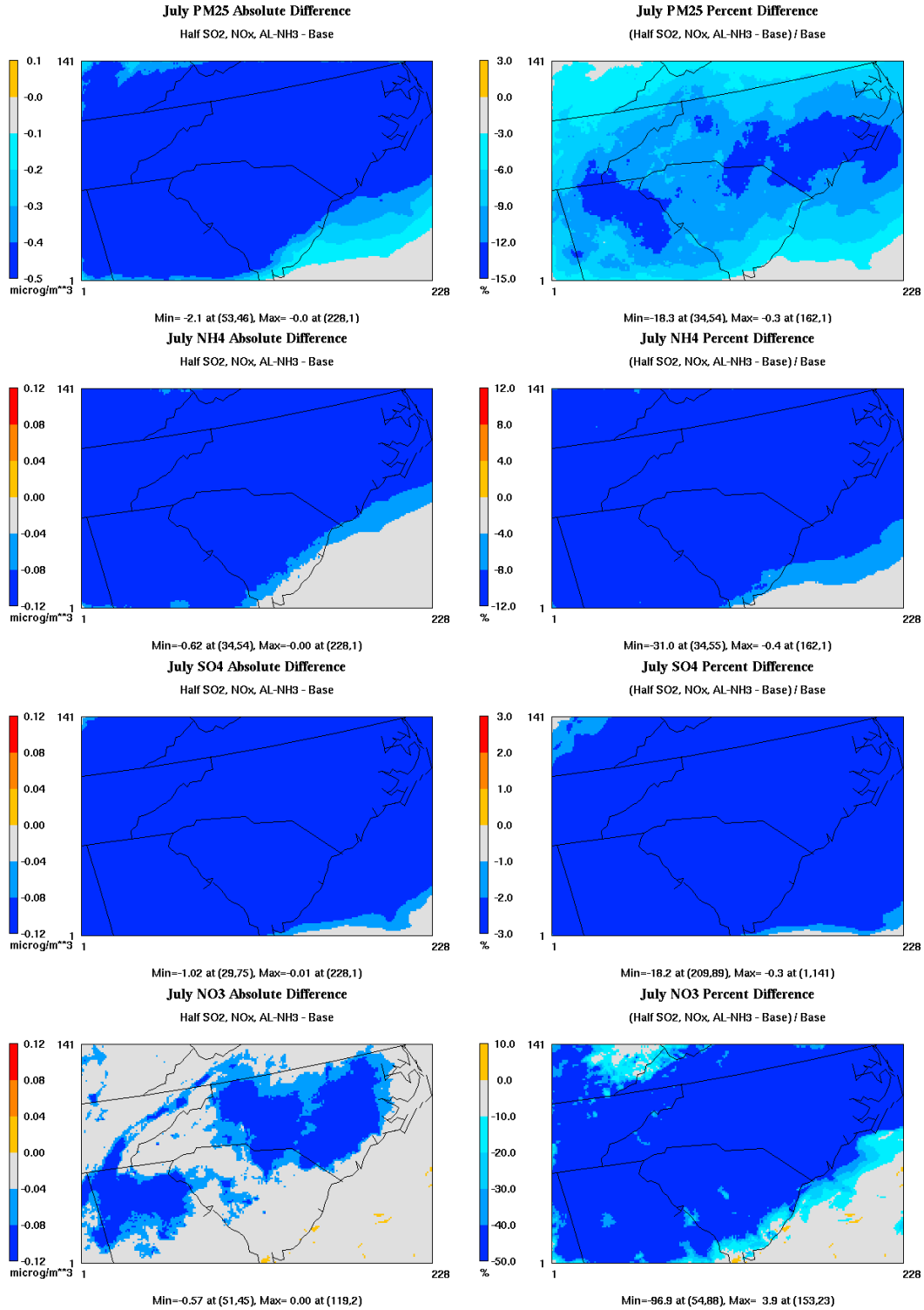


Figure 5.32. The absolute (left) and percentage (right) difference in PM_{2.5}, NH₄⁺, SO₄²⁻, and NO₃⁻ in July when AL-NH₃, NO_x, and SO₂ emissions are reduced by 50%.

Table 5.9. Absolute (abs., in $\mu\text{g m}^{-3}$) and percent (perc., %) change in domain-wide average $\text{PM}_{2.5}$, NH_4^+ , SO_4^{2-} , and NO_3^- as a result of emission reductions.

Month	Species Reduced	$\text{PM}_{2.5}$		NH_4^+		SO_4^{2-}		NO_3^-	
		Abs.	Perc.	Abs.	Perc.	Abs.	Perc.	Abs.	Perc.
Jan	AL- NH_3	-0.65	-7.06	-0.17	-15.49	-0.01	-0.62	-0.47	-28.27
	NO_x	-0.10	-1.09	-0.03	-2.37	0.04	1.96	-0.14	-8.23
	SO_2	-0.10	-1.11	-0.01	-1.32	-0.11	-5.00	0.02	1.16
	AL- NH_3 , NO_x , SO_2	-0.80	-8.60	-0.19	-17.67	-0.09	-4.10	-0.53	-32.06
Jul	AL- NH_3	-0.21	-2.59	-0.17	-16.66	0.00	-0.08	-0.04	-53.40
	NO_x	-0.10	-1.18	-0.01	-1.15	-0.03	-0.55	-0.03	-33.71
	SO_2	-0.48	-5.87	-0.05	-5.10	-0.43	-8.97	0.00	1.77
	AL- NH_3 , NO_x , SO_2	-0.74	-9.02	-0.20	-20.23	-0.45	-9.38	-0.05	-67.24

increase in NO_3^- contribution to $\text{PM}_{2.5}$ concentrations is insignificant. The largest reductions in domain-wide average $\text{PM}_{2.5}$ in both months occurs when the emissions of all three species are reduced by 50%. In January, the decrease is due to the decrease in AL- NH_3 emissions, decreasing NH_4NO_3 and is not much larger than when AL- NH_3 emissions alone are decreased. In July, the decrease in $\text{PM}_{2.5}$ is larger than the decrease due to emission reductions in any one of the individual species. The reduction of $\text{PM}_{2.5}$ is largely due to the reduced AL- NH_3 and SO_2 emissions. Although the percent reduction of NO_3^- is large, the concentration of NO_3^- in summer is small.

6. CONCLUSIONS AND RECOMMENDATIONS

Advancements in technology, as well as improved understanding and representation of atmospheric processes, have led to continued improvements in 3-D AQMs. Once the performance of a 3-D AQM has been verified through comparison with observations, the model can be used to conduct sensitivity evaluations on the impacts of future emission changes. The work in this thesis evaluates the performance of MM5/CMAQ and MM5/CAMx over the southeastern U.S. in January and July 2002 and assesses the sensitivity of MM5/CMAQ simulations to horizontal grid spacing and emission reductions. The air quality in the southeastern U.S. is of particular interest because of the high NH_3 emissions from agricultural sources and their impacts on the regional air quality and environment. NH_3 plays a key role in the nutrient and nitrogen cycle, neutralizes acids in the air, and participates in the formation of $\text{PM}_{2.5}$.

The baseline simulation of MM5/CMAQ at a horizontal grid spacing of 4-km is configured identical to the VISTAS simulations at 12-km in order to allow for a fair evaluation of sensitivity to horizontal grid resolution. Then, in order to complete a model inter-comparison between CMAQ and CAMx, the configurations for CAMx are selected to match CMAQ whenever available (i.e., CB-IV, RADM, and ISORROPIA). Differences between the two AQMs exist in the representation of vertical advection and PM size representation, secondary organic aerosol modules, and dry and wet deposition.

The meteorological variables evaluated from MM5 include hourly T2, RH2, WSP10, WDR10, u and v component of wind, and weekly total precipitation. T2 and RH2 of the baseline simulation are generally within $\pm 10\%$ of the observed values in both January and July. Wind speed is overpredicted in both months with a better performance in January. Precipitation, which impacts wet deposition, is slightly underpredicted in January by 11%, but significantly overpredicted in July by 151%. The large overprediction in July may be partially influenced by the fact that the weather in the southeast U.S. in 2002 was drier than the historical average for the region and the inability of the model in simulating dry conditions.

Both gaseous and PM species are evaluated from the air quality models. In January, both CMAQ and CAMx overpredict O_3 and $PM_{2.5}$, which may be a result of weaker vertical mixing in the models than what was observed, as indicated by the overprediction in CO and BC. The larger overprediction in CO and BC by CAMx indicates that CAMx simulates weaker vertical mixing than CMAQ. Despite CO predictions indicating weaker vertical mixing again in July, both models underpredict O_3 and $PM_{2.5}$, indicating other factors, such as underestimated emissions of their precursors or overpredicted wet deposition, have a larger impact than weaker vertical mixing in July. Both models are generally able to capture the diurnal variations of O_3 , but fail to capture the diurnal variations of $PM_{2.5}$ in both months. The formation mechanisms for O_3 are better understood than the complexities of $PM_{2.5}$ formation. Additionally, the volatility of some PM species, such as NO_3^- , makes simulating $PM_{2.5}$ more complicated than O_3 . To evaluate the potential impact of reduced NH_3 on $PM_{2.5}$, the AdjGR is calculated based on predicted concentrations of NH_3 , NO_3^- , and HNO_3 . The results indicate that the eastern NC and northeastern GA are NH_3 -rich in both January and July, so reductions in NH_3 emissions alone would result in little change in $PM_{2.5}$ in these regions. However, current regulations require reductions in the emissions of SO_2 and NO_x , which could change the impact of NH_3 . This was one of the foci in the sensitivity study. Satellite observations are used to evaluate the performance of CMAQ in simulating the total tropospheric column concentrations. This evaluation provides additional information on the spatial distribution of pollutants and the model's ability to replicate pollutant concentrations in the upper layers, which governs long-range transport of the pollutants. CO and NO_2 concentrations are well captured by CMAQ with NMBs of -4% and 14%, respectively, in January, and -14% and 7%, respectively, in July. The NMBs of O_3 and AOD are larger (60% and 29%, respectively in January; -30% and -48%, respectively in July), which may be due to uncertainties in the BCONs used in CMAQ, the calculation of AOD from CMAQ predictions, and the assumptions made by the AOD algorithm used in MODIS (i.e., removing very high and very low values).

The sensitivity to horizontal grid spacing is completed by evaluating MM5/CMAQ simulations at 12-, 4-, and 1.33-km horizontal grid spacings. July meteorological variables

display more sensitivity to horizontal grid spacing than January, with the 1.33-km performing the best for most variables. The more detailed topography of the domain, particularly near the mountains in the western NC, appears to be more detrimental than beneficial to the meteorological variables, especially RH2 in January; the lower RH2 on the leeward side of the mountains does not extend as far eastward as observed. The emissions in both months are also sensitive to horizontal grid spacing with the largest difference occurring between the 12-km and 1.33-km, as would be expected. The emissions at a horizontal grid spacing of 12-km are diffused into the larger grid cell, while at a finer grid spacing, the emissions remain confined in the grid cell near the source. The major differences in emissions between horizontal grid spacings occur along the roadways and in the major cities in both January and July, particularly in the case of SO₂, NO_x, and SO₄²⁻. Despite MM5 performing the best at 1.33-km in July, the 12-km simulation of CMAQ performs the best for almost all chemical species, indicating that other factors, such as emissions or removal through wet deposition, are more influential than meteorology. More mass is removed through wet deposition at the finer grid resolutions than the 12-km grid spacing in July, contributing to the larger underprediction of ambient concentrations. The simulation in January shows some improvement with finer grid spacing, which may also be influenced by emissions or more mass being removed through wet deposition at the finer grid spacings (which reduces the overprediction). Other factors impacting the model performance at finer grid spacings is the more detailed topography and land use data. Additionally, the short-range dispersion and mixing of agricultural species such as NH₃ are not explicitly treated in the air quality model, although the finer grid scales may better capture this process than the coarser grid scales. While these results indicate some improvement in simulating air quality at finer grid spacings, the number of available observations within the domain limits the extent of the evaluation. Additionally, the results indicate that the episode and domain of interest must be considered when determining if the use of finer grid spacing is beneficial.

By the year 2018, in order to reduce PM_{2.5} and improve the air quality of the region, the emissions of SO₂ and NO_x in the southeast are projected to be reduced by more than 50% from EGUs and mobile sources. Because NH₃ also plays an important role in PM_{2.5}

formation and there are high NH_3 emissions in the southeast from agricultural livestock, reducing NH_3 may also be beneficial in reducing $\text{PM}_{2.5}$. To assess this impact, the sensitivity of CMAQ to emission reductions in January and July is evaluated using four separate scenarios: reducing AL- NH_3 by 50%, reducing SO_2 by 50%, reducing NO_x by 50%, and combining the reduced AL- NH_3 , SO_2 , and NO_x emissions. This allows for the determination of the individual impact of reducing each species which is then compared to the impact of reducing all three. The largest reductions of $\text{PM}_{2.5}$ in both months occur when all three species are reduced by 50%, which results in a decrease of $\text{PM}_{2.5}$ by up to 19% in January and 18% in July. AL- NH_3 reductions result in the largest decrease in January at up to 16%, dominated by a reduction in NH_4NO_3 , while SO_2 reductions resulted in the largest decrease in July (up to 11%) due to decreases in NH_4^+ and SO_4^{2-} . This indicates that reducing AL- NH_3 emissions in conjunction with the projected SO_2 and NO_x reductions could act to reduce $\text{PM}_{2.5}$ concentrations more than reductions in SO_2 and NO_x alone. These results are consistent with previous studies including those reported by Tsimpidi et al. (2007) and Pinder et al. (2007).

Some of the limitations of this research are associated with available observations, while others are associated with the models. Limited observation sites within the fine scale simulation domain limit the evaluation of the spatial variations of meteorological and chemical variables. However, creating a denser network of observational sites would be costly. Using satellite data can provide some additional information on the spatial variability of pollutants; however, the resolution of some satellite data (i.e., O_3 and CO) is also coarser than the simulated grid spacing and may not provide information needed for small scale evaluation. Another limitation associated with model evaluation using observations is the time scale of observations. Hourly observations provide the most detail in understanding diurnal variations and associated processes, however, some surface observational data is only collected and reported as 24-hour averages once every three days. The use of satellite data is also limited by measurements made about once a day, not continuous over one location. The model evaluation is also limited in that the grid-averaged simulated values are being compared to pointwise observations. The AQMs themselves are limited by the

understanding and representation of atmospheric processes. For example, fine scale emissions and dispersion of agriculturally emitted NH_3 , the representation of PM size as modal or sections may not accurately capture the size distribution, and the inaccurate treatment of wet and dry deposition in the models. As new knowledge is obtained through field and laboratory research, it should be incorporated into the models in an effort to more accurately simulate the true atmosphere.

Future work to be completed based on this thesis includes completing additional simulations using the CFU (multi-sectional) scheme in CAMx and comparing the results to the bi-sectional simulation. Additional research on the complex, fine scale emissions of AL- NH_3 may be beneficial in improving the model simulation of NH_x through the development of chemical mechanisms for agriculturally-emitted species that includes the effects of bi-directionality of flux and short-range dispersion.

7. REFERENCES

- Aneja, V. P., P. A. Roelle, G. C. Murray, J. Southerland, J. W. Erisman, D. Fowler, W. A. H. Asman, and N. Patni (2001), Atmospheric nitrogen compounds II: emissions, transport, transformation, deposition and assessment, *Atmospheric Environment*, *35*, 1903-1911.
- Ansari, A. S. and S. N. Pandis (1998), Response of inorganic PM to precursor concentrations, *Environmental Science & Technology*, *32*, 2706-2714.
- Arunachalam, S., A. Holland, B. Do, and M. Abraczinskas (2006), A quantitative assessment of the influence of grid resolution on predictions of future-year air quality in North Carolina, USA, *Atmospheric Environment*, *40*, 5010-5026.
- Aubertin, G. M., D. S. Bigelow, and B. A. Malo (1991), Quality assurance plan: NADP/NTN deposition monitoring, report, National Atmospheric Deposition Program, Fort Collins, CO.
- Baker, K. R. (2004), Application of multiple one-atmosphere air quality models emphasizing PM_{2.5} performance evaluation, Air & Waste Management Association 2004 Annual Meeting, Air & Waste Management Association, Indianapolis, IN.
- Barnard, W. R. and P. Brewer (2004), Development of managed burning and wildland fire emission estimates for VISTAS, presented at 13th International Emission Inventory Conference, U.S. EPA, Clearwater, FL.
- Battye, R., W. Battye, C. Overcash, and S. Fudge (1994), Development and selection of ammonia emission factors, *EPA/600/R-94/190*, U.S. Environmental Protection Agency, Research Triangle Park, NC
- Binkowski, F. S. (1999), Chapter 10: Aerosols in Models-3 CMAQ, in *Science Algorithms of the EPA Models-3 Community Multiscale Air Quality (CMAQ) Modeling System*, edited by D. W. Byun and J. K. S. Ching, 24 pp., U.S. Environmental Protection Agency, Research Triangle Park, NC.
- Binkowski, F. S. and S. J. Roselle (2003), Models-3 Community Multiscale Air Quality (CMAQ) model aerosol component 1. Model description, *J. Geophys. Res.*, *108*, D6, doi:10.1029/2001JD001409.

- Binkowski, F. S. and U. Shankar (1995), The regional particulate matter model 1. Model description and preliminary results, *J. Geophys. Res.*, *100*, 26,191-26,209.
- Byun, D. W., J. E. Pleim, R. T. Tang, and A. Bourgeois (1999), Chapter 12: Meteorology-Chemistry Interface Processor (MCIP) for Models-3 Community Multiscale Air Quality (CMAQ) modeling system, in *Science Algorithms of the EPA Models-3 Community Multiscale Air Quality (CMAQ) Modeling System*, edited by D. W. Byun and J. K. S. Ching, 91 pp., U.S. Environmental Protection Agency, Research Triangle Park, NC.
- Byun, D. W., and J. K. S. Ching (Eds.) (1999), Science algorithms of the EPA models-3 community multi-scale air quality (CMAQ) modeling system. US EPA Report No. EPA/600/R-99/030. Office of Research and Development, Washington, DC.
- Byun, D. W., and K. L. Schere (2006), Review of the governing equations, computational algorithms and other components of the Models-3 Community Multiscale Air Quality (CMAQ) Modeling System, *Applied Mechanics Reviews*, *59*, 51-77.
- Chameides, W. L., C. Luo, R. Salor, D. Streets, Y. Huang, M. Bergin, and F. Giorgi (2002), Correlation between model-calculated anthropogenic aerosols and satellite-derived cloud optical depths: Indication of indirect effect?, *J. Geophys. Res.*, *107D10*, 4085, doi: 10.1029/2000JD000208.
- Chameides, W. L. and E. B. Cowling (2001), The state of the Southern Oxidants Study (SOS): Policy-relevant findings in ozone pollution research 1988-1994, North Carolina State University, Raleigh.
- Chow, J. C. and J. G. Watson (1998), Guideline on speciated particulate monitoring, report, Desert Research Institute, Reno, NV.
- Chu, D. A., Y. J. Kaufman, C. Ichoku, L. A. Remer, D. Tanré, and B. N. Holben (2002), Validation of MODIS aerosol optical depth retrieval over land, *Geophysical Research Letter*, *29*, doi: 10.1029/2001GL013205.
- Coffman, D. J., and D. A. Hegg (1995), A preliminary study of the effect of ammonia on particle nucleation in the marine boundary layer, *Journal of Geophysical Research*, *100D4*, 7147-7160.
- Cohan, D. S., Y. Hu, and A.G. Russell (2006), Dependence of ozone sensitivity analysis on grid resolution, *Atmospheric Environment*, *40*, 126-135.

- Cowling E. B. and C. Furness (2001), The state of the Southern Oxidants Study (SOS): Policy-relevant findings in ozone and PM_{2.5} pollution research 1994-2000, North Carolina State University, Raleigh.
- Dennis, R. L., P. V. Bhave, and R. W. Pinder (2008), Observable indicators of the sensitivity of PM_{2.5} nitrate emission reductions – Part II: Sensitivity to errors in total ammonia and total nitrate of the CMAQ-predicted non-linear effect of SO₂ emission reductions, *Atmospheric Environment*, 42, 1287-1300.
- Eder, B. and S. Yu (2006), A performance evaluation of the 2004 release of Models-3 CMAQ, *Atmospheric Environment*, 40, 4811-4824.
- Engel-Cox, J. A., C. H. Holloman, B. W. Coutant, and R. M. Hoff (2004a), Qualitative and quantitative evaluation of MODIS satellite sensor data for regional and urban scale air quality, *Atmospheric Environment*, 38, 2495-2509.
- Engel-Cox, J. A., R. M. Hoff, and A. D. J. Haymet (2004b), Recommendations on the use of satellite remote-sensing data for urban air quality, *Journal of the Air & Waste Management Association*, 54, 1360-1371.
- ENVIRON, 2006. User's Guide – Comprehensive Air Quality Model with extensions, Version 4.40. ENVIRON International Corporation, Novato, California.
<<http://www.camx.com/>>.
- Finkelstein, P. L., T. G. Ellestad, J. F. Clarke, T. P. Meyers, D. B. Schwede, E. O. Hebert, and J. A. Neal (2000), Ozone and sulfur dioxide dry deposition to forests: Observations and model evaluation, *Journal of Geophysical Research*, 105D12, 15365-15377.
- Grell, G. A., J. Dudhia, and D. R. Stauffer (1995), A description of the Fifth-Generation Penn State/NCAR Mesoscale Model (MM5), *NCAR Technical Report, NCAR/TN-398+STR*, 122pp.
- Hansen, D. A., E. S. Edgerton, B. E. Hartsell, J. J. Jansen, N. Kandasamy, G. M. Hldy, C. L. Blanchard (2003), The Southeastern Aerosol Research and Characterization Study: Part 1 – Overview, *Journal of the Air & Waste Management Association*, 53, 1460-1471.
- Hinds, W. C. (1999), *Aerosol technology: Properties, behavior, and measurement of airborne particles*, 2nd ed., 483 pp., John Wiley & Sons, Inc, New York.
- IMPROVE (2002), Quality Assurance Project Plan, report, IMPROVE, Fort Collins, CO.

- Jang, J.-C. C., H. E. Jeffries, D. Byun, and J. E. Pleim (1995), Sensitivity of ozone to model grid resolution – I. Application of High Resolution Regional Acid Deposition Model, *Atmospheric Environment*, 29, 3085-3100.
- Kinzig, A. P. and R. H. Socolow (1994), Human impacts on the nitrogen cycle, *Physics Today*, 47, 24-31.
- Kleeman, M. J., Q. Ying, and A. Kaduwela (2005), Control strategies for the reduction of airborne particulate nitrate in California's San Joaquin Valley, *Atmospheric Environment*, 39, 5325-5341.
- Lambert, J.-C. (Eds.) (2002), ERS-2 GOME GDP 3.0 Implementation and delta validation: Validation report for GOME level-1-to-2 data processor upgrade to version 3.0, ERSE-DTEX-EOAD-TN-02-0006, Space Aeronomy Institute of Belgium, Brussels, Belgium.
- Lefer, B. L., R. W. Talbot, and J. W. Munger (1999), Nitric acid and ammonia at a rural northeastern U.S. site, *J. Geophys. Res.*, 104, D1, 1645-1661.
- Liang, J., P. T. Martien, S.-T. Soong, and S. Tanrikulu (2004), A photochemical model comparison study: CAMx and CMAQ performance in Central California, paper presented at 13th Conference on the Applications of Air Pollution Meteorology with the A&WMA, American Meteorological Society, Seattle, WA.
- Liao, K.-J., E. Tagaris, K. Manomaiphiboon, S. L. Napelenok, J.H. Woo, S. He, P. Amar, and A. G. Russell (2007), Sensitivities of ozone and fine particulate matter formation to emissions under the impact of future climate change, *Environ. Sci. Technol.*, 41, 8355-8361.
- Li, Z. and V. P. Aneja (1992), Regional analysis of cloud chemistry at high elevations in the eastern United States, *Atmospheric Environment*, 26A, 2001-2017.
- MACTEC, Inc. (2007), Clean Air Status and Trends Network (CASTNET) Quality Assurance Project Plan (QAPP), report, MACTEC Engineering and Consulting, Inc., Alpharetta, GA.
- MACTEC, Inc. (2008), Documentation of the Base G2 and Best & Final 2002 base year, 2009 and 2018 emission inventories for VISTAS, report, MACTEC Engineering and Consulting, Inc., Alpharetta, GA.
- Malm, W. C. (1999), *Introduction to Visibility*, 70 pp., Cooperative Institute for Research in the Atmosphere, Colorado State University, Fort Collins, CO.

- Malm, W. C., J. F. Sisler, D. Huffman, R. A. Eldred, and T. A. Cahill (1994), Spatial and seasonal trends in particle concentration and optical extinction in the United States, *Journal of Geophysical Research*, 99D1, 1347-1370.
- Mass, C. F. D. Ovens, K. Westrick, and B. A. Colle (2002), Does increasing horizontal resolution produce more skillful forecasts? The results of two years of real-time numerical weather prediction over the Pacific Northwest, *Bulletin of the American Meteorological Society*, 83, 407-430.
- Mathur, R., U. Shankar, A. F. Hanna, M. T. Odman, J. N. McHenry, C. J. Coats Jr., K. Alapaty, A. Xiu, S. Arunachalam, D. T. Olerud Jr., D. W. Byun, K. L. Schere, F. S. Binkowski, J. K. S. Ching, R. L. Dennis, T. E. Pierce, J. E. Pleim, S. J. Roselle, and J. O. Young (2005), Multiscale Air Quality Simulation Platform (MAQSIP): Initial applications and performance for tropospheric ozone and particulate matter, *J. Geophys. Res.*, 110, D13308, doi: 10.1029/2004JD004918.
- McMurry, P.H., M. Fink, H. Sakurai, M.R. Stolzenburg, R.L. Mauldin III, J. Smith, F. Eisele, K. Moore, S. Sjostedt, D. Tanner, L.G. Huey, J. B. Nowark, E. Edgerton, and D. Voisin (2005), A criterion for new particle formation in the sulfur-rich Atlanta atmosphere, *Journal of Geophysical Research*, 110, D22S02, doi: 10.1029/2005JD005901.
- McPeters, R. D., et al. (1996), Nimbus-7 Total Ozone Mapping Spectrometer (TOMS) data products user's guide, NASA reference publication, NASA/Goddard Space Flight Center, Greenbelt, MD.
- Mebust, R. M., B. K. Eder, F. S. Binkowski, and S. J. Roselle (2003), Models-3 Community Multiscale Air Quality (CMAQ) model aerosol component 2. Model evaluation, *Journal of Geophysical Research*, 108D6, doi:10.1029/2001JD001410.
- Meyers, T. P., P. Finkelstein, J. Clarke, T. G. Ellestad, and P. F. Sims (1998), A multilayer model for inferring dry deposition using standard meteorological measurements, *Journal of Geophysical Research*, 103D17, 22645-22661.
- Morris, R. E., B. Koo, A. Guenther, G. Yarwood, D. McNally, T. W. Tesche, G. Tonnesen, J. Boylan, and P. Brewer (2006), Model sensitivity evaluation for organic carbon using two multi-pollutant air quality models that simulate regional haze in the southeastern United States, *Atmospheric Environment*, 40, 4960-4972.
- Morris, R. E., B. Koo, B. Wang, G. Stella, D. McNally, C. Loomis, C.-J. Chien, and G. Tonnesen (2007), Technical support document for VISTAS emissions and air quality modeling to support regional haze state implementation plans, *Draft Final Report*, ENVIRON, Novato, CA.

- Napari, I., M. Noppel, H. Vehkamäki, and M. Kulmala (2002), An improved model for ternary nucleation of sulfuric acid-ammonia-water, *Journal of Chemical Physics*, *116*, 4221-4227.
- Nguyen, K. and D. Dabdub (2002), NO_x and VOC control and its effect on the formation of aerosols, *Aerosol Science and Technology*, *36*, 560-572.
- Nolte, C. G., A. B. Gilliland, C. Hogrefe, and L. J. Mickley (2008), Linking global to regional models to assess future climate impacts on surface ozone levels in the United States, *J. Geophys. Res.*, *113*, D14307, doi: 10.1029/2007JD008497.
- Olerud, D. and A. Sims (2003), MM5 sensitivity modeling in support of VISTAS (Visibility Improvement – State and Tribal Association), draft report, Baron Advanced Meteorological System, LLC, Raleigh, NC, December.
- Olerud, D. and A. Sims (2004), MM5 2002 modeling in support of VISTAS (Visibility Improvement – State and Tribal Association of the Southeast), report, Baron Advanced Meteorological Systems, LLC, Raleigh, NC, August.
- Olerud, D. T., A. P. Sims, and M. Abraczinskas (2005), Annual meteorological modeling in support of visibility improvement in the southeast US, presented at AMS 85th Annual Conference/7th Conference on Atmospheric Chemistry, American Meteorological Society, San Diego, CA.
- Paerl, H. W. (1997), Coastal eutrophication and harmful algal blooms: Importance of atmospheric deposition and groundwater as “new” nitrogen and other nutrient sources, *Limnol. Oceanogr.*, *42*, 1154-1165.
- Pinder, R. W., P. J. Adams, and S. N. Pandis (2007), Ammonia emission controls as a cost-effective strategy for reducing atmospheric particulate matter in the eastern United States, *Environ. Sci. Technol.*, *41*, 380-386.
- Pinder, R. W., A. B. Gilliland, and R. L. Dennis (2008), Environmental impact of atmospheric NH₃ emissions under present and future conditions in the eastern United States, *Geophysical Research Letters*, *35*, L12808, doi: 10.1029/2008GL033732.
- Pitchford, M.L. and W.C. Malm (1994), Development and applications of a standard visual index, *Atmospheric Environment*, *28*, 1049-1054.
- Pun, B. K., R. T. F. Balmori, and C. Seigneur (2009), Modeling wintertime particulate matter formation in central California, *Atmospheric Environment*, *43*, 402-409.

- Pun, B. K. and C. Seigneur (2001), Sensitivity of particulate matter nitrate formation to precursor emissions in the California San Joaquin Valley, *Environmental Science and Technology*, 35, 2979-2987.
- Pun, B. K., C. Seigneur, E. M. Bailey, L. L. Gautney, S. G. Douglas, J. L. Haney, and N. Kumar (2008), Response of atmospheric particulate matter to changes in precursor emissions: A comparison of three air quality models, *Environ. Sci. Technol.*, 42, 831-837.
- Queen, A., Y. Zhang, R. Gilliam, and J. Pleim (2008), Examining the sensitivity of MM5-CMAQ predictions to explicit microphysics schemes and horizontal grid resolutions, Part I – Database, evaluation protocol, and precipitation predictions, *Atmospheric Environment*, 42, 3842-3855.
- Queen, A. and Y. Zhang (2008), Examining the sensitivity of MM5-CMAQ predictions to explicit microphysics schemes and horizontal grid resolutions, Part III – The impact of horizontal grid resolution, *Atmospheric Environment*, 42, 3869-3881.
- Remer, L. A., Y. J. Kaufman, D. Tanré, S. Mattoo, D. A. Chu, J. V. Martins, R.-R. Li, C. Ichoku, R. C. Levy, R. G. Kleidman, T. F. Eck, E. Vermote, and B. N. Holben (2005), The MODIS aerosol algorithm, products and validation, *Journal of the Atmospheric Sciences*, 62, 947-973.
- Robarge, W. P., J. T. Walker, R. B. McCulloch, and G. Murray (2002), Atmospheric concentrations of ammonia and ammonium at an agricultural site in the southeast United States, *Atmospheric Environment*, 36, 1661-1674.
- Roselle, S. J. and F. S. Binkowski (1999), Chapter 11: Cloud dynamics and chemistry, *Science Algorithms of the EPA Models-3 Community Multiscale Air Quality (CMAQ) Modeling System*, edited by D. W. Byun and J. K. S. Ching, 10 pp., U.S. Environmental Protection Agency, Research Triangle Park, NC.
- Sakurai, H., M.A. Fink, P.H. McMurry, L. Mauldin, K.F. Moore, J.N. Smith, and F.L., Eisele (2005), Hygroscopicity and volatility of 4-10 nm particles during summertime atmospheric nucleation events in urban Atlanta, *Journal of Geophysical Research*, 110, D22S04, doi:10.1029/2005JD005918.
- Seigneur, C., B. Pun, P. Pai, J.-F. Louis, P. Solomon, C. Emery, R. Morris, M. Zahniser, D. Worsnop, P. Koutrakis, W. White, and I. Tombach (2000), Guidance for the performance evaluation of three-dimensional air quality modeling systems for particulate matter and visibility, *J. Air & Waste Manage. Assoc.*, 50, 588-599.

- Seinfeld, J. H. and S. N. Pandis (2006), *Atmospheric Chemistry and Physics*, 2nd ed., 1203 pp., Wiley-Interscience, Hoboken, New Jersey.
- Slinn, S. A. and W. G. N. Slinn (1980), Predictions for particle deposition on natural waters, *Atmospheric Environment*, *14*, 1013-1016.
- Smith, J.N., K.F. Moore, F.L. Eisele, D. Voisin, A.K. Ghimire, H. Sakurai, and P.H. McMurry (2005), Chemical composition of atmospheric nanoparticles during nucleation events in Atlanta, *Journal of Geophysical Research*, *110*, D22S03, doi:10.1029/2005JD005912.
- Stockwell, W. R., J. G. Watson, N. F. Robinson, W. Steiner, and W. W. Sylte (2000), The ammonium nitrate particle equivalent of NO_x emissions for wintertime conditions in Central California San Joaquin Valley, *Atmospheric Environment*, *34*, 4711-4717.
- Stolzenburg, M.R., P.H. McMurry, H. Sakurai, J.N. Smith, R.L. Mauldin III, F.L. Eisele, and C.F. Clement (2005), Growth rates of freshly nucleated atmospheric particles in Atlanta, *Journal of Geophysical Research*, *110*, D22S05, doi:10.1029/2005JD005935.
- Tagaris, E., K. Manomaiphiboon, K.-J. Liao, L. R. Leung, J.-H. Woo, S. He, P. Amar, and A. G. Russell (2007), Impacts of global climate change and emissions on regional ozone and fine particulate matter concentrations over the United States, *J. Geophys. Res.*, *112*, D14312, doi: 10.1029/2006JD008262.
- Takahama, S., A. E. Wittig, D. V. Vayenas, C. I. Davidson, and S. N. Pandis (2004), Modeling the diurnal variation of nitrate during the Pittsburgh Air Quality Study, *J. Geophys. Res.*, *109*, D16S06, doi: 10.1029/2003JD004149.
- Tsimpidi, A. P., V. A. Karydis, and S. N. Pandis (2007), Response of inorganic fine particulate matter to emission changes of sulfur dioxide and ammonia: The eastern United States as a case study, *J. Air & Waste Manage. Assoc.*, *57*, 1489-1498.
- U.S. EPA (1991), Guidance for Regulatory Application of the Urban Airshed Model, *EPA-450/4-91-013*, US Environmental Protection Agency, Research Triangle Park, NC.
- U.S. EPA (1999), Particulate Matter (PM_{2.5}) Speciation Guidance: Final Draft, US EPA Office of Air Quality Planning and Standards, Research Triangle Park, NC, October 7, 1999. (<http://www.epa.gov/ttn/amtic/files/ambient/pm25/spec/specfinl.pdf>)
- U.S. EPA (2003), Guidance for Estimating Natural Visibility Conditions Under the Regional Haze Program, *EPA-454/B-03-005*, 66 pp., Battelle, Research Triangle Park, NC.

- U.S. EPA (2007), Guidance on the Use of Models and Other Analyses for Demonstrating Attainment of Air Quality Goals for Ozone, PM_{2.5}, and Regional Haze, *EPA -454/B-07-002*, US Environmental Protection Agency, Research Triangle Park, NC.
- Wang, K., Y. Zhang, C. Jang, S. Phillips, and B. Wang (2009), Modeling intercontinental air pollution transport over the trans-Pacific region in 2001 using the Community Multiscale Air Quality modeling system, *Journal of Geophysical Research*, *114*, D04307, doi: 10.1029/2008JD010807.
- Weber, R. J., P.H. McMurry, R. L. Mauldin, III, D. J. Tanner, F. L. Eisele, A. D. Clarke, and V. N. Kapustin (1999), New particle formation in the remote troposphere: A comparison of observations at various sites, *Geophysical Research Letters*, *26*, 307-310.
- Wesely, M. L. (1989), Parameterization of surface resistances to gaseous dry deposition in regional-scale numerical models, *Atmospheric Environment*, *23*, 1293-1304.
- Wu, S.-Y., S. Krishnan, Y. Zhang, and V. Aneja (2008a), Modeling atmospheric transport and fate of ammonia in North Carolina – Part I: Evaluation of meteorological and chemical predictions, *Atmospheric Environment*, *42*, 3419-3436.
- Wu, S.-Y., J.-L. Hu, Y. Zhang, and V. P. Aneja (2008b), Modeling atmospheric transport and fate of ammonia in North Carolina – Part II: Effect of ammonia emissions on fine particulate matter formation, *Atmospheric Environment*, *42*, 3437-3451.
- Yu, F. (2006), Effect of ammonia on new particle formation: A kinetic H₂SO₄-H₂O-NH₃ nucleation model constrained by laboratory measurements, *Journal of Geophysical Research*, *111*, D01204, doi:10.1029/2005JD005968.
- Yu, S., P. V. Bhave, R. L. Dennis, and R. Mathur (2007), Seasonal and regional variations of primary and secondary organic aerosols over the continental United States: Semi-empirical estimates and model evaluation, *Environ. Sci. Technol.*, *41*, 4690-4697.
- Yu, S., R. L. Dennis, P. V. Bhave, and B. K. Eder (2004), Primary and secondary organic aerosols over the United States: estimates on the basis of observed organic carbon (OC) and elemental carbon (EC), and air quality modeled primary OC/EC ratios, *Atmospheric Environment*, *38*, 5257-5268.
- Yu, S., B. Eder, R. Dennis, S.-H. Chu, and S. E. Schwartz (2006), New unbiased symmetric metrics for evaluation of air quality models, *Atmospheric Science Letters*, *7*, 26-34.

- Zhang, Y., B. Pun, S.-Y. Wu, K. Vijayaraghavan, and C. Seigneur (2004), Application and evaluation of two air quality models for particulate matter for a southeastern U.S. episode, *Journal of the Air & Waste Management Association*, 54, 1478-1493.
- Zhang, Y., P. Liu, B. Pun, and C. Seigneur (2006a), A comprehensive performance evaluation of MM5-CMAQ for the Summer 1999 Southern Oxidants Study episode - Part I: Evaluation protocols, databases, and meteorological predictions, *Atmospheric Environment*, 40, 4825-4838, doi:10.1016/j.atmosenv.2005.12.043.
- Zhang, Y., P. Liu, A. Queen, C. Misenis, B. Pun, C. Seigneur, and S.-Y. Wu (2006b), A comprehensive performance evaluation of MM5-CMAQ for the Summer 1999 Southern Oxidants Study episode - Part II: Gas and aerosol predictions, *Atmospheric Environment*, 40, 4839-4855, doi:10.1016/j.atmosenv.2005.12.048.
- Zhang, Y., P. Liu, B. Pun, and C. Seigneur (2006c), A comprehensive performance evaluation of MM5-CMAQ for the summer 1999 southern oxidants study episode, Part III: Diagnostic and mechanistic evaluations, *Atmospheric Environment*, 40, 4856-4873.
- Zhang, Y., K. Vijayaraghaven, X.-Y. Wen, H. E. Snell, and M. Z. Jacobson (2009a), Probing into regional O₃ and PM pollution in the U.S., Part I. A 1-year CMAQ simulation and evaluation using surface and satellite data, *J. Geophys. Res.*, (in review).
- Zhang, Y., X.-Y. Wen, K. Wang, K. Vijayaraghaven, and M. Z. Jacobson (2009b), Probing into regional O₃ and PM pollution in the U.S., Part II. An examination of formation mechanisms through process analysis technique and sensitivity study, *J. Geophys. Res.*, (in review).